Vibration and Sound Signal Analysis in Gas Stirred Ladles

Jaefer Yenus

A dissertation

Submitted for Fulfillment of the Degree of Doctor of Philosophy

Swinburne University of Technology

Melbourne, Australia

2017

Abstract

Ladle metallurgy operations are usually accompanied by gas stirring of the metal bath primarily to achieve chemical and thermal homogeneity, composition modification and removal of inclusions before the steel melt is poured to a caster. These all are important to produce a steel product with the desired quality. Hence, the quantity of volumetric gas flow rate passed through the metal bath needs to be monitored to maintain the desired level of stirring. In industry, the level of stirring is often evaluated manually by operators using visual observation of the top surface turbulence, close attendance of the sound imparted and gas flow rate indicators. In general, judgments drawn from manual observations are qualitative in nature, and not suited to providing a precise level of stirring. To quantify the level of stirring, credible, consistent and quantifiable signals and a technique to analyze these signals for online stirring process control are required. Several researchers have used one-dimensional vibration, sound and image signals measured during stirring to develop algorithms to predict the degree of stirring inside the ladles. However, the optimum location of the vibration sensor and measuring the stirring reliably at low volumetric flow rate is not fully understood. Also, how the depth of different phases in ladle affects these measurements is not fully understood.

The present work focuses on studying the low flow rate ladle stirring using vibration and bubbling sound signals generated during stirring. Vibration signal was used to quantify the amount of stirring and the sound signal was essential to determine the depth of the two layers. Laboratory experiments on two physical cold models and a plant trial were carried out. The data were analysed using various statistical and signal processing techniques.

There are several new findings from this research, which are important to ladle metallurgy in controlling the stirring process online. This study revealed that the accelerometer can be located on the ladle external wall, the ladle support or the tank external wall. The quality of information collected from the three locations provided was not significantly different.

Vibration data collected from the cold/water model as well as the plant is highly structured and the degree of correlation between latent variables and stirring power is very strong especially when the bath level is constant. The frequency ranges where these strong linear relationships reside are different for different flow rate ranges. It was also found that most of the results from plant trials are consistent with the cold model studies. Moreover, the study of the bubbling sound on the water model established that the bottom layer/molten steel depth and thickness of the top

layer/slag can be evaluated using the sound signal. The effect of plant variabilities such as porous plug position, number, and life, barrel life, slag line life on the vibration was not addressed in this study and these effects should be the focus of further research in this field.

In summary, the outcome of this study is significant for secondary steelmaking. The sound signal provides information regarding the amount of metal and slag whereas the vibration signal can predict the amount of stirring intensity in the reactor. Hence, a complete online automation system should be able to be developed for controlling the stirring process in gas stirred ladles.

Acknowledgement

I owe my deepest gratitude to my supervisor; Professor Geoffrey Brooks for the patient guidance, encouragement and advice he has provided throughout my Ph.D. journey. You have been a tremendous mentor. I would like to thank you for inspiring my research and for allowing me to grow as a researcher. Your advice on ways to approach a research problem and the need to be persistent to accomplish any goal is invaluable. Your bright face and funny talks are always unforgettable.

I express my warmest gratitude to my associate supervisor, Dr. Michelle Dunn for the encouragements and inspiring advice. She was helpful in building confidence and improving my skills on signal processing. Her commitment towards the project was significant.

I am forever thankful to all my friends for the wonderful times we shared. They made my stay at Swinburne memorable. Their inspiration, support and experience sharing was instrumental. It is my pleasure to a give special thanks to Dr. Hasnat for the valuable information and help he provided in a number of ways.

It is my pleasure to thank people from IT , the laboratory and the library for their instant support whenever I need. My special appreciation also goes to Krzysztof Stachowicz from Mechatronic Laboratory who gave me a hand in setting up my data acquisition system.

I am so grateful to the people at Tata Steel and Swindon Technology Center in Rotherham, the UK for their unlimited help during plant trials.

My deep and sincere gratitude also goes to my wife, Zeineb, for her continuous and unparalleled love, help and support. I am forever indebted to parents and family for their love, care, and cheer which is always the source of my strength.

Finally, yet importantly, I would like to thank the Swinburne University of Technology for providing me this opportunity and experience that improved my research skills and made me explore new directions in my life.

Declaration

"I, Jaefer Yenus, declare that this Ph.D. thesis entitled "Vibration and Sound Signal Analysis in Gas Stirred Ladles" is my work. It contains no material, which has been accepted for the award of any other degree or diploma, except where due reference is made in the text of the examinable outcome. To the best of my knowledge, this thesis contains no material previously published or written by another person except where due reference is made in the text of the examinable outcome.

Jaefer Yenus

September 2017

Certification

This is to certify that the above statement made by the candidate is correct to the best of our knowledge.

Professor Geoffrey Brooks

Dr. Michelle Dunn

Table of Contents

Abstract i

Acknowledgement iii

List of Figures xi

List of Tables xvii

List of Symbols and Abbreviations xix

1 Introduction 1

1.1 Theoretical Framework 1

1.2 Statement of the Problem 1

1.3 Aims 2

1.4 Methodology 2

1.5 Thesis Outline 3

2 Literature Review 5

2.1 Secondary Steelmaking 5

2.1.1 Ladle Stirring Phenomenon 9

2.1.2 Ladle Eye and Upper Layer/Slag 11

2.1.3 Ladle Metallurgy Control 13

2.1.4 Ladle Gas Stirring 15

2.2 Sound and Vibration Signals 17

2.2.1 Vibration Signals 17

2.3 Sound Signal 26

2.3.2 Sound of Bubbles 29

2.3.3 Bubble Formation 30

2.3.4 Sound Signal Measurements 32

2.4 Signal Analysis 33

2.4.1 Frequency Domain Analysis 33

2.5 Vibration Analysis Techniques 39

2.5.1 Multivariate Statistical Analysis 40

2.6 Ladle Vibration 48

3 Research Issues **55**

4 Methodology **57**

4.1 Experimental Method 57

4.1.1 Physical Modelling 59

4.1.2 Physical Cold Model Limitations 66

4.2 Data Collection 67

4.2.1 Data Acquisition System 67

4.2.2 Signal Measurement 70

4.3 Data Analysis 72

4.3.1 Signal Processing 73

4.3.2 Statistical Techniques 75

4.4 Error Analysis 79

4.4.1 Systematic Errors 79

4.4.2 Random Errors 79

4.5 Methodology Summary 81

5 Plastic Walled Cold Model Study **83**

5.1 Introduction 83

5.2 Experimental Setup 83

5.3 Experimental Conditions 85

5.3.1 Background Noise 87

5.3.2 Sampling Rate 88

5.3.3 Sampling Time 89

5.3.4 Analysis Procedure 90

5.4 Result and Discussion 92

5.4.1 Optimum Sensor Location 92

5.4.2 Single Layer Study 93

5.4.3 Double Layer Study 96

5.4.4 Comparison of Results 101

5.5 Conclusions 102

6 Steel-Walled Cold Model Study **105**

6.1 Introduction 105
6.2 Experimental Setup 105
6.3 Experimental Conditions 108
6.3.1 Accelerometer Locations 109
6.3.2 Air Flow Rate and Bath Height 109
6.4 Data Analysis 110
6.5 Result and discussion 111
6.5.1 Sensor Location 111
6.5.2 Single Layer Study 113
6.5.3 Double Layer Study 114
6.5.4 Peak Frequencies 125
6.6 Conclusion 126

7 Plant Scale Study: The Case of Vacuum Tank Degasser 129

7.1 Introduction 129
7.2 Experimental Setup 130
7.3 Experimental Conditions 131
7.4 Data Collection 131
7.5 Signal Treatment and Refining 133
7.6 Background Noise 134
7.7 Sample Time Determination 135
7.8 Result and discussion 139
7.8.1 Data Analysis for Combined Heats 143
7.8.2 Data Analysis with One Constant Parameter 145
7.8.3 Plug life 146
7.8.4 Comparison of Plant and Cold-Model Results 147
7.9 Conclusions and Recommendations 149

8 Bubbling Sound Signal Analysis 151

8.1 Introduction 151
8.2 Experiment Setup 151
8.3 Experimental Conditions 153
8.4 Analysis Procedure 154

8.5 Signal Analysis 154
8.5.1 External Noise 154
8.5.2 Sample Time Determination 157
8.6 Result and Discussion 160
8.6.1 Bubbling Sound in the Single Layer 160
8.6.2 Bubbling Sound in Double Layer 167
8.7 Conclusions 175

9 Discussion 177

10 Conclusions and Recommendations 185

10.1 Conclusions 185
10.2 Limitations, Recommendations, and Future Directions 187

References 189

Appendix A: Relationships Between PC1 and PC2 209

Appendix B Mean Square Error (MSE) of PLS Regressions 213

Appendix C: Matlab Based PCA and PLS Programs 215

Appendix D: Summary of Publications and Presentations 235

List of Figures

Figure 2-1 Steelmaking process route [5] 5
Figure 2-2 Schematic of ladle inner structure with steel and argon injection [35] 6
Figure 2-3 Vacuum Tank Degasser [62] 9
Figure 2-4 Schematic representation of liquid bath and the plume [63] 10
Figure 2-5 Sketch of ladle eye in ladle furnace 12
Figure 2-6 Kinds of purging plug systems [34] 16
Figure 2-7 Harmonic function [20] 18
Figure 2-8 Hysteresis loop for elastic materials [20] 19
Figure 2-9 Loss factor ranges of some common materials [113] 19
Figure 2-10 ladle wall cross section 20
Figure 2-11 Single-degree-of-freedom systems with viscous damper. [20] 20
Figure 2-12 Variation of X and ϕ with frequency ratio. [20] 22
Figure 2-13 Frequency response characteristics of accelerometers [23] 24
Figure 2-14 Comparison of frequency response curves using different mounting techniques [118] 24
Figure 2-15 Orientation of axis sensitivity, primary sensing axis and cross-axis plane for accelerometers [119] 25
Figure 2-16 bubble formation in a viscous liquid. [130] 30
Figure 2-17 Simultaneous breakups and coalescences [134] 31
Figure 2-18 Characteristics of the two-phase plumes profile during moderate gas injection in a cylindrical vessel. [137] 32
Figure 2-19 Ensemble of time History records defining random process [142] 34
Figure 2-20 FFT Resolutions [146] 35
Figure 2-21 Sampling and observation time [146] 35
Figure 2-22 Hanning window sampling [146] 37
Figure 2-23 Signal processing path [146] 37
Figure 2-24 Orthogonality of the first three PCs of a data set [179] 43
Figure 2-25 Schematic representation of PLS [31] 46
Figure 2-26 RMS values and peak frequencies as function of gas flow rate [10] 50

Figure 2-27 Increase of ladle vibration with the Froude number – Water scale models, pilot scale steel ladles, industrial plant data and numerical simulation.[15] 51
Figure 2-28 Relationship between stirring power and PC1.[7, 18] 52
Figure 2-29 RMS value of the detected vibration signal as a function of the gas flow rate for a 160-tonne ladle furnace.[8] 53
Figure 2-30 RMS value of the vibro-signal on the gas flow rate under various blowing conditions.[8, 14] 54
Figure 4-1 Characteristic dimensions of a full scale and a model 61
Figure 4-2 Sample flow path of a single particle 62
Figure 4-3 Data acquisition system setup 68
Figure 4-4 Schematic description of SNR [223] 70
Figure 4-5 Dividing the time history into N smaller time lengths. 72
Figure 5-1 Laboratory experimental setup 84
Figure 5-2 Sketch of experimental setup 85
Figure 5-3 Accelerometer locations 85
Figure 5-4 Vibration amplitude of background noise and main signal 87
Figure 5-5 Spectral variations of noise and main signal 88
Figure 5-6 Vibration frequency spectrum at 0.83x10^{-5} m^3/s and 0.10 m water bath height 88
Figure 5-7 Frequency spectra at 5 seconds sample time 89
Figure 5-8 Frequency spectra at 6 seconds sample time 90
Figure 5-9 Overall analysis scheme 91
Figure 5-10 Relationship between PC1 and a) stirring power b) steel bath recirculation speed for flow rate range of 0.17 to 0.83 x 10-5 m3/s 95
Figure 5-11 Relationship between PC1 and a) stirring power b) steel bath recirculation speed for flow rate range of 0.83 to 4.17 x 10^{-5} m3/s 95
Figure 5-12 Relationship between PC1 and a) stirring power b) steel bath recirculation speed for flow rate range of 3.33 to 10.83 x 10^{-5} m^3/s 96
Figure 5-13 Relationship between PC1 and stirring power for the flowrates of a) 0.17 to 0.83 x 10^{-5} m^3/s b) 3.33-10.83 x 10^{-5} m^3/s 97
Figure 5-14 Relationship between X-score and Y-score a) both layers varying b) fixed bath height (H=0.25 m, h=0.20 m) for a flow rate range of 0.17-0.83 x 10^{-5} m^3/s 98

Figure 5-15 Relationship between predicted response and a) stirring power b) bath recirculation speed for a flow rate range of 0.17 to 0.83 x 10^{-5} m^3/s 98
Figure 5-16 Relationship between X-score and Y-score a) both layers varying b) fixed bath height (H=0.25 m, h=0.20 m) speed for flow rate range of 0.83 -4.17 x 10^{-5} m^3/s....99
Figure 5-17 Relationship between predicted response and a) stirring power b) bath recirculation speed for a flow rate range of 0.83 -4.17 x 10^{-5} m^3/s 99
Figure 5-18 Relationship between X-score and Y score a) both layers varying b) fixed bath height (H=250 mm, h=20mm) speed for flow rate range of 3.33 to 10.83 x 10^{-5} m^3/s 100
Figure 5-19 Relationship between predicted response and a) stirring power b) bath recirculation speed for a flow rate range of 3.33 to 10.83 x 10^{-5} m3/s....100
Figure 5-20 Relationship between mean square error (MSE) and number of latent variables ...100
Figure 5-21 Relationship between vibration energy and Froude number for data taken from this study a) single layer b) double layer c) double layer....101
Figure 5-22 RMS value of the vibro-signal on the gas flow rate under various blowing conditions a) Single layer data b) Double layer data 102
Figure 6-1 160 ton ladle inside dimensions and bottom view showing porous plug locations..107
Figure 6-2 Overall experimental setup 108
Figure 6-3 Sensor locations (A and B and C) on ladle and vacuum tank degasser wall 109
Figure 6-4 Sensor candidate locations on the laboratory apparatus....109
Figure 6-5 Vibration Amplitude versus flow rate for each axes in each location 111
Figure 6-6 Relationship between PC1 and stirring energy in the frequency range of a) 170 to 180 Hz b) 150 to 160 Hz....113
Figure 6-7 Relationship between stirring power and PC1 in the range of 40 to 50 Hz 117
Figure 6-8 Relationship between response scores (Y) and predictor scores (X) in 80 to 90 Hz ..118
Figure 6-9 Relationship between response scores (Y) and predictor scores (X) in 70 to 80 Hz...118
Figure 6-10 Relationship between bath recirculation speed and $Yscore$....119
Figure 6-11 Relationship between stirring power and $Yscore$....119
Figure 6-12 Mean square root error (MSE) and number of variables taken....120
Figure 6-13 Relationship between stirring power and PC1 in the frequency range of 50 to 60 Hz 121
Figure 6-14 Relationship between X and Y-scores in the frequency range of 340 to 350 Hz.....123

Figure 6-15 Comparison between measured and predicted vibration signals (cross validation) 124
Figure 6-16 Peak frequencies in the three axes 126
Figure 7-1 Schematic diagram of vacuum tank degasser 129
Figure 7-2 Sketch of a ladle in the VTD: a) overall dimension b) porous plug position 130
Figure 7-3 a) Data acquisition setup in the plant and b) accelerometer orientation 131
Figure 7-4 Pressure profile for part of T0560Z heat 134
Figure 7-5 STFT of background noise: a) x-axis, b) y-axis, and c) z-axis 135
Figure 7-6 Vibration time history for a time length 60 seconds 136
Figure 7-7 Frequency spectra of a 15-second time sample time for X-axis 137
Figure 7-8 Frequency spectra of a 20-second sample time for the x −axis data 137
Figure 7-9 Frequency spectra of a 20-second sample time for the y −axis data 138
Figure 7-10 Frequency spectra of a 20-second sample time for the Z-axis data 138
Figure 7-11 Relationship between PC1 and gas flow rate: a) 0 to 914 Hz b) 40 to 50 Hz 141
Figure 7-12 Relationship between: a) input and output PLS components b) flow rate and predicted variable (Vibration) 142
Figure 7-13 Relationship between PLS components in the whole frequency range 142
Figure 7-14 Relationship between input and output latent variables in T0565Z, T0566Z, T0573Z and T0574Z heats 143
Figure 7-15 Relationship between input and output variables at a selected constant parameter 146
Figure 7-16 Vibration amplitude as a function of plug life number 147
Figure 7-17 Prediction of plant gas flow rate using PLS model developed from cold model data 148
Figure 8-1 Experimental setup for acoustic measurement 152
Figure 8-2 Cold model apparatus a) without insulation b) with insulation 154
Figure 8-3 Sound pressure at 0.25 m water level a) background noise b) noise + main signal at 16.67x10-6 m^3/s c) noise + main signal at 33.33x10-6 m^3/s 155
Figure 8-4 Comparison of noise signal with main signal containing noise a) no stirring (external noise) and with insulation b) flow rates of 16.67x10-6 m^3/s and c) flow rates of 33.33x10-6 m^3/s) 156

Figure 8-5 Sound pressure level (dB) for a) no stirring (external noise) b) flow rates of 16.67x10-6 m^3/s and c) flow rates of 33.33x10-6 m^3/s) 156
Figure 8-6 Spectral patterns of sound pressure at sample time of 30 seconds 157
Figure 8-7 Spectral patterns of sound pressure at sample time of 10 seconds 158
Figure 8-8 Spectral patterns of sound pressure at sample time of 6 seconds 159
Figure 8-9 Spectral patterns of sound pressure at sample time of 5 seconds 160
Figure 8-10 Relationship between average sound pressure and flow rate 161
Figure 8-11 Sound waves for a fixed flow rate of $1.67x10^{-6}$ m^3/s and variable bath level 161
Figure 8-12 Peak frequencies at 0.15 m water level and 10^{-5} m^3/s volumetric air flow rate 162
Figure 8-13 Global peak frequency at different flow rate and bath heights 163
Figure 8-14 PSD of sound pressure at 10^{-5} m^3/s flow rate and the various heights 163
Figure 8-15 Sound power at $33.3x10^{-6}$ m^3/s and 125 to 130 Hz 164
Figure 8-16 Sound pressure at $33.3x10^{-6}$ m^3/s and 160 to 185 Hz frequency range 164
Figure 8-17 Sound pressure at $33.3x10^{-6}$ m^3/s and 160 to 185 Hz frequency range 165
Figure 8-18 Relationship between air flow rate and average sound pressure 166
Figure 8-19 Peak frequencies at 10.83 $x10^{-6}$ m3/s a) 0.15 m and b) 0.25 m bath level 166
Figure 8-20 First peak frequency at different flow rate and bath heights 167
Figure 8-21 Second peak frequency at different flow rate and bath heights 167
Figure 8-22 Relationship between sound pressure and flow rate 168
Figure 8-23 Peak frequencies as a function of flow rate. 168
Figure 8-24 Relationship between amplitude at peak frequencies and flow rate at four oil depths. 169
Figure 8-25 Sound pressure level at $36.67x10^{-6}$ m^3/s, 0.250 m thick lower layer and varying upper layer 170
Figure 8-26 Sound pressure level for the flow rate of $36.67x10^{-6}$ m3/s and H=0.25 m 171
Figure 8-27 Variation of average sound pressure level with the depth of the upper layer in between 760 and 775 Hz 171
Figure 8-28 Peak frequency values at different upper layer depths 172
Figure 8-29 Spectral patterns of sound pressure in the range of 700 to 800 Hz a) single layer: 172
Figure 8-30 Peak frequencies when H= 0.10 and h=0.005 to 0.020 m. 173
Figure 8-31 Peak frequencies at 66.67 m^3/s a) single layer: H= 0.10 m and b) double layer, H=0.10 and 0.020 m thick oil 173

Figure 8-32 Sound pressure level at 36.67×10^{-6} m^3/s and water level of 0.25 m with oil as an upper layer 174
Figure 8-33 Variation of sound pressure level with the depth of the upper layer in between 1700 and 1710 Hz 174
Figure 8-34 Peak frequency variation in the double layer for water level of 0.15 m and oil depth that varies from 0.005 to 0.020 m 175

List of Tables

Table 2-1 Summary of SIMPLS algorithm 48
Table 4-1 Mechanical properties of steel, stainless steel and acrylics [216-220] 65
Table 4-2 PCB Industrial Accelerometer general specification (ICP Model 604B31) 68
Table 4-3 PCB Microphone (ICP Model 130A23) general specification 68
Table 4-4 Key Instruments Airflow meter descriptions 69
Table 5-1 working conditions in laboratory and plant scales 84
Table 5-2 Experimental conditions for single layer study 86
Table 5-3 Experimental conditions for double layer study 86
Table 5-4 Experimental conditions for accelerometer location selection 86
Table 5-5 PC1 and PC2 values for the single (without the top) layer study 93
Table 5-6 PC1 and PC2 values for the double (with the top) layer study 93
Table 5-7 PC1 and PC2 values at different frequency ranges and flow rates for the single (without the top layer) layer study 94
Table 5-8 PC1 values for double layer (with oil on top) bubbling at different frequency ranges. 97
Table 6-1 Parameters and their values in the full and the laboratory scales in the 160-ton ladle 107
Table 6-2 Values of experimental parameters the three accelerometer locations 110
Table 6-3 Values of experimental parameters for a fixed accelerometer location 110
Table 6-4 Values ($PC1$) and the degree of correlation ($R2$) 112
Table 6-5 Values of loading vectors and PC for the single layer blowing data 114
Table 6-6 Values of loading vectors and PC for the double layer blowing data 115
Table 6-7 PC1 values of small frequency ranges 115
Table 6-8 Values of PCVAR of different frequency ranges 116
Table 6-9 Values of β for the frequency range of 80 to 90 Hz 120
Table 6-10 Values of PC1 for 23.33 to 40x10^{-6} m^3/sec 121
Table 6-11 Values of PCVAR for different frequency ranges 122
Table 6-12 Values regression coefficient, β 123
Table 6-13 PC1 values for the flow range of 41.67 to 83.33x10^{-6} m^3/sec 124
Table 6-14 Values of PCVAR in the flow rate range of 41.67 to 83.33x10^{-6} m^3/sec 125
Table 7-1 List of measured heat and related information availability 132
Table 7-2 Heats with respective parameter values 133

Table 7-3 PC1 values for three samples of T0561Z heat at different frequency ranges 139
Table 7-4 PC values of each heat 140
Table 7-5 Values of Loading vectors, Eigenvalues and principal components for 60 to 70 Hz.. 141
Table 7-6 PC values for combined data..... 144
Table 7-7 PC values when one parameter was kept constant..... 145
Table 7-8 PC1 values of plant and water model data..... 147
Table 8-1 Experimental conditions for sound pressure experiment 153
Table 8-2 First and second peak frequencies for four water levels and varying flow rates 162
Table 8-3 First and second peak frequencies at different flow rate and water height 165
Table 8-4 First and second peak frequencies and their respective sound pressure amplitude value 169
Table 8-5 Peak frequency values within the frequency range of 700 to 800 Hz 171

List of Symbols and Abbreviations

Abbreviation/Symbol	Description
U_P	Plume velocity (m/s)
α_f	Void fraction
g	Gravitational acceleration (m/s^2)
H	Bottom layer depth (m)
ε	Stirring power (w/tonne)
Q_0	Volumetric gas flow rate (Nm^3/min)
T	Temperature (K)
M	Weight of liquid metal (tonne)
P_0	Atmospheric pressure(bar)
$\bar{U}$	Bath recirculation speed (m/s)
R	Vessel radius (m)
h	Top layer/oil thickness (m)
D_m	Cold model diameter (m)
H_m	Cold model height (m)
D_f	Full-scale diameter (m)
H_f	Full-scale height (m)
λ	Geometric scaling factor
Q_m	Volumetric air flow rate in the model
Q_f	Volumetric air flow rate in the full scale
A	Acceleration amplitude (m/s^2)
$PC1$	First principal component
$PC2$	Second principal component
A^*	Dimensionless area
A_{es}	Spout area exposed to air (m^2)
η	Internal loss factor
η_s	Structural energy loss
ρ	Density (kg/m^3)
V	Volume (m^3)
η_{rad}	Acoustic radiation loss factor

p	Pressure
L_p	Sound pressure level
T_{obs}	Total sample time
N	Number of samples
β	Regression coefficient of PLS model
Y_{res}	Residual matrix of PLS model
f_1	First peak frequency
f_2	Second peak frequency
f	Frequency (Hz)
x	Acceleration along x-axis (m/s^2)
y	Acceleration along y-axis (m/s^2)
z	Acceleration along z-axis (m/s^2)
X	Matrix of H, h and Q
Y	Matrix of x , y and z
E_r	Residuals of X
F_r	Residuals of Y
T	X −score
P	X −loading
U	Y-score
C	Y-weights
W	x −weight
$PCVAR$	Percent of variation

1 Introduction

1.1 Theoretical Framework

Ladle Metallurgy is an important step in producing high-quality steel. After tapping of molten steel from a primary steelmaking furnace such as Electric Arc Furnace (EAF) or Basic Oxygen Furnace (BOF), the liquid steel is subjected to additional refining in different processes grouped under ladle metallurgy or secondary steelmaking for high quality or specialty applications. Ladles are equipped with various accessories such as porous plugs/tuyeres or lances to facilitate the refining process. Strict control of secondary steelmaking operations is associated with producing high grades of steel in which the tolerances in chemistry and consistency are narrow.

Ladle metallurgy processes comprise alloying, homogenization of temperature and composition, desulfurization, deoxidation, inclusion removal, and degassing processes.[1, 2] Ladle metallurgy (or the secondary steelmaking process) is a crucial stage where thermal and composition homogenization of the liquid metal takes place in ladles. In addition, chemistry adjustments and inclusion removal are also carried out in these reactors.[3, 4] These processes produce a steel with fewer impurities, and lower inclusion content resulting in uniform casts, better mechanical properties, and surface quality.[1, 2, 5]

The secondary steelmaking refining processes are frequently facilitated by stirring the melt using inert gas purged through porous plugs usually located at the bottom of the vessel. The gas stirring plays an important role in achieving the key objectives of secondary steelmaking.[4, 6] Hence, monitoring the stirring process is vital in attaining the required steel quality from ladle metallurgy.

1.2 Statement of the Problem

The status of the stirring process is often assessed by looking at the turbulence on the top surface, paying attention to the audible sound imparted and observing flow meter gauges.[7, 8] However, this method of control may not be efficient because of several reasons. First, the evaluation of the process from the top surface not only needs experienced operators but is also a qualitative approach. Second, gas losses at different parts of the ladle gas line result in a disparity between the actual amount of gas entering the metal bath and the measured flow rates outside the vessel.

In addition, the working conditions do not allow direct measurement of the process characteristics like temperature and composition.[9]. As a result, the true magnitude of stirring is difficult to estimate correctly.[7, 10-13] Moreover, the problem of visual control worsens when ladles are agitated at low gas flow rates because of leakage and working conditions.

Hence, researchers have searched for signals that can be directly measured from the process and reliably used to evaluate stirring. In recent times, there has been much attention on the application of vibroacoustic and image signals to regulate the process online i.e. using these signals to predict the actual gas flow rate or stirring intensity in real time.[7, 8, 10, 12-19]. Vibration is the oscillation of a physical object about a fixed equilibrium position initiated by disturbances or forces.[20-23] The sound is created by alternate contraction and relaxation of waves in the medium. The propagation of sound is affected by the temperature, density, and viscosity of the medium. The sound intensity indicates the wave strength along a perpendicular surface the sound is passing through.[24] The multidimensional dynamic fluid turbulence during gas stirring inside causes the ladle wall to vibrate. In a similar manner when inert gas rises forming bubbles, the bubble formation, and disintegration process generates sound pressure.[25, 26] Hence, sound and vibration signals can be directly and continuously measured from the process to provide online information about the status of the stirring.[10]

1.3 Aims

This study has focused on studying the stirring process using sound and triaxial vibration signals. Specifically, this research paid particular attention to selecting the best vibration sensor location, using triaxial vibration signals to characterize stirring at low flow rates, and using the sound signal to estimate the amount of slag and liquid metal.

1.4 Methodology

This study was carried out on two physical cold models; one was constructed from a transparent material (Perspex) and the other built from stainless steel. A full-scale industrial gas stirred ladle was also investigated. A vibration study was carried out on plant and laboratory scales whereas the sound signal investigation was carried out on a laboratory cold model only. The physical cold models were designed based on geometric and dynamic similarity criteria. Water and motor oil were used as working fluids to replicate liquid metal and slag respectively. The water-oil bath

was stirred by air. Vibration and sound signals caused by air/gas stirring were measured using a three-axis accelerometer and microphone respectively. Captured data was analysed by various signal processing and multivariate statistical techniques.

Time domain triaxial vibration and sound signals are converted to the frequency domain using the Fast Fourier Transform (FFT). In the plant trials, since vibration data was noisy, the Short-Time Fourier Transform (STFT) was used to locate the power of the noise signal. The frequency range where the noise signal was dominant was ignored in the vibration analysis. Once the data was processed, the vibration data was analysed using principal component analysis (PCA) and partial least squares (PLS). Principal component analysis is a well-established tool for revealing highly structured data and reducing the number of variables by linearly suppressing the dimension of the variables to a reasonably few number of linear combinations which are known as principal components.[27-29] After the highly structured frequencies were discovered, the next step was to find the relationship between the input data and output in these frequency ranges using partial least square (PLS). PLS is a widely used tool in different fields for modeling linear relations between a multivariate input matrix, $\boldsymbol{X}$, and output matrix, $\boldsymbol{Y}$.[30] PLS deals with the variation in $\boldsymbol{X}$ (predictors) and $\boldsymbol{Y}$ **(**responses**)** spaces simultaneously which makes it an ideal choice for process monitoring.[31] During PLS analysis, the input parameters were the airflow rate and depths of the top and bottom layer whereas the output matrix consisted of the vibration in the x, y and z axes.

1.5 Thesis Outline

The thesis consists of ten chapters. Chapter 2 introduces secondary steelmaking and the gas-stirring phenomenon. It reviews the literature on stirring process control using vibration, sound and image signals. This chapter also introduces basic concepts of vibration and sound signals and their analysis techniques. The statistical techniques used in this study are also described in this chapter. Chapter 3 discusses the research questions that are addressed in this study. Chapter 4 describes the methods applied in this study to address the research issues listed in chapter 3.

The experimental results and discussion are presented in chapters 5, 6, 7 and 8. In Chapter 5 and 6 cold model results are discussed whereas Chapter 7 describes the outcomes of the plant trial and the comparison with the cold model study. The laboratory scale study of bubbling sound is

discussed in Chapter 8. The discussion chapter, Chapter 9, explains the importance of the research outcome to industry and the limitations encountered. Finally, Chapter 10 summarizes conclusions from the results found in the current study and points out recommendations for future research.

2 Literature Review

2.1 Secondary Steelmaking

The modern steelmaking process begins with charging raw material (iron ore) to the blast furnace to produce pig iron. This hot iron and some steel scrap are then charged into the Basic Oxygen Furnace (BOF) where oxygen is injected to produce molten steel that has specific chemical and physical properties. In a similar manner, cold scrap metals are also used to produce molten steel using an Electric Arc Furnace (EAF).[32, 33] However, the BOF and EAF, which can be taken as primary steelmaking processes, cannot produce high-quality steel that can meet customer demand.[34] This problem led to the development of secondary steelmaking or ladle metallurgy. In secondary steel making, molten steel is tapped from the BOF and EAF for further refining and processing to a ladle furnace. Figure 2-1 shows the general process layout of steelmaking from the raw material to the continuous casting stage.

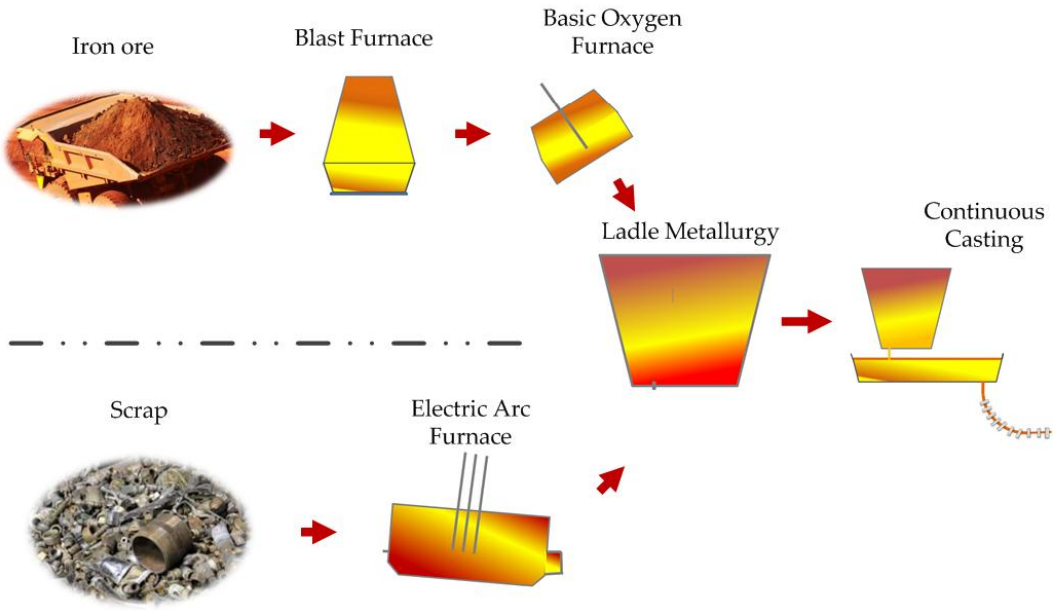

Figure 2-1 Steelmaking process route [5]

Secondary steelmaking processes are generally carried out in cylindrical vessels that are internally lined with refractory materials to protect the shell from melting due to the high heat. Figure 2-2 shows the general sketch of a ladle furnace and the other geometries related to it.[35]

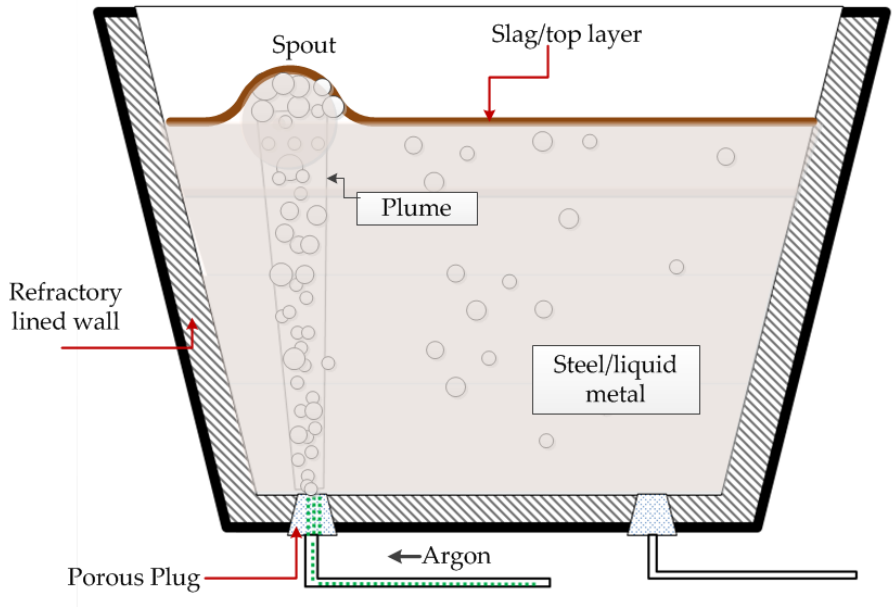

Figure 2-2 Schematic of ladle inner structure with steel and argon injection [35]

A common technique to all these processes is the injection of pressurized gas (usually argon) through the porous plugs (also known as lances or tuyeres) to create the desired bath stirring.[34, 35] The magnitude of the flow rate may vary from 0.001 to 0.015 Nm^3/min per tonne depending on the particular goal of the ladle refining operation. Inert gases can be injected by either symmetrical or asymmetrical positioned porous plugs. Studies have shown that nozzle geometries have no significant effect on bubble and liquid upward acceleration and therefore are not critical under ladle refining conditions [36, 37] On the other hand, inert gas flow rate, nozzle position and ladle geometry do have a large influence on the fluid dynamics and interaction and are being studied extensively.[38] Generally, the roles of ladle stirring comprise all or some of the following essential activities:[34, 35, 39]

- Temperature regulation and homogenization
- Composition modification and homogenization
- Removal inclusions

Hence, ladles should be thoroughly agitated to achieve high thermal and compositional homogeneity while the final values of temperature and composition are attained. Gentle bubbling through the vessel can easily homogenize the temperature and facilitate the rate of removal of inclusions while strong stirring conditions can lead to slag droplet entrainment into the steel melt.[40] Pretorius defined a slag as "ionic solutions consisting of metal oxides and fluorides that

float on the top of the steel (completely liquid or partially liquid). Slags often contain both liquid and solid fractions.[41] As the solid fraction increases the fluidity of the slag decreases and it is evident that it changes eventually to a "crust" on the surface." Slag is a by-product of steelmaking and refining process.[42, 43]

The scope of secondary steelmaking (or Ladle metallurgy) is large and encompasses desulfurization, deoxidation, inclusion removal, alloying, and degassing processes.

a. **Desulfurization**: Sulfur is usually a harmful impurity in steel. Excess amounts of sulfur reduce weldability and tend to aggravate brittleness.[44] The concentration of sulfur in the continuous casting route should below 0.02 wt % for line pipe and ship plates. Some special steel plates require the percent composition of sulfur below 0.005 wt%. Other ultra-low-sulfur products should have steel with as low as 0.001% wt %.[45] Sulfur removal in primary steelmaking is not significant because of the oxidizing environment. Hence, further desulfurization is carried out in ladles. The process can reduce the sulfur content to or below 0.01% and is a vital part of a modern integrated steel plant. This can be achieved by treatment of molten steel with synthetic slag on top and gas stirring.[4]
b. **Deoxidation:** The drive to steel deoxidation is to remove most of the dissolved oxygen and in the oxides from the liquid steel.[46] Liquid metal dissolves some oxygen and this solubility decreases as the metal starts to solidify. Consequently, the remaining oxygen is rejected during solidification of the steel in ingot or continuous casting. This leads to defects such as blow holes and non-metallic inclusions and affects the structure of the cast metal. Hence, deoxidation takes place in secondary steelmaking operations to bring down the level of oxygen in the melt.[4] The stirring of the melt causes homogenization and promotes dissolution of the deoxidizer.[47]
c. **Inclusion Removal:** Reactions that mainly develop during secondary steelmaking and solidification can result in inclusions such as oxides, sulfides, and other binary or more complex aggregates in steel products. It well understood that distribution, size, composition, and shape of these inclusions significantly affect corrosion and mechanical properties, castability, cold and hot workability, and machinability of steel.[48] Vigorous mixing in the melt is carried out by argon-rinsing to promote inclusion removal.[48]
d. **Alloy Addition:** Additions of ferrous alloys to the metal bath is carried out to provide for chemical control. The process of alloying steel melts in ladles comprises three partial steps:

alloy addition, alloy solution, and alloy mixing.[49] Gas stirring mixes the alloys and homogenizes the composition of the liquid metal.[50]

e. **Vacuum Degassing:** Generally, vacuum degassing refers to the exposure of molten steel to a low-pressure environment to removes gases from the steel bath. Vacuum degassing is a vital secondary steel making process. The existence of pressure dependent reactions makes this process essential. Gases such as nitrogen, oxygen, and hydrogen are found dissolved in liquid steel during steelmaking. Solubilities of these gases in a solid steel are very low. When liquid steel is solidified, excess nitrogen and hydrogen may form stable nitrides and unstable hydrides respectively. As a result, the excess hydrogen in solid steel tends to formH_2. Hydrogen gas, precluded by solid steel, accumulates in holes and develops high gas pressure inside the hole. When the steel is forged, the combination the high gas pressure in holes near the surface and hot working stresses have a tendency to form fine cracks in the surface region. Hydrogen also increases the brittleness of steel. Nitrogen can be detrimental to steel because it affects aging and toughness characteristics.[4] There are also applications where nitrogen can be beneficial.[51, 52] Attempts to avoid these cracks, brittleness, aging and toughness characteristics led to the development of vacuum degassing processes.[4] Degassing is used to remove nitrogen and hydrogen from liquid steel.[33, 53-59] At low pressure (vacuum), the deoxidation product acquires much smaller values than in the atmospheric pressure which signifies the vacuum degassing can also be used for deoxidation and decarburization. [60]

   In order to carry out degassing, a low pressure/vacuum must be maintained inside the tank/vessel by means of a pump system. There are generally three types of vacuum degassing processes: ladle degassing, vacuum tank and circulation degassing.[4, 6] Tank degassing speeds-up intensive metal-slag interactions during the entire degassing process.[6, 61] This promotes sulfur and nitrogen removal from the liquid steel during the degassing treatment. However, carryover slag from primary steelmaking contains FeO, which may increase the O_2 content of the steel melt. Therefore, it is essential that carry over slag from primary steelmaking furnace be as low as possible to improve the effectiveness of degassing.[62] A schematic diagram of a tank vacuum degasser is shown in Figure 2-3.

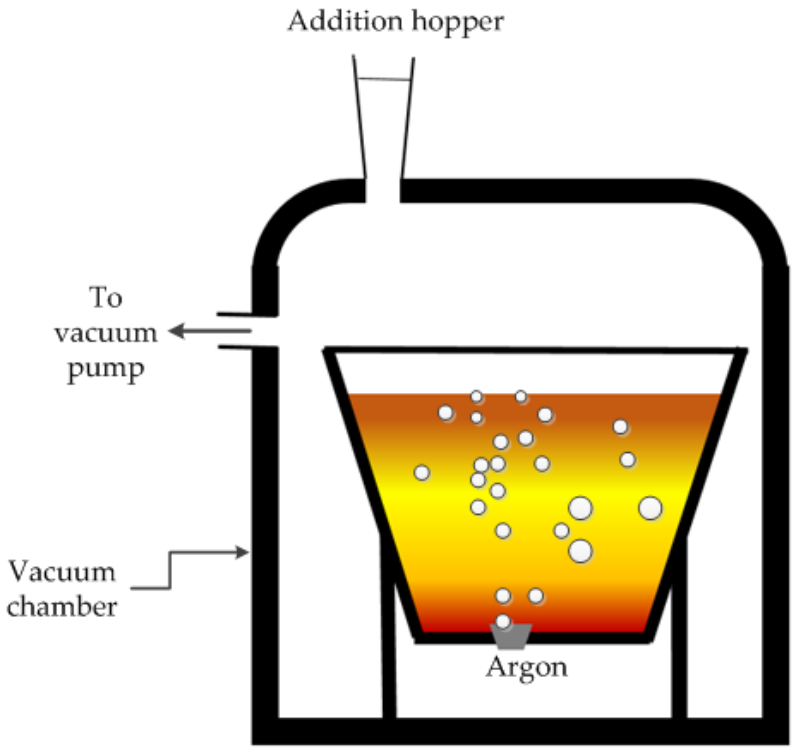

Figure 2-3 Vacuum Tank Degasser [62]

Percolation of argon below the melt is used for efficient mass transfer, homogenization and inclusion removal. The locations of porous plugs play an important role in achieving the objectives of degassing. Argon injection facilitates the rate of vacuum degassing and decarburization by imparting stirring to the melt, causing circulation of liquid metal and enhancing the gas–metal interfacial area through the generation of bubbles that rise and drop.

2.1.1 Ladle Stirring Phenomenon

When gas is injected into the melt through the bottom plugs, jets or large bubbles are formed depending on the magnitude of the gas velocity. These bubbles collapse into tiny bubbles as they travel upward and entrain the melt to form a two-phase region called the plume.[38, 63] The plume rises to the surface in a conical shape. Themelis et al.[63] observed that the liquid around the cone also speeds up and travels upward together with the plume. On the surface, the gas bubbles detach from the two-phase plume while the melt moves upwards and returns to the bath.[63] This is shown in Figure 2-4.

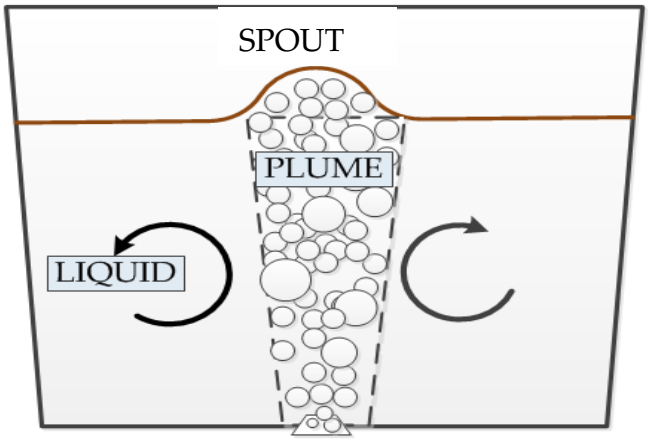

Figure 2-4 Schematic representation of liquid bath and the plume [63]

The energy exchange undertaken in this manner between the inert gas and the melt is responsible for mixing and other metallurgical interactions. According to Krishnapisharody and Irons[36], the momentum of the injected gas is lost after a short travel from the injector and it is the buoyancy of the rising gas that drives the plume afterward. Hence, plume properties are related to the plume Froude number, which is the ratio of inertial force to buoyancy force. The plume Froude number is defined using the plume velocity (U_p), void fraction (α) and bath height (H) and is shown in Equation 2-1[36] Void fraction is the fraction of the volume that is occupied by the gas phase.

$$Fr_P = \frac{U_P^2}{\propto_f gH} \qquad 2\text{-}1$$

The stirring power, defined as the capacity to homogenize the melt, is then due to the rising bubbles are driven by buoyancy.[40, 64] Szekely et al.[39] showed that the rate of mixing in ladle furnace depends on the rate of energy input or energy dissipation and the geometry of the vessel.[65] The rate of energy dissipation, which defines the rate of energy input is given by Equation 2-2a.

$$\varepsilon = 14.2\frac{Q_0 T}{M}\log(1+\frac{H}{1.46}P_0) \qquad 2\text{-}2a$$

$$\bar{U} = 0.86Q^{0.86}H^{0.25}R^{-0.58} \qquad 2\text{-}2b$$

where ε is the rate of energy dissipation (watt/tonne),$Q_0$is the volumetric gas flow rate (Nm^3/min), T is bath temperature (Kelvin), M is liquid weight (tonne), H is depth of gas injection or the bath

height (m), and P_0 is the pressure at the melt surface (bar). Some studies [66, 67] show that part of the energy imparted by gas to a two layer liquid bath is dissipated due to interfacial phenomenon such as emulsification. Minion et al.[10] indicated that the steel bath recirculation beneath the surface is crucial in studying and overcoming the problem of low flow rate stirring.[10] Sahai and Guthrie derived a macroscopic model that estimates the average steel bath recirculation from water model data shown in Equation 2-2b.[68] In Equation 2-2b, Q is volumetric gas flow rate (l/min), H is the depth of liquid (m) and R is the radius of the vessel (m). This gas stirring also aims to refine and remove inclusions from the molten steel.[69] Hence, monitoring the steel stirring process plays a vital role in ensuring the inert gas is doing its work properly and its consumption is efficient.[7]

The relatively large size of ladles and harsh operating conditions imposes obstacles to the close study of the stirring process. Physical models, which obey geometric, kinematic and dynamic similarities with the full-scale industrial vessel, have been applied to study stirring and another related phenomenon.[35, 64, 70-79] Steel melt and slag are commonly replicated by water and oil respectively. The density difference between these two fluids is crucial in that the oil floats above the water making it suitable to study various aspects of the ladle stirring process.[74-79]

2.1.2 Ladle Eye and Upper Layer/Slag

When pressurized gas is purged to the molten metal, the gas rises towards the top surface and tries to push the upper layer/slag upward creating a bulged region termed the spout. This can be easily recognized in Figure 2-4. In the case of very thin upper layer/slag or if the horizontal flow near the surface has the ability to push the slag away, the molten metal is exposed to air in the spout region. This area of bare metal is known the ladle eye and is shown schematically in Figure 2-5.[73, 77, 80] Ladle eye area is an important industrial phenomenon as it is the location of harmful reactions between the air and the metal.[80] It is the region where slag metal interaction, slag entrainment, metal losses to slag, and transport phenomenon linked with refining reactions take place. Other unwanted effects like energy losses, re-oxidation of steel, splash and fume formation occur in this region.[79, 80] There have been several studies on the spout and ladle eye.[72, 73, 76-82]As a result, various models have been proposed to demonstrate the relationships between the eye area and the operating parameters of the ladle furnace and geometry.[80]

Xu, Brooks, and Yang[80] compared the various models (which are based on industrial and laboratory data) of ladle eye area proposed by Subagyo et al.[74], Mazumdar et al.[81] and Krishnapisharody et al.[82] According to their analysis, Krishnapisharody and Irons' model which is based on industrial data, had better reliability.[80] Krishnapisharody's dimensionless ladle eye area model based on the assumption that the plume expands in conical fashion is given in Equation 2-3 and 2-4 [73]

$$A^* = \frac{A_e}{H^2} \qquad 2\text{-}3$$

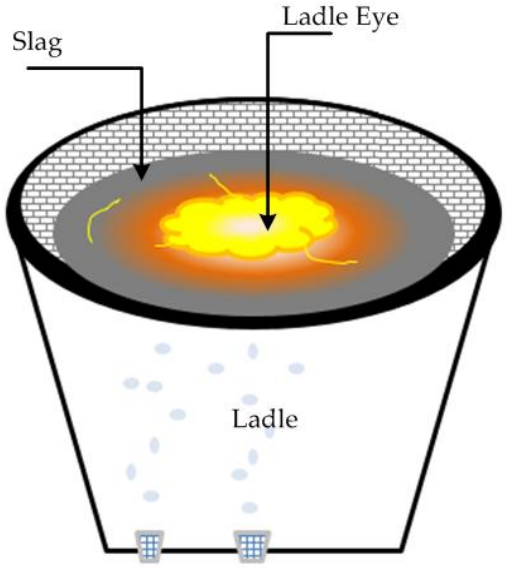

Figure 2-5 Sketch of ladle eye in ladle furnace

$$A^* = \alpha' + \beta' \left(\frac{\rho}{\Delta\rho}\right)^{0.5} \left(\frac{U_p^2}{gh}\right)^{0.5} \qquad 2\text{-}4$$

Where α' and β' are numerical constants, A^* is a dimensionless area, A_{es} is the exposed spout area measured at the slag air interface (m^2), A_e is the spout area (the surface area between liquid metal and air) (m^2), H is height of the bulk fluid (liquid steel/water) (m) and h -height of the upper layer (slag/oil) (m). Thus, the nondimensional area A^* is dependent on non-dimensional density difference and Froude number. Equation 2-4 can be used for eccentric ladle stirring, if the eye does not interact with the ladle wall, which is the normal regime of industrial operations.[73]

The close control of ladle eye dynamics is challenging in an industry. This is often because no mechanism is developed to provide continuous feedback data and the gas flow rate purged

through porous plugs is often monitored manually. Ladle eye dynamics should reliably be controlled for better quality products.[83]

The height of metal and slag has significant importance in ladle metallurgy operations especially in terms of controlling heat loss, metal chemistry (O and N pick up), eye size and the heating characteristics of the electric arc heating system. The slag height and its rheology essentially depend on operating conditions and chemical composition respectively. Consequently, the determination of its physical characteristics like density, surface tension, viscosity, and thickness is not easy.[3, 39] Literatures show that the properties of the slag such as density, surface tension and viscosity are also dependent on the composition of each component and working temperature.[84]Similar to the ladle eye, regulating slag characteristics is beneficial in developing a comprehensive process control in ladle metallurgy.[85]

2.1.3 Ladle Metallurgy Control

Ladle metallurgy is a common unit operation in most steelmaking melt shops and plays a vital role in ensuring the quality of steel products. The quality is achieved through adjusting and fine tuning of the molten steel's composition and temperature and removing inclusions prior to casting.[86, 87] Hence, the parameters that should be monitored to make sure the final product is of quality are chemistry, temperature and inclusion characteristics. The common controlling techniques of these parameters are briefly described by Brooks et al.[39]

a) Chemistry Control

The chemical composition of the liquid steel should be homogenous and the final values of carbon, sulfur, phosphorus, oxygen, nitrogen, calcium, silicon, manganese, aluminum and other alloying elements have to be at the desired level. Measurement techniques range from direct methods, which are accurate but expensive, to indirect methods, which are fast and low-cost, but only reliable as relative indicators.[88] The composition values of these metals are often measured at three stages of the heat: initial, intermediate and final stages. Samples taken from the melt are analysed using optical emission spectrometry (OES), or destructive distillation techniques (LECO). The latter, though it is slow, it is better in accurately determining steel chemical composition of carbon levels, sulfur, oxygen, and nitrogen. OES performs rapid elemental analysis of solid metallic samples with optical emission spectrometry.[89, 90]

The composition of a slag is also commonly sampled manually at the initial and final stages. The analysis of samples using Inductively Coupled Plasma (ICP) or X-ray Fluorescence (XRF) techniques can take few hours to get the composition values. So, these results are more often used for analysis rather than for control purposes.[90]

b) Temperature Control

Thermal homogeneity as well as final melt temperature are critical to achieving a consistent quality in the production of castings and should be at proper values before casting takes place. Several techniques have been developed to measure liquid metal temperature. These include "spot" measurement, ladle wall temperature measurement, infrared pyrometry, radiation spectrometry [91], resistance thermometers, heat flow meters and computer models.[39, 89]

Spot measurements are measured using a thermocouple several times during a heat. These sensors can give a reading within 10ms response time and associated error of $\pm 5℃$.[89] Thermocouples installed to the refractory base can indirectly measure the temperature of the steel melt in a real time. However, this continuous monitoring technique can be hampered by metal build-ups and sensor damage, which can interfere with the main signal. Continuous temperature monitoring can also be done using infrared pyrometry. These contactless sensors measure the infrared radiation from the surface of the body to estimate its temperature. This method is common in areas where surface conditions, geometry, and emissivity are not difficult to express. Due to the harsh working conditions surrounding the hot metal, these probes may not be convenient for use in steelmaking. Thermal numerical models have been developed for online applications in ladle furnace. The parameters evaluated include heat loss to the refractory lining, heat loss due to purging and heat gain due to arcing and heating effects.[92] These models do not contain any feedback parameters from the process. They are generally used as part of an operator guidance system.[39]

c) Inclusion Characteristics

To cope with the increasing demand for a high-quality steel, the amount of non-metallic oxide inclusions should be minimum and their composition, morphology, size, and distribution should be monitored during the process. Many traditional techniques directly evaluate inclusions in a two-dimensional section through solidified product samples.[88] In general, the chemistry,

number, size, and morphology of inclusions are not directly measured from heat to heat. Microscopic examinations of different grades of steel leaving the plant are used to evaluate these parameters.[39] Optical Microscopes (OM), rapid scanning electron microscope (SEM), spark emission, ASPEX[93], Electron Microprobes (EMF) and Scanning Electron Microscopes (SEM) with Energy Dispersive Spectrometry (EDS) are used to evaluate the chemical composition of the inclusions in the steel. Total oxygen measurement and nitrogen pick up are indirect methods for inclusion measurement.[39, 88, 94]

d) Metal and Slag Depth

Evaluating the depth of the molten metal and thickness of the slag on the top help in monitoring the chemical composition (oxygen and nitrogen pickup), heat loss and heating characteristics of electric arc heating systems, and ladle eye size.[39, 95]

The common way of slag thickness determination is dipping a steel rod into a ladle and measuring the melted part. This is usually used to determine the slag point of slag-metal interface.[96] Techniques such as radar reflectance, microwave radars, oxygen probes, electromagnetic field disturbance, and non-contact microwave have been developed by different industries/researchers to assess the metal-slag interface and slag thickness.[96-101] Inductive sensors have also been suggested for liquid metal measurement in the beginning of 1980s.[95]

In ladle operations, monitoring the chemistry, temperature, inclusions and bath depths is achieved through the manipulation of melt gas stirring, electrode heating, and the addition of fluxes and reagents.[39]

2.1.4 Ladle Gas Stirring

Stirring is an important part of secondary steelmaking. It is usually performed by gas purging. Electromagnetic stirring is also another method of stirring. Electromagnetic stirring, EMS, is possible by the interaction between the magnetic field from the static induction coil placed outside the ladle furnace and the electrically conducting metal bath.[102]

Argon gas can be injected in the steel ladle either through a deeply inserted refractory lance from the top into the molten steel bath or through a bottom purge-plug. Argon gas introduced via a

bottom purge plug is the more effective method of gas rinsing an argon injection on top of the bath through the top lance.[62, 103] Generally, purging plugs need to be resistant to thermal shock and deformation at working temperatures. These plugs are made of high alumina refractories. There are three types of purging plugs: porous purging plug, slot purging plug, and linear core purging plug.[104]

Figure 2-6 shows the different types of purging plugs. In capillary plugs, gas flows around channels whereas in linear plugs argon flows predominantly straight. Porous plugs are sintered high alumina refractory materials that have controlled porosity to allow for gas flow.[104] In purging plugs durability, permeability, and operational safety are important. Plugs are damaged by penetration of liquid metal into them through the back attack, as well as by peeling at the surface in contact with the melt. The back attack is caused by pressure fluctuations in the gas line due to formation and release of gas bubbles during molten metal stirring.[34]

This image is unable to be reproduced online.

Porous plug Slot/Capillary plug Linear/ Slit plug

Figure 2-6 Kinds of purging plug systems[34]

One purpose of stirring is to make a well-mixed metal. This helps in minimizing the thermal and compositional gradient, which is one crucial step in attaining high-quality steel products.[40]. Depending on the objective of the ladle operation, the volumetric gas flow rate ranges from 0.001 to 0.015 Nm^3/ min/tonne.[38] Other authors have reported the range of volumetric gas flow rate to be from 0.000833 to 0.0167 Nm^3/ min/tonne.[105] Moderate flow rate ranges (15 to 1020 l/min) are also applied to various ladle operations.[106-109]

The nature of the operation does not give easy access to measure and quantify the degree of homogeneity inside ladle furnaces from the beginning to the end of the process. As a result, experts who are well accustomed to the operation tend to observe various features of the process

like injected gas flow rate, top surface dynamics, and bubbling sound to estimate the ladle stirring.[7, 8, 12, 39] Monitoring this process on this basis has its own shortcomings. The degree of mixing inside the bath may not be equivalent to the turbulence on the surface. The low flow rate stirring is also difficult to evaluate visually.[8] In addition, the amount of gas shown on flow meters may not be equal to the actual amount of gas entering the molten metal. This is because of the losses encountered during service in various parts like refractories, pipes and hook-ups and resistance to gas flow developed by porous plugs.[7, 8, 10, 12-16, 39] This emphasizes that the measurement of the actual level of stirring is essential in establishing a control system and thereby enhancing process efficiency.

In recent decades, there have been attempts to search for reliable signals that can be used in automating the stirring process.[17] The melt inside the vessel experiences high turbulence during inert gas bubbling. This dynamic behavior, in turn, forces the ladle wall to vibrate. Moreover, during the stirring process sound can be emitted due to the bubbling of the gas and certain metallurgical activities. Consequently, scholars started to use vibration and sound signals to analyse and predict the stirring power, ladle eye size, and optimum stirring conditions.[7, 15, 17, 39] Hence, a reasonable understanding of these signals is indispensable. The subsequent section introduces some of the concepts of vibration and sound signals.

2.2 Sound and Vibration Signals

2.2.1 Vibration Signals

Vibration is a back-and-forth movement about a specific equilibrium position. This dynamic oscillation is due to a sudden or continuous application of force on a physical object. The nature of oscillations may be random, harmonic or periodic.

Harmonic motion is the fundamental and simplest type of periodic motion expressed by sinusoidal functions. It represents the commonly encountered types of motion in many dynamic systems.[110] The relationship between time and position, of the object is given by Equation 2-5.[20, 22, 110]

$$x = x_o \sin(2\pi f t) \qquad 2\text{-}5$$

where x_0 is the amplitude, and f is the frequency in Hz. The corresponding velocity and acceleration can be found by the first and second derivatives of Equation 2-5 respectively. Figure 2-7 shows a periodic function which represents a repeating pattern.

This image is unable to be reproduced online

Figure 2-7 Harmonic function[20]

Vibration can also be described as free or forced. If the object continues to vibrate after an applied force is removed it is free vibration, otherwise, it is forced.[20, 111] In general, vibratory systems are represented by three basic parameters. These are the spring, mass (or inertia) and damper. Each of them characterizes specific properties of the physical object. The elasticity or the ability to store potential energy of the object is modeled by springs whereas the mass and damper signify the ability to store kinetic energy and the way of losing energy respectively. The loss of energy due to damping is very small but taking it into account is essential for an accurate prediction of system's vibration response.[20, 22] The resistance offered by a fluid such as water, air, or oil when mechanical systems vibrate in a fluid medium is termed viscous damping. Rao explained that the amount of dissipated energy is a function of size and shape of the vibrating body, the viscosity of the fluid, the frequency of vibration, and the velocity of vibrating body.[20] Coulomb or dry friction damping is due to friction between rubbing surfaces that are either dry or have insufficient lubrication.[20, 22]

When a material is deformed, the internal planes slip and the friction between these planes cause energy to be absorbed or dissipated inside the material. This type of damping is known as hysteresis or material damping. For elastic materials, the area of the loop in Figure 2-8 represents the energy loss per unit volume of the body per cycle due to damping.

The internal loss factor, η, is a parameter useful in studying the response of vibrating structures. It consists of various energy loss mechanisms. The two most common are: 1) structural (hysteretic

or viscoelastic) which is dependent on material property and 2) acoustic radiation which represents the loss to fluid medium from the surface.[23] The total internal loss factor or damping mechanism is given in Equation 2-6.

$$\eta_{total} = \eta_s + \eta_{rad} \qquad 2\text{-}6$$

This image is unable to be reproduced online.

Figure 2-8 Hysteresis loop for elastic materials [20]

Here η_s is the loss factor associated with energy dissipation within the structural element itself and η_{rad} is related to the acoustic radiation damping. Acoustic radiation damping is the radiation of a sound wave to the external environment.[112] Figure 2-9 shows the relative and approximate loss factor values of commonly used materials. From this figure, steel and bricks have less loss factors than plastics.

This image is unable to be reproduced online.

Figure 2-9 Loss factor ranges of some common materials [113]

Ladle furnaces are often close to being cylindrical in shape and its approximate cross section is shown in Figure 2-9. 70-80% ladle refractory linings are made of alumina bricks and the shell is made of steel.[3, 114] These materials have loss factors less than that of a plastic as shown in Figure 2-10. The structural loss factor of steel is 0.006 and that of refractory is 0.015.[112] Thus, the material's loss factors need to be considered when ladles are modeled for dynamic analysis.

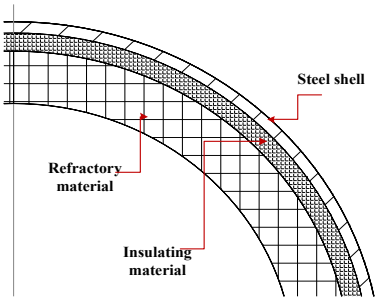

Figure 2-10 ladle wall cross section

2.2.1.1 Forced Vibration with Viscous Damping

Varieties of forces are applied to mechanical systems that result in vibration. The applied forces or displacement excitations can be harmonic, periodic, non-periodic or random in nature. Random excitation is unpredictable with time and must be presented using probability and statistics. If a force, $F(t)$, is applied on a viscously damped spring-mass system shown in Figure 2-11, the equation of motion can be obtained using Newton's Second Law and is given by Equation 2-7.[20]

$$m\ddot{x} + c\dot{x} + kx = F_0 cos\omega t \qquad 2\text{-}7$$

This image is unable to be reproduced online.

Figure 2-11 Single-degree-of-freedom systems with viscous damper.[20]

Where m is the mass or inertia, c is the damping constant, k is spring constant, t is time , F_0 the applied force and ω is the angular frequency. The general solution is the sum of the homogeneous solution, $X_h(t)$, and the particular solution, $X_p(t)$ given by Equation 2-8.

$$X_v = X_h(t) + X_p(t) \quad \text{2-8}$$

The homogenous solution is given in condition of free vibration, which dies out with time.

$$X_p(t) = C_1 e^{\left(-\xi+\sqrt{\xi^2-1}\right)\omega_n t} + C_2 e^{\left(-\xi-\sqrt{\xi^2-1}\right)\omega_n t} \quad \text{2-9}$$

Where ξ is damping factor and ω_n is the natural frequency. The particular solution for a harmonically excited system is given by Equation 2-11.[20]

$$X_p = X\cos(\omega t - \phi) \quad \text{2-10}$$

Where,

$$X = \frac{F_0}{\sqrt{[(k - m\omega^2)^2 + c^2\omega]}} \quad \text{2-11}$$

and

$$\phi = \tan^{-1}\left(\frac{c\omega}{k - m\omega^2}\right)$$

The amplitude ratio ($M = \frac{X}{\delta_{st}}$) and frequency ratio ($r$) are given by Equation 2-12 and 13.

$$r = \frac{\omega}{\omega_n} \quad \text{2-12}$$

$$M = \frac{X}{\delta_{st}} = \frac{1}{\sqrt{(1 - r^2)^2 + (2\xi r)^2}} \quad \text{2-13}$$

where X is the dynamic amplitude and δ_{st} is the static amplitude. In regions of $\approx \omega_n$, the damping ratio has a significant effect on the amplitude and phase values. Figure 2-12 shows the relationship between amplitude and frequency ratios.

This image is unable to be reproduced online.

Figure 2-12 Variation of X and ϕ with frequency ratio.[20]

2.2.1.2 Response to Random Inputs

The pattern of a random signal is not clear or predictable making it difficult to focus on its details. To overcome this, the signals are manipulated in terms of their statistical properties. In this case, a vibration response $x(t)$ is an ensemble of possible time histories resulting from the similar conditions.[21, 22] The mean and root-mean-square values of a random signal are defined and denoted in Equations 2-14 and 2-15.[21, 22]

$$\bar{x} = \lim_{T-\infty} \frac{1}{T} \int_0^T x(t)\, dt \qquad 2\text{-}14$$

$$\overline{x^2} = \lim_{T-\infty} \int_0^T x^2\,(t) dt \qquad 2\text{-}15$$

The autocorrelation, $R_{xx}(\tau)$, gives a measure of how fast the signal $x(t)$ is changing and is computed using Equation 2-16.[21, 22]

$$R_{xx}(\tau) = \lim_{T-\infty} \frac{1}{T} \int_0^T x(t)\, dt \qquad 2\text{-}16$$

The Fourier transform of the autocorrelation function, given in Equation 2-17, defines the power spectral density (PSD) [21]. For a stationary signal, it shows the rate of change of mean square value with frequency:

$$S_{xx} = \frac{1}{2\pi} \int_{-\infty}^{\infty} R_{xx}(\tau) e^{-j\omega\tau}\, d\tau \qquad 2\text{-}17$$

Averaging of several signals is important to diminish the noise of similar frequencies and get the actual signal. The signal to noise ratio for time record averaging is given by Equation 2-18.[23]

$$\frac{S}{n}(dB) = 10\log_{10} n \qquad 2\text{-}18$$

where n is the number of measurements in a sample.

2.2.1.3 Vibration Measurements

Measurement of steelmaking operation quantities is crucial in analyzing processes using physical models or full scales. [35] Vibration, as one measurable physical quantity, can be described in terms of displacement, velocity, or acceleration. The frequency content of these signals may be identical but low frequencies correspond to larger displacements while higher acceleration occurs at higher frequencies. The amplitude-time curves of displacement, velocity, and acceleration show the phases are different.[23]

During the vibration analysis of basic oxygen steelmaking by Bramming et al[115]., when determining a feasible end-point sensor to control basic oxygen steelmaking process by O'Leary[116], and by Burty et al.[13, 15, 16] during ladle vibration analysis, the most practical method of vibration measurement was selected to be an accelerometer.[16, 115] Moreover, accelerometers have been the first choice in measuring absolute motion because of their specific characteristics.[23, 117] Accelerometers have negligible mass and physical dimensions, and wide frequency ranges. The ability to achieve corresponding velocities and displacement from measured acceleration using electronic integrators is also one advantage of accelerometers.[23, 117]

When choosing an accelerometer, there are significant issues related to its performance, to be taken into account before commencing measurements. These are accelerometer-cold model mass, accelerometer mounting, and environmental conditions. The mass of the accelerometer greatly affects the actual vibration level measured especially on a light structure and at high frequencies. This results in a trade-off between frequency range and sensitivity as shown in the Figure 2-13 below [23].

Generally, the mass of the structure (cold model or full scale) should be greater than ten times of the mass of the accelerometer.[118] Inappropriate accelerometer mounting can result in false measurements. Five commonly used mounting techniques are via a threaded stud, cementing the stud, a thin layer of wax, a magnet, and a hand held probe. Among these, the threaded stud and the cement stud give better frequency responses.[23, 118] Figure 2-14 shows the comparison of frequency response curves at various mounting techniques.

This image is unable to be reproduced online.

Figure 2-13 Frequency response characteristics of accelerometers [23]

This image is unable to be reproduced online.

Figure 2-14 Comparison of frequency response curves using different mounting techniques [118]

The proper selection of the accelerometer position is also important in getting repeatable measurements [118]. Working temperature is an environmental factor that can influence the accuracy of the accelerometer. This is due to the piezoelectric material being sensitive to

temperature increases beyond the design limit.[23, 118] Hence, the temperature where the measurement is taking place should be within the permissible range of the transducer. This is particularly important in steelmaking operations where extreme temperature is common.

2.2.1.4 Accelerometer Cross-axis sensitivity

An accelerometer measures the vibration along a certain axis, the primary axis, and this measured value is affected by values in the other axes. This condition is termed cross axis sensitivity of the accelerometer. The maximum transverse sensitivity often does not go beyond 5%.[119] McConnell et al. developed a theoretical model for a three-axis accelerometer cross-axis characteristics from a single axis accelerometer.[119] Figure 2-15 shows the orientation of axis sensitivity, primary sensing axis and cross-axis plane for an accelerometer.[119]

The actual acceleration, a, can be found by multiplying the apparent acceleration, b, by the correction matrix $[C]$ as shown in Equation 2-19.[119]

$$\{a\} = [C]\{b\} \qquad 2\text{-}19$$

The correction matrix, [C], is given approximately in Equation 2-20.

$$[C] = \begin{bmatrix} 1 & -\varepsilon_{xy} & \varepsilon_{xz} \\ -\varepsilon_{yx} & 1 & -\varepsilon_{yz} \\ -\varepsilon_{zx} & -\varepsilon_{zy} & 1 \end{bmatrix} \qquad 2\text{-}20$$

This image is unable to be reproduced online.

Figure 2-15 Orientation of axis sensitivity, primary sensing axis and cross-axis plane for accelerometers [119]

Where ε is cross axis sensitivity coefficient that represent the i^{th} direction acceleration-contribution to the actual axis measured. The true acceleration can be estimated using Equation 2-21.[119]

$$\begin{aligned} a_x &= b_x - \varepsilon_{xy} b_y - \varepsilon_{xz} b_z \\ a_y &= \varepsilon_{yx} b_x + b_y - \varepsilon_{yz} b_z \\ a_z &= \varepsilon_{zx} b_x - \varepsilon_{zy} b_y + b_z \end{aligned} \qquad 2\text{-}21$$

2.3 Sound Signal

A wave in a material medium is a process by means of which a disturbance from equilibrium is transported through the medium carrying energy and momentum in the absence of mass transfer.[120] The longitudinal propagation of vibration as mechanical waves of pressure and displacement in a medium (solid, liquid or gas) with alternative expansion and compression of the medium with defined frequency is referred to as a sound wave.[18, 121] Animals including humans have specific sound perception frequency ranges. The frequency range of sound that can be sensed in a human being is 20Hz to 20kHz.[24]

The characteristics of sound propagation are influenced by density and pressure of the medium. These factors, in turn, are affected by temperature, motion, and viscosity of the medium even though for media like air and water the viscosity effect is insignificant.[121]

2.3.1.1 Sound waves in gas and liquids

In the air, the sound is an adiabatic and nonlinear phenomenon in which the pressure and density are related by Equation 2-22.

$$P = \alpha \rho^{\gamma} \qquad 2\text{-}22$$

where α is a constant and γ is the specific heat ratio of air.[120] For infinitesimal mass M inhabiting a mean volume of V_0 and an infinitesimal change of volume δV and density $\delta\rho$, the acoustic pressure, $\delta p = p - P_0$, is given by Equation 2-23 [120]:

$$\delta p = -(\gamma R \rho_0 T_0)\left(\frac{\delta V}{V}\right) \qquad 2\text{-}23$$

The way sound is created is similar in both gases and liquids and the volumetric strain is the key factor for sound wave existence [120]. However, small fractions of the gas can reside in liquids and

this influences the speed and intensity of sound. In addition, these gas bubbles can relieve the stress produced by volumetric strain and this lowers the bulk modulus but the average density doesn't change significantly.[120]

The speed of sound, c , considering one-dimensional fluid motion is given by Equation 2-24.[113, 120]

$$c = \sqrt{\frac{M_s}{\rho_0}} = \sqrt{\frac{\gamma P}{\rho_0}} \qquad 2\text{-}24$$

Where M_s is adiabatic bulk modulus, P is pressure, γ is specific heat ratio and ρ_0 is density at equilibrium. Fahy explained that the bulk modulus is essentially a function of the type of liquid, hydrostatic pressure and temperature [120]. Similarly, a sound wave in a solid can propagate in either longitudinal or transverse mode and its speed is given by Equation 2-25.[113, 120]

$$c = \sqrt{\frac{E}{\rho}} \qquad 2\text{-}25$$

where ρ and E are the density and elastic modulus of the solid respectively.

For one-dimensional sound propagation, the sound wave disturbances travel by a constant speed c where the air particle oscillates back and forth in the direction of wave propagation (*x-axis*) with a velocity, u. For any plane wave traveling in the positive x-direction at any instant, the relationship in Equation 2-26 can be developed.[113]

$$\frac{p}{u} = \rho c \qquad 2\text{-}26$$

For any plane wave traveling in the opposite (negative x) direction, Equation 2-27 is established.

$$\frac{p}{u} = -\rho c \qquad 2\text{-}27$$

The quantity ρc is known as the characteristic impedance, Z, of the fluid.

Acoustic impedance is important in regulating the transmission of sound and vibration through a system by properly selecting its value for the different components of the system forming the

transmission route. Impedance is also a key factor in the study of the interaction between solid and fluid systems in relation to sound absorption, reflection, and transmission [120]. Impedance heavily depends on frequency and the impedance at specific frequency shows how much sound pressure is generated by a given air vibration at that frequency.[122]

The rate at which the sound wave does work on a surface of unit area in a direction perpendicular to the surface is the sound intensity and for one-dimensional plane wave, the sound intensity, I, is given by Equation 2-28.

$$I = \frac{p^2}{\rho c} \qquad 2\text{-}28$$

The sound power, P transmitted per unit area is given by integrating the intensity over any surface, S, around the source and is given by Equation 2-29.[113]

$$P = \int_S \langle I \rangle dS \qquad 2\text{-}29$$

where $\langle I_n \rangle$ is the time averaged normal component of the intensity. Sound waves can be reflected, refracted or diffracted when traveling in a non-uniform medium or they come across a variable geometrical path. Interference of sound waves can also take place when identical waves meet from the same or different direction.[121]

Since sound pressure magnitudes and sound power experienced by a particle are huge, the logarithmic measures are often applied. The decibel, which represents a relative measurement, is the most common and the result is called level. The sound pressure level is the physical variable used to describe sound strength is given by Equation 2-30.[24, 121]

$$L_p = 10 \log \left(\frac{p_{rms}^2}{p_{ref}^2} \right) \qquad 2\text{-}30$$

where p_{ref} is the reference pressure. The same manipulation is applied for the power and intensity levels.

2.3.2 Sound of Bubbles

When liquid entrains gas bubbles, the volume pulsation of the bubbles imparts high sound pressure to the medium. The volume pulsation is explained by bubble wall oscillation that decays with time due to damping characteristics.[123] Strasberg et al. computed the instantaneous radius, r ,of the bubble using Equation 2-31.[123]

$$r(t,\theta,\varphi) = R_0 + \sum_n r_n S_n(\theta,\varphi)\exp(2\pi i f_n t) \qquad 2\text{-}31$$

Where R_0 is mean bubble radius, S_n is surface harmonics of order n as a function of angles θ and φ, r_n is the oscillation amplitude related to the n^{th} order, and $f_n$is the frequency of oscillation. The magnitude of sound pressure from bubble oscillation due to volume pulsation is given by Equation 2-32.[123]

$$p_0 = 3\gamma P_0(\frac{r_0}{d}) \qquad 2\text{-}32$$

Where d is distance from the centre of the bubble, γ is the ration of specific heats of the gas in the bubble, and P_0 is the static pressure. The sound pressure decreases with distance from the center of the bubble but increases with bubble radius.

When bubbles divide or coalescence, the decaying sinusoidal pulse of sound is released like bubble formation. The excitation of volume pulsation in this regard is because of the difference between the equilibrium pressure inside the single larger bubble and that inside the smaller bubbles. The reduced surface tension pressure on the single larger bubble is the reason for the pressure difference.[25, 123, 124] On coalescence, the size and number of secondary bubbles increased with flow rate and result in an increase of sound amplitude.[25, 124] Larger bubbles rising along somewhat irregular paths can generate continuous low-intensity sound concentrated at the frequency of free volume pulsation. The irregular ascending of the bubble is influenced by the rate of change of pressure fluctuation. This causes pulsation and thereby sound emission.[123]

2.3.3 Bubble Formation

Bubble phenomena such as formation and growth are much-studied topics because of their importance in a wide range of the industrial process.[125-129] Various theories exist on how bubbles are formed.

This image is unable to be reproduced online.

Figure 2-16 bubble formation in a viscous liquid.[130]

Lubetkin [131] reported that bubble generation can be spontaneous or nonspontaneous. In a thermodynamic sense, the former is accompanied by a reduction in the free energy whereas the latter is accompanied by an increase in free energy. According to Lubetkin, bubbles may originate spontaneously from six rather separate and fundamentally independent sources. These six sources are cavitation, homogeneous nucleation, heterogeneous nucleation, Harvey nuclei, electrolysis, and pre-existing stable free bubbles.[131] The formation of bubbles from each source is often followed by bubble growth to a microscopic level.[131] Large bubbles are unstable in a turbulent liquid. They often break up to form a swarm of smaller bubbles.[132] Lubetkin also categorized non-spontaneous bubble formation into attrition, entrainment, and sparging. Sparging refers to the injection of gas bubbles directly into the liquid using a pressurized gas. This is the same phenomenon as "stirring" in the case of secondary steelmaking.[131] Figure 2-16 shows the formation of a bubble at a constant gas flow rate in an orifice of diameter 9.6 10^{-3} m.

Gas bubbles exist in gas-liquid-solid, gas-liquid and gas-solid systems. The process of bubble formation in gas-liquid systems can be static or quasi-static in that it occurs slowly for a system with very small and/or constant gas flow rate conditions.[129, 133] The bubble formation is often

followed by a dynamic process such as bubble break-up, coalescence etc. A simultaneous breakup and coalescence of bubbles in viscous liquids is shown in Figure-17.[134]

The size of the bubbles formed influences the direction of the rise, velocity, overall turbulence and trajectory in the liquid bath, which in turn can affect the performance of the reactor.[129]

This image is unable to be reproduced online.

1 2 3 4 5 6

Figure 2-17 Simultaneous breakups and coalescences [134]

Kulkarni and Joshi reviewed the factors that affect the formation of bubbles. They reported that the operating parameters govern bubble formation. According to these authors, the factors that affect these phenomena are: [129]

- liquid properties such as viscosity, surface tension, liquid density and nature of liquid (polar or non-polar)
- the orifice configuration
- the gas flow rate through the orifice
- mode of operation
- flow/static condition of the liquid

The motion of a bubble in a liquid bath is possible mainly due to drag, viscous, gravity or/and buoyancy forces. A bubble detached from an orifice rises through a liquid due to buoyancy forces. The dynamics related to the rise are large because of bubble characteristics or/and the variation in the system properties with time. This phenomenon is very common in many industrial gas-liquid reactors such as flotation tanks, absorbers, bubble columns, stirred gas-liquid hydrogenation reactors, etc. The rise of a bubble in the liquid is affected by many parameters like the properties of gas-liquid systems (density difference between gas and liquid, viscosity, surface

tension and density), liquid motion (direction), operating conditions (temperature, pressure, gravity), and bubble characteristics (shape and size).[129]

Gas is usually percolated into the steel melt through porous plugs to stir the melt, thereby homogenizing the chemistry, and temperature throughout the liquid steel and promote metal-slag interactions.[125] The injected gas rises vertically through the liquid steel due to buoyancy and lower density of the injected gas. The rate at which the bubbles ascends is a function of bubble size, and the bulk flow (in a "plume") driven by gas flow.[26] As a bubble rises from an orifice and the static pressure decreases, the bubble expands and breakup can take place.[135, 136] Figure 2-18 shows the flow phenomenon observed during gas bubbling. The gas-liquid two-phase region is subdivided into two physically different regions: primary bubble, free bubble, plume, and spout respectively.[137]The bubble sizes, their spatial distributions and rise velocities are not significantly affected by inlet operating conditions.[38]

This image is unable to be reproduced online.

Figure 2-18 Characteristics of the two-phase plumes profile during moderate gas injection in a cylindrical vessel.[137]

2.3.4 Sound Signal Measurements

Measurement of sound is undertaken by transducers known as microphones. Three main types of microphones exist today. These are ceramic, condenser and dynamic microphones. The sensing element in ceramic microphones is a piezoelectric crystal. These microphones have a very high

dynamic range as well as high-frequency response. They are the good choice for research applications where very small microphones are needed. However, care has to be taken in measuring sound pressure for vibrating structures, as they are equally sensitive to mechanical vibrations. Thus, they should be isolated from any vibrating surface.

Dynamic microphones work on the generation of an electrical signal via a moving coil in a magnetic field. They exhibit superior sensitivity characteristics and are relatively unaffected by humidity fluctuations. However, the frequency response is lower than the other types of microphones.[23]

In a condenser microphone, the sensing element is a capacitor in which the pressure difference deflects the diaphragm of the capacitor. Because of their wide frequency range, insensitivity to vibrations and extreme temperatures, they are the most universally used microphones. On the other hand, they are vulnerable to humidity and for small microphones, the sensitivity is lower.[23] Generally, condenser microphones are directly connected to a high input impedance, low output impedance preamplifier with a cable leading to the analyzing/recording instrumentation. The use of a preamplifier is purposely to isolate the device from the processing element and to amplify the transducer signal.[23] In almost all types of microphones, there exists a membrane, which reacts to the pressure or the particle velocity of an impacting sound wave. The dynamics of this membrane is transformed into electric currents or alternating electromotive forces by a linear transducing technique.[138]

2.4 Signal Analysis

2.4.1 Frequency Domain Analysis

Physical phenomena that vary with time are usually described in terms of their amplitude fluctuation with time. These fluctuations are often difficult to anticipate because of their random nature.[139] Figure 2-19 is an illustration where several sample time records are taken at different times. Here, the maximum and minimum values in each of the recordings may vary considerably with time. According to Cohen, the frequency domain is useful in locating the source of the wave and provides an easier understanding of the waveform than in the time domain.[140]

The principles of the Fourier Transform help in transforming time functions of waves to the frequency domain. The Fourier method assumes waves are the sum of sinusoids of unequal frequency and thus the Fourier transform identifies each sinusoid with corresponding amplitude and phase to make a wave as a function of frequency.[141]

This image is unable to be reproduced online.

Figure 2-19 Ensemble of time History records defining random process [142]

In digital computers where signals are analysed, the continuous point wave functions need to be presented by a discrete number of sample points to suit the analysis. The Fourier transform that does this is the Discrete Fourier Transform (DFT).[143-145]

The main parameters that can affect the quality of the resulting data from FFT are the resolution, the number of averages, the maximum frequency, the type of window and the percent overlap. Here, the main objective is to optimize the data quality by making appropriate selections for the values of the parameters.[146] FFT resolution represents the number of lines of information that appear on the FFT plot as shown in Figure 2-20. Each line will contain a range of frequencies, and the resolution of each line can be calculated simply by dividing the overall frequency (f_{max}) by the number of lines. The maximum frequency, f_{max}, is the highest frequency recorded by an instrument. The waveform recorded by an instrument should be sampled at least twice the maximum frequency to avoid aliasing according to the Nyquist Theorem. This helps in generating the true waveform. Aliasing is the phenomena where a high frequency component

appears as if it is a lower frequency due to the selection of a low sampling frequency. The total sample time for getting valid FFT data can be manipulated from the maximum frequency and lines of resolution by the formula given in Equation 2-33 and 2-34.[141, 146]

This image is unable to be reproduced online.

Figure 2-20 FFT Resolutions[146]

$$T_{obs} = \frac{\#lines}{f_{max}} \quad \text{2-33}$$

or

$$T_{obs} = N_{sample} \quad \text{2-34}$$

where, f_{max} is highest analysed frequency (Hz.), #lines is total number of lines of FFT resolution, N is sample number collected and T(sample) is sample period (in seconds.). The above terms are illustrated in the Figure 2-20 and 2-21. The application of FFT to manipulate Fourier transform requires the careful choice of values of N and T.[141]

This image is unable to be reproduced online.

Figure 2-21 Sampling and observation time [146]

To improve the spectral resolution, the sample signal is multiplied by a time function, a window, before performing FFT. This is termed as windowing. A window is a mathematical function that is zero-valued outside of some chosen interval. Windowing may result in a good frequency resolution but the amplitude may be of weak resolution i.e. both cannot be achieved the same time. Hence, there are different window functions each having their own strength and weakness in achieving the specific resolution. In addition, windowing can help in minimizing leakage, which occurs when FFT algorithms are performed at sample discontinuities.[38, 141, 147]

Several windowing functions are available. Hamming, Kaiser-Bessel, Flat-Top, Hanning, Rectangular (actually no window), are some window types.[38, 147] The most frequently used window is Hanning (raised cosine). In sine waves, it gives a better trade-off between amplitude and frequency resolution. It is a discrete window function given by Equation 2-35.[147]

$$\omega(n) = 0.5\left[1 - \cos(\frac{2\pi n}{N})\right] \quad 2\text{-}35$$

where $n = 0, 1, 2, 3, \dots, N-1$. As it can be seen in Figure 2-22 the Hanning Window creates an improved signal than the rectangular one. The Rectangular Window has a better trade–off between amplitude and frequency when sampled signal is periodic and the window fits exactly at the initial and final points. The Hamming window gives better frequency resolution at the expense of the amplitude. Its time window function is given by Equation 2-36.[147]

$$\omega(n) = 0.54 - 0.46\left[\cos(\frac{2\pi n}{N})\right] \quad 2\text{-}36$$

where $n = 0, 1, 2, 3, \dots, N-1$.

The flattop is useful in providing very accurate amplitude and its time function is given by Equation 2-37.[146, 147]

$$\omega(n) = a_0 - \left[a_1 \cos\left(\frac{2\pi n}{N}\right) + a_2 cos\left(\frac{4\pi n}{N}\right)\right] \quad 2\text{-}37$$

Where $a_0 = 0.281, a_1 = 0.521, a_2 = 0.198$.

This image is unable to be reproduced online.

Figure 2-22 Hanning window sampling [146]

The typical signal path from measurement to storage is shown in the Figure 2-23 where the A/D converter represents the analogue to digital conversion. The A/D converter accomplishes the digitalization of analogue signals by sampling the applied analogue input signal and quantizing it to its digital representation.[148, 149] Mostly the A/D converter is specified by its amplitude resolution. Computer processing circuits work with binary numbers as 8-bit, 12-bit, 16-bit, etc. For example, an A/D converter specified with 8-bit resolution offers 256 intervals (or quantization levels) on an amplitude scale.[146] As the resolution increases, the dynamic range improves. After signals are processed as shown in Figure 2-23, they can be stored for further analysis such as with statistical techniques.

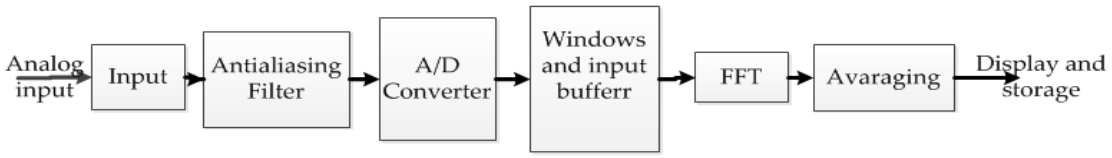

Figure 2-23 Signal processing path[146]

2.4.1.1 Statistical Errors Associated with Signal Analysis

An infinite ensemble or a single data record of infinite time is difficult to analyse. During signal treatment, various errors may arise. Generally, in any signal, errors exist which can be random errors that come from statistical sampling or bias errors, which appear during data acquisition. Bias errors are systematic and occur in the same direction [23]. Errors that are created in the digital signal analysis are aliasing and leakage. Aliasing is due to an inappropriate sampling interval and leakage is the result of window selection.[23]

Random and Bias Errors:

In signal analysis, there is a trade-off between analysis time and bandwidth [23]. A filter with a bandwidth of B Hz takes roughly 1/B seconds to respond to a signal that is applied to its input [23, 150, 151]. The relationship is as shown in Equation 2-38.

$$BT \geq 1 \qquad 2\text{-}38$$

where B is resolution bandwidth in the case of digital signal analysis and a filter bandwidth of measurement for analogue signal analysis and T is the duration of the measurement. While averaging the data of a number of measurements, it is essential to make sure the correlation BT $\geq$1 is fulfilled and several periods of the lowest frequency of interest are incorporated [23]. For a measurement acquired by an analogue spectrum analyser, the normalized random error is formulated by Equation 2-39.[23]

$$\varepsilon_r = \frac{\sigma}{m} \approx \frac{1}{(BT)^{0.5}} \qquad 2\text{-}39$$

where σ is the standard deviation and m is the mean value. Therefore, $BT \geq 1$ for small standard deviations. Equation 2-39 reveals two preconditions that oppose each other: compared to 1/T, B has to be large for better statistical reliability whereas, for good resolution, B has to be small.[23]

The smallest obtainable frequency resolution bandwidth, for a time record, T, digitized in a sequence of N equally spaced sampled values is expressed by Equation 2-40.[23]

$$\Delta f = \frac{1}{T} \qquad 2\text{-}40$$

It is clear from this that individual time record length, T, not the total amount of data ($T_t = nT$), is taken to determine resolution bandwidth [23]. Nevertheless, the normalized random error is dependent on the overall volume of digitized data, T_t and is given by Equation 2-41.[23]

$$\varepsilon_b = \frac{\sigma}{m} \approx \frac{1}{(B_e T_t)^{0.5}} \qquad 2\text{-}41$$

where B_e is resolution bandwidth for digital signal analysis. The normalized random error relationships given above are applicable to auto-spectral measurements.[23]

Unlike the random error, the normalized bias error is a function of resolution bandwidth, B_e and half-power bandwidth, $B_r \approx 2\xi f_d$, of the system frequency response function, where f_d is the damped natural frequency and ξ is damping ration. The normalized bias error is approximately given by Equation 2-42.[23]

$$\varepsilon_r = -\frac{1}{3}\left(\frac{B_e}{B_r}\right)^2 \qquad 2\text{-}42$$

The normalized bias error is applicable to both digital and analogue signals, and auto and cross-spectral density measurements. Bias error appears at resonance frequencies in spectral approximations and has the influence in limiting the dynamic range of an analysis thereby underrating spectral peaks and overestimating spectral troughs[23]. The normalized RMS error for both analogue and digital signals can be expressed by Equation 2-43.

$$\varepsilon = (\varepsilon_r^2 + \varepsilon_b^2)^{0.5} \qquad 2\text{-}43$$

Aliasing and leakage are avoided by choosing an appropriate sample interval and selecting suitable window type. Normalized random errors can be minimized by boosting the number of samples. Since bias errors occur at resonance frequencies, this error can be taken as negligible if signals are taken below the resonance.[23]

2.5 Vibration Analysis Techniques

Vibration data are frequently captured in the form of continuous electrical (analogue) signals generated by transducers, where each analogue signal portrays the instantaneous value of motion (displacement, velocity or acceleration) as a function of time. The Fourier transform of this time history data is known as frequency domain. Thus, techniques used to analyse vibration data can be grouped into two main categories: the time and frequency domain analysis.[110, 151] The most fundamental descriptions of a stationary vibration with a time history $x(t)$ are given by overall values of mean μ_x, the mean-square ψ_x^2, and/or the variance σ_x^2 .[151] These values are defined in Equation 2-44, 2-45 and 2-46 respectively.

$$\mu_x = \lim_{T\to\infty} \frac{1}{T}\int_0^T x(t)\,dt \qquad 2\text{-}44$$

$$\psi_x^2 = \lim_{T\to\infty} \frac{1}{T}\int_0^T x^2(t)\,dt \qquad 2\text{-}45$$

$$\sigma_x^2 = \lim_{T\to\infty} \frac{1}{T}\int_0^T [x(t)-\mu_x]^2\,dt \qquad 2\text{-}46$$

The mean value describes the central tendency (a static value) of the vibration, while the standard deviation defines the dispersion of the vibration. The root means square (RMS) value is a measure of both the central tendency and dispersion. The (RMS) value of a vibration signal provides the information about the power content of the signal in time domain. Other time domain approaches include kurtosis and crest factor. Kurtosis is used as an indicator of major peaks in a set of data and crest factor is used to detect changes in the signal pattern.[152] An increase in overall RMS level may indicate that something has changed internally but not give any information to the cause. These causes can be picked up by spectrum monitoring or frequency domain analysis. Frequency domain analysis is the most common technique performed on signals.[117] This technique is briefly discussed in section 2.4.

Vibration analysis has been widely used as the main diagnostic tool for most mechanical systems. Vibration analysis has also been used to investigate metallurgical operations.[10, 13, 15, 16, 153-155] Measurement and analysis of vibration in three axes have been also applied in steelmaking operations. The three signals in x-, y- and z- have been combined successfully using the multivariate statistical technique to analyse the process.[156] In gas stirred ladles, vibration signals are combined using certain multivariate techniques, which are described in the subsequent section.

2.5.1 Multivariate Statistical Analysis

Multivariate statistical analysis, unlike univariate, involves observation and analysis of more than one independent /outcome variable in a multivariate system. Regression analysis, canonical correlation, multiple modeling, cluster analysis, discrimination function analysis, factor analysis, principal component analysis (PCA), and Multi-Dimensional Scaling are some of the multivariate statistical techniques. Most of these techniques are applied to reduce the number of dimensions to establish a hypothesis.[27]. Multivariate techniques can be applied to data analysis, monitoring and control while multivariate statistical techniques can be used to establish nonparametric

models for process monitoring.[157, 158] Multiple regression, canonical correlation, and structural modeling try to investigate relationships among two or more variables and this relationship is used for the prediction of dependent variables. Cluster analysis is applied to a group of population or sample based on specific characteristics. The two common techniques that deal with internal data structure are factor analysis and principal component analysis. They are both variable reduction methods but they have basic differences. Principal components account for a maximal variance but factor analysis accounts for a common variance in the data.[159] There are various techniques, which can be regarded as PCA extensions. Complex Principal Component Analysis (CPC), Nonlinear Principal Component Analysis (NLPCA), Probabilistic Principal Component Analysis, and Sparse Principal Component Analysis (SPCA). The above-mentioned techniques are described in the literature.[18, 30, 154, 158, 160-172]

In steelmaking, after the melt is transferred from electric arc furnace and basic oxygen furnace to ladle furnaces, inert gas (usually argon) is injected to agitate the metal. During the stirring process, there is bubbling acoustic emission, ladle wall vibration and disturbance of the top surface initiated by the inert gas flow. These phenomena can be taken as multivariate signals to analyse the mixing process inside the ladle.[18] Thus, the application of multivariate techniques like multivariate statistical techniques, fuzzy logic, and neural networks is advantageous.[18] An artificial neural network (ANN) is a mathematically adjustable structure important in uncovering complex nonlinear relationships between inputs and outputs especially for processes that are not easy to be described by physical equations.[173] Fuzzy logic control is an attempt to simulate human thinking and natural language through computers. It uses expert knowledge to transform linguistic control techniques to automate one. As ANN offers many advantages, it may also have some limitations. It may have greater computational burden, "black box" nature, and proneness to overfitting.[174] The application of artificial neural networks and fuzzy logic for online ladle stirring process based on vibroacoustic technology may not be easy due to limited vibration and acoustic data.[18] The small amount of data on inert gas losses may not be sufficient to exactly know the trend of the losses.[18] In addition, the application and success story of artificial neural networks and fuzzy logic in the industry is very limited.[18, 175]

Several researchers engaged in ladle stirring process online control used single axis vibration signals to analyse the mixing strength.[8, 10, 12-16, 18] Due to the random nature of the signal, its statistical properties like the RMS value have been used to estimate the degree of agitation inside

the ladle. Recently Xu et al. introduced a multivariate statistical technique to analyse the signals related to the process. They used principal component analysis (PCA) to combine sound, one-dimensional vibration and ladle eye area as one signal to monitor the process online.[18]

The current study deals with three-axis vibration and bubbling sound measurement from cold models and full-scale industrial ladles to investigate the actual stirring power. In the literature, triaxial vibration has been described as crucial signals but the technique to analyse them is not well established. Triaxial vibration data can be either analysed taking each axis individually or combining the three axes using mathematical techniques.[176] Irem and Edward applied principal component analysis (or PCA) on their triaxial data to combine the three axes of measurement in into one "principal component" with the highest variance.[156, 176] It demonstrated the potential value of using triaxial vibration measurements in conjunction with a PCA-based methodology to regulate the vibrational behavior during helicopter flight.[156, 176] Other studies that used PCA have also shown its effectiveness.[157, 158] Liu et al. used PCA model to design a control system on a multivariable and nonlinear maize production process.[157] Luis and his co-researcher tried to include an adjustable gain and tuning rules for processes using PCA as a control method.[158] The output from PCA is also suitable to use for further multivariate statistical techniques.[177]

2.5.1.1 Principal Component Analysis

Principal component analysis (PCA) is a statistical procedure that was developed by Pearson I in 1901.[157] Due to its simplicity and non-parametric technique for collecting important information from most intricate data, PCA has emerged as a standard tool in modern data analysis.[28] The main goals of PCA are to extract essential information, simplify the representation and investigate the structure of the dataset.[178] It applies an orthogonal transformation to achieve linearly uncorrelated variables from sets of observations of possibly correlated ones. The new set of variables is called principal components (PC). Principal components are uncorrelated to each other and are sorted such that the k^{th} PC has the biggest variance of the remaining. The k^{th} PC is orthogonal to the $k^{th} - 1$ PCs i.e. it is the direction of largest variation. Figure 2-24 shows the orthogonality of the first three PCs. The notion is to take the first few PCs as they catch most of the variation in the original dataset. [179] However, during the analysis important and very powerful assumptions are made. These are linearity, orthogonality of principal components and the assumption that a large variance indicates useful structures.[28]

This image is unable to be reproduced online.

Figure 2-24 Orthogonality of the first three PCs of a data set [179]

Mathematically if '$\boldsymbol{X}$' is the original dataset matrix and '$\boldsymbol{Y}$' is the new transformed matrix of the original dataset, then the goal of PCA is to find orthonormal matrix $\boldsymbol{G}$ in Equation 2-47.

$$\boldsymbol{Y} = \boldsymbol{G}\boldsymbol{X} \tag{2-47}$$

The rows of *P* are the principal components of $\boldsymbol{X}$.[28]

PCA comprises of several steps.[29] Let $\boldsymbol{X_0}$ be the original data matrix where its rows and columns correspond to process variables(n) and set of measurements(m) respectively, the first step is to scale or make it mean centred. Then the new $m \times n$ matrix, $\boldsymbol{X}$, is defined by Equation 2-48.

$$\mathbf{X} = \begin{bmatrix} x_{11} & x_{12}. & \dots & x_{1n} \\ x_{12} & . & . & x_{2n} \\ \dots & . & . & \dots \\ x_{m1} & x_{m2} & .. & x_{mn} \end{bmatrix} \tag{2-481}$$

The covariance matrix is of $\boldsymbol{X}$ then defined by Equation 2-49.

$$\boldsymbol{S_x} = \frac{1}{n-1}\boldsymbol{X}\boldsymbol{X}^T \tag{2-49}$$

$\boldsymbol{S}$ is a square symmetric $m \times m$ matrix and its diagonals are the variances of the process variables. By assumption, the diagonal large values correspond to interesting dynamics. The algebraic solution of PCA lies in the fundamental property of eigenvector decomposition. PCA computes

the orthogonal vectors (loading vectors) in order of variance defined by direction of loading vectors.[157] Singular value decomposition can be applied in manipulating the orthogonal vectors from the covariance; this is shown in Equation 2-50.

$$\boldsymbol{S_x} = \frac{1}{n-1}\boldsymbol{XX^T} = \boldsymbol{E\Lambda E^T} \qquad 2\text{-}50$$

where $\boldsymbol{\Lambda}$ is a diagonal $m \times m$ matrix. Here, the diagonal matrix $\boldsymbol{\Lambda} = \boldsymbol{V^T V}$ comprises non-negative real singular values with magnitude in a decreasing order. This is represented by Equation 2-51.

$$\lambda_1 \geq \lambda_2 \geq \lambda_3 \ldots \lambda_m \geq 0 \qquad 2\text{-}51$$

To effectively obtain the variation of the dataset, the loading vector corresponding to the largest 'k' singular values are kept in PCA. 'k' is the number of principal components that grasp most of essential information. The proportion of variation explained by the first k^{th} principal components, r_k , is given by Equation 2-52.

$$r_k = \frac{\lambda_k}{\sum_{1 \to k} \lambda} \qquad 2\text{-}52$$

The final step in PCA is driving the new dataset, $\boldsymbol{Y}$, by multiplying the original dataset, $\boldsymbol{X}$, by a diagonal matrix of principal components, as follows by Equation 2-53.

$$\boldsymbol{Y} = \boldsymbol{GX} \qquad 2\text{-}53$$

PCA deals with one set of the matrix only. To deal with two sets of the matrix, which are input and output, partial least square method becomes important in computing the latent variables on both sides simultaneously in a way to maximize the covariance between input and output. In ladle metallurgy, PCA has been used by Xu et al. and Graham et al. in their research to examine its importance in online process control.[7, 83]

2.5.1.2 Partial Least Square Method (PLS)

One of the most frequently encountered data-analytical challenges in science and technology is modeling responses using independent variables.[172] The traditional technique used to find a linear combination of the independent variables to predict the dependent variable is multiple linear regression analysis (MLR). However, MLR has its own limitations that influence the power

of prediction. MLR fails to handle a dataset that consists any two linearly dependent columns i.e. a matrix that is not full column rank.[172, 180, 181] In MLR, independent variables are assumed to be error free which indicates the ability to handle noisy data is poor. In addition, it may be difficult to analyse heterogeneous data using MLR.[172]

The partial least-squares regression method (PLS) is widely used in many areas of chemistry in this regard. This method was originally used in the field of econometrics in the 1960s by Herman Wold.[169, 171] It gives few latent variables (LV) that pick up the majority of the information in the independent variables. This LVs are important to predict the dependent variable.[180] As the PLS model deals with variation in input as well as output space simultaneously, nowadays it is becoming of great interest in industrial process control.[31, 172] PLS regression is essentially useful when a set of dependent variables are required to be predicted from a significant number of independent variables known as predictors.[169] This multivariate statistical technique has the ability to handle data that is noisy, collinear and data with incomplete variables in both dependent and independent sets. Another outstanding characteristic of PLS is that the accuracy of its model parameters can be enhanced by increasing the number of relevant observations and variables.[172] Hence, it can be regarded as a generalization of multiple linear regression.

PLS regression (which also means projection to latent structure) tries to find a common structure between dependent variables and predictors by undertaking simultaneous decomposition to compute latent vectors which explain maximum covariance between dependent and predictor variables.[169] In other words, it uses a two-block predictive PLS model to describe the correlation between the two blocks of matrices.

A simplified clarification of PLS is given by Figure 2-25. There are five input variables X_1, X_2, X_3, X_4 and X_5 and one output variable y_1. If the change in X_2 and X_5 also affects the product quality y_1 at same time period, the variation in y_2 is probably related to variation in X_2 and X_5. In this scenario, the first latent variable t_1 is a weighted average of X_2 and X_5 whose circumstances best describes y_1.[31]

This image is unable to be reproduced online.

Figure 2-25 Schematic representation of PLS[31]

The algorithm used to compute the PLS model can vary depending on the pattern/distribution of the data such as skewness, symmetry, uniformity, and number of peaks.[30, 172, 182-184] The two common PLS algorithms discussed in the successive sections are the standard PLS termed as NIPALS (Nonlinear Iterative Partial Least Square) and SIMPLS PLS.

2.5.1.3 Nonlinear Iterative Partial Least Square (NIPALS)

Nonlinear Iterative Partial Least Square (NIPALS) algorithm was first introduced by Wold et al.[170] It has been discussed in detail elsewhere.[171, 172, 185-187] The model parameters are computed by the following three main phases.[171, 188] The first phase is termed the outer relation and is the decomposition of the predictor, $\boldsymbol{X}$, and response, $\boldsymbol{Y}$, in to their scores and loadings as shown in Equation 2-54 to 2-56.

$$\mathbf{X} = \mathbf{TP}' + \mathbf{E}_r \quad \text{2-54}$$

$$\mathbf{Y} = \mathbf{UC}' + \mathbf{F}_r \quad \text{2-55}$$

$$\boldsymbol{Y} = \boldsymbol{XCWT} \quad \text{2-56}$$

$$\boldsymbol{Y} = \boldsymbol{\beta X} + \boldsymbol{Y_{res}} \quad \text{2-57}$$

The residual matrices, E_r and F_r, are worked to be minimum. The final PLS model is given by Equation 2-57. $\boldsymbol{T}$, $\boldsymbol{P}$, $\boldsymbol{U}$, $\boldsymbol{C}$, $\boldsymbol{W}$, $\boldsymbol{\beta}$, and $\boldsymbol{Y_{res}}$ are x −score, x −loadings, y −scores, y −weights , x −weights, regression coefficient and residual matrices respectively.[31, 172, 180, 181, 188]In the second phase which results in an improved predictive capacity of the model, scores of both datasets are manipulated to provide rotated components of $\boldsymbol{X}$ and $\boldsymbol{Y}$ blocks. As a result, the model parameters

such as regression coefficient are computed in this step. The third step is to use the determined parameters to build the final prediction model.[181, 188]

The PLS regression model is established from a training set of N observation with K $X-$ independent variables denoted by $x_k(k = 1, \dots, K)$ and M $Y-$dependent variables y_m $(m = 1, \dots, M)$. Transformations on both input and output variables are done in order that their distributions be reasonably symmetrical. Logarithmic transformation is one way to transform data. To make analysis result easier to understand and visualize, $\boldsymbol{X}$ and $\boldsymbol{Y}$ variables usually scaled and centered before analysis. Scaling is achieved by dividing each variable by the standard deviation to a unit variance and centering is computed by subtracting the average from each variable.

In the PLS model, information regarding similarities /differences of variables is explained by the scores $\boldsymbol{T}$ and $\boldsymbol{U}$ in the given model. The weights $\boldsymbol{W}$ and $\boldsymbol{C}$ provide information on how the variables come together to build the quantitative relationship between Y and X. In other words, the relative importance of each $\mathbf{X}-$variable is given by the weights $\boldsymbol{W}$. Residuals are part of the data that are not included in the model. Small $\boldsymbol{Y}$-residuals are the evidence for a good fit in the model while large residual are a sign of weak prediction power. Outliers are data that does not fit in the model. Residual of $\boldsymbol{X}$ and $\boldsymbol{Y}$ data are used to identify these outliers.

2.5.1.4 SIMPLS-PLS

The algorithm proposed by de Jong, SIMPLS, computes the PLS parameters directly as a linear combination of the original variables. It is easy to interpret because it does not apply a breakdown of the dataset. It meets normalization and orthogonality constraints and computes PLS parameters to maximize the covariance criterion.[7]

The name "SIMPLS" is given to this method because it applies a straightforward statistical concept used to modify the standard PLS. The intention of this alternative PLS approach is to develop a predictive linear model $\widehat{\boldsymbol{Y}} = \boldsymbol{XB}$ like NIPALS-PLS. The PLS factor T is directly computed as a linear combination of the original centered X- variables. Compared to NIPALS, this approach has several advantages. Firstly, datasets $\boldsymbol{X}$ and/or $\boldsymbol{Y}$ need not be deflated which as a result improves the analysis speed and memory requirements. Secondly, the interpretation of the analysis outcome is relatively easy. The derivation of the PLS regression model is also easier as the factors are represented as a linear combination of the original variables.

The generalised procedure according to SIMPLS algorithm for PLS is summarized by de Jong as Table 2-1.[30]

Table 2-1 Summary of SIMPLS algorithm

N	Procedure	Remark
1.	Compute the cross product	$\boldsymbol{S = X'_0 Y_0}$
2.	Compute singular value decomposition (SVD) of S	for a=1 (a is number of output variables)
3.	Compute SVD of $S - P(P'P)^{-1}P'S$	for a>1
4	Get weights r = first singular vector	
5.	Compute scores	$\boldsymbol{t = X_0 r}$
6.	Compute loadings	$\boldsymbol{P = \frac{X'_0 t}{(t't)}}$
7.	Compute regression coefficient, B_{PLS}	$\boldsymbol{B_{PLS} = RT^{-}Y_0}$

In both NIPALS and SIMPLS, the covariance criterion is maximized and orthogonality of the successive scores is met. However, the final results are identical only when the number of $\boldsymbol{Y}$-variables is one.[30]

Yenus et al. applied PLS techniques to find the correlation between process parameters and vibration in a cold model investigation of ladle stirring.[154] It was also applied in this research to analyse the cold model and plant data. Other studies that used vibration, sound or image signal by applying different analysis methods to automate the stirring process are reviewed in the next section.

2.6 Ladle Vibration

The improvement of steel product quality in ladle metallurgy depends on the ability to achieve high thermal and compositional homogeneity, slag metal interactions and inclusion removal rate through pressurized inert gas stirring of the ladle furnace. The gas is usually argon and purged through porous plugs placed at the bottom of the vessel.[39] However, in reality, having direct and persistent control over temperature and composition is difficult due to the harsh operating conditions. Hence, the usual practice is to monitor the stirring process manually by giving more

attention to the sound imparted, observing the uppermost surface turbulence and magnitude of the gas flow in the gauges.[7, 8, 12, 39] Nevertheless, this approach has its own limitations. Firstly, the degree of mixing inside may be different even though the disturbance on the upper surface is similar. Secondly, at low flow rates, the visual control of weak stirring is difficult and complex.[8] Thirdly and most importantly, the indicated flow quantity may not be equal to the flow entering the ladle because of high resistance to gas flow by porous plugs and leaks developed during use in connections between pipes, hook ups, and refractories. Consequently, the resulting level of intensity may not be identical to that shown by the flow meters.[7, 39]

Various researchers from both the academic and industrial communities have studied to use the vibration and sound signals imparted from the ladle furnace to control the steelmaking processes. The bubbling of inert gas causes molten steel turbulence and this, in turn, forces the ladle wall to vibrate.[17] Hence, measuring the wall vibration and bubbling sound and analyzing them may be helpful in understanding the status of the stirring process.[7, 15, 17, 39] Furthermore, ladle eye area has also been studied using laboratory- and full-scale models in combination with other signals to describe the situation.[7] Vibration of the wall is the most frequently used signal to describe the stirring intensity.[10, 12, 14-16, 19] Hydrophones, accelerometers, video cameras and signal processing instruments have been used to measure and process the signals.[7, 10, 12, 14-16, 18]

Mucciardi[19] used an accelerometer to measure ladle vibration due to stirring to correlate the mixing power and vibration signal. He reported that the degree of agitation in the metal bath is proportional to a representative value of the accelerometer signal raised to the power of 1.6. This investigation also showed that an accelerometer is a viable transducer for controlling the interaction between liquids and gases when direct contact with the liquid phase is not practical.

Minion et al.[10] stated that there were no direct means of stir indication at lower flow rates during reheating and proposed a method, which utilizes the vibration signal to control the process.[10, 12] They took plant measurements and analysed it using the Fast Fourier Transform. They found that the vibration amplitude increases as the argon flow rate increases and the energetic frequency range are 50 to 70 Hz. Figure 2-26 shows the increase of RMS with an increase of bubbling rate. The peak frequency remains constant. They developed a control system based on continuous FFT analysis and a Programmable Logic Controller.[10] However, this control system had limited application at low flow rates and could not succeed commercially.[12]

This image is unable to be reproduced online.

Figure 2-26 RMS values and peak frequencies as function of gas flow rate[10]

Kemeny et al.[12, 189] have measured the stirring energy using vibration signals to control the amount of flow of gas to the desired level. The measurement of the vibration was performed by an accelerometer attached radially on the wall of the ladle. They showed that the energetic frequency ranges are from 30 to 50 Hz and 70 to 90 Hz. According to Kemeny, since the frequency range, 70 to 90 Hz did not contain noise; their control system was devised in this range of frequency.[12] Kemeny and his co-researchers have not described in the open literature the effect of slag thickness, molten steel level on vibration signal. Vibration based control system (TruStir) developed by Nupro Corporation was implemented in various steel plants such as Hadeed[190] and Dongbu[191]. It was reported that the monitoring system improved steel cleanliness and reduced argon consumption.[190]

Burty and his co-researchers carried out a relatively comprehensive investigation on lab-scale water models, pilot scales and industrial ladles ranging from 90 to 300 tonne.[15, 16]. Measurements of vibration signals from all scales and liquid pressure fluctuation from the cold water were made using accelerometers and hydrophones respectively.[15, 16] The root means square value was used

to indicate the stirring energy. According to this research, the vibration and pressure fluctuation increases in a logarithmic way with flow rate. In addition, the slag layer between 0.1 to 0.4m thick has no significant influence on the ladle vibration.[16] For the 90-tonne ladle, the finding is that the energetic frequency range is between 20 and 200 Hz and the open eye appears when the flow rate is higher than 150 to 200 l/min and the vibration index is over 0.025 m/s^2 per tonne [16]. According to the work of Burty et al., the optimum rinsing flow rate for the 90-tonne ladle was found to be 100 l/min.

Furthermore, they developed a relationship between the Froude number and vibration index (in m/s^2) which is valid in the region between bubbling and coalescence.[13, 15, 16] Figure 2-27 is drawn from Equation 2-58 for water and full-scale models. The figure shows a linear relationship between the vibration and Froude number. The values of A and B are given as 0.2939 and -0.4265 respectively.[15]

This image is unable to be reproduced online.

Figure 2-27 Increase of ladle vibration with the Froude number – Water scale models, pilot scale steel ladles, industrial plant data and numerical simulation.[15]

They reported that the open eye area increases with flow rate and the trend were affected by the presence of thick slag in the range of 0.15 to 0.28 m. This finding conflicts with their result that the slag depth in the range of 0.1 to 0.4 m does not affect the vibration value. In addition, the recommended flow rate of 1.67×10^{-3} m^3/s for inclusion removal is not clear as to whether it applies

to all ladle size. The research work by same authors published in 2011 claims that the quantity and rheology of slag do not affect the vibration signal.[13]

A cold model-based experimental investigation was performed by Xu et al. to study ladle stirring.[7] This study used water and oil to simulate the molten steel and upper layer respectively. The aim of this investigation was primarily to show that the stirring control system can rely on a single signal which is a combination of vibration, sound and ladle eye area.

$$k = A \log \frac{Q^2}{g^{0.5} D^{2.5}} + B \qquad 2\text{-}58$$

This image is unable to be reproduced online.

Figure 2-28 Relationship between stirring power and PC1.[7, 18]

Principal component analysis (PCA) was the main tool applied to reduce the number of variables. Based on this work, the sound and vibration signals can pick up most of the variation in the system. Figure 2-28 shows that removing the image signal does not destroy the relationship between the combined signal and the stirring power. They also showed that the vibration amplitude increases with volume and flow rate. The dominant frequencies discovered by these authors were in the range of 1 to 120 Hz for vibration and 100 to 1500 Hz for sound signals. The sound intensity increases with flow rate but does not vary much when the upper layer is thicker than 0.015 m. The main limitation of this study is that it does not address the low flow rate-stirring phenomenon where there is no open eye. Moreover, the overall results of this analysis are not verified using industrial data of the corresponding vessel and experimental conditions.

Further research was carried out by Yuriy et al. on the vibration of a ladle furnace using cold models. They used flasks of 1000, 2000 and 2400 ml, and 2000 ml of water mixed with 400 ml of

alcohol.[8] They placed the sensor near the base of the flask.[8, 14] Their finding was similar in that the RMS value increases with an increase of flow rate and the energetic frequency range lies in the range of 0 to 200 Hz. They reported that the maximum correlation of flow rate and vibration amplitude is exhibited in the range of 0 to 40 Hz. According to these authors, the number of blowing units does not affect the vibration signal. In addition, they found that as the volume of water increases, the RMS value increases as shown in Figures 2-29 and 2-30.[8, 14] With regard to surface tension, at low flow rates there is a significant influence on vibration amplitude i.e. with a decrease of surface tension, the RMS value reduces.[8, 14] They also established a relationship between the RMS value and flow rate, Q, based on their laboratory experiment shown in Equation 2-59.[8, 14]

This image is unable to be reproduced online.

Figure 2-29 RMS value of the detected vibration signal as a function of the gas flow rate for a 160-tonne ladle furnace.[8]

$$V_{RMS} = kQ^{0.285} \quad \text{2-59}$$

where k is fluid height coefficient. Figure 2-30 illustrates the gas flow rate, the RMS value, and the effect surface tension. Even though, some of their results seem to agree with previous works, there are some issues not well addressed in their work. First, it is not clear whether the flasks tubes/cold models and flow rates were based on geometric, kinematic or dynamic similarities with the plant ladle furnaces. Secondly, the effect of upper layer was not studied. The argument behind their sensor's position near the bottom of the tube was not explained. In addition, the issue of low flow rate stirring detection has not been well addressed.

This image is unable to be reproduced online.

Figure 2-30 RMS value of the vibro-signal on the gas flow rate under various blowing conditions.[8, 14]

The research on ladle vibration to monitor stirring was also undertaken by Pylvänäinen et al.[192] and Fabritius et al.[193] Pylvänäinen et al.[192] pointed out that the results of their investigation supports the use of vibration measurements to effectively monitor gas stirring intensity online.

In the present study, the low flow rate-stirring problem in gas stirred ladles has been addressed by measuring the real-time vibration of the ladle wall and the sound generated due to the liquid metal bath bubbling. The following Chapter describes the main objectives/issues of this research.

3 Research Issues

Ladle metallurgy operations are very crucial to producing high-quality steels that is a steel product with appropriate physical, chemical and mechanical properties for the intended application, which can serve reliably for the designed length of time. In ladle metallurgy, stirring is a mechanism through which the melt is well agitated to achieve a refined, and thermally and compositionally homogeneous liquid metal. These phenomena play a great role in producing the desired steel quality. The common and effective way of stirring is often carried out by purging argon through the bottom. Gas is injected through porous plugs at high pressure. The refining, mixing and inclusion removal processes may require a different degree of stirring. Vigorous gas stirring may lead to slag-steel mixing and slag entrainment, and this should be avoided. Hence, the argon flow to the metal bath should be in an appropriate quantity to achieve the intended liquid metal chemistry and temperature at the end of the operation and before the metal is poured to a caster. Ladle operators often evaluate the amount of bath stirring by observing the flow indicators, the size of bare metal on the top slag layer, and /or listening to the bubbling sound. This method of control generally focuses on system stability rather than system optimization. It is more of qualitative judgment and may not exactly evaluate the stirring status. In addition, gas leakage that occurs at various ladle components makes the flow gauges in particular and the manual monitoring, in general, less reliable.

Researchers from academia and industry have tried to automate the stirring process using signals that are generated during the process. The multidimensional dynamic fluid turbulence inside causes the ladle wall to vibrate. This vibration signal can be constantly measured by an accelerometer to provide online information about the status of the process.[10] In a similar manner, when inert gas rises forming bubbles, the bubble formation, coalescence, and disintegration process often generate sound.[25, 26] Hence, the sound and vibration signals that can be directly measured from the stirring process and used to explain various phenomena of the ladle stirring. These signals may continually change to manifest the changes in the degree of stirring occurring in the metal bath.

This study has focused on studying low flow rate stirring process using sound and vibration signals. The key objectives of this study were as follows:

- To assess the effect of mounting a tri-axial accelerometer at different locations and then choose the optimum accelerometer location for efficient data gathering.
- To investigate how the three-axis vibration signal measured at various experimental conditions describe low flow rate stirring. This includes investigating the structure of the vibration data and how these data are correlated with the process parameters and the amount of stirring inside the ladle/cold model apparatus.
- To assess vibration data collected from the actual industrial ladle. This includes analyzing the structure of the data, the correlation between stirring indicators and latent variables and comparing with water model study results.
- To compare and contrast laboratory and plant scale studies.
- To investigate how bubbling sound is correlated with low flow rate stirring
- To investigate the effect of the bottom and top layer depths on the vibration and sound signals.

These research questions were mainly addressed experimentally in the laboratory using physical cold models of 200 and 160-tonne ladles. Some plant trials have also been carried out in a Tata Steel site in the United Kingdom. The details of the physical modeling, experimental conditions, and analysis techniques are described in the next chapter.

4 Methodology

This chapter describes the approaches used to address the research issues described in Chapter 3. The study was experimental using physical cold models in a controlled environment and actual ladles in an industrial setting. Laboratory scale models were designed, constructed, and used in the laboratory to carry out the majority of the experiments to study the stirring process. Vibration and sound signals were measured from these laboratory scale models and a plant trial was undertaken to gather vibration in gas stirred ladle in a vacuum tank degasser. Appropriate data acquisition hardware and software were applied to acquire and process the data. Data were analysed using various signal processing and statistical techniques. The procedure and theory of physical modeling, collection of data and analysis techniques are described in this chapter.

4.1 Experimental Method

McLeod defined an experiment as " an investigation in which a hypothesis is scientifically tested. In an experiment, an independent variable (the cause) is manipulated and the dependent variable (the effect) is measured; any extraneous variables are controlled"[194] The author classified an experiment as with laboratory/controlled or field experiments. In a similar manner, McLeod defined an independent variable as a "Variable the experimenter manipulates (i.e. changes) – assumed to have a direct effect on the dependent variable." and dependent variable as a " Variable the experimenter measures, after making changes to the independent variable that are assumed to affect the dependent variable." [194] A scientific experiment may begin by defining problems followed by collecting, organizing and evaluating data to reach conclusions.[194] This research method helps clear out extraneous and unwanted variables that exist in the actual system. It gives higher control over relevant independent variables as compared to other research methods. In the experimental study, the cause and effect relationship can be easily determined by manipulating the independent variables. Another benefit of experimental research is that experiments can be repeated to verify if the already obtained results are reproducible.[194]

Laboratory experimental designs are often replicated scenarios that may not represent all things that happen in the system being studied. Hence, the extent that results can be generalised to all conditions and real world applications may not be comprehensive. In this study, the issues are

addressed by carrying practical experiments on an actual industrial system and comparing results with the laboratory study.

The current study used triaxial vibration signal and sound pressure as dependent variable and air flow rate and bath height as independent variables. It manipulated three independent variables to determine their effect on the dependent variables. Other process parameters related to ladle stirring such as pressure, temperature, plug position, number, and life were not varied during the laboratory study.

The experiment was performed on two cold models and one full-scale industrial ladle. The first cold model was a plastic walled apparatus that has been used previously by Xu et al. for studying the stirring process using three different signals i.e. vibration, ladle eye size, and sound.[18] The second cold model was built from steel material aimed at comparing results with the plastic model and investigating the effect of the material on the vibration signal. It involved the physical modeling of gas stirred ladles consisting of two liquids that are immiscible with each other.

Ladle metallurgy operations are often accomplished in ladles that vary in size and shape.[195] ladles are often slightly tapered cylindrical vessels, which are internally lined with refractory materials. The design of the bottom of the ladle has traditionally been flat but in recent times it is being restructured to a funnel shape.[196] The later geometry has been observed to enhance metallurgical performance in gas stirred ladles.[197, 198] The external shell is made of steel plates with a thickness that depends on the ladle capacity. The thickness ranges from 0.012 to 0.032 m for ladle capacities of 10 to 200 tonne and above.[199] Internally, a ladle is multi-layered to protect the outer shell from high temperature, decrease heat loss and increase mechanical strength. Specialized refractory bricks are located on the inner face and are important to contain the molten metal. A mass layer, safety layer, and insulation layer are layered in sequence from the brick to the external steel shell. The overall thickness of the ladle wall can reach up to 0.30 m. The top of the ladle is covered by a lid.[200, 201]

During pyrometallurgical operations, pressurized gas injection into liquid metal through one or two purging plugs has been the foundation for several advances in steelmaking.[35, 195] A large number of purging types and designs are available.[202] Plugs may be porous refractory material or segment-purging plugs.[104] The location, number, and size of purging plugs may also differ

from one ladle to the other. Plugs can be positioned at the center or on the sidewalls. Standard stirring operations are carried out by percolating argon gas through the porous plug to the metal bath. The choice of argon is due to its low solubility in steel and chemical inertness.

The geometry, location of porous plugs and gas flow rates of two industrial ladles were replicated in a laboratory using established concepts in the literature on physical modeling.[36, 203, 204]

4.1.1 Physical Modelling

Modeling is a widely established scientific approach and has been used in steelmaking for decades. The two most common scientific models are physical and mathematical models. A general definition of a physical model is given by Steven Hughes [205] as "a physical system reproduced (usually at reduced scale) so that the major dominant forces acting on the system are represented in the model in correct proportion to the actual physical system". It is an important precision device for estimating the behavior of a physical phenomenon.[206] Svendsen mentioned three research scenarios that can be studied using a physical model. These are listed below:[207]

a) Verifying a theoretical model from the acquired data

b) Obtaining data for phenomena that are not been yet reachable to theoretical approaches

c) Looking for a qualitative understanding of a phenomenon not yet known in detail

Physical models have several distinct benefits.[205]They are cost effective considering the size and complexity of the actual full scales, more variables of the process can be included to establish complex relationships, they provide the opportunity to measure and monitor the physics in a controlled environment and they demonstrate visually what is happening. The inability to reproduce all real phenomenon in the model is the most important limitation of a physical model.[205]

In ladle metallurgy, a physical model has been used to understand liquid metal flows and associated mass transfer.[35] Designing a reasonably realistic model is not a straightforward procedure because steelmaking operations involve complex processes such as multi-phase turbulent flow, chemical reactions and mass transfer among metal, slag and gas. As a result, assumptions and idealizations are often applied. However, it is fundamental that certain

conditions are fulfilled in order for the model to correctly describe the events happening in the actual reactor. During ladle metallurgy operations, the fluid flow in a liquid metal cannot be visualized, the working temperature is very high, toxic or corrosive substances are usually present and industrial metal processing reactors are relatively large. These all make a direct experimental study of fluid flow, mixing and mass transfer in full-scale liquid processing ladles difficult.[35, 195] Representing the industrial ladle by a physical model makes a measurement of desired parameters more manageable and easier observation/visualization of the process at a reasonable cost.[35, 195, 208]

A physical model of secondary steelmaking process can be a cold model or a high-temperature model depending on the working fluid. High-temperature models use molten steel while cold models may use mercury, water etc. to simulate molten metal. When building a physical model, four conditions of similarity need to be satisfied. These are:[35]

a. Geometric similarity

b. Mechanical similarity

c. Chemical similarity

d. Thermal similarity

4.1.1.1 Geometric Similarity

The geometric similarity requires the ratio of every corresponding geometric dimension of the model and the real system to be equal, constant and linear while respecting similarity of shapes at the same time. The geometric scaling factor, λ, can be defined using full-scale ladle geometric dimensions, diameter (D_f) and height (H_f), and respective dimensions in the physical model. The ratio of corresponding lengths, between model and full-scale systems is mathematically given in Equation 4-1.[204]

$$\frac{D_m}{D_f} = \frac{H_m}{H_f} = \lambda \qquad 4\text{-}1$$

where m and f refer to model and full-scale respectively.

Figure 4-1 shows the diameter and height on both scales. In the case of a tapered cylindrical ends, the extent of the taper should be identical i.e. the top and bottom diameters should be related by the geometric scaling factor.

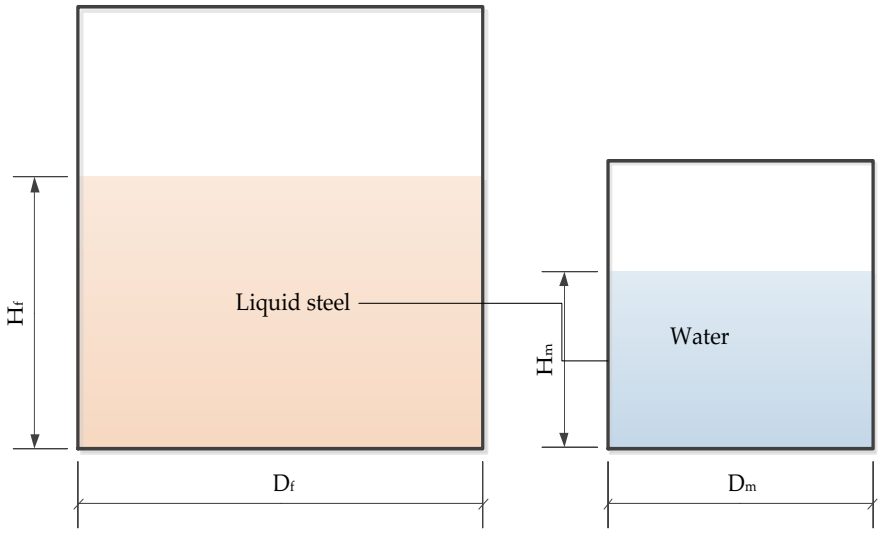

Figure 4-1 Characteristic dimensions of a full scale and a model

It is not always possible to replicate every length and shape in the physical model. This is because it is time-consuming and expensive to manufacture every single detail. Sometimes some parts may also be less important to include during modeling. In addition, the geometry of some parts of an industrial ladle may be affected by various phenomena such as slag and metal solidification, and refractory erosion occurring during ladle operations. Hence, some reasonable assumptions and approximations are done to simplify these problems during physical modeling.[35]

4.1.1.2 Mechanical Similarity

In general, mechanical similarity refers to the similarity of forces between the two scales. It constitutes three types of similarity criteria: static, kinematic and dynamic similarities.[203] Static similarity is useful when studying the behavior of structures. It mainly focuses on forces required to move or rotate the reactor. In secondary steel making, the ladle is normally kept stationary.[35, 195] In this study, the main aim is to investigate movement caused by gas stirring. Hence, for stationary ladles, a static similarity criterion was not considered in this investigation. Kinematic similarity requires that the geometrical shape of the flow paths of a particle in the full scale and the corresponding particles in the model are similar i.e. the length and time scales which refers

to velocities at corresponding points be similar between model and full-scale.[195, 204] In Figure 4-2, the velocity of a sample particle at 1, 2, 3 and 4 should be similar between the two scales.

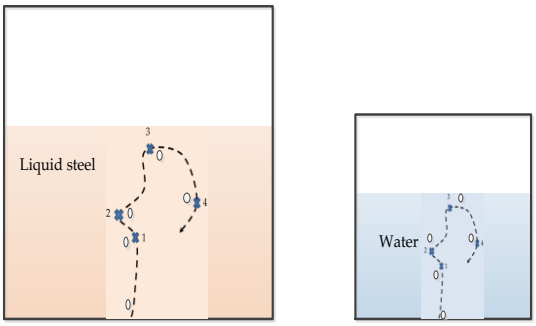

Figure 4-2 Sample flow path of a single particle

In gas stirred ladles, ascending gas bubbles cause melt flow. The speed of the motion is a function of various interacting forces such as viscous, buoyancy, and inertial forces. The third form of mechanical similarity which is most important in this study is the dynamic similarity and is concerned with such forces.[195] This similarity criterion necessitates that forces in the full scale should be similar to the forces on the model at corresponding time and location. Guthrie and Mazumdar proposed the mathematical expression that shows the dynamic similarity between a full-scale system and a physical model. This is shown Equation 4-2.[35, 204]

$$\frac{F_{I,m}}{F_{I,f}} = \frac{F_{P,m}}{F_{P,f}} = \frac{F_{V,m}}{F_{V,f}} = \frac{F_{G,m}}{F_{G,f}} = C_F \qquad 4\text{-}2$$

Where $I, P, V,$ and G refer to inertial, pressure, viscous and gravity forces. Equation 4-2 can be rearranged to show equalities of ratios of forces that ensure dynamic similarity at corresponding times and locations.[35] These are given by Equation 4-3 to 4-5. Equation 4-3 to 4-5 make evident that the dynamic similarity criteria needs to respect equality of different dimensionless quantities. A list of these dimensionless numbers that are relevant to steelmaking can be found in literature.[35, 204] These dimensionless quantities contain the physical properties of the model and full-scale important in developing mechanical and geometric similarities.[195] Some of them are useful in modelling steelmaking reactors.

$$\left(\frac{F_I}{F_V}\right)_{mod} = \left(\frac{F_I}{F_V}\right)_{full} \qquad 4\text{-}3$$

$$\left(\frac{F_I}{F_G}\right)_{mod} = \left(\frac{F_I}{F_G}\right)_{full} \quad 4\text{-}4$$

$$\left(\frac{F_I}{F_P}\right)_{mod} = \left(\frac{F_I}{F_P}\right)_{full} \quad 4\text{-}5$$

In geometrically similar systems, velocity boundary conditions are naturally comparable and therefore may not be a problem during physical modeling.[35] In this study, the ladle operation was assumed to have fluid flow, which is multidimensional, steady and isothermal.

In ladle metallurgy, equality of all dimensionless groups may not be respected during physical modeling of liquid metal flow.[35] In homogeneous isothermal flows, viscous, inertial, pressure, and gravitational forces are significant and hence Froude, Reynolds, and Euler numbers are vital.[35] Dynamic similarity is fulfilled through the equality of Reynold and Froude numbers between the model and full scale. Mathematically, Froude number and Reynold are given by Equations 4-6 and 4-7 respectively.[195, 203]

$$\text{Froude Number (Fr)} = \frac{\text{Inertial Force}}{\text{Buoyancy Force}} \quad 4\text{-}6$$

$$\text{Reynolds Number } (R_e) = \frac{\text{Inertial Force}}{\text{Viscous Force}} \quad 4\text{-}7$$

In argon stirred ladles containing only liquid metal simulated by a physical cold model of water and air where $\lambda < 1$, it is difficult to respect equivalence of these two numbers at same time.[35, 195, 203] This is because the kinematic viscosity of steel at 1873 K is basically the same to that of water at room temperature.[203] Hence, it is vital to identify which forces are more important to construct dynamic similarity in argon stirred ladles. It was reported that inertial and buoyancy forces dominate in isothermal flow phenomenon in model studies of gas stirred ladle systems. The Froude number equality is more important than the other factors. As a result, it was used as the modelling criterion in this research.[36, 195, 203] Fluid flow in large-scale industrial refining ladles is turbulent in nature. Hence, the flow in the reduced scale model must ensure turbulent flow conditions as well.[203] This Froude number criterion is used to derive a relationship between plant flow rates and airflow rates in the model. The relevant ladle Froude number is defined in the literature using plume rise velocity (U_p) and the molten metal depth (H).[36, 209]

$$Fr = \frac{U_p^2}{gH} \quad 4\text{-}8$$

Equation 4-8 shows that the plume rise velocity is a vital parameter in determining the amount of energy going to the system. In addition, the buoyancy is a function of liquid metal depth. The momentum of the plume is due to the buoyancy of the bubbles, not the injected gas momentum. Therefore, hydrodynamic conditions at the orifice or nozzle are not essential to the overall flow recirculation induced in ladles.[36, 203]

For geometrically and dynamically similar systems, the scaling equation between plant operating flow rate (Q_f) and its corresponding air flowrate in the laboratory scale (Q_m) was derived by equating the Froude numbers in Equation 4-8 and the plume velocity definition in Equation 4-9.[68]

$$U_p \approx Q^{0.33} H^{0.25} R^{-0.58} \quad 4\text{-}9$$

Where Q, H and R refer to gas flow rate, metal bath height and vessel/ladle radius. Thus, the relationship between model and full scale gas flow rates expressed as a function the geometric scaling factor, λ, is given by Equation 4-10.[203]

$$\frac{Q_m}{Q_f} = \lambda^{2.5} \quad 4\text{-}10$$

The geometric scaling factor, λ, is selected in such a way that the type of liquid flow regimes in the ladle are preserved in model. Generally, flows in steelmaking are turbulent and therefore the reduced model should not be too small to respect flow similarity.[203] The models built for this study are 1/10 of the full-scale industrial ladles. Several studies have used this scaling factor successfully.[7, 154, 155, 210, 211] the selection flow rates in laboratory study were computed using Equation 4-10 from their corresponding plant gas flow rates. Once the scale factor was chosen, the next step was to select the working fluids that simulate liquid metal and slag.

4.1.1.3 Selection of Slag and Simulation Fluid

The kinematic viscosity of molten steel at 1873 K is almost equal to that of water at 298 K. This guarantees the similarity of flows of both fluids.[35] In addition, water has other advantages that

make it popular for replicating liquid metal. It is readily available, suitable to work, economical, and makes flow visualization possible.[35]

Steel slag is a by-product of steelmaking and steel refining processes. Most steel slags consist primarily of CaO, MgO, SiO_2 , and FeO. The proportions of these oxides and the amount of other minor components change from batch to batch even in one plant depending on furnace conditions, raw materials, and type of steel made.[212] In ladles, the chemical composition of the slag depends on the grade of steel produced. Therefore, compared to BOF and EAF slags, the chemical composition of ladle slag is highly variable.[43] The viscosity of slag varies with temperature, oxide composition, basicity, and volume fraction of solid phases.[213] Hence, the composition and dynamic and physical property of slag are highly variable and are difficult to mimic with a single material. Though oil is far from being perfect to simulate slag, because of its immiscibility with water and availability, it has been successfully used in steelmaking water model investigations. [7, 8, 14-16, 18, 37, 73, 76-80, 97, 214, 215] In this investigation, water and motor oil (ϱ= 850 kg /m^3) were used to simulate molten steel and slag respectively.

4.1.1.4 Model Material and Stirring Gas

Two physical cold models that simulate ladles of different capacities are considered in this study. One is made of a transparent material (Perspex) and the other built from stainless steel. In both cases, the water-oil bath was stirred by pressurized air. Stainless steel has similar mechanical damping properties to steel. A damping factor is a dimensionless number that explains how the structure or material oscillations die away.

Table 4-1 Mechanical properties of steel, stainless steel and acrylics [216-220]

Material	**Damping factor**
Steel	0.0016-0.005
Stainless steel	0.00085-0.006
Acrylic (Perspex)	0.01-0.07

The higher the damping factor the quicker the dampening of the vibration. As it is shown in Table 4-1, the damping factor collected from different sources shows that Perspex dampens vibration more than steel. Hence, stainless steel with similar damping properties was used to build the cold

model. In addition, stainless steel can easily be drawn in a conical shape to replicate the actual ladle geometry.

4.1.1.5 Thermal and Chemical Similarity

Thermal similarity is achieved if the ratio of temperature differences at corresponding times and locations is constant between two non-isothermal systems that already respect dynamic or kinematic similarity.[35] In this study, the ladle refining process is assumed isothermal at a constant temperature of 1873 K. In addition, during the cold model study, different working fluids were used at constant ambient temperature. Hence, the thermal similarity was not important in this research.

Chemical similarity requires the ratio of the concentration of all chemical species in the full scale and model to have fixed relationship. This is useful to the model distribution and the reaction of constituents in the gas stirred metal bath.[35, 195] As the objective of the research is to assess the dynamic movement of ladle wall and bubbling sound due to fluid flow because of gas agitation, the chemical aspect of the process was not taken into account.

Once the design of the physical model was completed, the physical dimensions were determined using the geometric scale factor and workshop drawing prepared to manufacture the cold model. The apparatus was then installed and data collection commenced.

4.1.2 Physical Cold Model Limitations

Dynamic similarity and idealization of flow require equality of Froude as well as Reynolds numbers between models and full scales. This is difficult to satisfy for other than full-scale models, which can be expensive, to some extent tiresome and can lead to uncertainties.[35, 221] The multiphase nature of steelmaking systems that consists of slag, gas, and metal make it difficult to ideally mimic through water models. Reasonable slag– metal interfacial tensions and slag–metal density are difficult to attain in any aqueous system. In addition, melt flow can be slowed by the interaction of the slag with liquid bath. This cannot be observed in water model, which contributes to the weakness of physical cold modeling.[222] Physical model investigations with oil as a top layer/phase and water as bottom layer/liquid are therefore approximate.[35]

4.2 Data Collection

For vibration and sound pressure signal measurement, a measurement system that comprises sensors, data acquisition hardware, computer, software, data visualization techniques and storage formats were designed. The main elements of this system are described in section 4.2.1.

4.2.1 Data Acquisition System

Data acquisition (DAQ) systems are processes and/or products used to gather information to analyse or document some phenomenon. In this study, DAQ systems were used to collect vibration and sound signals from water models as well as an industrial ladle. The system consisted of sensors, signal conditioning, an Analogue to Digital Converter, cables, and a computer. Figure 4-3 shows how the DAQ components are arranged to collect data.

A. Sensors

Sensors were used to measure physical variables or signals emanating from gas/air stirred ladles/models and convert these into their proportional electrical signals suitable for the DAQ system to process. Essentially, two measurements were carried out in this study. These are wall vibration in terms of acceleration and bubbling sound in terms of sound pressure. Additional sensors like flow meters and pressure gauges were also used to monitor the volumetric air/gas flow rate and the pressure respectively.

The selection of the vibration sensor, an accelerometer, was based on cost, sensitivity, mounting technique, application environment, frequency and amplitude range. The accelerometer was used in both the laboratory and the plant trial. Hence, it was selected to meet the operating requirement in both environments. A low-cost triaxial industrial accelerometer that measures acceleration in x, y and z directions was selected. Its specifications are presented in Table 4-2. The accelerometer was mounted using a standard stud on a smooth and flat surface on the external wall of the cold model. The mounting surface was wiped out and a light film of oil was spread prior to installation. The film of oil increases vibration transferability and improves the stiffness of the mounting. The high frequency operating range of the accelerometer is more efficient when the installation is made with a stud.

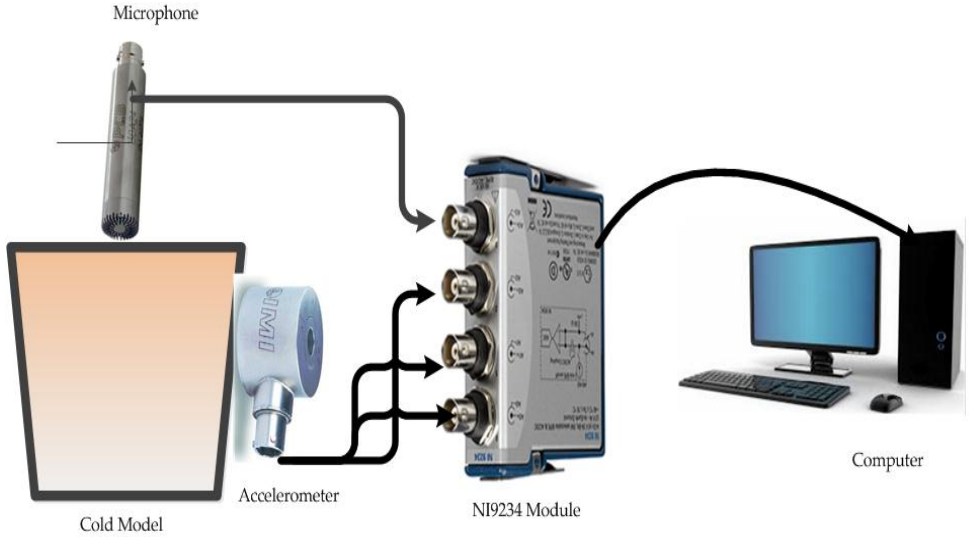

Figure 4-3 Data acquisition system setup

Table 4-2 PCB Industrial Accelerometer general specification (ICP Model 604B31)

No.	Performance	Value
1	Sensitivity	95 mV/g
2	Measurement range	±50 g
3	Frequency range	0.5 to 5000 Hz
4	Operating temperature	219 to 394 K
5	Mounting technique	Through threaded hole

Sound pressure imparted from a bottom stirred physical cold model was measured using a microphone. The microphone selection considered the cost, polar pattern or directionality, frequency response, dynamic range and working temperature. The microphone has a preamplifier coupled with it to amplify weak signals. Table 4-3 shows the basic specification of the microphone used. The microphone was placed on the top with its head facing the water bath during signal capturing from the cold model.

Table 4-3 PCB Microphone (ICP Model 130A23) general specification

No	Performance	Value
1	Sensitivity	14 mV/Pa
2	Dynamic range (High)	150 dB
3	Frequency range	20 to 20000 Hz
4	Operating temperature	263 to 323 K
5	Directionality	Unidirectional

The amount of pressurized air injected through the nozzle located on the bottom of the vessel was monitored by Acrylic flow meters of various volumetric airflow rate ranges. The meter uses a ball float to determine the flow rate reading. The flow meters were installed in a way that minimizes external vibrations and internal flow variations. A detailed description of the airflow meters used in this study is shown in Table 4-4.

To prevent pressure fluctuation of the compressed air source, a pressure regulator was installed between a flow meter and the source. The pressure regulator can regulate up to 700 kPa and has an operating temperature range of 263 to 333 K.

Table 4-4 Key Instruments Airflow meter descriptions

No	**Performance**	**Value**	
1			Accuracy
			±5% Full Scale
			±3% Full Scale
			±3% Full Scale
3	Floats	black glass	
4	Maximum temperature	338 K	
5	Maximum pressure	690 kPa	

B. Analogue to Digital Converter Module

The electrical signal coming from the sensors was transported to a module where analogue to digital conversion and further signal conditioning was carried out. This module was a four-channel dynamic signal acquisition module with each channel having a maximum sampling rate of 51.2 kHz. It has a built-in anti-aliasing filter that adjusts to the given sampling frequency automatically. The operating temperature can go up to 343 K. Each sensor was connected to this module with a standard coaxial cable. This module, in turn, was linked to a computer with a USB cable.

C. Computer

The national instrument module (NI) was connected to a computer installed with Signal Express and MATLAB software. SignalExpress is used to as an interface to interact with NI9234 module, process and export data. MATLAB was mainly used to analyse data collected from the experiment.

4.2.2 Signal Measurement

Vibration and sound pressure signals were captured using the accelerometer and microphone respectively as described in the previous section. Before starting the collection of data, the issue of background noise, sampling frequency, and sampling time was addressed.

4.2.2.1 Background Noise

The first step of the signal measurement was to evaluate the background noise by measuring the noise signal separately and comparing it with the actual signal. The signal to noise ratio (SNR) was used to determine the strength of the main signal with respect to noise. A sketch of the main, and noise signals and SNR is shown in Figure 4-4. SNR is given by Equation 4-11 [223]

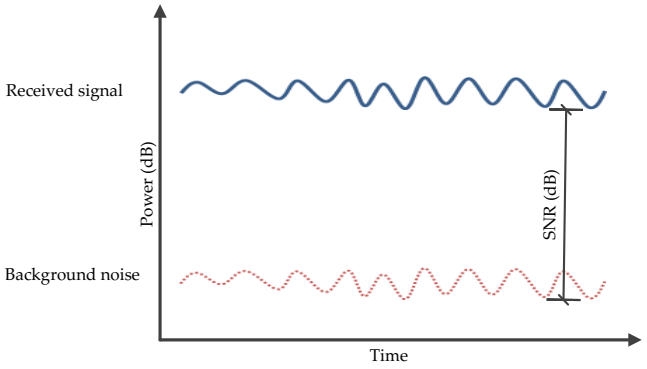

Figure 4-4 Schematic description of SNR [223]

$$SNR_{dB} = 10\log_{10}\left[\left(\frac{P_{signal} - P_{noise}}{P_{noise}}\right)\right] \quad 4\text{-}11$$

where P is the signal's power given by the root mean square (RMS) of the amplitude. SNR is a dimensionless number.

The other technique used to filter out the noise signal was to determine the frequency range where the power of the noise signal is concentrated and ignore this frequency range in the analysis.

4.2.2.2 Sampling Frequency

In signals where the frequency content is roughly known, the sampling frequency has to be at least twice the highest frequency of the expected signal using the Nyquist criterion.[224] Due to

turbulent fluctuation caused by fluid flow in gas stirred ladles, the ladle wall vibration signal may not have distinct peaks in its frequency spectrum; instead, the spectrum may be composed of a broad range of frequencies. Cimbala [224] proposed a trial and error procedure to determine the sampling rate in such phenomenon. The principle is to sample the signal at different sampling rates and observe the location of two or more peak frequencies in the frequency spectra. The procedure is summarized below:

i. Starting with sampling rates f_1'
ii. Sample at a high rate f_2' , which is not integer multiple of f_1'
iii. Check the location of the two peak frequencies in both frequency spectrums. Peaks in the frequency spectra that appear at different frequencies indicate some aliasing errors are happening.
iv. Continue sampling at a higher rate till the peaks in the spectra do not change or shift
v. Sampling at a very high rate may cause poor frequency resolution

Another criterion to be fulfilled is that the frequency spectrum should fall to zero amplitude near the folding frequency of the spectrum if the sampling frequency is high enough. If this is not the case, aliasing of higher frequency components may have occurred.[224] The sampling frequency of the sound pressure was determined using this method.

4.2.2.3 Sample Time

The recording length of the data acquisition of vibration and sound signals was computed by observing the spectral wave pattern at different sampling times. This involved taking the measurement for an extended period, T, and dividing the time history into N divisions as shown in Figure 4-5. Once the signal is divided, the two divisions ($T2$) are compared. If there is no difference between them, the sample time can be reduced to the time of the division. When a difference is noted, then the larger time is taken as a sampling time. The division starts with two and continues until the smallest division, t, is found. This smallest time, t, represents the smallest sampling time that provide similar frequency spectrum among the dividends. Dividing further will cause the similarity of frequency spectrum to be distorted. Hence, a sample time of t seconds was determined and used throughout the experiment assuming that reducing the sample time to t seconds does not affect the quality of the data.

After determining the sampling rate and sample time, the data was collected from the physical cold model. The sample time for the industrial data was determined from a single heat in which the flow rate remained constant. The gathered data was analysed using various techniques of signal processing and statistics.

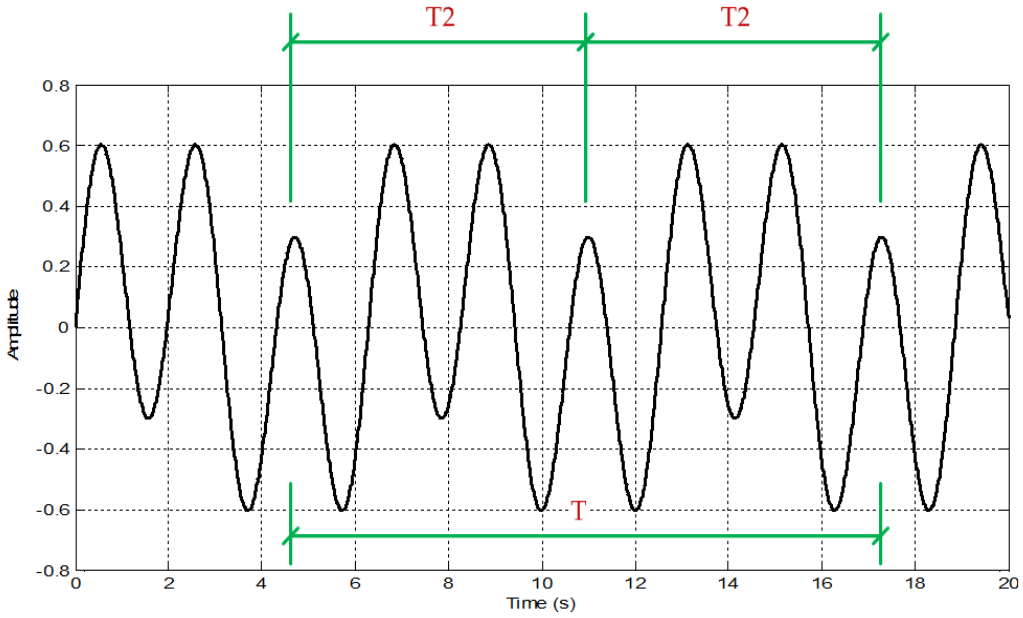

Figure 4-5 Dividing the time history into N smaller time lengths.

4.3 Data Analysis

The time-dependent data collected from the laboratory and plant scales was put into a different group of datasets based on the objective of the study and/or to make it suitable for analysis. The specific grouping is discussed in detail in each particular chapter and its sections. In this section, the general analysis procedure and the techniques are briefly described.

The datasets were analysed in the time and frequency domains. Time domain analysis involved the computation of the sum of the vibration and sound pressure amplitudes to observe the variation/trend with process parameters such as volumetric airflow rate, bottom layer depth, and top layer thickness. The sum of the absolute values of the amplitudes for a sample time t was calculated using Equation 4-11.

$$A_{sum} = \sum |A(t)| \qquad 4\text{-}11$$

where A is the vibration amplitude in m/s^2 or sound pressure in Pa. the majority of the investigation was carried out in the frequency domain that applied various signal-processing methods.

4.3.1 Signal Processing

The acquired time varying signals from the transducers were brought into a mathematical integrator for conversion to individual frequency components by an FFT (Fast Fourier Transform). In some portions of the study, the Short-Time Fourier Transform (STFT) and Power Spectral Density (PSD) were used to analyse the frequency content and the power of the signal as a function of the frequency. STFT was applied to locate the frequency range where the power of the noise signal is concentrated in the industrial data. In addition, the Savitzky-Golay (S-G) filter was used to smooth the digital plant data to minimize further the presence of background noise.

During the bubbling sound study, PSD was applied to find the power present in the sound signal as a function of frequency.

4.3.1.1 Fast Fourier Transform

The concept of Fourier helps in transforming time functions of waves to the frequency domain.[141, 225-227]. It shows how fast or how randomly the signal is changing. The vibration signal collected from the laboratory model and plant has three component signals: y and z components. The sound pressure is a one-dimensional time signal. Each time function signal was transformed to its respective frequency domain using the Fast Fourier Transform (FFT) algorithm. A detailed explanation of the Fourier Transform can be found in the literature.[141, 143, 144, 228-230] The mathematical definition of the FFT for any signal $x(t)$ is given by Equation 4-12.

$$X(f) = \int_{-\infty}^{\infty} x(t) e^{-j2\pi ft}\, dt \qquad 4\text{-}12$$

where $x(t)$, $\exp(-j2\pi ft)$, t are the time signal, frequency, complex oscillation, and t is the time axis of the signal respectively. f is the single frequency parameter that determines the basis function in the family. There is one basis function for every f. The purpose of the transformation of the vibration signal was to prepare the data for further statistical analysis.

4.3.1.2 Short Time Fourier Transform

Raw plant vibration data is often full of noise. The sources of this unwanted signal can be crane movement, nearby ladle furnaces, and other related operations. In order to obtain the characteristic vibration signals caused by gas stirring from the vacuum tank degasser, the background noise has to be filtered out or reduced to a level that does not alter the end computation outcome. In this study, the industrial data was processed by STFT to remove the heavy noise. The Short-Time Fourier Transform (STFT) is a Fourier-related transform that can convert a non-stationary one-dimensional time signal to the two-dimensional frequency-time domain.[231-233] Mathematically it is defined by Equation 4-13.[233, 234]

$$TF(t,f) = \left| \int_{-\infty}^{+\infty} y(\tau) h(\tau - t) e^{-i2\pi f\tau} d\tau \right| \qquad 4\text{-}13$$

where $h(t)$ is a short-time analysis window centred at $t = 0$. This technique was applied here to identify the frequency band where the power of the noise is concentrated. The frequency ranges that contain high noise signal were not considered for further analysis. The frequency ranges that have less noise component were further processed using Savitzky-Golay filter.

4.3.1.3 Savitzky-Golay Filter

To capture essential patterns and improve the signal to noise ratio without greatly destroying the signal, the plant data was smoothed using the Savitzky-Golay filter (S-G filter). S-G filter a widely used filter for reducing noise.[235-238] The benefits of this filter are: it adjusts boundaries automatically, it easy to program, it can deal with missing values, it performs smoothing faster, one parameter provides continuous control of the smoothness and permits quick cross validation.[239] It smooths data using a local least square (LS) polynomial approximation.[236] It acts on a vector of input samples $x(k)$ to give a smoothed vector of *y(k).* This filter is defined mathematically in Equation 4-14.[234, 237, 238, 240-242]

$$Y_j = \sum_{i=-(m-1)/2}^{i=(m-1)/2} C_i Y_{j+i} \qquad \frac{m+1}{2} \leq j \leq n - \frac{m-1}{2} \qquad 4\text{-}14$$

where n is sample size of the data (Xj, Yj) and $j = 1, \ldots, n$. m is number of convolution coefficients ,Ci. In this analysis, the S-G filter in MATLAB is utilized. The window width over which to do the polynomial fit and the order of the polynomial were chosen in a way that gives the best fit and better correlation between the latent variable and process parameters.

4.3.1.4 Power Spectral Density

Knowing the distribution of the signal's strength in the frequency domain is important in order to use it in many applications. The power spectrum of a time series signal, $x(t)$, is used to compute power distribution across frequency components constituting that signal.[243-246] The average power spectral density, $S_x(f)$, of a random time signal $x(t)$ is computed from the Fourier Transform and its autocorrelation, $R_x(\tau)$.[244, 247, 248] The autocorrelation and power spectral density are given in Equation 4-15.

$$S_x(f) = \int_{-\infty}^{\infty} R_x(\tau) e^{-2j\pi f\tau} d\tau, \quad \text{where} \qquad R_x(\tau) = \int_{-\infty}^{\infty} x(t)\, x(t+\tau) \mathrm{d}t \qquad 4\text{-}15$$

To analyse the acoustic pressure variation generated during bubble flow in gas stirred ladles, investigation of the frequency components was important. In the study of the bubbling sound from the physical cold model, the power spectral density of the sound pressure was used to compute the energy content of different frequency ranges. This was used to characterize the sound pressure with respect to process parameters such as volumetric gas flow rate and bath volume. The PSD was not applied to the vibration data.

The vibration data, once transformed to the frequency domain, was further analysed by two statistical approaches. These approaches were crucial in discovering essential relationships in the large vibration dataset.

4.3.2 Statistical Techniques

Most of the industrial processes are not so simple to be explained and controlled by simple laws of nature or a scientific law.[18] This is partly because the number of variables affecting a certain process is large. Hence, these variables have to be measured and manipulated to be used as an

input to the control system.[249] In a similar manner, ladle metallurgy operations involve complex processes such as compositional changes through chemical reactions and multi-dimensional fluid flows and therefore a single mathematical model may not be sufficient to predict the process.[250] Xu et al. successfully measured vibration and sound signals generated from the metallurgical processes and used the multivariate statistical method to analyse the data. These methods are used to a summarized data to analyse the correlation between process variables and to unveil underlying structure.[27, 251-255]

In this study, two multivariate statistical methods were applied to the three-variable frequency-domain vibration data collected from the laboratory and plant scales. These are linear principal component analysis (PCA) and partial least square (PLS). The main weakness of these techniques is that they can only detect linear relationships but they also have many other advantages.

The choice of PLS was due to its ability to analyse data with many, noisy, collinear, and even incomplete variables in both input and output data. PLS also has a desirable property that the precision of the model parameters improves with the increasing number of relevant variables and observations. PLS and PCA based industrial multivariate monitoring schemes have been shown good progress in the last two decades. PCA was selected to be one of the analysis tools because of the following reasons. It is a reliable, simple and nonparametric method of extracting important information from a large dataset. It has simple mathematical operations, which make it convenient for online analysis. PCA has success stories in industrial applications.[31, 175, 256]Its first few principal components can account for the maximum variance of the data. The reduced components can also be utilized for further analysis. In ladle stirring where several different signals can be extracted, it is very important if the most process descriptive variables are identified and used for its online control process. The three vibration signals (along x, y and z) and sound signal have been found more important to effectively describe the stirring phenomenon in ladle metallurgy.[7] PCA was used to find the structure in the vibration data.

4.3.2.1 Principal Component Analysis (PCA)

In gas stirred ladles different signals can be extracted that can describe the process and used for its online control. During ladle stirring, vibration and sound signals are generated during bottom gas agitation. The measured vibration signal has three components: $x-$, $y-$, and $z-$axis. PCA

was applied to combine these three signals and compute the structure of the datasets. PCA was applied in various frequency ranges in order to identify any highly structured frequency ranges. In addition, the best accelerometer location was chosen based on PCA. The vibration data used to construct the state matrix for PCA was prearranged in the order of increasing flowrate, bottom layer depth and top layer thickness. Then, the data was subdivided into different frequency ranges. In every frequency range, the absolute values of the vibration amplitudes that were captured at a specific flow rate and bath height were summed before PCA was applied. PCA was then performed on the treated data.

PCA comprises several steps.[29] Let X_0 be the original data matrix where its rows and columns correspond to three axes of vibration (n) and set of measurements (m) respectively. The first step was to mean centre and scale X_0. Then the new mean centered and scaled mxn matrix X was used to calculate the covariance matrix. The covariance matrix is given by Equation 4-16.[28, 257]

$$\boldsymbol{C}_x = \frac{1}{n-1} XX^T \qquad 4\text{-}16$$

C_X is a square symmetric mxm matrix and its diagonals are the variances of the process variables. These diagonal variables are assumed to describe the variability in the stirring process. The next step was to compute the eigenvectors and eigenvalues of the covariance matrix. These provide vital information about the vibration data. It is important to remember that the sum of the lengths of the eigenvectors is equal to 1.[28, 29, 31, 158, 165, 226, 246, 257]. Solving the singular value decomposition (SVD) of the sample covariance, C_X , gives the loading vectors. Loading vectors are computed loading and ordered by the amount of variance explained in the loading vector directions.[158]

$$C_X = \frac{1}{n-1} X^T X = V \Lambda V^T \qquad 4\text{-}17$$

In Equation 4- 17, the diagonal matrix Λ contains the singular/eigenvalues in decreasing order. These singular values are non-negative quantities shown in Equation 4-18.

$$\lambda_1 \geq \lambda_2 \geq \lambda_3 \geq \cdots \geq \lambda_m \geq 0 \qquad 4\text{-}18$$

A vital property of the Eigenvalues that their sum is equal to the sum of the diagonal elements of the covariance. In Equation, 4-18, λ_i corresponds to the i^{th} principal component (PC). PC_i is the linear combination of the variables given by Equation 4-19.

$$PC_i = V_{i1}x_1 + V_{i2}x_2 + \cdots V_{in}x_n + \quad 4\text{-}19$$

These principal components show the amount of variance/data structure explained in each latent variable. Depending on the values of PCs, the frequency ranges with high data structure were identified. The identified frequency ranges were further analysed by partial least square (PLS). In PLS both input and output matrices are considered. The input matrix contained the experimental parameters whereas the output matrix consisted of the three accelerations in the three axes.

4.3.2.2 Partial Least Square Regression

PLS regression tries to find a common structure between dependent variables/output matrix and predictors/ input matrix by undertaking simultaneous decomposition to compute latent vectors that explain maximum covariance between dependent and predictor variables. The procedure used to apply PLS is discussed in detail by de Jong.[30] The summary of the procedure is summarized in Table 4-5.[30] This aims to develop predictive models for stirring status using vibration signals. In Equation 4-20 X is the predictor, B is regression coefficient and $\boldsymbol{Y_{res}}$ is the residual data. PLS analysis was carried out in different frequency ranges for a wide variety of data sets that are collected from two cold models and the plant scale.

$$\mathrm{Y} = \beta\mathrm{X} + Y_{res} \quad 4\text{-}20$$

4.3.2.3 PLS Model Validation

To check how well the PLS model predicts new data, Cross-validation (CV) is a practical and reliable way to test this predictive significance. CV is a standard in PLSR analysis. CV is performed by dividing the data into a model training/learning and model test/validation set.[172]

Divide the learning data L randomly in to K segments L_k of equal size. let f_k be the predictor trained on $L \backslash L_k$, the $k - fold$ cross validation estimate is given by Equation 4-2.[258]

$$MSEP_{CV,K} = \frac{1}{n_k}\sum_{k=1}^{K}\sum_{i \epsilon L_k}\left(f_k(y_{pi}) - y_{ri}\right)^2 \quad 4\text{-}21$$

where y_p and y_r are the predicted and response/measured variables The Root Mean Square Error of Prediction (MSEP) was calculated to quantify how well each model predicted the training set

or test set. PLS models with low MSE have higher performance. PLS in Matlab uses either k-fold cross validation or x and y both to fit the model and to estimate the mean-squared errors without cross-validation.

In this study, models developed by training data were validated by a new/test dataset. MSEP was also computed to observe how well these models predict the required parameters. Plant data was also used in PLS models derived from cold model data.

4.4 Error Analysis

In an experiment, there are two kinds of errors: systematic and random errors.[259] Generally, in any signal processing, errors can be random which are due to statistical sampling or bias errors, which appear during data acquisition. Bias errors are systematic and occur in the same direction [23]. Bias errors occur at resonance frequencies, this error can be negligible because signals were taken below the resonance Errors that are generated in the digital signal analysis are aliasing and leakage. Aliasing is due to an inappropriate sampling interval and leakage is the result of window selection.[23]

4.4.1 Systematic Errors

Systematic errors affect the accuracy of measurement.[259] They cannot be avoided or reduced by repeating the measurement. Common sources of systematic errors are a faulty reading of instruments by the user, faulty calibration of measuring instruments, or poorly maintained instruments. To avoid systematic errors in the experiments of this study, accelerometers, flow meters and microphones were properly calibrated before used in the laboratory. Calibration was performed in compliance with ISO 9001, ISO 10012-1, ANSI Z540.3, and ISO 17025. In addition, sensors with relatively high sensitivity were selected for vibration and sound measurement.

4.4.2 Random Errors

Random errors are errors that influence the precision of a measurement. If random errors exist in an experiment, the measurements can vary from each other due to random and unpredictable variations in the measurement process. Common sources of random errors are problems

estimating a quantity that lies between the graduations (the lines) on an instrument and the inability to read an instrument because the reading fluctuates during the measurement.

In laboratory scale study, the external sources of sound and vibration were minimized to a negligible value by using proper insulation and tightly fixing the apparatus to the ground. This helped to diminish the random error generated due to unwanted signals in the measurement. This is described in section 5.3.1 and 8.5.1. Selection of appropriate sample time, sampling frequency, and windows was also performed to eliminate or reduce aliasing and leakage. In plant data, various noise filtering and smoothing techniques were applied. This is discussed in section 7.5 and 7.6.

Errors caused by a flow meter and level reading were addressed by repeating the measurements in each experiment three times. The standard deviation and mean were used to observe how the first principal components (PC1), the degree of linear correlation (R^2), and the percent of variation (PACVAR1) are close to each other for the three measurements. Since the most repeatable values were taken, the difference between the three selected values of each parameter was very small.

To compute how precise these measurements are, statistical analysis was carried out. This consists of computing a central value and observing the distribution of the data around this central value. It uses two numbers: the mean and the standard deviation. For a set of N measured values for some quantity x , the mean and the standard deviation are computed from Equations 4-22 and 4-23.[260]

$$\bar{x} = \frac{1}{x}\sum_{i=1}^{N} x_i \qquad 4\text{-}22$$

$$\sigma_x = \sqrt{\frac{1}{N-1}\sum_{i=1}^{N}(x_i - \bar{x})^2} \qquad 4\text{-}23$$

In general, PCA and PLS are techniques that can filter out noise, irrelevant or redundant data to reveal the underlying structure. This can help to minimize various errors introduced in the data.

4.5 Methodology Summary

In summary, this research was carried out experimentally mostly in the laboratory using physical cold models of actual ladles of capacity 200 and 160 tonne. The 200-tonne ladle is constructed from plastic (Perspex) material and the 160-tonne ladle is built from stainless steel. Physical models were designed mainly based on geometric and dynamic similarity criteria. The two signals collected to study the ladle stirring are sound and vibration. The vibration was also measured from a vacuum degasser ladle in an industry. Appropriate data acquisition hardware and software were used to acquire process and analyse this data. Vibration data was mostly analysed by PLS and PCA whereas sound signal was investigated using signal processing techniques. Error analysis and cross-validation were also carried out to check the accuracy of data and validity of models. The research began by studying a plastic walled water model, which will be described in the following chapter.

5 Plastic Walled Cold Model Study

5.1 Introduction

This chapter describes the cold model study of a 200-tonne ladle. It was focused on measuring the amount of stirring in ladles using a three-axis vibration signal. It commenced by analyzing the optimum accelerometer location on the external wall of the plastic model. As described in Chapter 2 section 2.6, there is limited literature on detecting stirring of molten metal in ladle metallurgy by using vibration signal. Moreover, the low flow rate inert gas stirring phenomena is not fully understood. The issue of sensor location was also not addressed in the open literature. In addition, previous studies measured ladle vibration in one dimension only. Hence, this chapter describes the investigation that addresses the issue of accelerometer location, vibration data structure and the degree of stirring at various flow rate ranges and bath depths using a plastic walled physical cold model. The study measured triaxial vibration signal, applied PCA, and PLS to analyse the data.

5.2 Experimental Setup

A cold model, prepared using dynamic and geometric similarity criteria proposed by Krishnapisharody and Irons, was used in this study.[36] The detail theory and procedure of physical modeling is discussed in section 4.1.

The cold model simulated a 200-tonne capacity industrial ladle that is scaled down to 1/10. Then the geometric dimensions and other process parameters were determined using this scaling factor. The vessel's inner diameter is 0.42 m and the height is 0.50 m. The nozzle (diameter =0.003 m) through which compressed air is injected is located at the bottom center. A summary of the parameters, which were used in the laboratory scale, is presented in Table 5-1.

The compressed air flow rate was controlled by a standard acrylic rotameter which was assembled between a ball valve and pressure regulator. The air pressure was made to be at a fixed value by a pressure regulator at 0.20 MPa to prevent any fluctuation that may originate from the source. The ball valve was significant to halt the backflow of fluid from the vessel. A stud mounted triaxial PCB accelerometer was used for simultaneous multi-axis (x, y and z) vessel wall vibration measurement. Analogue vibration data obtained from the accelerometer was digitized

using a 4-channel C series dynamic signal acquisition module (National Instrument 9234) before it was exported to a computer.

Table 5-1 working conditions in laboratory and plant scales

Parameter	**Industrial ladle**	**Cold model (293 K)**			
			Density , kg/m^3	**Kinematic Viscosity ,m^2/s**	**Surface Tension, N/m**
	Molten metal	water[261]	998.2	1.003x10^{-6}	0.0728
	slag	oil	878.7	326.00 x10^{-6}	0.031
Bubbling gas	Argon	air	1.23	15.11 x10^{-6}	0.0729
Plug/nozzle position	centre	centre			
Scale factor	1	0.1			
Temperature	1873 K	293 K			

National Instrument SignalExpresss 2013 software was used to acquire, generate and save the signals. The list of sensors and accessories used in this experiment are described in Chapter 4 and shown Table 4-2 and Table 4-4. The vessel frame was tightly fixed to the concrete floor to make background noise negligible. The overall experimental setup is shown in Figure 5-1 and 5-2. Candidate locations of the accelerometer are positioned along the vertical axis on the external vessel wall. Figure 5-3 shows the three locations for mounting the accelerometer.

Figure 5-1 Laboratory experimental setup

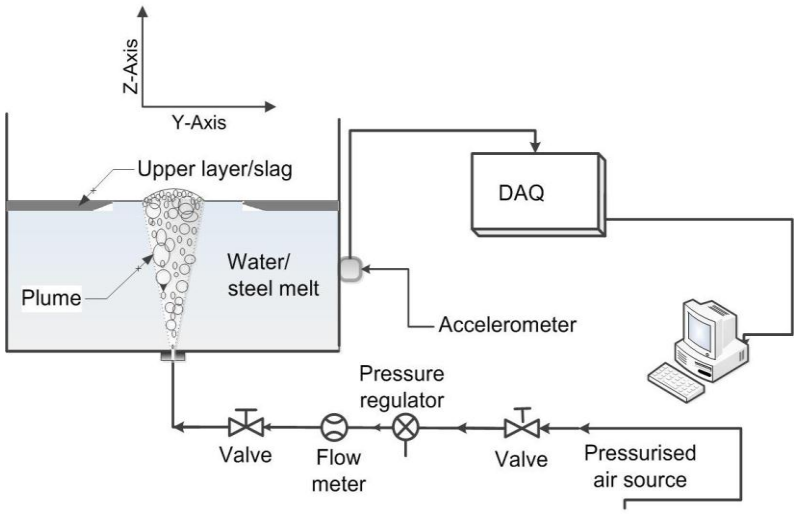

Figure 5-2 Sketch of experimental setup

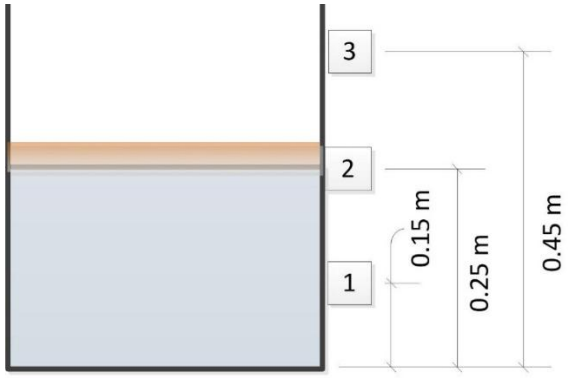

Figure 5-3 Accelerometer locations

5.3 Experimental Conditions

The main parameters of the stirring process that involved in this study are the depth of the molten metal (H), slag thickness (h), and volumetric gas flow rate (Q). Applying geometric and dynamic similarity criteria, the parameters' values in the lab-scale were determined. Equation 4-10 which is based on plume Froude number similarity ($(Fr_p)_m = (Fr_p)_f$) was applied to determine the volumetric flow rates for cold model study. Flow rates considered in this study were computed from Equation 4-10 ($Q_m = \lambda^{2.5} Q_f$) in order to be within the range of flow rates applied in ladle metallurgy.

The experiment was carried out with a single layer (without top layer/ oil) and double layer (with the bottom and top layers). Generally, the bottom layer depth was varied from 0.1 m to 0.25 m at

intervals of 0.05 m through the experiment. Similarly, four top layer thicknesses were considered in this study: 0.005, 0.01, and 0.015 and 0.02 m.

Three volumetric airflow rate ranges in the interval of $0.17x10^{-5}$ to $10.83x10^{-5}$ m^3/s were considered in this study. This flow interval corresponds to a range of $53.3 x10^{-5}$ to 3416.7 m^3/s in actual industrial ladles. This flow rate range is within the operational range of flow rates in ladles.[38, 105, 262] The vibration data was gathered by varying the parameters according to Table 5-2 for the single layer and Table 5-3 for the double layer studies. The single and double layer investigation done after the accelerometer location was selected.

Table 5-2 Experimental conditions for single layer study

Parameter	**Water depth (m)**	**Air flow rate (m^3/s) x 10^{-5}**
	0.1 to 0.25 at 0.05 interval	0.17 to 0.83 at 0.17 interval
	0.1 to 0.25 at 0.05 interval	0.83 to 4.17 at 0.83 interval
	0.1 to 0.25 at 0.05 interval	3.33 to 10.83 at 0.83 interval

Table 5-3 Experimental conditions for double layer study

Parameter	**Water depth (m)**	**Oil depth(m)**	**Air flow rate (m^3/s) x 10^{-5}**
	0.1		
	0.15		
	0.2		
	0.25		
	0.1		
	0.15		
	0.2		
	0.25		
	0.1		
	0.15		
	0.2		
	0.25		

Vibration data from each of the three locations shown in Figure 5-2 was collected using the experimental conditions presented in Table 5-4.

Table 5-4 Experimental conditions for accelerometer location selection

Water depth (m)	**Oil thickness (m)**	**Flow rate(m^3/s) x 10^{-5}**
0.1 to 0.25 , 0.05 interval	None	0.83 to 4.17 at 0.83 interval
0.2	0.01	0.83 to 4.17 at 0.83 interval

The values of the key process parameters were determined so that the data acquisition covers a range of operating conditions that can generalise the outcome. The data acquisition began by measuring the background noise and comparing it with the main signal generated from the air bubbling of vessel bath. Then, sampling rate (F_s) and sampling time/period (T) were determined. These parameters were then used throughout the data acquisition process.

5.3.1 Background Noise

The vibration signal measured in the absence of vessel bath stirring was analysed in the time and frequency domains. This signal was compared to the vibration signal imparted during bath stirring. Figure 5-4 shows the amplitudes of the noise and main signal. It is evident that the amplitude of the background noise was insignificant. This outcome was also repeated in the frequency domain investigation, which is shown in Figure 5-5.

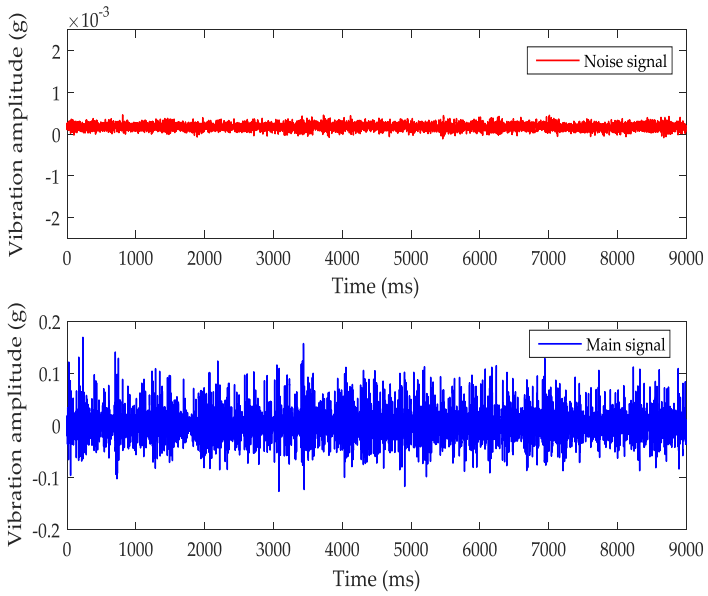

Figure 5-4 Vibration amplitude of background noise and main signal

The signal to noise ratio (SNR) was computed and was found to be very large which also confirms that the other sources of vibration do not affect the main signal. This signifies that filtering was not important for the cold model study.

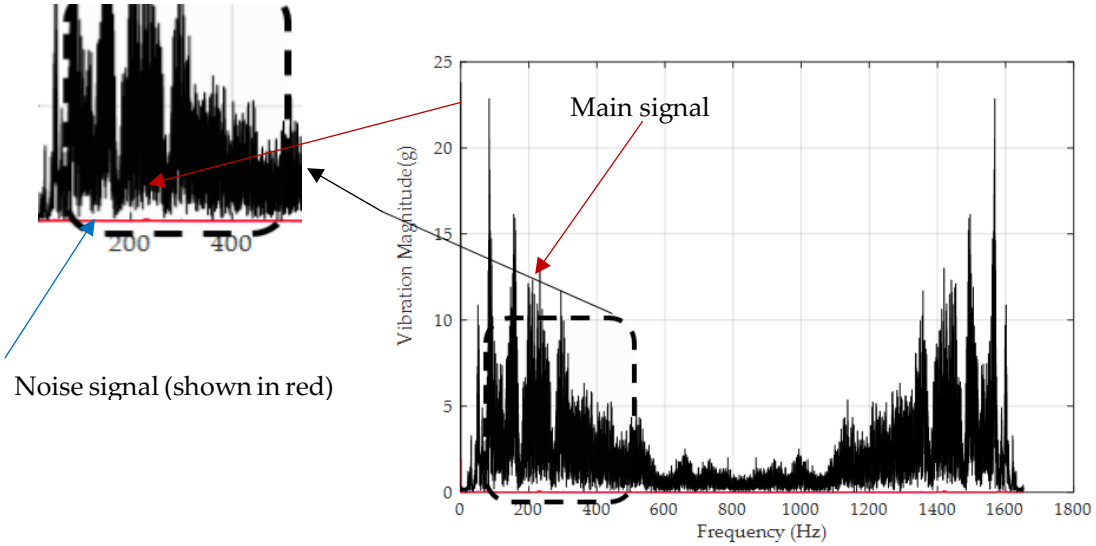

Figure 5-5 Spectral variations of noise and main signal

5.3.2 Sampling Rate

The vibration signal was sampled at 1828 Hz. This was computed using the trial and error procedure proposed by Cimbala.[224] The procedure is described in section 4.2.2.2. In addition, the minimum sampling frequency of the data acquisition module is 1828 Hz. At this sampling rate, the vibration frequency spectrum drops off towards zero amplitude near folding/Nyquist frequency. This is shown in Figure 5-6. According to literature, this sampling frequency is high enough to sample the vibration signals.[224] This sampling rate was also compared with other studies, which were conducted on ladle vibration due to stirring, and was found to be higher. [7, 12] Hence, 1828 Hz was used to sample the vibration data throughout the experiment.

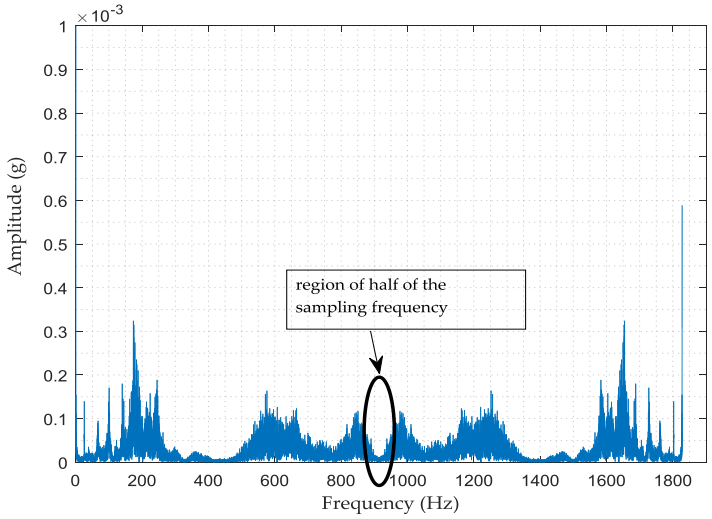

Figure 5-6 Vibration frequency spectrum at 0.83x10^{-5} m^3/s and 0.10 m water bath height

5.3.3 Sampling Time

The minimum sampling time was computed by observing the frequency spectra at various sample times. The vibration signal was recorded for 120 seconds. Then, this recording was divided into smaller segments and a comparison of their frequency-amplitude plots was made. The smallest time length that provides identical frequency spectrum graphs was taken as the sample time. At this sample time, the quality of the measured data was not affected.

Figures 5-7 and 5-8 represent what has been found during sample time manipulation. Figure 5-7 shows the frequency-amplitude graph at 5-second sample time. It can be observed that the three plots are not identical. On the other hand, Figure 5-8 shows that the spectral variation of the amplitude is quite similar in the two plots. Hence the period or sample time for the whole vibration data gathering was taken to 6 seconds. Other studies have also shown that this sample time gives the desired data quality.[18]

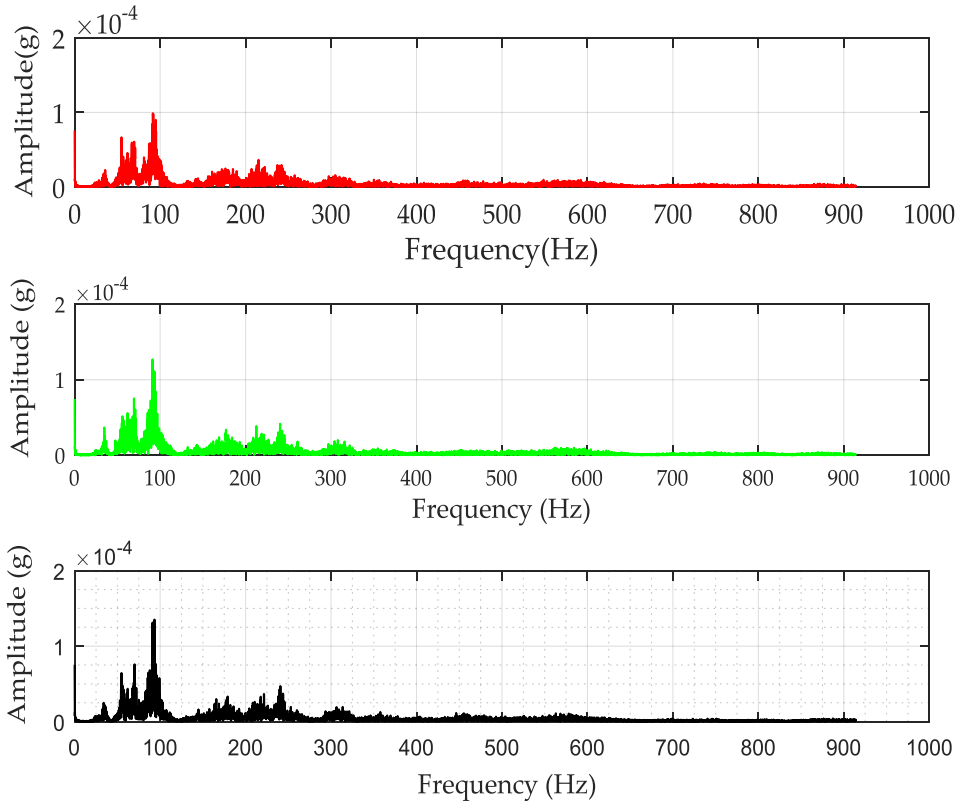

Figure 5-7 Frequency spectra at 5 seconds sample time

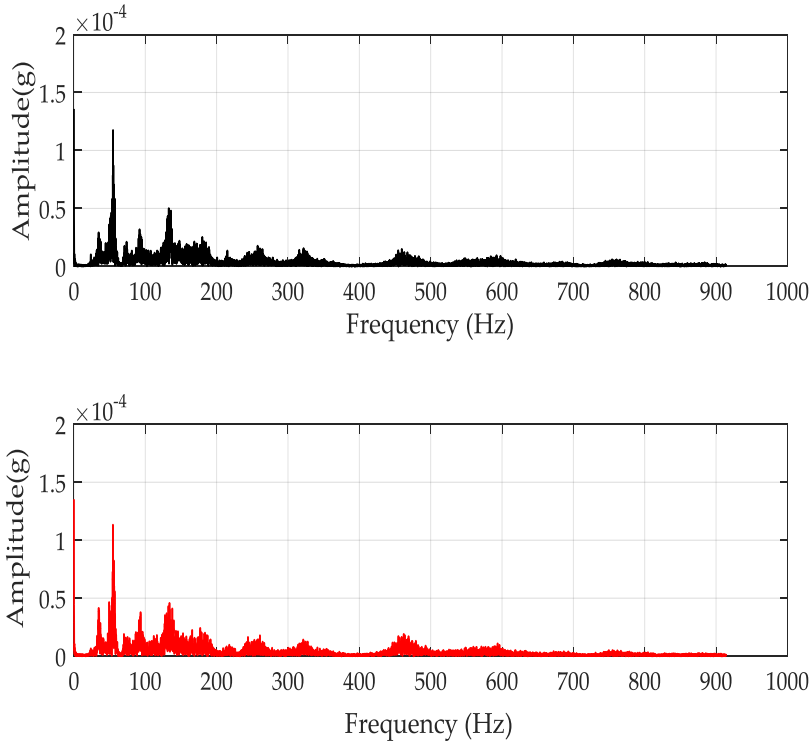

Figure 5-8 Frequency spectra at 6 seconds sample time

5.3.4 Analysis Procedure

The time-domain vibration signal was transformed into the frequency domain using FFT algorithm, found in Matlab version 2013a, before principal component analysis was applied.

To identify the most informative frequency range, the whole frequency range was split into smaller ranges. The vibration amplitudes within these specific frequency ranges were analysed by principal component analysis. The analysis starts from a large to a smaller frequency range (10 Hz). The sum of the vibration amplitude within the considered frequency range was calculated using Equation 5-1. This was used to build a matrix, which is an input for PCA analysis.

$$v_k = \sum_{i}^{i+10} v(i) \qquad 5\text{-}1$$

Where $k = x, y$ and z accelerations and $i = 0, 10, 20 \ldots 90{,}900$ Hz.

The matrix consists of the acceleration in the x, y and z directions at different experimental conditions. The goal was to linearly combine and suppress them to one or two latent variables using the algorithm of PCA found in Matlab 2013a. These helped to identify the most informative

frequency ranges. The data within these informative frequency ranges were analysed using the algorithm of PLS in Matlab 2013a. The concept of PCA and PLS are described in section 4.3.2. In the PLS analysis, airflow rate, water depth, and top layer/oil thickness make the predictor matrix while the measured vibration along x, y and z-axis make the response matrix. The number of variables is equal to three in each matrix. With the PLS, the aim is to extract a set of orthogonal matrices/latent variables with the best predictive power. The model to predict the vibration response is given by Equation 5-2.

$$\boldsymbol{Y} = \boldsymbol{\beta X} + \boldsymbol{Y_{res}} \qquad 5\text{-}2$$

where $\boldsymbol{X}$ is the predictor matrix, $\boldsymbol{\beta}$ is the regression coefficient, and $\boldsymbol{Y_{res}}$ is the residual matrix. The resulting response is correlated with the stirring power and average bath recirculation speed defined in Equation 2-2a and 2-2b respectively. The overall analysis scheme is presented in Figure 5-9.

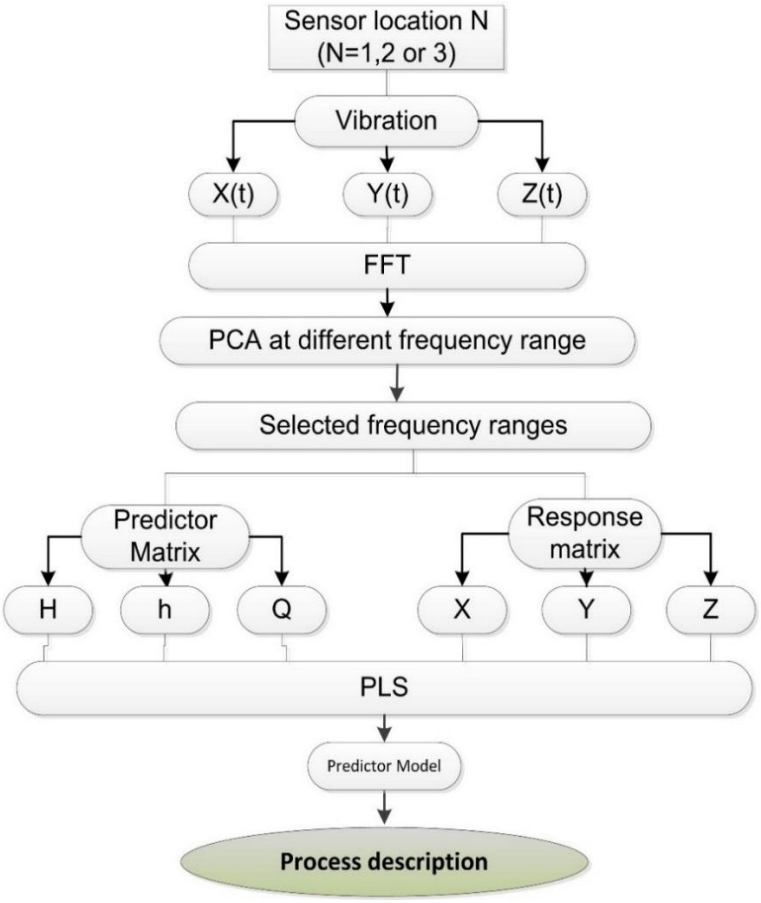

Figure 5-9 Overall analysis scheme

During PCA and PLS analysis, mean values of first principal components (PC1) and percent variation (PCVAR1) were used to evaluate the structure in the data and the amount of variation explained by the first latent variables. The standard deviation was also computed using Equation 4-22 to examine the precision of the results. The maximum standard of deviation varied from 0.3 to 1 in most of the calculations as the most repeatable outcomes were taken.

5.4 Result and Discussion

5.4.1 Optimum Sensor Location

To determine the optimum sensor location, data gathered from the three locations were analysed using PCA. The sum of the first two principal components (PC1+PC2) was used to identify which location provided the maximum process variation.

Table 5-5 shows the values of the first and second principal components different frequency ranges. Similarly, Table 5-6 shows the values of principal components from the double layer data analysis. The result shows that the signals with higher PC1 were found in two different frequency ranges for the single layer experiment. Moreover, the analyses reveal that the first principal component retains almost all of the structure in the data. The finding highlights that the frequency range where the useful information is situated varies slightly for the three locations with no significant differences for information. Less structured frequency ranges are included in both tables for comparison purposes. Though the sum of the two principal components is high, the choice of the best location was based on the value of the first latent variable. Therefore, location 2, which is at the mid-height of the rig, is chosen because of easy accessibility for mounting the accelerometer.

Table 5-5 PC1 and PC2 values for the single (without the top) layer study

Sensor location	**1**		**2**		**3**	
Flow rate(m^3/s) x 10^{-5}	0.83-4.17		0.83-4.17		0.83-4.17	
Frequency range (Hz)	**50-60**	**70-80**	**30-40**	**50-60**	**60-70**	**80-90**
PC1 (%)	98	96	97	97	96	95
PC2 (%)	1	2	2	3	3	4
PC1+PC2	99	98	99	100	99	99
Frequency range (Hz)	**80-90**		**10-20**		**50-60**	
PC1 (%)	82		72		89	
PC2 (%)	17		17		10	
PC1+PC2	99		89		99	

Table 5-6 PC1 and PC2 values for the double (with the top) layer study

Water level =0.20 m , oil depth=0.01 m						
Sensor location	**1**		**2**		**3**	
Flow rate (m^3/s) x 10^{-5}	0.83-4.17		0.83-4.17		0.83-4.17	
Frequency range (Hz)	**60-70**	**110 to 120**	**50-60**	**60-70**	**70-80**	**160-170**
PC1 (%)	99	72	99.5	90	99	71
PC2 (%)	1	27	0.5	9	1	29
PC1+PC2	100	99	100	99	100	100

5.4.2 Single Layer Study

The study conducted on the cold model in the absence of the upper layer/slag shows that the frequency range where the highest process variation obtained is different for low and high flow rate bubbling. Table 5-7 shows the frequency ranges in the investigated flow rates for the single layer study. It was found that specific frequency ranges capture the majority of the variation in the process and these frequencies vary with flow rate range.

Table 5-7 PC1 and PC2 values at different frequency ranges and flow rates for the single (without the top layer) layer study

Flow rate(m^3/s) x 10^{-5}	0.17-0.83			
Frequency range(Hz)	40-50	160-170	180-190	190-200
PC1 (%)	76	68	96	90
PC2 (%)	20	23	3	4
PC1+PC2	96	91	99	94
Flow rate (m^3/s) x 10^{-5}	0.83-4.17			
Frequency range (Hz)	10-20	50-60	60-70	170-180
PC1 (%)	72	95	84	85
PC2 (%)	19	3	13	11
PC1+PC2	91	98	97	96
Flow rate(m^3/s) x 10^{-5}	3.33-10.83			
Frequency range(Hz)	60-70	220-230	240-250	250-60
PC1 (%)	76	79	88	74
PC2 (%)	17	12	9	13
PC1+PC2	93	91	97	91

The first principal component or latent variable with maximum structure in each flow rate range was compared to the stirring power defined by Szekely et al.[65] in Equation 2-2a, and the average steel bath recirculation speed as defined in Equation 2-2b. The results are shown in Figures 5-10 to 5-12. Figure 5-10, 5-11 and 5-12 show a linear relationship between stirring energy and PC1 as well as bath recirculation speed and the dominant principal component. The first principal component predicts the stirring energy and bath recirculation speed quite well at all flow rates ($0.96 \geq R^2 \geq 0.85$) analysed in this study.

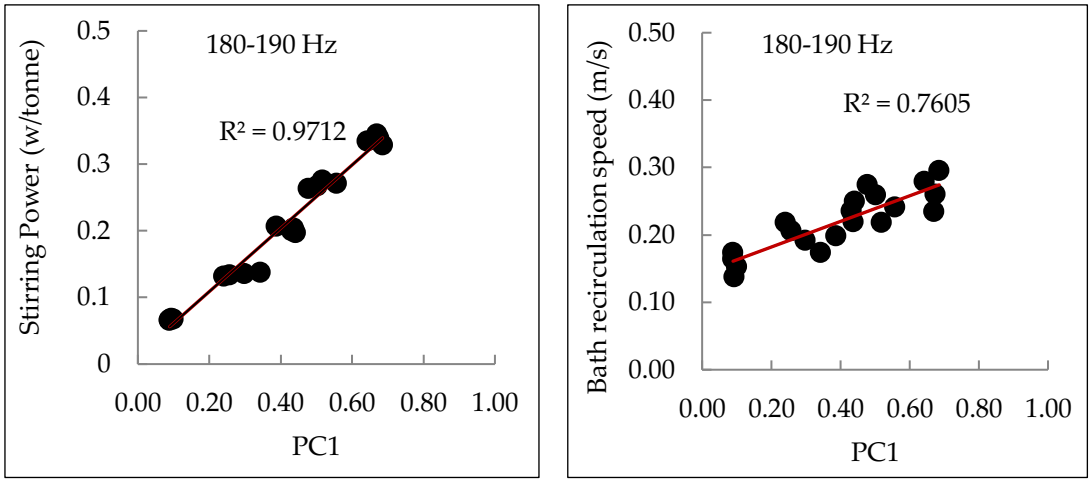

(a) (b)

Figure 5-10 Relationship between PC1 and a) stirring power b) steel bath recirculation speed for flow rate range of 0.17 to 0.83 x 10-5 m3/s

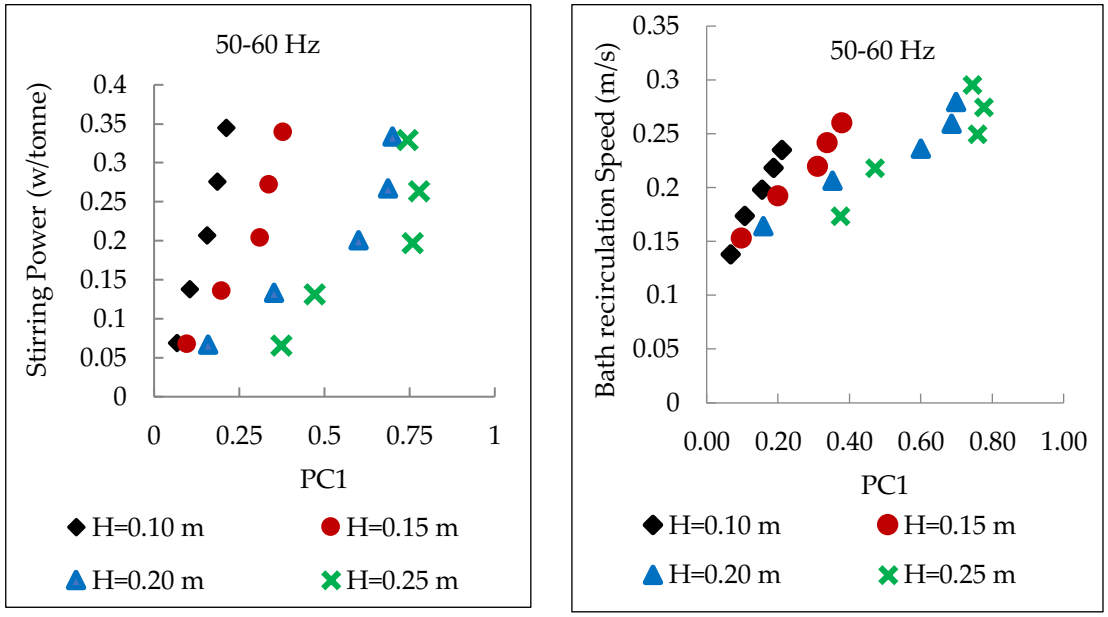

(a) (b)

Figure 5-11 Relationship between PC1 and a) stirring power b) steel bath recirculation speed for flow rate range of 0.83 to 4.17 x 10^{-5} m3/s

$$PC1 = 0.57x + 0.58y + 0.58z \qquad 5\text{-}3$$

Equation 5-3 shows the loading vector of the first principal component/latent variable for the low flow rate range in the frequency range of 180 to 190 Hz. This reveals that the contribution of vibration along x, y and z-direction to the overall stirring process variation is almost equal (33,

33 and 34 %). This implies that vibrations in the three axes are equally useful in estimating the mixing status and developing on-line ladle stirring control.

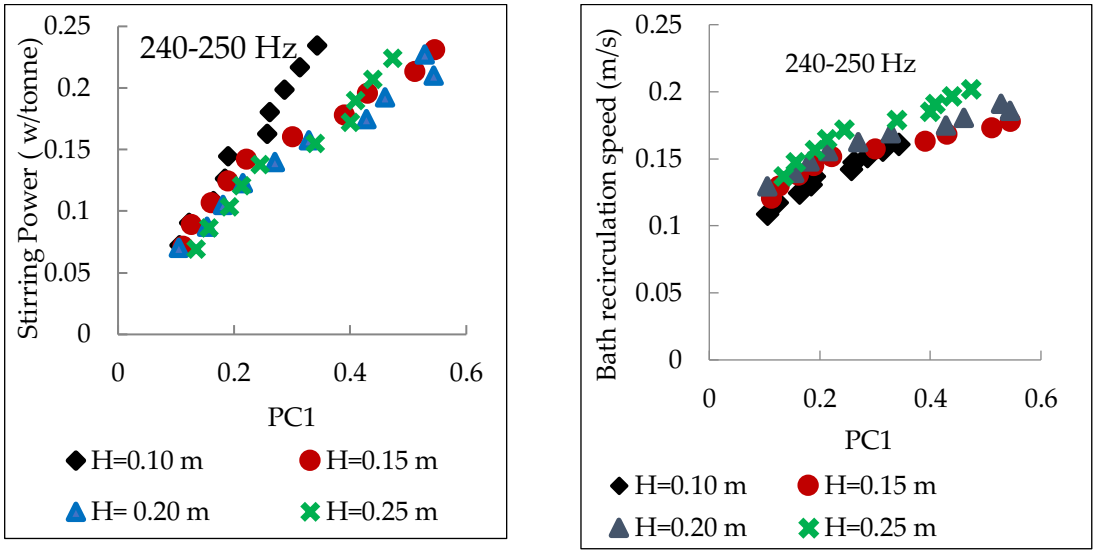

(a) (b)

Figure 5-12 Relationship between PC1 and a) stirring power b) steel bath recirculation speed for flow rate range of 3.33 to 10.83 x 10^{-5} m^3/s

5.4.3 Double Layer Study

The double layer data was analysed using PCA and PLS. PCA was applied in a similar manner to the single layer study to find the frequency ranges with maximal structure. PLS was applied in the identified frequency ranges on the input and output data to extract latent variables with high predictive power. Principal component analysis at a fixed water level and variable oil depth show that there are specific informative frequencies for of each the flow rate range selected. These informative frequency ranges are presented in Table 5-8. Table 5-8 shows that there is a strong structure in the data in specific frequency ranges in the flow rate ranges investigated. The maximum standard deviation computed for these values is ± 0.76.

Vibration data gathered by varying the depth of both layers have also been analysed using PCA. Most of the informative frequency ranges in the double layer have been found identical to those of the single layer study. Some of the informative frequency ranges that were found on the higher flow rate double layer stirring study are found to be similar to the study of Minion et al[4]., Kostetskii et al.[9] Kemeny et al.[11] and Yuriy et al.[15] These frequency ranges are 50 to 60 Hz, 60 to 70 Hz.

Table 5-8 PC1 values for double layer (with oil on top) bubbling at different frequency ranges

Flow rate (m^3/s) x 10^{-5}	0.17-0.83				
Frequency range(Hz)	10-20	30-40	70-80	180-190	240-250
PC1 (%)	46	98	76	96	90
Flow rate (m^3/s) x 10^{-5}	0.83-4.17				
Frequency range(Hz)	10-20	30-40	80-90	50-60	320-330
PC1 (%)	70	98	83	95	98
Flow rate (m^3/s) x 10^{-5}	3.33-10.83				
Frequency range(Hz)	10-20	70-80	30-40	250-260	270-280
PC1 (%)	80	85	98	97	83

The identified frequency ranges in the double layer experiment retain most of the stirring process variation. However, the correlation of the first principal component with macroscopic models of stirring power and bath recirculation speed is not linear as in the single layer analysis. Figure 5-13 shows the relationship between the highly structured vibration data in the frequency range of 180 to190 Hz and 250 to 260 Hz.

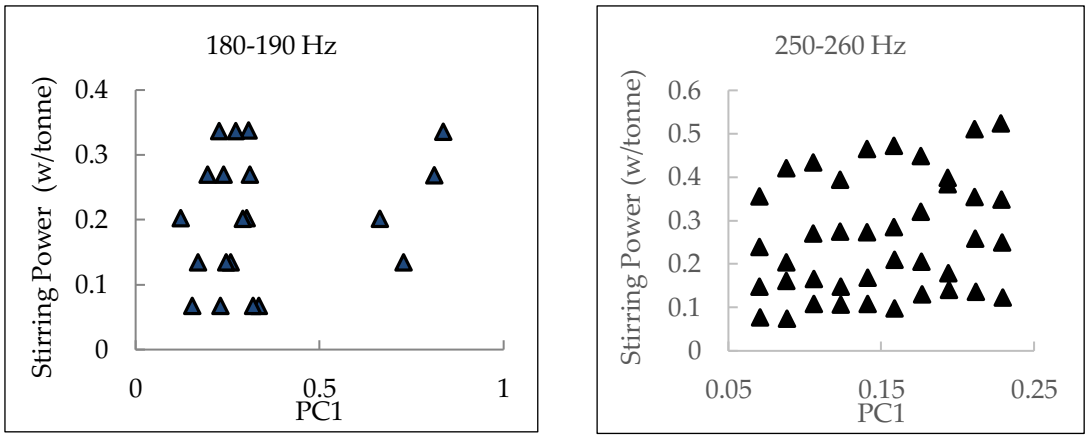

(a) (b)

Figure 5-13 Relationship between PC1 and stirring power for the flowrates of a) 0.17 to 0.83 x 10^{-5} m^3/s b) 3.33-10.83 x 10^{-5} m^3/s

To alleviate this problem another multivariate statistical technique was used. PLS was applied to extract latent variables, which explain the highest variations in the process data (vibration) and most predictive of the stirring energy. Figure 5-14 shows the relationship between the latent variables of the input $\boldsymbol{X}$ and output $\boldsymbol{Y}$ for the flow rate range of 0.17 to 0.83 x 10^{-5} m^3/s, with

varying depths of the lower layer(water) and the top layer (oil). This figure uncovers that the correlation is satisfactory. Considering a fixed bath level depth, i.e. both top and bottom layers depth remain constant, the correlation between the latent variables of predictor and response is found to be strong (Figure 5-14b). Figure 5-15a and 5-14b also show the linear relationship between the response variable and stirring energy and bath recirculation speed for different oil/slag depths. A similar analysis was also done on the other flow rate ranges (0.83 to 4.17 x 10^{-5} m^3/s and 3.33 to 10.83 x 10^{-5} m^3/s).

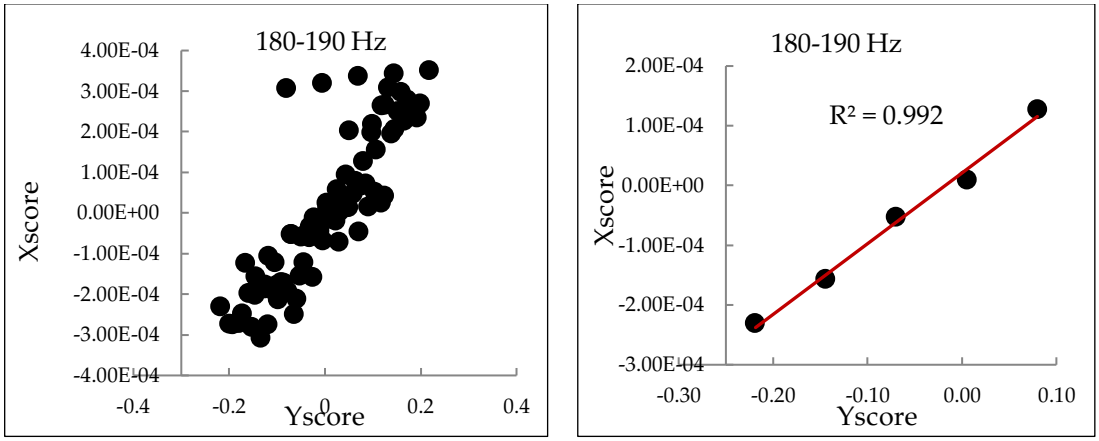

(a) (b)

Figure 5-14 Relationship between X-score and Y-score a) both layers varying b) fixed bath height (H=0.25 m, h=0.20 m) for a flow rate range of 0.17-0.83 x 10^{-5} m^3/s

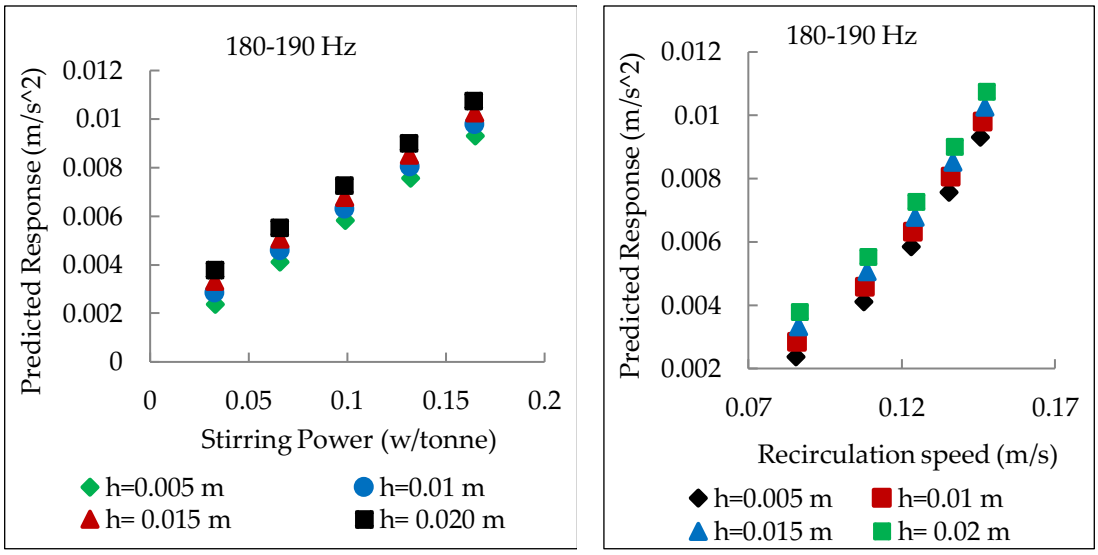

(a) (b)

Figure 5-15 Relationship between predicted response and a) stirring power b) bath recirculation speed for a flow rate range of 0.17 to 0.83 x 10^{-5} m^3/s

The results are shown in Figures 5-16 to 5-19. The degree of linear correlation between the variables and parameters at fixed bath heights are very strong in all the three analyses , with R^2 is between 83 and 98 %.This indicates that if the slag depth and molten metal height are known, the control of mixing in ladles can be managed by studying the data in selected frequency ranges . Figure 5-16 (a) and (b) reveal that the stirring power does not significantly change with changes in oil/slag depth.

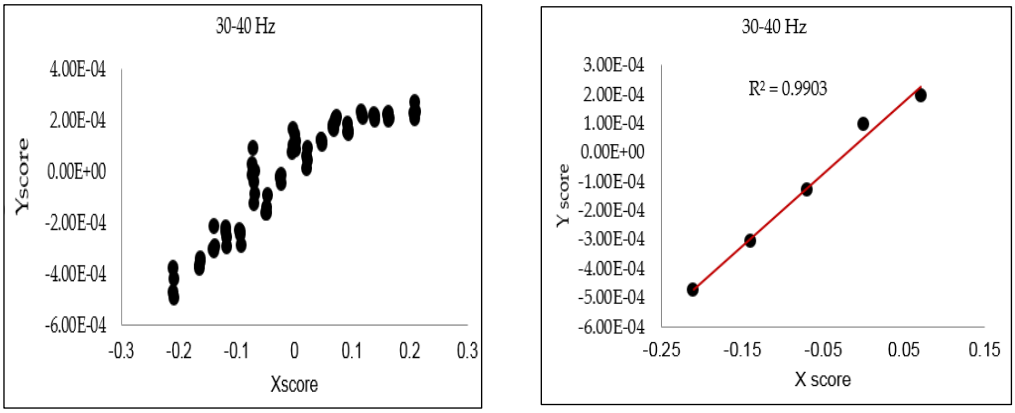

(a) (b)

Figure 5-16 Relationship between X-score and Y-score a) both layers varying b) fixed bath height (H=0.25 m, h=0.20 m) speed for flow rate range of 0.83 -4.17 x 10^{-5} m^3/s

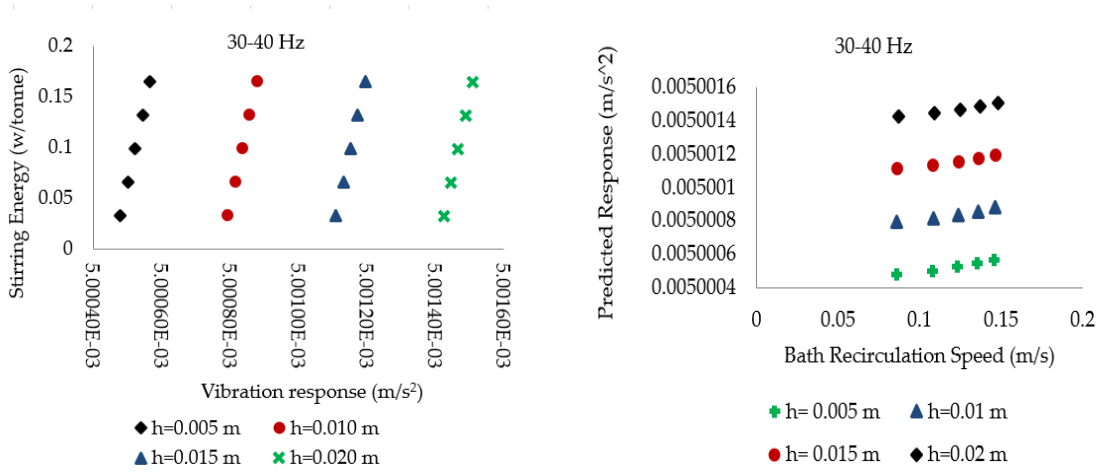

(a) (b)

Figure 5-17 Relationship between predicted response and a) stirring power b) bath recirculation speed for a flow rate range of 0.83 -4.17 x 10^{-5} m^3/s

The other finding from the partial least squares analysis is that the mean square error (MSE) is minimized if three latent variables are extracted to predict the response for double layer stirring. This is shown in Figure 5-19 for the high flow rate range. The phenomenon is similar to the two

other flow rate ranges. This demonstrates that in order to predict the vibration with minimal error, the value of the flow rate, water depth, and oil thickness need to be known and considered in the PLS model.

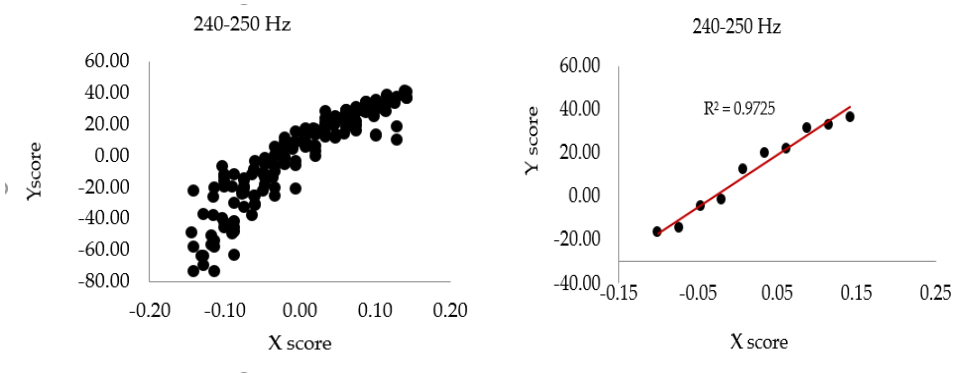

(a) (b)

Figure 5-18 Relationship between X-score and Y score a) both layers varying b) fixed bath height (H=250 mm, h=20mm) speed for flow rate range of 3.33 to 10.83 x 10^{-5} m^3/s

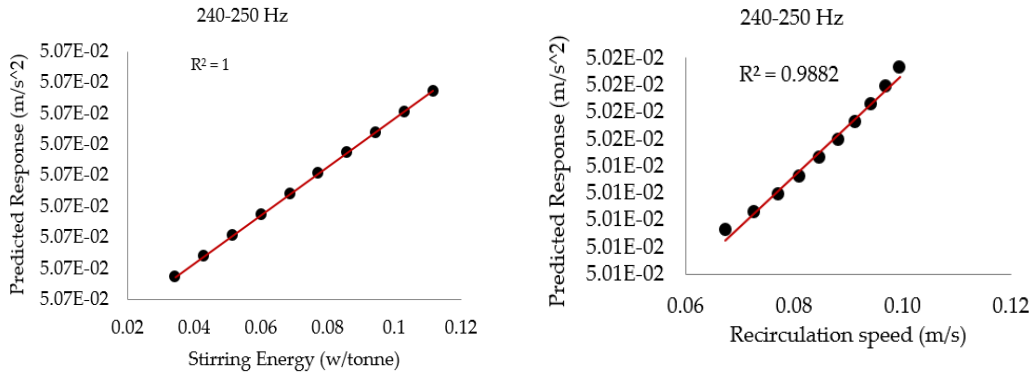

(a) (b)

Figure 5-19 Relationship between predicted response and a) stirring power b) bath recirculation speed for a flow rate range of 3.33 to 10.83 x 10^{-5} m3/s

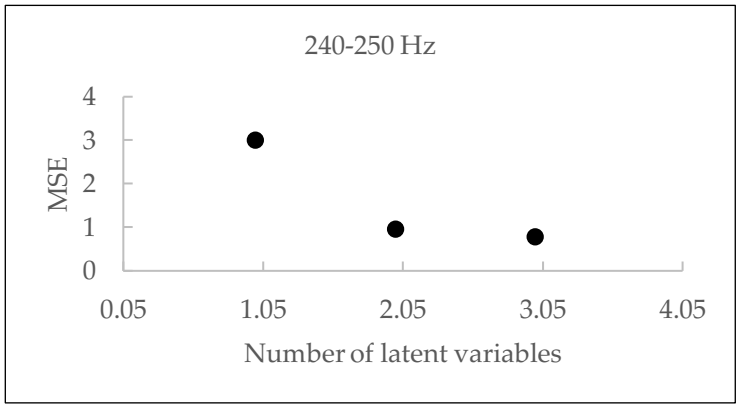

Figure 5-20 Relationship between mean square error (MSE) and number of latent variables

5.4.4 Comparison of Results

The relationships established by Burty et al. and Yuriy et al. described by Equation 2-58 and 2-59 respectively were checked using the vibration data collected from the plastic-walled model. It was found that Equation2-58 agrees with the single layer bubbling vibration data. The double layer data could not show any linear relationship between vibration and their Froude number. Figure 5-21a shows the correlation between vibration and Froude number in the single layer. In Figures 5-21b, the vibration data was collected for double layer bubbling where the top layer varies.

In similar manner, Figure 5-22a and 5-22b were constructed from data collected by the current from the plastic walled cold model to compare the result with Equation 2-59. The vibration data was measured at low flow rates with and without the top layer. For the single layer data, it was found that the relationship is consistent in terms of an increase in RMS value with flow rate which is shown in Figure 5-22a. On the other hand, no distinct relationship was found in the data collected in the presence of a varying top layer using Equation 2-59. This is shown in Figure 2-22b.

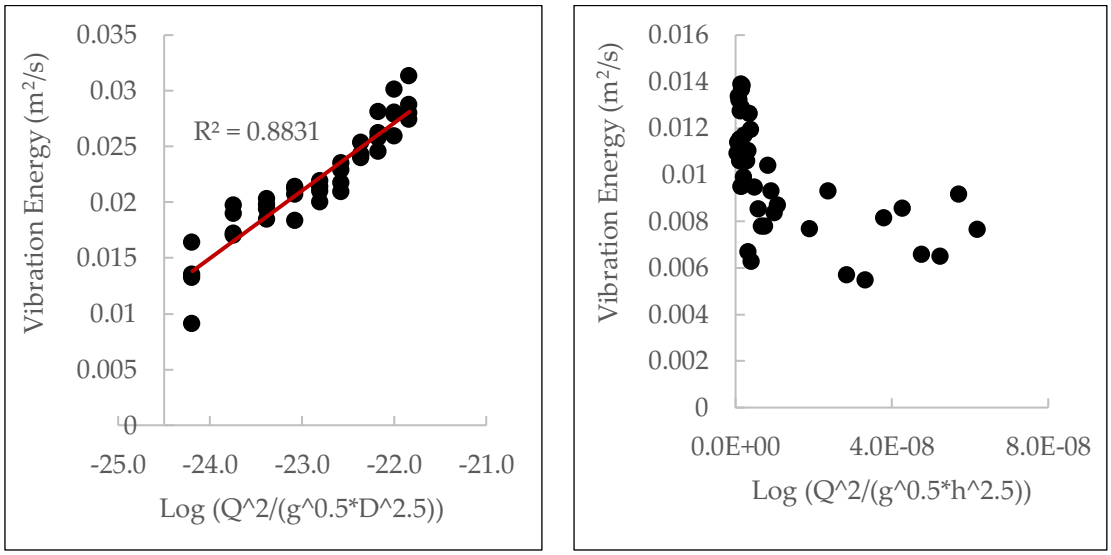

(a) (b)

Figure 5-21 Relationship between vibration energy and Froude number for data taken from this study a) single layer b) double layer c) double layer

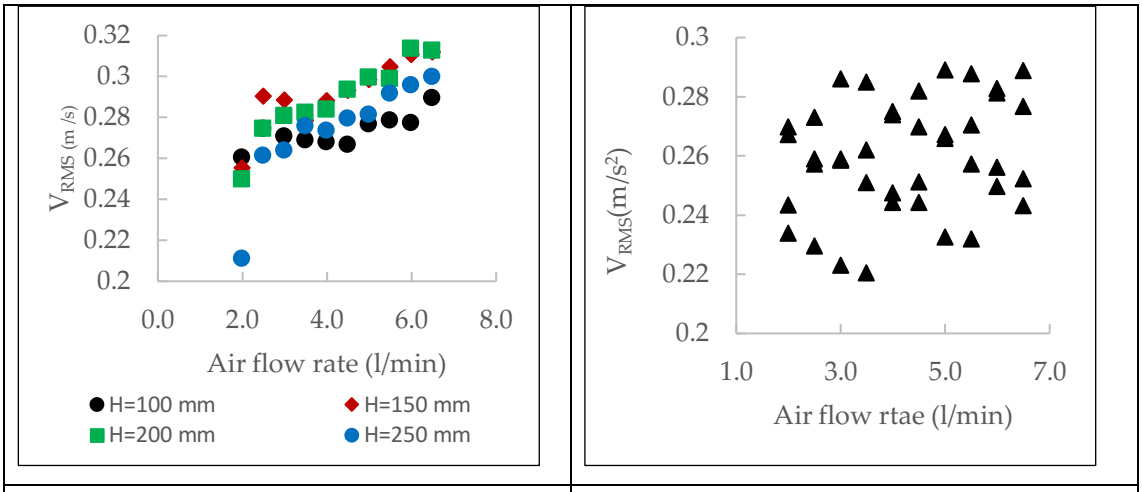

(a) (b)

Figure 5-22 RMS value of the vibro-signal on the gas flow rate under various blowing conditions a) Single layer data b) Double layer data

5.5 Conclusions

The objective of this study was to find the frequency ranges in the measured vibration signal that can retain the majority of the structure based on the percentage of variation explained by the first principal component. The partial least squares method was then applied to the input/predictors and output/response variables to obtain latent variables that maximize the covariance between predictor and response. The study was performed on three different airflow rate ranges and various bath levels for both single and double layer conditions on a plastic cold model. This lab-scale model is a 1/10 scale of the actual 200-tonne ladle.

It has been found that for the low flow rate range considered in this study, the frequency range that retains maximum structure is 180 to 190 Hz. The first principal component in this frequency range can effectively predict both the amount of stirring energy and bath recirculation speed adequately for single layer data. However, for data gathered by varying the water and oil depth, the relationship has not been found to be linear. This was especially exhibited in the low flow rate range. On the other hand, PLS analyses unveiled a strong linear relationship between the predictor score and response score of the double layer data of fixed bath height in the frequency range of 180 to 190 Hz. Both the stirring power and bath recirculation speed showed a strong linear relationship with the response variable (vibration) predicted using PLS.

In the intermediate flow rate range study, the frequency ranges with strong structure are different from that of low flow rate ranges. The result of the present study reveals that the frequency ranges that capture most of the data variation are 50 to 60 Hz and 30 to 40 Hz for single and double layer data. An additional frequency range of 320 to 330 Hz was found in the double layer data. The dominant principal component in these flow ranges predicts the stirring energy and bath recirculation speed effectively ($R^2 \geq 0.90$). PLS analysis on the double layer data in the frequency range of 30 to 40 Hz shows that the latent variables of the predictors have a good predictive power of stirring in the vessel with a small mean square error. This is especially effective if the bath height is fixed and only the flow rate is varying.

In general, the study shows that for a specific flow rate range, there is a corresponding frequency range where the experimental data is highly structured. This implies that process control can be more effective if the frequency range is chosen carefully. The latent variable of PCA in each frequency range predicts the amount of energy transferred to the ladle adequately in the single layer. Double layer data has also shown strong linear relationships when analysed using partial least squares. This is an important step in building a linear predictive model for the stirring status in ladles.

Finally, this work strengthens the significance of triaxial vibration signal in developing online ladle stirring control by one or two latent variables if the frequency ranges are chosen wisely. PCA and PLS were important tools in this study to reveal a structure in the data and predict the stirring status respectively. The following chapters will focus on analyzing the vibration data from cold models of steel material and a subsequent industrial trial.

6 Steel-Walled Cold Model Study

6.1 Introduction

One of the most important requirements of a steel is its purity. The level of impurities such as phosphorous, sulfur, hydrogen, residual elements and inclusion determines its cleanness level. The removal of these impurities is a significant challenge for steelmakers. In steel plants, ladle metallurgy operations are responsible for reducing these impurities. Specifically, vacuum tank degassing in ladle metallurgy helps remove undesirable gases, harmful inclusions and reduce carbon content.[46] In the vacuum degassing process, ladles are stirred by pressurized argon gas to achieve low hydrogen, oxygen, and carbon contents. The stirring energy can be calculated knowing the injected argon flow and liquid steel temperature.[263] Nevertheless, for industrial systems, accurate measurements of the argon flow are not rigorous, due to leakages in the system that are hard to assess.[263] As a result, the optimum stirring magnitude may not be correctly determined from the process. Measuring vibration from a tank degasser may help in evaluating the status of melt stirring. The study of stirring in Vacuum Tank Degasser (VTD) using tri-axis vibration signals was first carried out at a laboratory scale using a physical cold model of the VTD.

In this chapter, the cold model study of ladle stirring in a Vacuum Tank Degasser (VTD) is discussed. This was part of an industrial study in collaboration with Tata Steel. The study started by building a replicate of the VTD using physical modeling concepts and procedures described in the methodology chapter. Vibration data was collected from the cold model to study the low flow rate-stirring phenomenon. The main objective of this project was to study the stirring process at low volumetric airflow rates using vibration signals measured from the cold model of the VTD. In the cold study, the second aim was to choose the optimum location of the accelerometer from the three candidate locations: the ladle wall, the ladle support, and the tank external wall. Vibration data measured from this VTD cold model was analysed using signal processing and multivariate statistical techniques described in the methodology chapter.

6.2 Experimental Setup

Physical cold models made of steel materials are not common in ladle metallurgy research. This is because the steel material is not transparent and cannot show fluid flow behavior during

experiments of secondary steelmaking studies. The objective of this research was to investigate the stirring phenomenon by measuring the vibration of the ladle wall during bubble flow in the steel melt. Hence, the transparency of the plastic walled tanks was not required and the study could be carried out on a steel walled model that more accurately represents the industrial reactor. This study was carried out in a laboratory using a cold model of the VTD operated by Tata Steel plant in the UK. Since the vibration response depends on the nature of the tank material [112, 217, 220, 264-267], the newly built physical cold model was made to replicate the material, tapered shape, and geometric dimensions of a 160-tonne ladle of the VTD. The VTD comprises a tank, a ladle and ladle supports together with gas purging and material addition apparatuses. During physical modeling, these three structures were replicated using geometric and dynamic modeling procedures discussed in the methodology chapter. The model was rigidly attached to a four-legged metal frame. The frame was in turn firmly tightened to the ground.

The laboratory model was a 1/10 geometric scale of a 160-tonne industrial ladle of the VTD. The geometric dimensions and amount of air flow rate in the cold model was computed using Equations 4-1 and 4-10. Molten metal and slag were simulated by water and oil respectively. Air was used to stir the liquid from the bottom of the vessel. Figure 6-1 is a schematic drawing showing the main dimensions of the ladle and the two porous plug positions at the bottom of the furnace. This basic geometry was used to construct the laboratory scale. Table 6-1 contains detailed information of the full scale and its corresponding laboratory scale. The flow rate ranges mentioned in this table are within the operational range of flow rates in ladles.[38, 105, 262]

The compressed air flow rate was controlled using standard rotameters (±3 and ±5 % full-scale errors). The air pressure was set to a fixed value by a pressure regulator at 0.20 MPa. A stud mounted triaxial accelerometer (95 mv/g sensitivity and ±50 g measurement range) was used for simultaneous multi-axis (x, y, and z) vessel wall vibration measurement. The analogue vibration data coming from the accelerometer was digitized using a 4-channel C series dynamic signal acquisition module (NI 9234) before it was exported to a computer. National Instrument SignalExpresss 2013 software was used to acquire, generate and save signals. The overall experimental setup is shown in Figure 6-2. The vessel frame was tightly fixed to the concrete floor to make background noise negligible. A sample time of 6 seconds was taken throughout the experiment as it had been observed that reducing the sample time to 6 seconds resulted in no

reduction of the quality of the data.[154, 155] Data was sampled at 1828Hz to avoid any aliasing errors as explained in section 5.3.2.

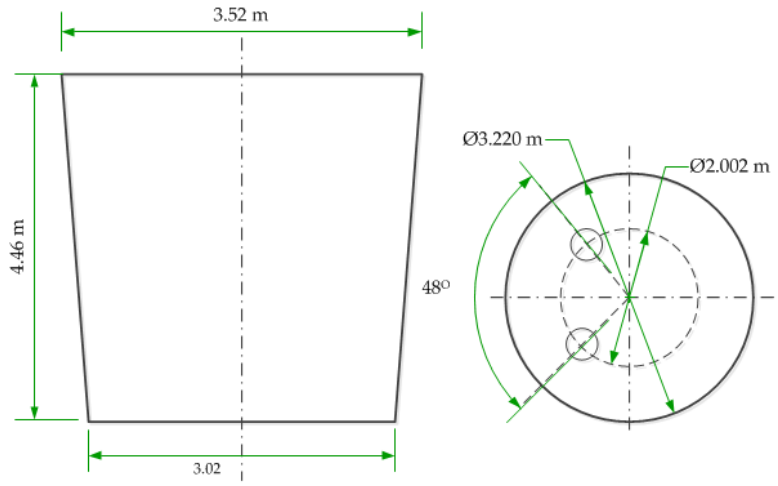

Figure 6-1 160 ton ladle inside dimensions and bottom view showing porous plug locations

Table 6-1 Parameters and their values in the full and the laboratory scales in the 160-ton ladle

Parameter	**Industrial ladle**	**Model(λ=1/10)**
Vessel		
Height (m)	4.460	0.446
Top diameter (D1)* (m)	3.520	0.352
Bottom diameter (D2)* (m)	3.025	0.302
Nozzle		
Diameter (m)	0.110	0.003
Number	2	2
Position (m)	R1.001@48^o	R100@48^o
Working fluid		
Bath Liquid	Steel melt + slag	Tap water +motor oil
Stirring gas		
Stirring gas	Argon	Air
Gas flow rate ($^{m^3}/_s$)	0-1.6x10^{-2}	0-6.67x10^{-5}
Gas pressure (Pa)	10^6	2 x10^5
Material	Steel and refractory	Stainless steel

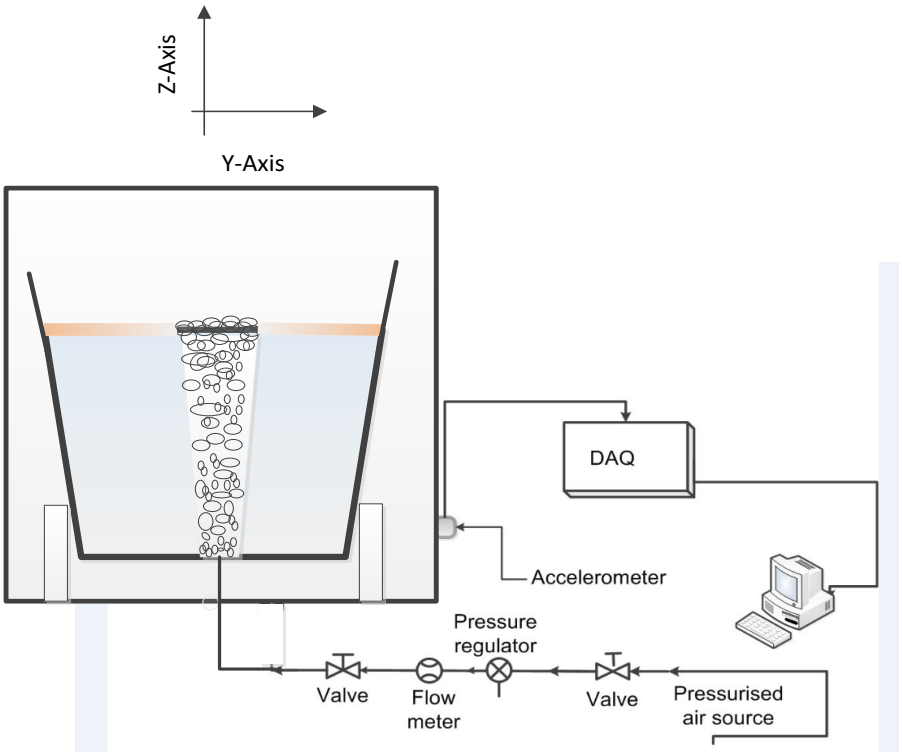

Figure 6-2 Overall experimental setup

6.3 Experimental Conditions

The experiment was carried out with and without the top layer of oil at different volumetric airflow rates. The depth of both layers was varied during the course of the study. Other parameters such as pressure, nozzle position, and number of nozzles were kept constant. Two nozzles were used to inject air and the amount of flow was identical in both nozzles. The accelerometer was located at three different positions for gathering wall acceleration at various flow rates and bath volumes. Applying geometric and dynamic similarity criteria, the parameters' values in the lab-scale were determined. Equation 4-10 which is based on plume Froude number similarity ($(Fr_p)_m = (Fr_p)_f$) was implemented to compute the volumetric flow rates for cold model study. Flow rates considered in this study were computed from Equation 4-10 ($Q_m = \lambda^{2.5} Q_f$) in order to be within the range of flow rates applied in ladle metallurgy. Table 6-1 consists the flow rates computed using this relationships.

6.3.1 Accelerometer Locations

The choice of an optimum location of the sensor depends on many factors like accessibility, ease of mounting, signal quality, and other industrial environmental factors. For this study, the candidate locations considered were the vessel wall (C), the vessel support (B) and the tank external wall (A) which are shown in Figure 6-3 on a sketch of the actual vacuum degasser. The accelerometer was stud mounted on a flat smooth surface covered with a thin oil film. Figure 6-3 shows these locations on the physical cold model.

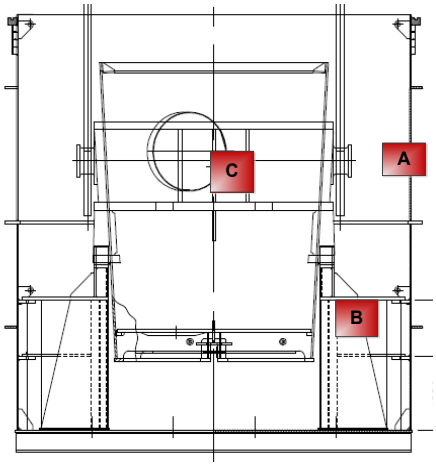

Figure 6-3 Sensor locations (A and B and C) on ladle and vacuum tank degasser wall

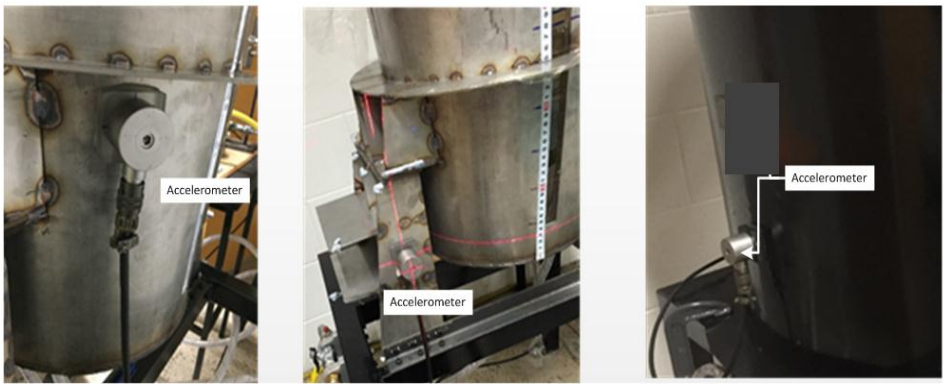

Figure 6-4 Sensor candidate locations on the laboratory apparatus

6.3.2 Air Flow Rate and Bath Height

Air was injected into the bath through two-sidewall 0.003 m flush nozzles on the bottom plate of the apparatus. The airflow rate taken in this experiment was in the range of 6.67×10^{-6} to 40×10^{-6} m^3/s, which corresponds to 20.83×10^{-4} to 126.7×10^{-4} m^3/s in the industrial ladle using the Froude

number similarity criteria for the 160-tonne capacity vacuum tank degasser. Relatively higher flow rates were also considered. Water/steel melt and oil/slag depths are determined based on geometric similarity criteria with the scaling factor (λ=0.1). The water level was varied from 0.220 to 0.280 m and the oil depth was varied from 0.005 to 0.02 m at 0.02 and 0.005 intervals respectively. The thorough set of experimental parameters is summarized in Table 6-2 and 6-3. Table 6-2 shows the experimental conditions used to choose the optimum location for the vibration sensor. The values of experimental inputs used to study the stirring flow rate are shown in Table 6-3.

Table 6-2 Values of experimental parameters the three accelerometer locations

S.N	Layers	Water Depth (m)	Oil Depth (m)	Air Flow Rate(m^3/s)
1	Single	0.15		
2	Single	0.20		
3	Single	0.25		
4	Single	0.30		
5	Double	0.28	0.02	

Table 6-3 Values of experimental parameters for a fixed accelerometer location

S.N	Layers	Water Depth (m)	Oil Depth (m)	Air Flow Rate(m^3/s)
1		0.15		
2		0.20		
3		0.25		
4		0.30		
5		0.22		
6		0.24		
7		0.26		
8		0.28		

6.4 Data Analysis

Vibration data collected at different blowing conditions was first treated with the FFT and then analysed by PCA and PLS. FFT, PCA, and PLS are discussed in the methodology chapter. The analysis started by investigating the data gathered for the selection of the optimum accelerometer placement. PCA was applied to the three variables of the vibration i.e. acceleration along the $x-$,$y-$, and $z-$axis in different frequency ranges. The best sensor position was selected based

on the strength of the underlying structure, accessibility and mounting suitability. Data captured at the nominated sensor location was investigated first by PCA to unveil the underlying structure and then by PLS to find the relationship between latent variables of the blowing parameters and vessel wall accelerations. The overall analysis procedure is similar to the scheme shown in Figure 5-9.

6.5 Result and discussion

6.5.1 Sensor Location

The time-domain vibration signals from the three locations were first compared using the sum of the amplitudes at each sample time. Figure 6-5 shows a comparison of acceleration amplitudes for identical axes for the three locations. It is found that for the same experimental conditions, the amplitudes along two identical axes are not equal.

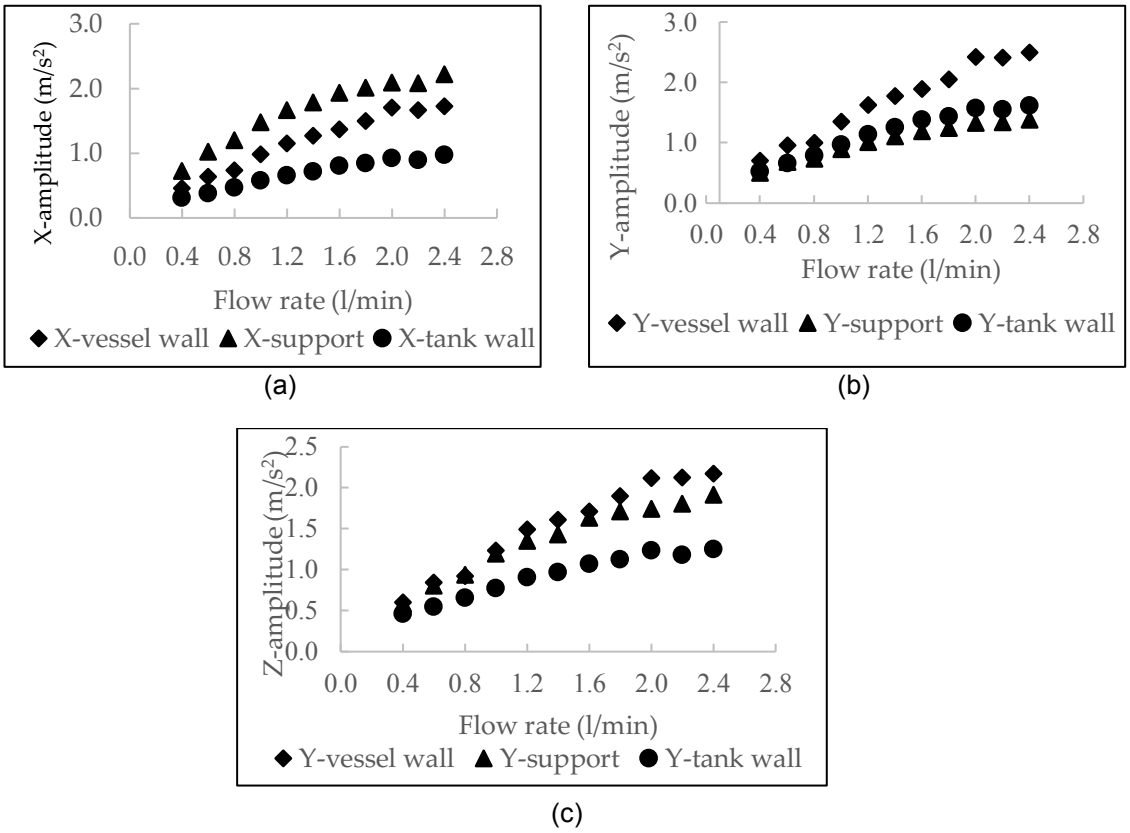

Figure 6-5 Vibration Amplitude versus flow rate for each axes in each location

Furthermore, principal component analysis was carried out to combine the three axes vibration data to see if any structure exists at various frequency ranges. This would allow the comparison

of the underlying relationship among the three candidates. The underlying relationship is explained by the data structure. PCA analysis shows that the structure of the data is high at the three locations and in similar frequency ranges. Table 6-4 shows the values of the first principal components (PC1) and degree of linear correlation coefficients (R^2) in the selected frequency ranges. The linear correlation coefficient (R^2) shows how strongly the flow rate (Q) and latent variable ($PC1$) predict the vibration and stirring energy respectively. They were used to select a frequency range among the highly structured frequency ranges at each location. As can be seen from Table 6-4, the frequency ranges which show better structure and prediction at each location are different but the values of $PC1$ and R^2 do not have a significant difference. Hence, the sensor can be mounted on wall, support or tank as the structure is high in the three positions. This implies that the amount of information of the stirring process of the cold model does not depend on the sensor locations considered in this study. This result is useful in industry in many ways. It simplifies the difficulty of locating the sensor caused by hot components, accessibility and safety issues. In in the lab-scale and plant scales studies, the accelerometer was mounted on the tank external wall near the support. This location is convenient to mount and relatively cooler surface and hence less likely to affect the accelerometer's performance.

Table 6-4 Values ($PC1$) and the degree of correlation (R^2)

Single Layer	**Vessel Wall**		**Vessel support**		**Tank Wall**	
Frequency range (Hz)	30-40		20-30		170-180	
$\boldsymbol{PC1}$	82		99		95	
$\boldsymbol{PC2}$	14		0.5		3	
	(Q, V)	$(PC1, \varepsilon)$	(Q, V)	$(PC1, \varepsilon)$	(Q, V)	$(PC1, \varepsilon)$
$\boldsymbol{R^2}$	0.87	0.88	0.86	0.88	0.89	0.87
Double layer						
Frequency range (Hz)	90-100		90-100		150-160,	
$\boldsymbol{PC1}$	99%		98%		99%	
$\boldsymbol{PC2}$	0.5		1		0.5	
$\boldsymbol{R^2}$	0.95	0.95	0.98	0.98	0.96	0.96

Vibration data was then measured at different stirring conditions such as water height, oil depth and flow rate (shown in Table 6-3) with the accelerometer mounted on the tank external wall

shown in Figure 6-4 (right). The study was undertaken in the absence and presence of the top layer. In the double layer study, the data was subdivided into two volumetric airflow rate ranges. These are 6.67 to 23.33x10^{-6} m^3/sec and 23.3 to 40 x10^{-6} m^3/sec to study the stirring phenomenon in each range on the cold model. The flow rate varied from 6.67 to 40 x10^{-6} m^3/sec during single layer study.

6.5.2 Single Layer Study

Single layer refers to the water bath without oil on the top. Using the parameters in Table 6-3, the air was injected through two nozzles at the bottom to stir the water bath and the corresponding tri-directional wall movement was logged. PCA showed that the single layer data is highly structured. The whole frequency range, as well as most of the small frequency ranges, exhibits this strong structure. In Table 6-4, specific frequency ranges were picked because the data in this frequency ranges show a strong relationship between latent variables and process parameters.

Figure 6-6 shows the relationship between the first latent variable, which is a combination of the three axes vibration, and the stirring power for two frequency ranges. The stirring power is a function of the flow rate and bath volume. In Figure 6-6b, the relationship shows that though the 150 to 160 Hz is highly structured frequency range, its correlation with the string energy is not strong for the single layer bubbling. The total variance explained by each principal component (PC) is shown in Table 6-5.

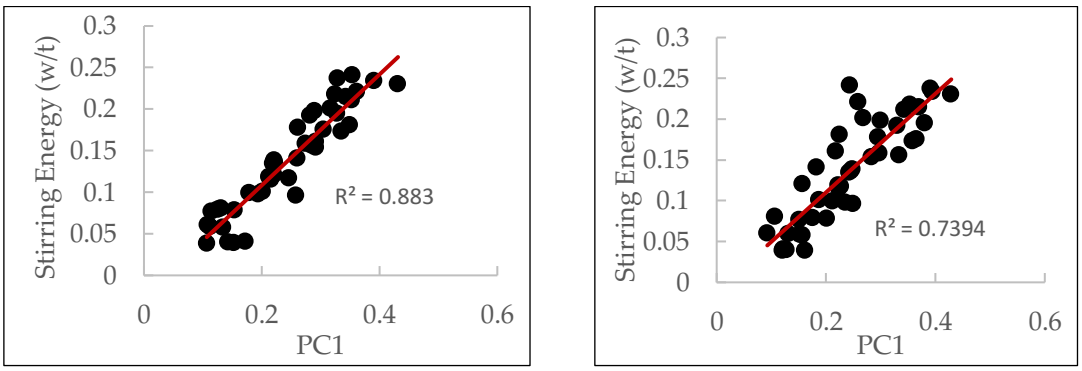

(a) (b)

Figure 6-6 Relationship between PC1 and stirring energy in the frequency range of a) 170 to 180 Hz b) 150 to 160 Hz

For the frequency range of 170 to 180 Hz, the contribution of each variable to the total variance in each PC is obtained from the loading vectors in Table 6-5. Equation 6-1 shows that the variation

explained by PC1 comes proportionally from the variation in x, y and z. The percentage variation of the system explained by x, y, and z accelerations in the single layer is 38%, 32% and 30 % respectively

Table 6-5 Values of loading vectors and PC for the single layer blowing data

Score	**Loading vector**		
x	0.65	0.72	-0.25
y	0.55	-0.22	0.80
z	0.52	-0.66	-0.54
Eigen value	0.0078	0.00037	0.00017
Variance (PC)	94	4	2

$$PC1 = 0.65x + 0.55y + 0.52z \quad (6\text{-}1)$$

6.5.3 Double Layer Study

The double layer refers to a water bath with a top layer/oil on it. Air was injected into the water-oil bath through dual sidewall nozzles located at the bottom. The amount of volumetric air flow rate was identical for each nozzle. Two airflow rate ranges were studied independently. In each flow rate range, the water depth and oil depth were varied according to Table 6-3 at an increment of 0.02 and 0.005 m respectively. Vibration datasets were analysed first by PCA to find the hidden structure in specific frequency ranges and then by PLS to unveil the linear relationship and construct a linear prediction model.

a) *Flow rate range: $6.67x10^{-6}$ to $16.67\ x10^{-6}$ m^3/s*

The tri-axis acceleration data captured from the steel-walled cold model in this volumetric airflow rate range was treated first by FFT to transform the time domain signal to a spectral form. To unveil the structure in the data, PCA was applied to the whole dataset. The structure explains how much variation is explained by the principal components (PCs) or latent variables, which each are a linear combination of the signals in the three axes. It was found that the whole frequency range has a strong structure.

The loading vector in Table 6-6 shows that the total variation in PC1 has equal contributions from the variation in x, y and z data.

In addition, the whole frequency range was subdivided into smaller ranges and analysed using PCA. The objective was to find the small frequency range where the structure concentrates. Industrial data is noisy and taking the full frequency range has a greater chance of including other sources of vibration, which may result in weakening the efficiency of the vibration-based online monitoring system. A small frequency range would prevent this from happening.

Table 6-6 Values of loading vectors and PC for the double layer blowing data

Score	**Loading vector**		
x	0.57	-0.41	0.71
y	0.577327	-0.41258	-0.70
z	0.58	0.812	0.002
Eigen value	0.00223	1.41E-05	5.07E-06
Variance (PC)	99	0.6	0.4

Table 6-7 PC1 values of small frequency ranges

Frequency range (Hz)	0 to 10	10 to 20	20 to 30	30 to 40	40 to 50
PC1 (%)	94.41	82.40	75.10	86.50	99.33
Frequency range (Hz)	50 to 60	60 to70	70 to 80	80 to 90	90 to 100
PC1 (%)	98.87	96.12	97.74	99.10	91.63
Frequency range (Hz)	100 to110	110 to120	120 to130	130 to 140	140 to 150
PC1 (%)	90.61	94.44	95.22	92.80	97.88
Frequency range (Hz)	150 to 160	160 to 170	170 to 180	180 to 190	190 to 200
PC1 (%)	97.95	93.69	95.63	94.15	94.47
Frequency range (Hz)	200 to210	210 to 220	220 to 230	230 to 240	240 to 250
PC1 (%)	89.04	88.20	92.57	86.24	92.14
Frequency range (Hz)	250 to 260	260 to 270	270 to 280	280 to 290	290 to 300
PC1 (%)	77.25	78.03	87.57	72.16	85.98

Table 6-7 shows that most of the small frequency ranges are highly structured. On the other hand, the linear relationship between the first latent variable (PC1) and the stirring power was found

to be poor especially if both the top and bottom layers were varying. Figure 6-7 shows that the frequency range 40 to 50 Hz, though it has the high structure (PC1=99 %), its linear relationship with the stirring power is not strong. This procedure was repeated for the highly structured frequency ranges shown in Table 6-6 and similar results were obtained.

Table 6-8 Values of PCVAR of different frequency ranges

Frequency range (Hz)	PCVAR1 (%)		Total PCVAR (%)	
	Y	X	Y	X
0 to 10	14	33	17	100
40 to 50	47	33	47.1	100
50 to 60	68.5	33	69	100
60 to 70	79	33	80	100
70 to 80	89	33	90	100
80 to 90	91	33	91.5	100
90 to 100	82	33	86	100
100 to 110	72	33	77	100
110 to 120	76	33	79	100
120 to 130	78	33	79	100
130 to 140	70	33	71	100
140 150	78	33	79	100
150 to 160	79.5	33	79.5	100
160 to 170	78	33	80	100
170 to 180	64	33	64	100
180 to 190	67	33	68	100
190 to 200	66.5	33	68	100
220 to 230	74	33	77	100
240 to 250	72.5	33	75	100

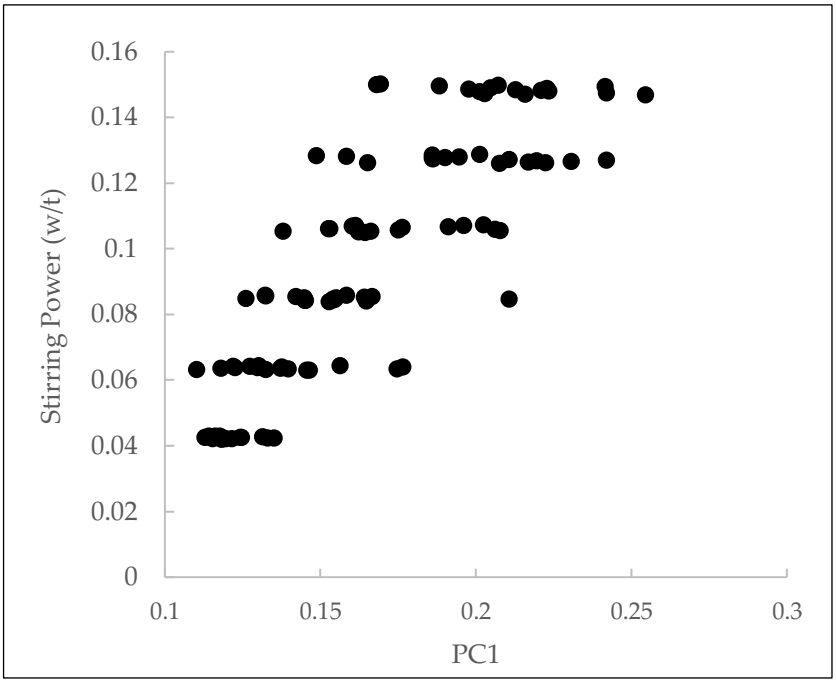

Figure 6-7 Relationship between stirring power and PC1 in the range of 40 to 50 Hz

To alleviate this problem, partial least square regression was applied. This technique deals with the variation in the three process parameters (regarded as the input matrix) and three accelerations (regarded as the output matrix) simultaneously to unveil a common structure. In Table 6-8 PCVAR refers to the percent of variation and PCVAR1 refers to the amount of variation explained by the first latent variable of PLS analysis. X and Y are matrices containing the input (flow rate and bath levels) and output (vibration) parameters. Table 6-8 shows that in the frequency ranges of 70 to 80 and 80 to 90 Hz three latent variables explain most of the linear variation in the stirring process. Though PCA results showed that most of the frequency ranges of the vibration data have maximum structure, PLS showed that the hidden linear relationship between input parameters and wall vibration is best explained in specific frequency ranges. Figure 6-8 and 6-9 show how the input variable X can predict the output variable Y in the frequency range of 80 to 90 Hz and 70 to 80 Hz respectively. In an industrial scenario, Y_{score} which is the linear combination of the three axes vibration signals, can be measured but X_{score} which is the linear combination of the process parameters, is difficult to measure. Thus, Y_{score} can be used to predict the process parameters especially the volumetric gas flow rate.

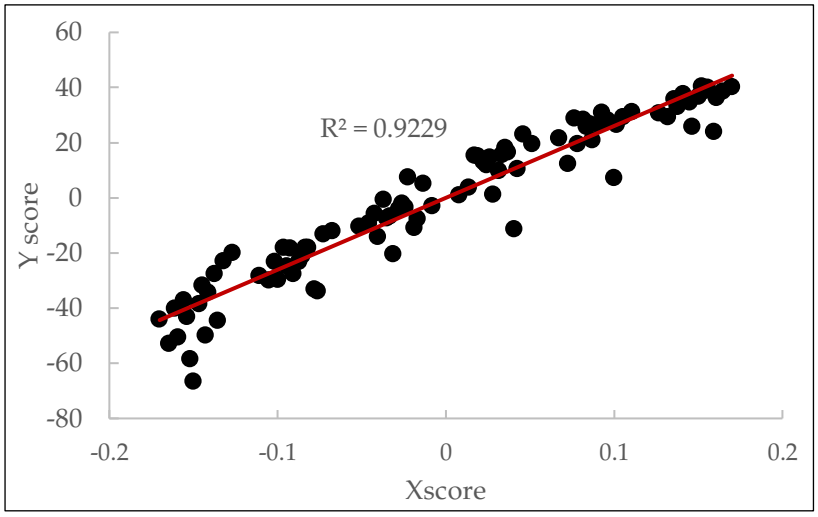

Figure 6-8 Relationship between response scores (Y) and predictor scores (X) in 80 to 90 Hz

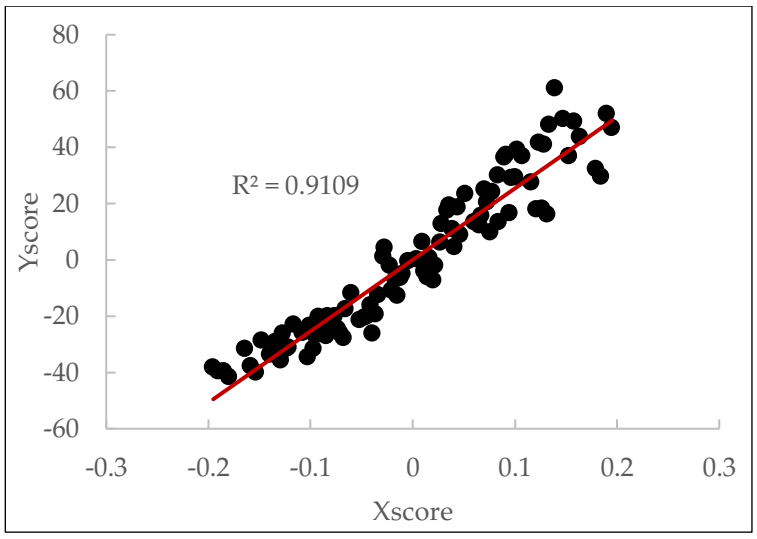

Figure 6-9 Relationship between response scores (Y) and predictor scores (X) in 70 to 80 Hz

To observe how the first latent variable of the vibration data predicts the amount and energy of agitation, the Y_{score} was correlated with bath recirculation speed (U) and stirring power (ε). Figure 6-10 and 6-11 shows these correlations. Figure 6-10 indicates that the speed of melt circulation can be estimated by measuring wall vibration. Figure 6-11 shows that the amount of energy imparted by the purged gas per unit time can be evaluated using the vibration signal along the three axes coming from the wall.

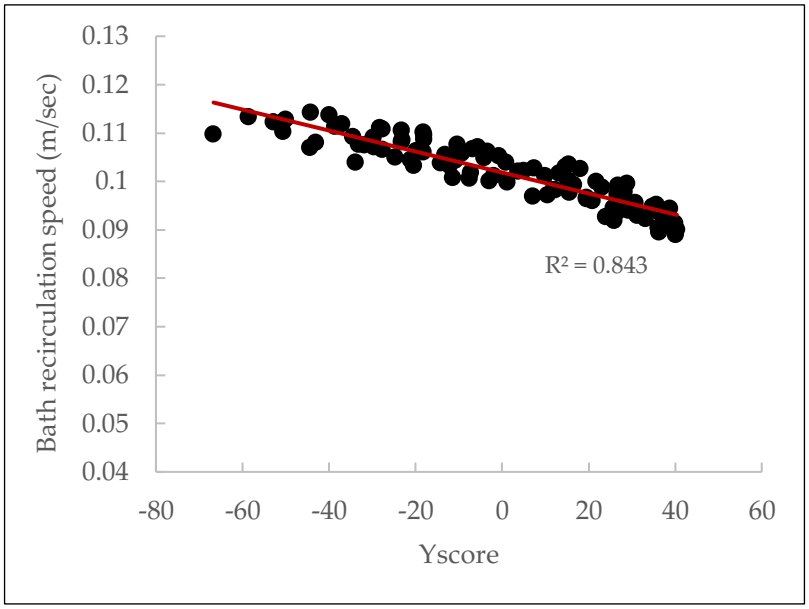

Figure 6-10 Relationship between bath recirculation speed and Y_{score}

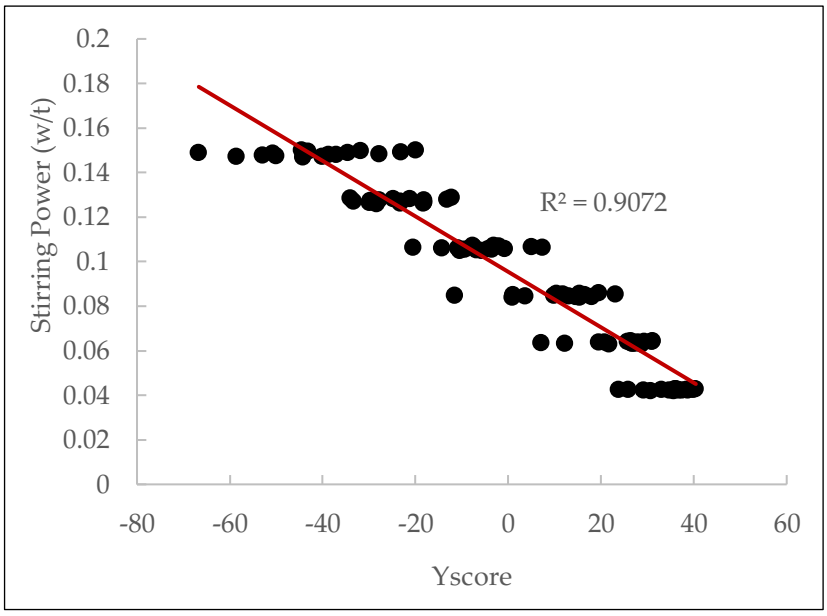

Figure 6-11 Relationship between stirring power and Y_{score}

The aim of PLS is to develop a predictive model like Equation 6-2 of the stirring status using vibration signal. In Equation 6-2 X is the predictor, β is regression coefficient and Y_{res} is the residual data.

$$Y = \beta X + Y_{res} \qquad 6\text{-}2$$

The values of regression coefficient, β, are shown in Table 6-9. This shows the change in the output variable,Y is largely contributed to the quantity adjustment of the flow rate.

The accuracy of prediction can be influenced by the number of latent variables taken. Figure 6-12 shows that in PLS analysis, the error generated when using a different number of latent variables for the vibration data. This, in turn, affects the prediction of gas flow rate using Equation 6-2. The minimum deviation or residual data is achieved when three latent variables are used.

Table 6-9 Values of β for the frequency range of 80 to 90 Hz

Parameter	Coefficients(β)		
H	0.024	0.081	0.063
h	0.08797	0.107641	0.090
Q	0.945	0.939	0.965

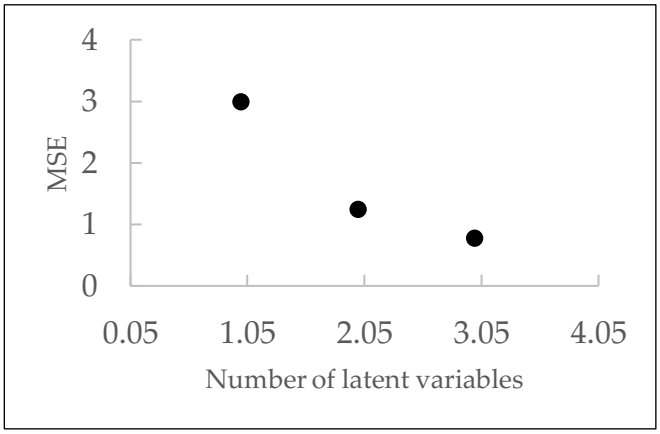

Figure 6-12 Mean square root error (MSE) and number of variables taken

b) Flow rate: 23.33 to 40x10^{-6} m^3/sec

The analysis procedure of the vibration data captured in this flow rate range was similar to the previous volumetric flow rate range study. The vibration data at the different top and bottom layer depths were measured when the water-oil bath was stirred by varying the volumetric airflow rate. Figure 6-13 shows that there is no linear relationship between the first latent variable, PC1, and the stirring power for vibration data obtained from double layer experiment. The values

of the first principal components at various frequency ranges for the double layer experiment are shown in Table 6-10.

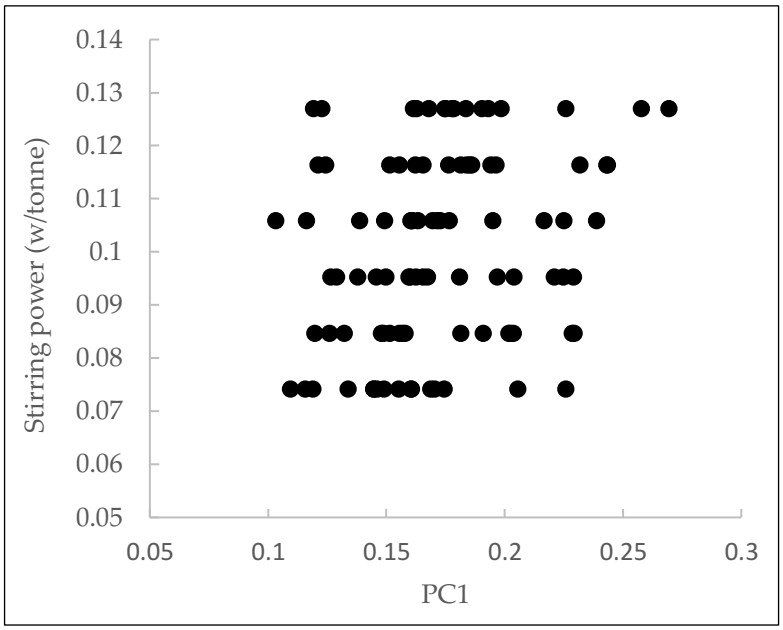

Figure 6-13 Relationship between stirring power and PC1 in the frequency range of 50 to 60 Hz

Table 6-10 Values of PC1 for 23.33 to 40x10^{-6} m^3/sec

Frequency range (Hz)	0 to 10	10 to 20	20 to 30	30 to 40	40 to 50
PC1	84.38	80.11	67.50	74.40	99.19
Frequency range (Hz)	50 to 60	60 to 70	70 to 80	80 to 90	90 to 100
PC1	98.14	82.85	89.19	92.24	57.21
Frequency range (Hz)	100 to 110	110 to 120	120 to 130	130 to 140	140 to 150
PC1	65.52	81.47	86.22	80.23	91.28
Frequency range (Hz)	150 to 160	160 to 170	170 to 180	180 to 190	190 to 200
PC1	91.05	73.43	86.45	82.31	79.02
Frequency range (Hz)	200 to 210	210 to 220	220 to 230	230 to 240	240 to 250
PC1	70.86	79.75	85.78	93.44	80.34
Frequency range (Hz)	310 to 320	320 to 230	330 to 340	340 to 350	350 to 360
PC1	70.86	75.8	88.4	92.2	81.03

Table 6-11 shows that the percentage of variance explained in Y (vibration data) by the three PLS components (total PCVAR) is higher for the frequency range of 340 to 350 Hz than the other frequency ranges. Hence, this frequency range explains the maximum common structure between stirring process parameters and the vibration signal when both layers are varied.

Table 6-11 Values of PCVAR for different frequency ranges

Frequency range (Hz)	PCVAR1 (%)		Total PCVAR (%)	
	Y	X	Y	X
40 to 50	31.7	33.3	32	100
50 to 60	47.7	33.3	48	100
60 to 70	19.6	33.3	26.5	100
70 to 80	44	33.3	47.5	100
80 to 90	40.5	33.3	43	100
120 to 130	38	33.3	43	100
140 to 150	60	33.3	62	100
150 to 160	51	33.3	52	100
170 to 180	51.5	33.3	53	100
180 to 190	44	33.3	49	100
220 to 230	56	33.3	59	100
230 to 240	73	33.3	74	100
240 to 250	58	33.3	69	100
310-320	67	33.3	69	100
320-330	78	33.3	79	100
330-340	73.5	33.3	74.5	100
340 to 350	79.6	33.3	80.5	100

In this frequency range, the correlation between vibration and stirring process parameters scores were found to be strong. This is shown in Figure 6-14. Each score is a linear combination of its respective three variables i.e. the input or the output variables. Table 6-12 contains the values of regression coefficient, which indicates most of the vibration is caused by the gas flow rate.

In the PLS regression model given by Equation 6-2, the regression coefficients for the input parameters shown in Table 6-12 shows that majority of the vibration response is contributed from the airflow rate. To examine the difference between the measured vibration and the vibration predicted using Equation 6-2, a new set of stirring parameters were used and the respective

vibration amplitude was computed. The new set of inputs used to test the model consists of the following parameters:

- a constant water depth of 0.24 m
- an oil thickness that varies from 0.005 to 0.02 m and
- a volumetric airflow rate that increases from 41.67 to 83.33x10^{-6} m^3/sec

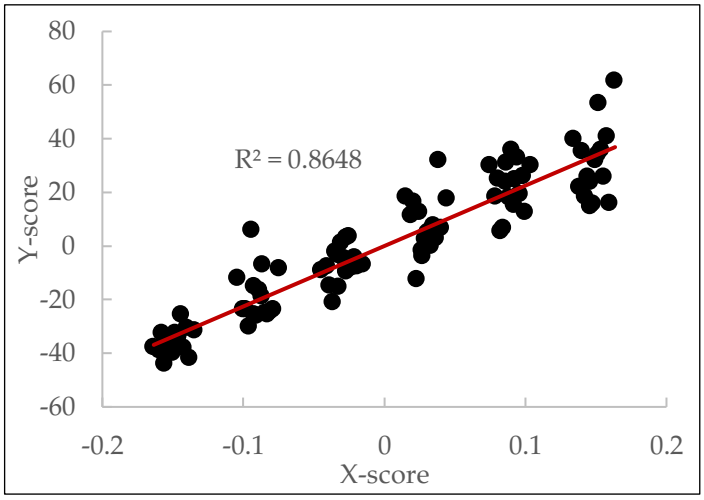

Figure 6-14 Relationship between X and Y-scores in the frequency range of 340 to 350 Hz

Figure 6-15 shows that the predicted and measured vibration signals are almost equivalent with an average deviation of 10 % in each axis. This shows that the measured vibration from the ladle wall can predict the stirring power and bath recirculation speed with some tolerable error, which are functions of flow rate, and bath volume.

Table 6-12 Values regression coefficient, β

X	Coefficients		
H	-0.044	-0.211	0.074
h	0.026	-0.0819	-0.063
Q	0.911	0.827	0.919

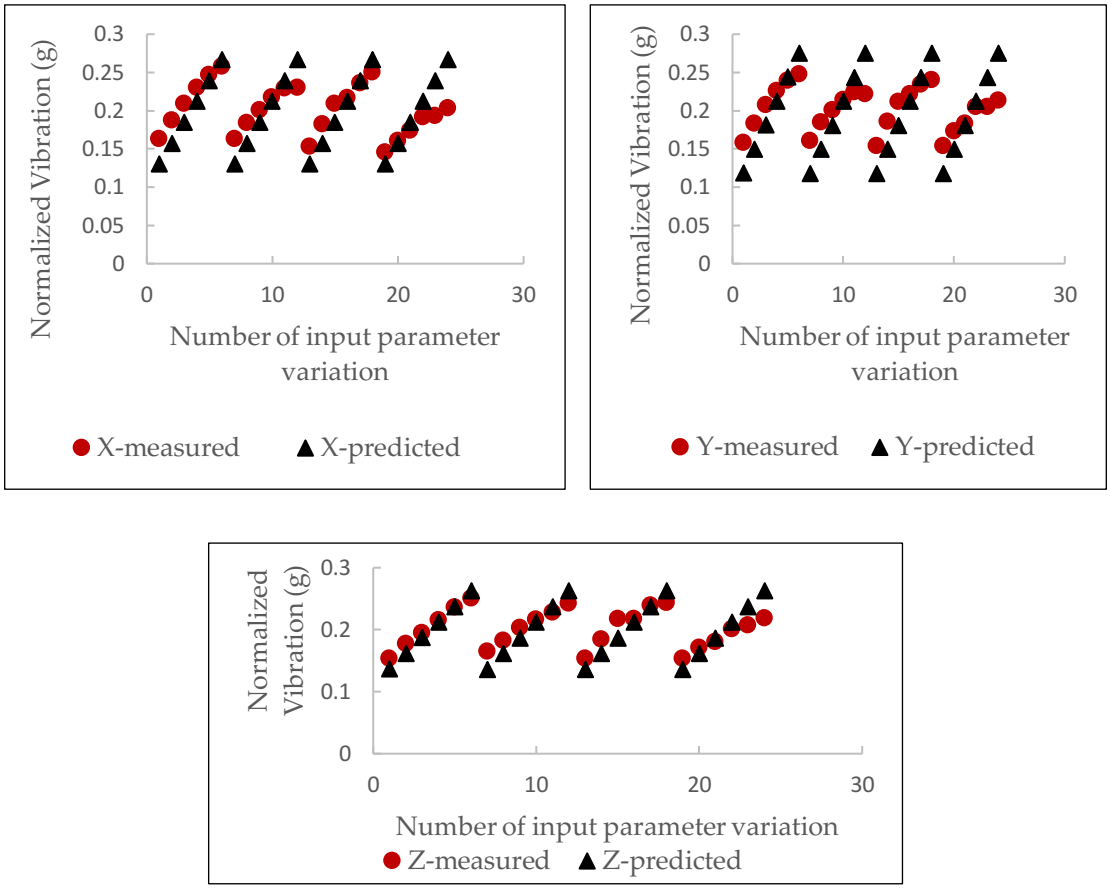

Figure 6-15 Comparison between measured and predicted vibration signals (cross validation)

c) Flow rate:(41.67 to 83.33)x10-6 m3/s

The flow rate in the steel walled cold model was varied from 41.67 x10^{-6} to 83.33x10^{-6} m^3/s. This flow rate range corresponds to 131.67 to 263. 33 x10^{-6} m^3/sec in the industrial scale.

Table 6-13 PC1 values for the flow range of 41.67 to 83.33x10^{-6} m^3/sec

Frequency range (Hz)	0 to 10	10 to 20	20 to 30	30 to 40	40 to 50
PC1	83.86	71.53	79.48	87.07	99.80
Frequency range (Hz)	50 to 60	60 to 70	70 to 80	80 to 90	90 to 100
PC1	99.42	93.78	78.08	96.15	95.40
Frequency range (Hz)	100 to 110	110 to 120	120 to 130	130 to 140	140 to 150
PC1	93.62	99.21	87.54	92.83	96.79
Frequency range (Hz)	150 to 160	160 to 170	170 to 180	180 to 190	190 to 200
PC1	84.17	85.96	96.55	96.01	90.70
Frequency range (Hz)	200 to 210	210 to 220	220 to 230	230 to 240	240 to 250
PC1	93.83	95.23	90.35	68.50	65.19

The vibration signal was measured for a fixed water height of 0.24 m and varying oil depth from 0.005 to 0.020 m. As ladle operations usually have a constant liquid metal depth, this assumption was reasonable. The smaller frequency ranges of the vibration signal with their respective first principal component (PC1) are shown in Table 6-13. There are few frequency ranges that can describe the majority of the structure in the data. However, similar to the findings in the previous sections, the linear relationship was not strong. PLS was applied taking two of the process parameters and vibration data as output and input matrices.

Table 6-14 Values of PCVAR in the flow rate range of 41.67 to 83.33x10^{-6} m^3/sec

Frequency range (Hz)	PCVAR1 (%)		Total PCVAR (%)	
	Y	X	Y	X
50 to 60	99.4	22	0.5	79
80 to 90	96	36	100	74
130 to 140	93	87	100	92
180 to 190	90	76	100	94
190 to 200	90	90	100	92
200 to 210	94	91	1	92
210 to 220	95.5	94	100	96

PLS analysis identified certain informative frequency ranges that best explain the variation in vibration as well as the stirring parameters simultaneously in these flow rates. These frequency ranges are shown in Table 6-14. In Table 6-14, Y is a matrix of the flow rate and working fluid depths whereas X consists the vibration signals. The frequency range 210 to 220 Hz is highly informative and can be used to predict the gas flow rate using the PLS model in Equation 6-2.

6.5.4 Peak Frequencies

Frequencies with maximum amplitude may indicate intensified stirring status[10] but in this investigation, they have not been found to significantly affect the overall stirring process variation. The peak frequencies of the three axes were computed for data where only oil depth varied. The results show that peak frequencies computed from the $x-$, $y-$ and z-axes do not vary much with the oil depth. Frequencies along the $y-$axis are higher than the other axes.

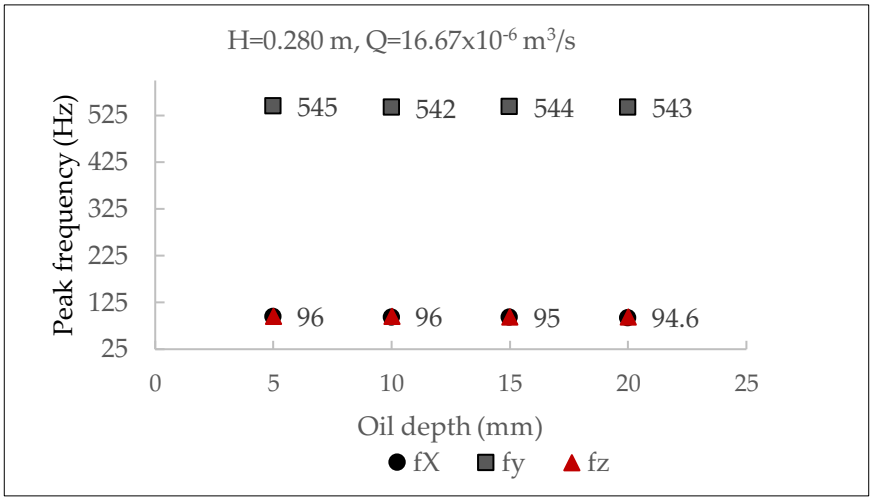

Figure 6-16 Peak frequencies in the three axes

Figure 6-16 shows the peak frequencies as a function of oil/slag depth. This trend is similar when the water level and airflow rate are varied.

6.6 Conclusion

The study of the physical cold model of a bottom purged Vacuum Tank Degasser (VTD) discovered several findings that can improve and simplify the online monitoring of the low flow rate-stirring problem. This study was focused first on analyzing the effect of the accelerometer location on the amount of stirring information that can be harnessed. Three main locations were taken in this investigation. These were the ladle external wall, the ladle support and the exterior wall of the tank. Vibration data captured from each position was analysed using PCA to find the quantity of information present per dataset and then select the optimum location. Vibration signals were then measured at different bubbling rates with and without the top layer. PCA and PLS were applied in order to find the structure of the vibration data and the correlation between stirring process parameters respectively.

The investigation on optimum accelerometer location unveiled that the amplitude information harnessed from the three sensor positions considered in this study were not significantly different but the informative frequency ranges were different. Hence, placing the accelerometer on the tank external wall near the ladle supports can give the desired vibration signals. This result is valuable in the industry in many ways; it simplifies the difficulty of locating the sensor caused by temperature and accessibility and safety issues.

In general, this study was able to detect stirring using three-dimensional vibrations in the laboratory cold model. The detected vibration signals have a strong linear correlation with the stirring indicators like stirring power and bath recirculation speed. It was found that the combined vibration signal can predict the stirring power and recirculation speed effectively for the studied experimental conditions. In addition, specific frequency ranges that contain the majority of the variation in the vibration data were identified for each flow rate range considered.

Furthermore, both in the single and double layer vibration data, the overall variation was contributed equally from x, y and z axes. Thus, it can be concluded that measuring vibration from the three axes is advantageous. This result was also displayed during the plastic-walled cold model study.

Finally, to verify the results of this investigation, an additional study was carried out at an industrial scale for the same VTD capacity and configuration. This is described in the following chapter.

7 Plant Scale Study: The Case of Vacuum Tank Degasser

7.1 Introduction

In this chapter, an industrial trial carried out at Tata Steel UK to supplement the cold model studies as described. The trial was carried out for a ladle in a vacuum tank degassing (VTD) plant. A sketch of this VTD is shown in Figure 7-1.Vibration measurement was undertaken at various working conditions and data was analysed by principal component analysis and partial least square regression.

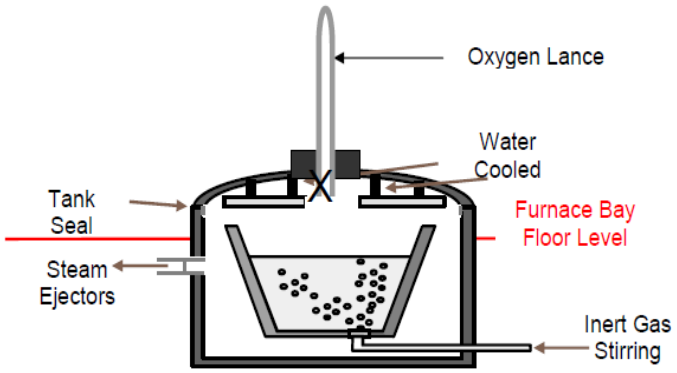

Figure 7-1 Schematic diagram of vacuum tank degasser

Vacuum degassing of steel is carried out after the molten steel has left the furnace and before the steel is poured into ingots or processed through a caster. A vacuum tank degassing (VTD) plant is frequently used to produce steel grades with the best quality. A ladle containing the liquid steel melt is placed in a vacuum tank and is treated in a low-pressure environment below 1.33 KPa. Due to the equilibrium conditions under vacuum, unwanted elements dissolved in liquid steel such as nitrogen, hydrogen, and sulfur can be removed. A pressurized stirring gas (normally argon) is injected from the bottom to guarantee the necessary mixing of the liquid metal and to facilitate the refining reactions.

The adjustment of the stirring intensity is usually difficult due to leakage and other various reasons discussed in the literature review section. To address these issues further, a physical cold model of a VTD was studied and described in Chapter 6. This chapter outlines a continuation of the study carried out on the steel-walled physical cold model. The work in this chapter is a study on an actual 160-tonne Vacuum Tank Degasser (VTD) to investigate the bottom gas stirring of the ladle in the VTD using tri-axes vibration signals. In the cold model study, investigation of

vibration data found that the data is highly structured. In certain frequency ranges, there is a relationship between the stirring indicators and the latent variables of the vibration data. This study was aimed at investigating the stirring phenomena at an industrial scale. This was essential to verify the results found in the cold model study.

The collection, noise filtering, and analysis of the plant vibration data are described in different sections of this chapter.

7.2 Experimental Setup

The VTD process at Tata Steel UK is characterized by a ladle bottom diameter of 3.02 m, a heat weight of 140 to 160 tonne and melt temperature of 1873K. The porous plugs are in the circle of radius 1 m at the angle of~ 48^o. Figure 7-2 shows the major dimensions of a ladle of the VTD. The data for this experiment was gathered from this reactor.

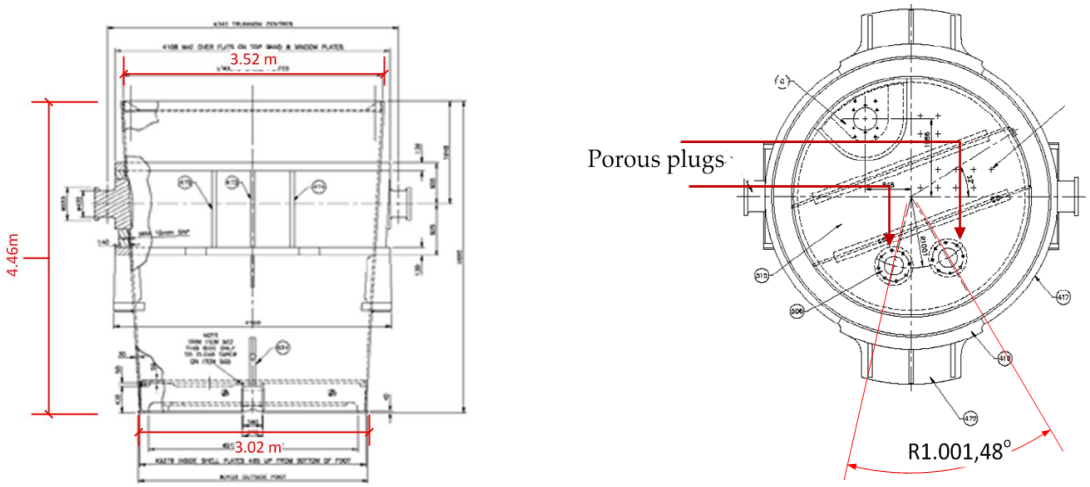

(a) (b)

Figure 7-2 Sketch of a ladle in the VTD: a) overall dimension b) porous plug position

In the cold model study of the VTD, it was found that the amount of information collected from the ladle wall, ladle support and tank external wall was similar. Hence, in this industrial study, the accelerometer was installed on the tank external wall 1.7 m from the base of the tank. Figure 7-3 shows the position of the accelerometers, ladle configuration, and overall setup. The vibration sensor was a piezoelectric ICP Accelerometers and its detail specification is found in the methodology chapter section 4.2.1.

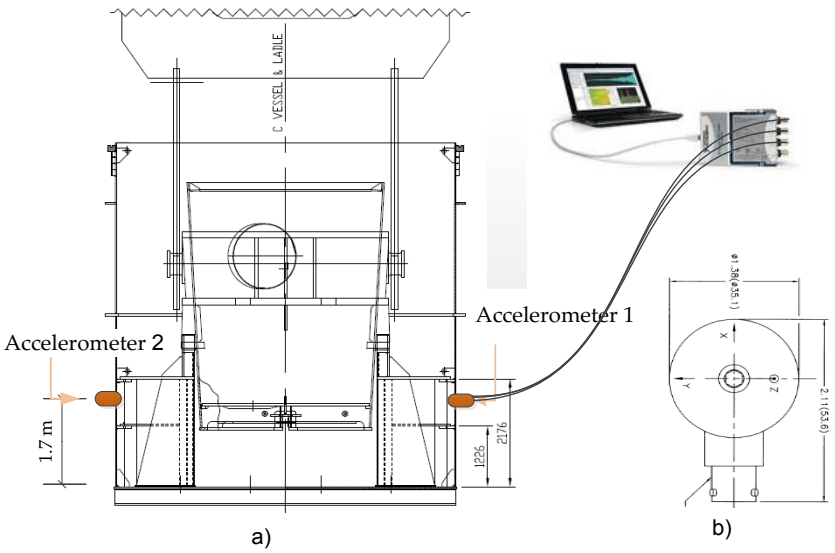

Figure 7-3 a) Data acquisition setup in the plant and b) accelerometer orientation

7.3 Experimental Conditions

Argon gas was injected through two sidewall porous plugs at the bottom of a 160-tonne ladle. During the plant vibration measurement, the amount of metal and slag, plug life, plug position, barrel life and slag line life were different in each of the heats. One heat corresponds to one ladle operation. The barrel and slagline are distinct parts of the ladle lining. The slagline is a slightly thicker lined part of the lining at the height where the steelmaking slag is going to be in contact with it. This wears more rapidly than the ladle lining below the slag line, which is known as the barrel. The numbers of barrel and slag line lives are simply the number of heats that have been in contact with the ladle slagline and barrel since they were installed. It is common to see a barrel life in excess of the slagline life, as the slagline can be replaced independently of the barrel. A ladle of barrel life number 16 to 21 and slagline number 1 to 4 were used during the data collection. The steel weight generally varied from 130 to 150 tonnes while the slag weight was between 1.8 and 3.6 tonnes. Some heats were carried out with new porous plugs and others with old plugs that served two to four heats. The volumetric gas flow rate generally varied from (583.33 to 16650) $x10^{-6}$ m^3/s. For a single ladle operation, only the gas flow rate was assumed to vary throughout the stirring process.

7.4 Data Collection

Vibration data logging started and finished immediately after the ladle was placed on and was lifted from the supports respectively. The starting and finishing time was recorded for each heat

considered. Background noise was also measured in different circumstances when the vacuum degasser was not running. The main purpose was to analyse the background noise signal separately in order to understand how it affects the main signal's strength.

Vibration data was captured from 18 heats but due to incomplete supplementary information, only data from eight heats were used in the study. A list of the heat and the corresponding information required is listed Table 7-1. A complete heat information refers to the heat that has time, flow rate, pressure and logging time information. The logging start time is the exact time the sensor/data logger started recording. This was required to locate the useful vibration data from the signal's time history. Table 7-2 shows the values of various parameters for each heat during vibration measurement. This data helped to create different datasets that explain various heating scenarios.

Table 7-1 List of measured heat and related information availability

S.N	Heat ID	Complete Heat information	Logging start time
1	T0552Z	Available	Not available
2	T0553Z	Available	Not available
3	T0560Z	Available	Available
4	T0561Z	Available	Available
5	T0565Z	Available	Available
6	T0566Z	Available	Available
7	T0569Z	Available	Available
8	T0571Z	Available	Available
9	T0573Z	Available	Available
10	T0574Z	Available	Available
11	T0577Z	Available	Not available
12	T0578Z	Available	Not available
13	T0655Z	Not available	Available
14	T0662Z	Not available	Available
15	T0668Z	Not available	Available
16	T0671Z	Not available	Available
17	T0698Z	Not available	Available
18	T0709Z	Not available	Available

Table 7-2 Heats with respective parameter values

Heat ID	Ladle ID	Steel Weight (kg)	slag weight	Ladle Plug	Barrel Life	Slagline Life	Plug Life	Ladle Tare
T0560Z	16	146840	2803	2	16	4	3	77.6T
T0561Z	19	145881	1814	2	19	1	1	77.1T
T0565Z	21	136681	4842	3	21	1	1	79T
T0566Z	19	135261	3366	2	19	2	2	79.6T
T0569Z	19	147995	1853	2	19	3	3	80.5T
T0571Z	21	129166	3591	3	21	2	1	79T
T0573Z	19	140869	2072	2	19	4	4	80.4T
T0574Z	4	154295	1874	2	4	1	1	79.9T

7.5 Signal Treatment and Refining

In the VTD, the ladle is equipped with a porous plug at its bottom to purge argon gas and is placed in a vacuum tank. The vacuum is created through a vacuum pumping system. Vacuum pump system is the motive power for the vacuum degassing processes for the liquid steel. Pressure is often kept below 0.5 KPa for efficient degassing.[62] Hence, purging of argon begins when the pressure reaches this value.

Vibration data that corresponds to a stirring at or below 0.5 kPa of pressure was first separated out from each heat. Then, the data was arranged in a way that the flow rate is in an increasing order. During a ladle heat, the steel weight and slag depth are assumed constant. Figure 7-4 shows the pressure-time profile during argon injection. This profile help identify the duration of time where bubbling gas flows below the desired pressure i.e. 0.5 kPa. During each heat, the pressure was brought to a value less than 10 mbar for the actual stirring to commence. Three sample datasets were taken for analysis to compare the results and the most repeatable outcome was taken to describe the process

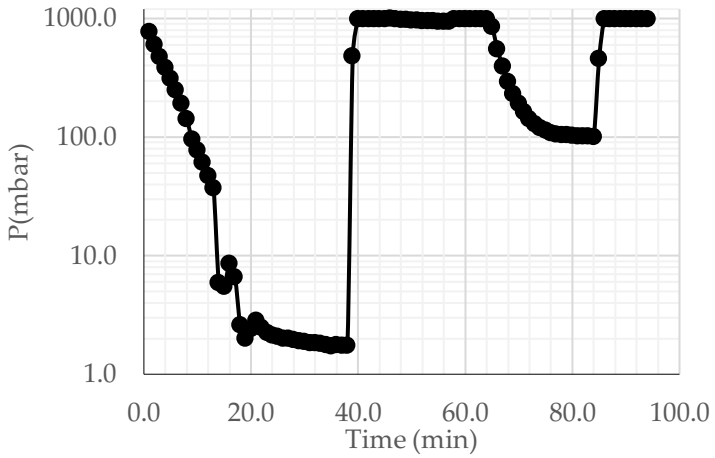

Figure 7-4 Pressure profile for part of T0560Z heat

7.6 Background Noise

While the degassing process was running, there were other sources of vibration viz. overhead crane, ladle furnace etc. The vibration signal coming out from these sources need to be filtered out to minimize its effect on the result of the plant trial. Short-time Fourier Transform (STFT) was applied to treat the noise signal.

The Short Time Fourier Transform (STFT) is a Fourier-related transform that can convert a non-stationary one-dimensional time signal to the two-dimensional frequency-time domain. This technique was applied here to identify the frequency band where the power of the noise is concentrated. There were various sources of background noise during vibration measurement of the vacuum degasser.

Noticeable vibration sources that come from crane movement and nearby ladle furnaces are considered as significant vibration sources. By applying STFT on signals measured for these phenomena only, the frequency ranges where the power of these noise signals can be identified. Figure 7-5 illustrates the frequency-time graph of a vibration signal when the ladle furnace was running but the vacuum degasser had not started. In the $x-axis$, the power of the noise is concentrated between 0 and 50 Hz as it is indicated by enclosed boxes. This distributed power is also seen in the other $y-$ and $z-$axes. In the $y-axis$ the frequency range 220 to 250 Hz shows higher power values. In the $z-axis$ the power of the noise is distributed between 500 to 550 Hz, and 700 to 800 Hz. Therefore, to minimize the effect of these noise signals in the analysis, these signals within these frequency ranges were disregarded. In addition, to capture essential patterns

and improve the signal to noise ratio without greatly destroying the signal, the plant data was smoothed using the Savitzky-Golay filter (S-G filter). After the signal is filtered and smoothed, the analysis started by determining the minimum sample time.

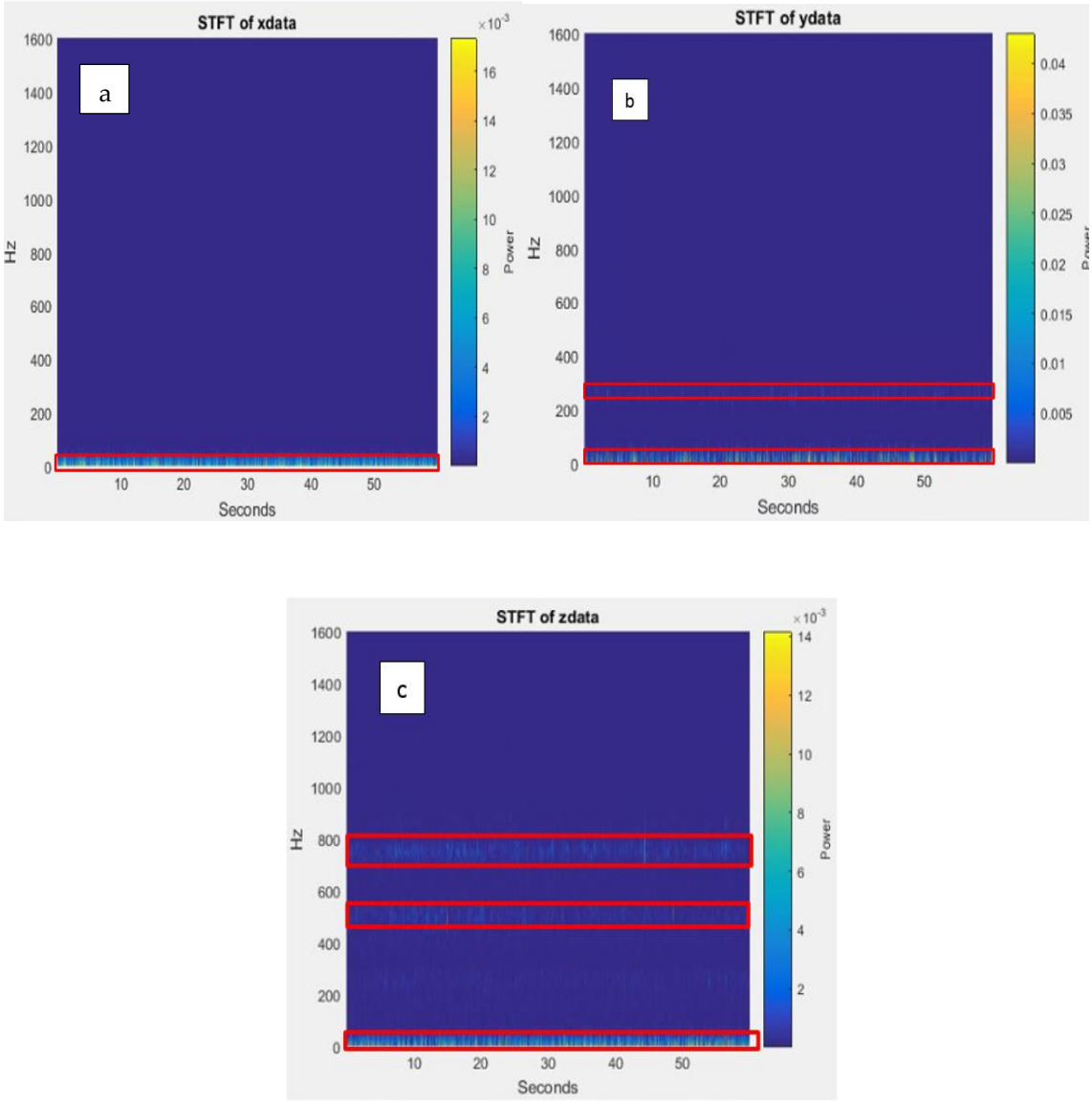

Figure 7-5 STFT of background noise: a) x-axis, b) y-axis, and c) z-axis

7.7 Sample Time Determination

In a similar manner to the cold model studies, the minimum sample time for plant data needs to be determined. This sample time was determined for a constant gas flow rate. During the vacuum degassing process, the flow rate of argon remains constant for a minimum of 60 seconds. This

was observed from the collected data. Hence, the 60 seconds was taken as an initial value for computing the smallest sample time. First, a one-minute time history was observed. As it can be seen from Figure 7-6, the time history of the three axes may not indicate how long the minimum sample time should be.

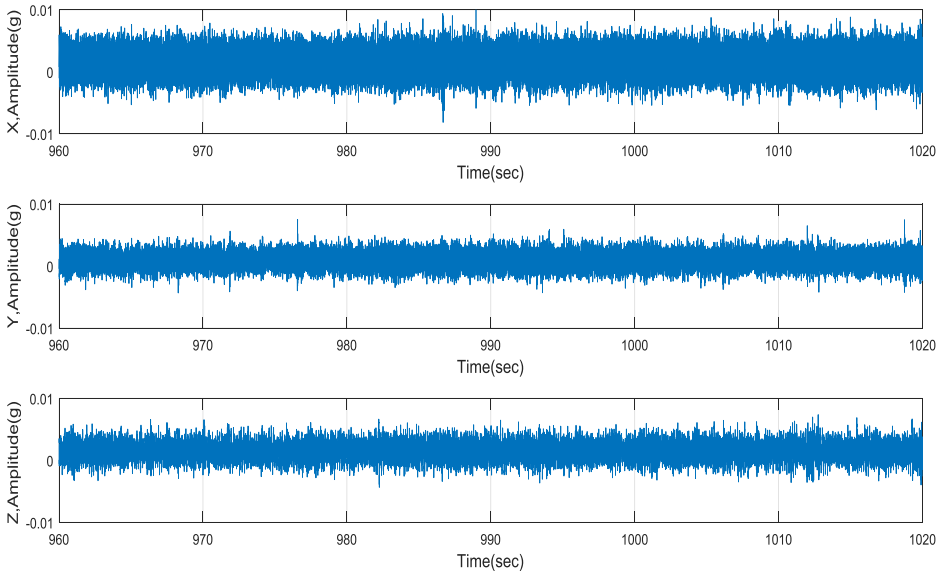

Figure 7-6 Vibration time history for a time length 60 seconds

The procedure for determining the sample time is similar to the water model study. The one-minute vibration data of each heat was divided into small parts and then the spectrum of each compartment was observed. The divisions, which show similar frequency-amplitude plots, were taken as a minimum sample time. The vibration time history of 60 seconds was subdivided into 2, 3, 4, 6 and 12 parts at a time. The time lengths of these divisions correspond to 30, 20, 15, 10 and 5 seconds respectively. Applying the Fast Fourier Transform on each part, the frequency spectra were observed. When a sample time of 15 seconds was considered, the frequency spectra of the four parts are not similar to each other. Figure 7-7 is the frequency spectra of the x-axis signal with 15-second sample time. The spectral variations of the amplitudes show better similarity when a 20-second sample time is taken than the other sample times. The corresponding spectra for 20-second samples are shown in Figures 7-8 to 7-10 $x-$, $y-$ and $z-$ axes data respectively. Hence, 20 seconds was taken as a sample time for the entire plant data analysis.

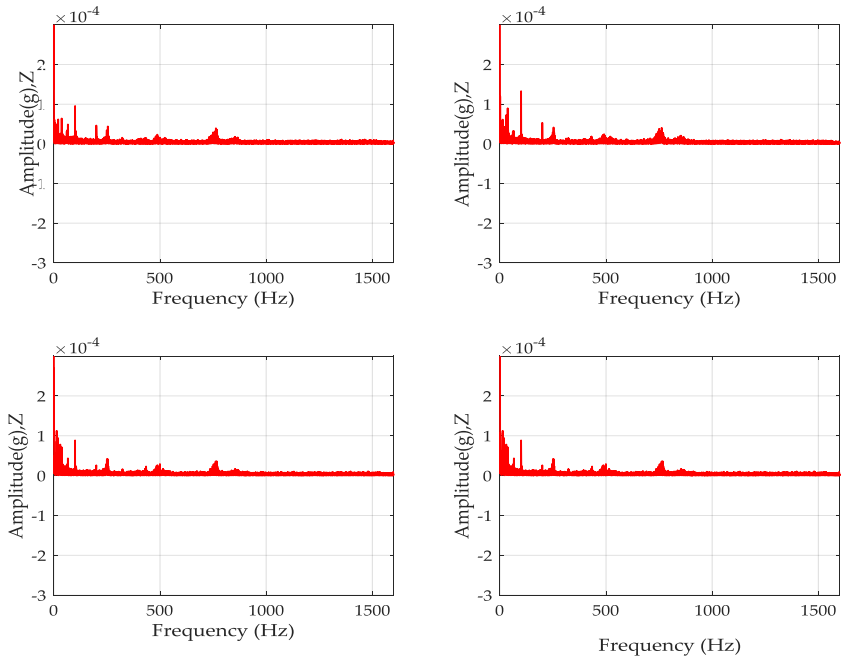

Figure 7-7 Frequency spectra of a 15-second time sample time for X-axis

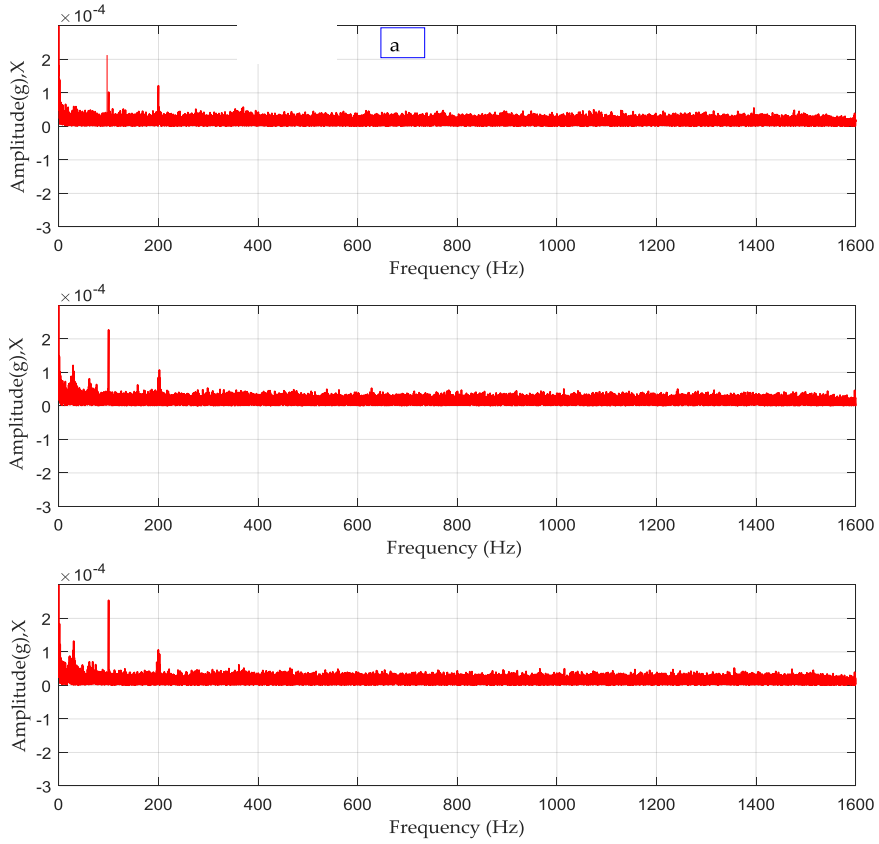

Figure 7-8 Frequency spectra of a 20-second sample time for the x −axis data

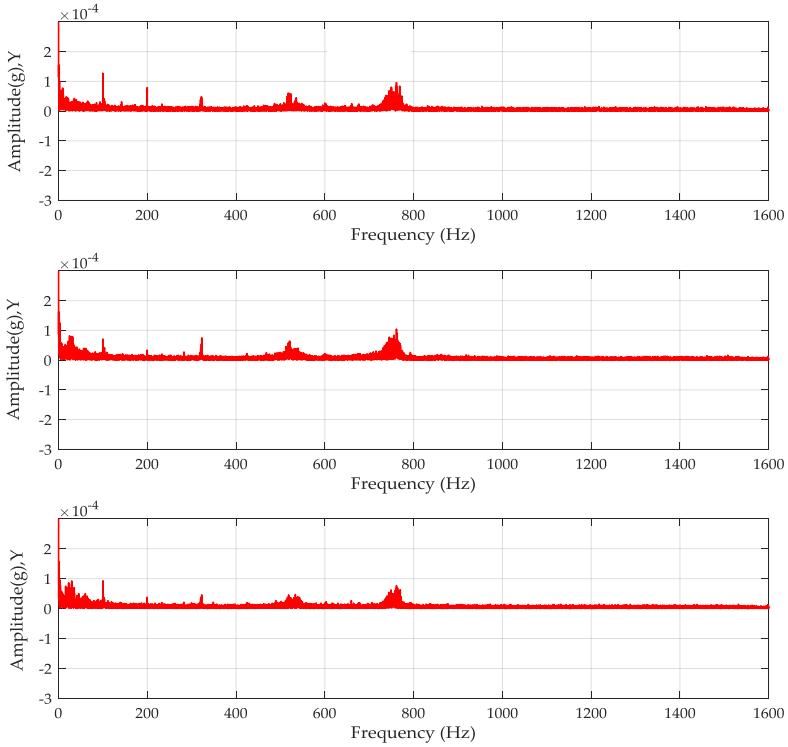

Figure 7-9 Frequency spectra of a 20-second sample time for the y −axis data

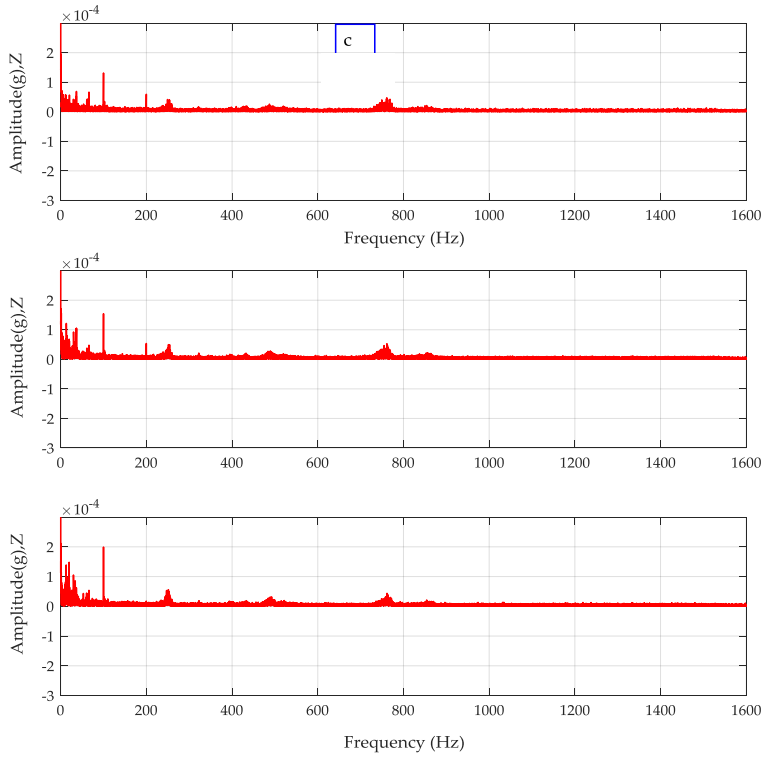

Figure 7-10 Frequency spectra of a 20-second sample time for the Z-axis data

In the cold model, the sample time was 6 seconds. The variation may be due to different reasons. Scaling and the factors not included when physical modeling the process may have affected the sample time. A separate study may be required to identify the actual reason.

Once the minimum sample time was determined, the time history of the vibration data from each heat was sub-divided where each division is 20 seconds long. Different datasets that correspond to different operating conditions were constructed. Each dataset was first analysed by PCA and then by PLS.

7.8 Result and discussion

Principal component analysis of the vibration data within each heat shows that the plant data is highly structured in specific frequency ranges. Table 7-3 shows the values of the first components for the three sample datasets taken from the T0561Z heat. These principal components are a combination of the vibration signal in the x, y and z-axes.

Table 7-3 PC1 values for three samples of T0561Z heat at different frequency ranges

Frequency range (Hz)	**PC1 values**			**Frequency range (Hz)**	**PC1 values**		
	1	2	3		1	2	3
0 to 10	95	68.3	96.4	50 to 60	97.9	97.9	96
10 to 20	98	99.5	99.3	60 to 70	94.3	87.1	87.0
20 to 30	100	99.8	99.5	70 to 80	87.4	97.6	85.1
30 to 40	100	98.5	99	80 to 90	88.5	80.0	70.8
40 to 50	98	99.3	99	90 to 100	86.7	98.1	90.2
0 to 914	98	98.3	98.3				
	1	2	3		1	2	3
100 to 110	97.7	93.5	97.3	150 to 160	70.7	58.7	70.7
110 to 120	75.5	95.7	90.9	160 to 170	53.6	86.4	92.4
120 to 130	58.6	71.4	80.8	170 to 180	79.7	84.2	97.7
130 to 140	91.3	85.0	85.1	180 to 190	57.7	62.4	77.4
140 to 150	80.7	82.4	77.5	190 to 200	69.0	83.5	70.1
	1	2	3		1	2	3
200 to 210	82.6	62.9	70.0	250 to 260	97.7	96.4	99.4
210 to 220	82.7	68.8	76.4	260 to 270	93.6	95.9	88.3
220 to 230	90.9	98.2	92.7	270 to 280	75.7	90.0	94.9
230 to 240	98.2	98.7	96.9	280 to 290	75.4	74.8	96.3
240 to 250	95.8	98.3	96.0	290 to 300	96.4	90.2	58.5

The values PC1 and PC2 in Table 7-3 indicate that most of the underlying structure in the stirring process can be explained by the first principal component in many of the studied frequency ranges. In the other heats, the sum of first and second principal component can explain the variation in most of the frequency ranges. This is shown in Table 7-4 for selected frequency ranges and the six heats considered in this study

The contribution of the x-,y- and z-axis vibration data was found to be similar. In Table 7-5, the loading vectors of the first latent variable are the coefficients of x, y and z. This is shown in Equation 7-1. This agrees with the steel-walled cold model results.

$$PC1 = 0.54x + 0.53y + 0.65z \quad 7\text{-}1$$

Table 7-4 PC values of each heat

Heat ID	Frequency (Hz)	PC1 (%)	PC2 (%)	Heat ID	Frequency (Hz)	PC1 (%)	PC2 (%)
	50-60	97	1		50-60	80	16
	60-70	89	8		60-70	85	9
	70-80	86	10		70-80	70	12
	80-90	75	12		80-90	83	11
	90-100	92	3		90-100	87	5
	180-190	60	31		180-190	92	4
	50-60	94	4		50-60	70	13
	60-70	97	2		60-70	88	10
	70-80	96	3		70-80	80	9
	80-90	98	1		80-90	82	13
	90-100	96	2		90-100	65	21
	180-190	93	1		180-190	62	31
	50-60	85	12		50-60	74	17
	60-70	83	15		60-70	85	7
	70-80	65	25		70-80	83	8
	80-90	72	16		80-90	77	14
	90-100	85	14		90-100	65	26
	180-190	73	11		180-190	70	18

Table 7-5 Values of Loading vectors, Eigenvalues and principal components for 60 to 70 Hz

Score	Loading vector		
x	0.54	0.84	0.074
y	0.53	-0.40	0.74
z	0.65	-0.36	-0.67
Eigen value	0.01052	0.01052	0.01052
Variance (PC)	94	5	1

No linear relationship between the latent variable and the volumetric gas flow rate is found. Figures 7-11a and 7-11b show the flow rate as a function of the latent variable when considering the data within the whole frequency range. This was also the case in the cold model study. Hence, plant data was further analysed by PLS to attempt to find any common structure between the stirring parameters and the vibration signal i.e. to uncover any linear relationship between input variables and the latent variable that is a combination of the three-axis vibration signal. PLS was applied to each dataset of a single heat and in the combination of heats. Various datasets were also formed by taking one varying parameter while keeping the others constant.

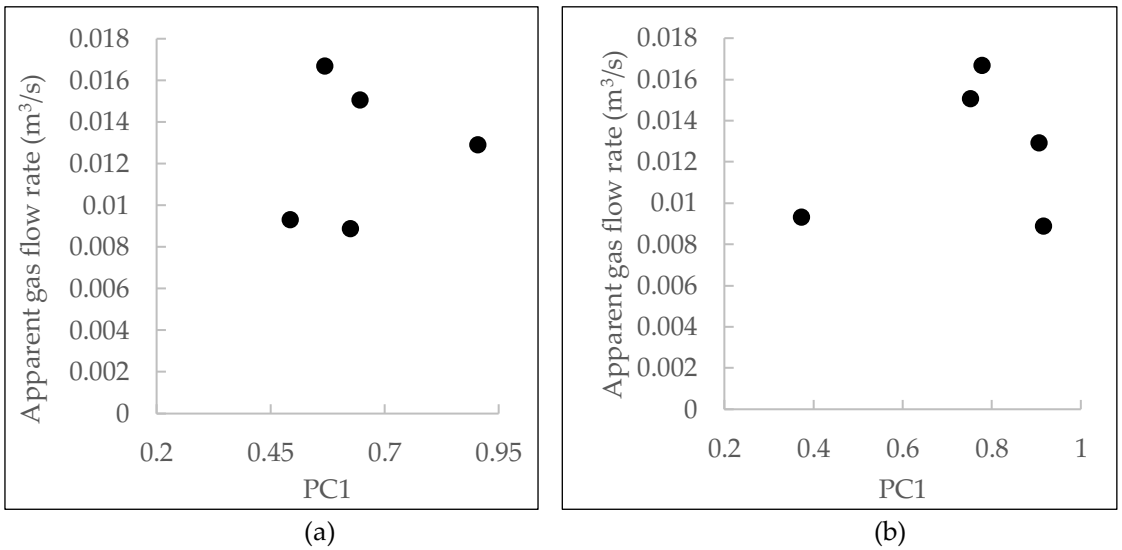

Figure 7-11 Relationship between PC1 and gas flow rate: a) 0 to 914 Hz b) 40 to 50 Hz

Taking one heat at a time, the only input parameter that is assumed to vary throughout the process is the gas flow rate and hence the variation is mostly related to this parameter. Figure 7-

12a shows a good linear correlation between the input and output PLS latent variable. Figure 7-12b shows how vibration can linearly predict volumetric gas flow rate. The frequency range that consistently gives this result is 60 to 70 Hz.

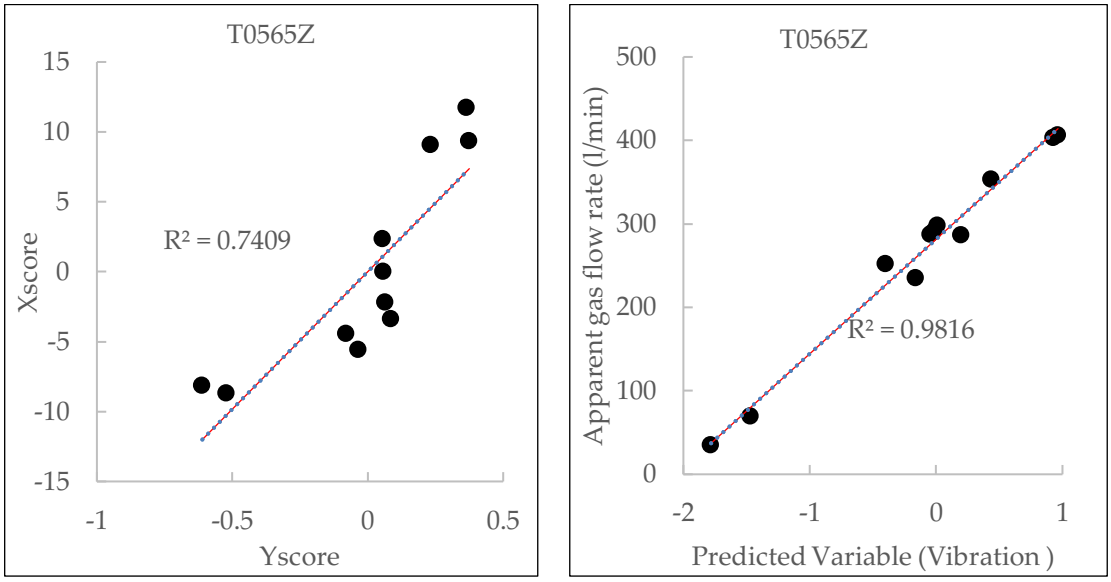

(a) (b)

Figure 7-12 Relationship between: a) input and output PLS components b) flow rate and predicted variable (Vibration)

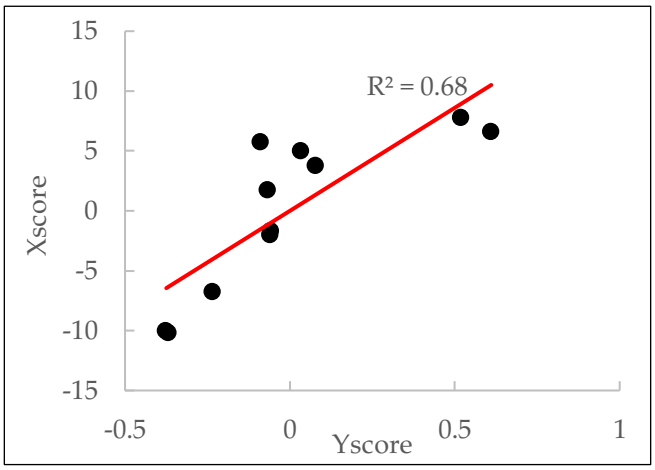

Figure 7-13 Relationship between PLS components in the whole frequency range

The same procedure was followed to analyse each heat independently. The result found was similar to the single heat study with slight variation in the degree of correlation. This is illustrated in Figure 7-13 and 7-14. The frequency range 60-70 Hz was consistently giving similar results in

the investigated heats. When the whole frequency range was analysed, the linear relationship was found to be weaker compared to the smaller frequency ranges. This is shown in Figure 7-13 where the value of the linear correlation coefficient, R^2 is less than the value in the 60 to 70 Hz range shown in Figure 7-14.

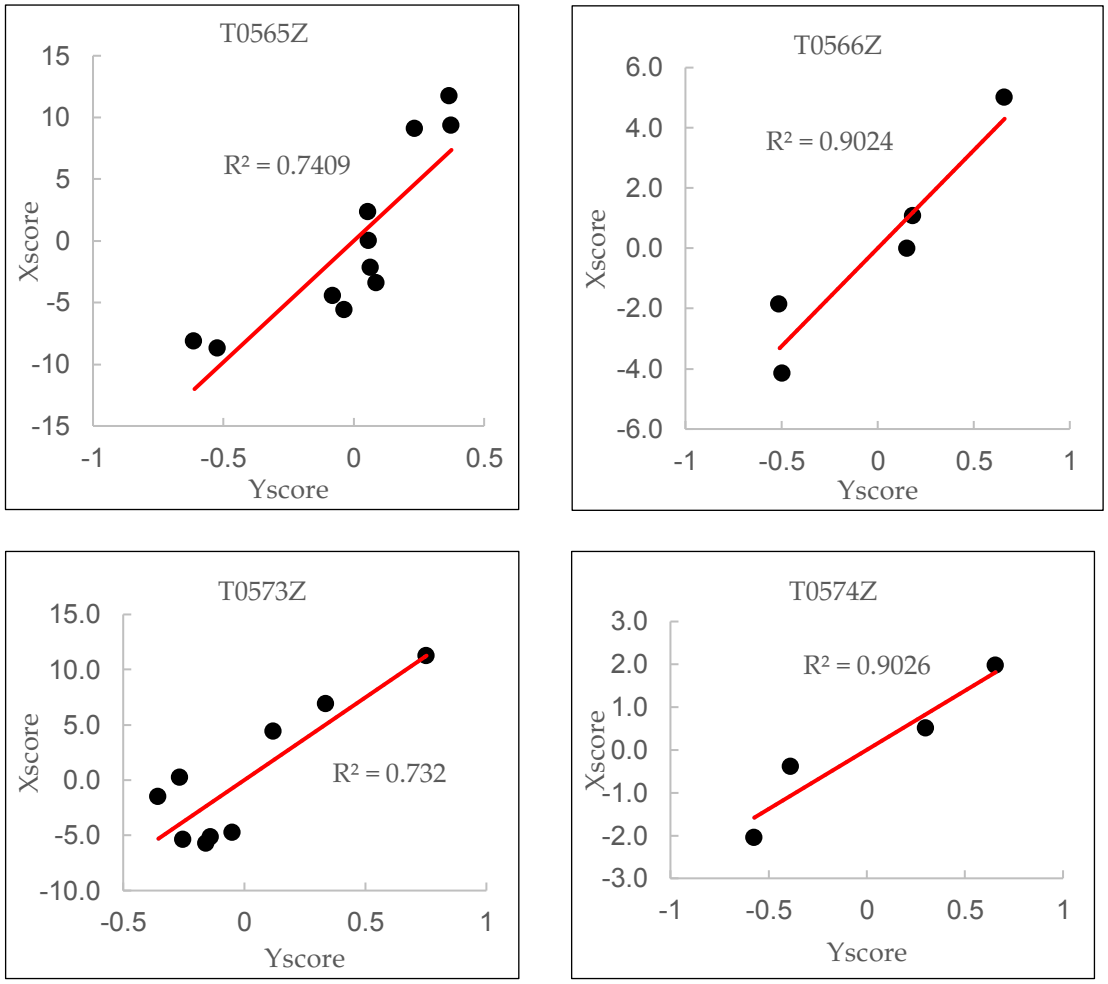

Figure 7-14 Relationship between input and output latent variables in T0565Z, T0566Z, T0573Z and T0574Z heats.

Data from all heats were also combined and analysed by PLS in order to generalise the relationship and use it with any ladle operation.

7.8.1 Data Analysis for Combined Heats

After analyzing each heat individually, the next step was to analyse the entire combined data to unveil any structure or relationships. The flow rates were taken from each heat and ranked in an

increasing order. The respective vibration data was then used to construct a matrix for PCA analysis. PCA revealed the strong structure in the data in specific frequency ranges. Table 7-6 contains the values of principal components (PC) for the combined data.

Table 7-6 PC values for combined data

Heat ID	PC1 (%)	PC2 (%)	Frequency Range (Hz)
	92	4	50-60
	94	3	60-70
	95	2	70-80
	93	6	80-90
	88	7	90-100
	95	3	180-190

To examine the linear relationship between process parameters and vibration signal, the data within these frequency ranges were investigated using partial least squares. The gas flow rate varied from 583.33 to 16650 m^3/s, which is the sum of the flows from the two porous plugs. The steel weight varied from 130 to 150 tonnes while the slag weight was between 1.8 and 3.6 tonnes. In addition, some heats were carried out with new porous plugs and others with old plugs that served from two to four heats. The location of these plugs was also different among the six heats.

No linear relationship between stirring indicators and the latent variable was found in the combined data. This disparity could be due to a couple of reasons. Firstly, the underlying relationship could be non-linear. Secondly, the data comes from heats that have different process parameter values such as plug position, plug life, steel weight, slag weight, plug life, and barrel life that can contribute to data scattering. The sample size may be also too small, compared to the varying parameters, to construct the desired linear correlation. Hence, the relationship could be improved by carrying out separate and sufficient plant measurements for each parameter and analyzing the combined data by both linear and nonlinear data analysis techniques.

To try to determine any relationships in the data when certain parameters are controlled, heats that have similar parameter value such as plug position, steel weight, plug life or slag weight were grouped to form five datasets. Each dataset has one constant parameter with the others varying.

7.8.2 Data Analysis with One Constant Parameter

The parameters taken here are slag weight, metal weight, plug life, and position. In each dataset, one parameter is maintained constant and the other three are varying. The intention of this analysis was to identify which parameter affects the variation in the vibration signal during bubbling. Table 7-7 shows the underlying structure in each dataset when analysed by PCA. When the slag weight is kept constant, the data shows higher structure implying the variability of this parameter can play a larger role.

PLS analysis of individual dataset could not find any linear relationship between PLS components of the vibration and the stirring parameters. This is shown in Figure 7-15.

Table 7-7 PC values when one parameter was kept constant

Const. Plug Position 2	PC1 (%)	PC2 (%)	Frequency (Hz)	Constant Plug life 1	PC1 (%)	PC2 (%)	Frequency (Hz)
	80	13	50-60		94	3	50-60
	88	7	60-70		89	8	60-70
	90	6	70-80		96	1	70-80
	93	4	80-90		95	2	80-90
	92	5	90-100		89	6	90-100
	85	12	180-190		97	1	180-190
	79	8	50-60		94	3	50-60
	88	9	60-70		96	2	60-70
	93	1	70-80		96	1	70-80
	94	3	80-90		98	1	80-90
	93	2	90-100		91	4	90-100
	84	11	180-190		94	2	180-190

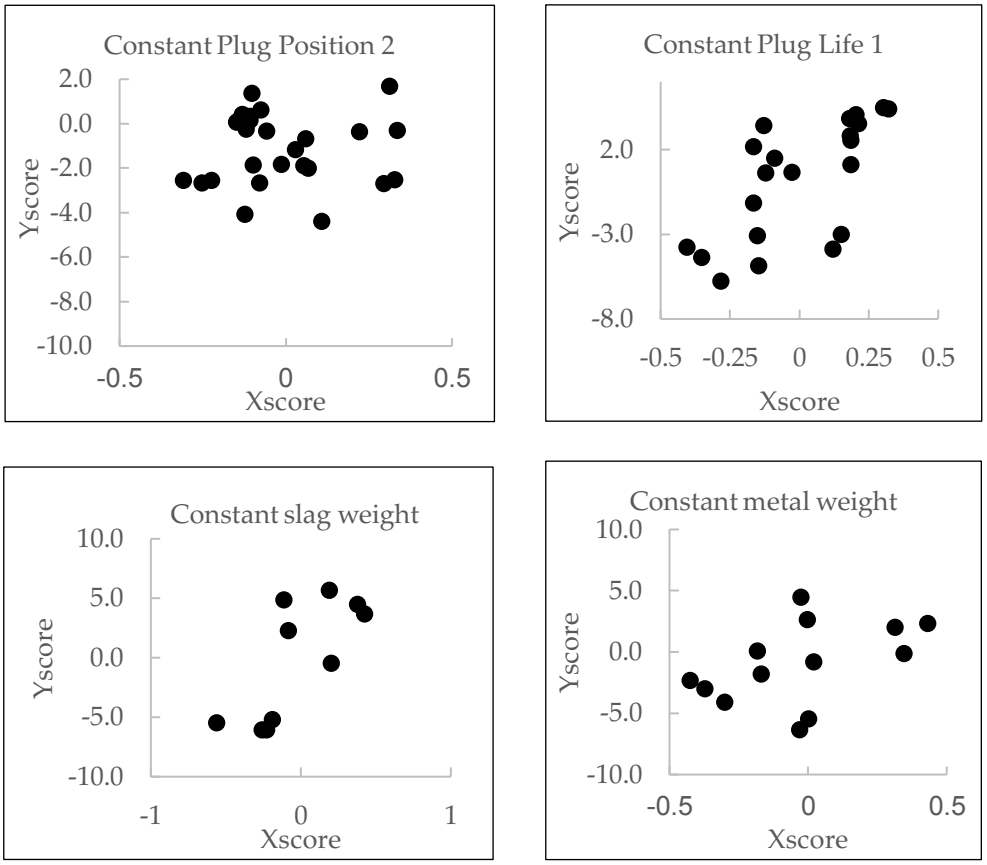

Figure 7-15 Relationship between input and output variables at a selected constant parameter

7.8.3 Plug life

Porous plugs are a means to inject gas through the bottom of the ladle. During service, the life of the plug may be exposed to metal build up, corrosion, cracking etc. that in turn affect the efficiency of the plugs in terms of gas purging into the steel melt.[268] The plug life number indicates the number of times the plug is used to inject gas. This section deals with investigating how the plug life affects the vibration. As the vibration is assumed to reflect the actual bubbling inside, the trend of vibration with plug life may indicate how the actual gas flow is affected as the plug becomes older.

To observe how the amplitude of the vibration signal behaves with plug life, four plug lives (1 to 4) were taken for analysis. All other parameters remain constant for these selected plug lives. Plug life 1 and 4 represent the newest and oldest respectively. The vibration signal with similar flow rate and vacuum pressure is recorded from each plug life. The result shows that the sum of vibration amplitudes within the 20-second time history slightly decreases as the plug becomes

older. Figure 7-16 shows summated amplitude as a function of plug number in the time domain. This may indicate that as the plug serves longer; metal build up prevents the passage of the gas. This results in less fluid turbulence and therefore decaying in ladle wall vibration.

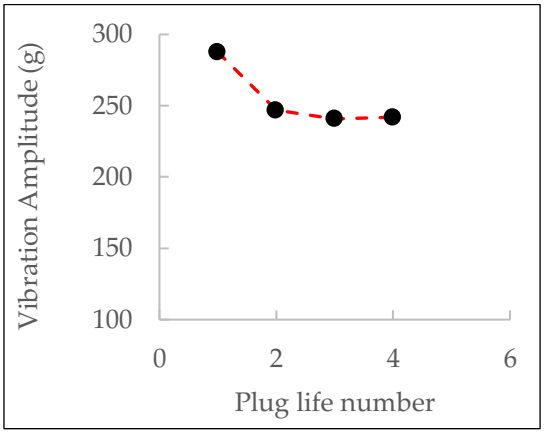

Figure 7-16 Vibration amplitude as a function of plug life number

7.8.4 Comparison of Plant and Cold-Model Results

When the results from both the data and steel-walled cold model data groups are examined, there are similarities and differences. In both cases, the structure is strong and the frequency ranges where this structure resides are the same. These frequency ranges include 60 to 70, 70 to 80, 80 to 90 and 90 to 100 Hz. Table 7-8 shows the values of the first latent variable in the cold model and the plant data. There is a good agreement between cold model and plant studies in that the hidden structure is similar.

Table 7-8 PC1 values of plant and water model data

Frequency (Hz)	**PC1 (%)**	
	Plant	**Model**
60-70	94	96.3
70-80	95	98
80-90	93	99
90-100	88	91

The degree of correlation between the latent variables and process parameters in the plant data analysis was comparable to that of the cold model but only for a single heat data in the frequency ranges of 60 to 70 Hz. The plant data in the other frequency ranges show a poor linear

relationship. The strong structure identified in the data, however, suggests that further study is required to discover the underlying relationship.

The PLS model developed from the cold model data was used to predict the gas flow rate of a plant and to observe how close this model can compute the flow rates taking ladle vibration as an input. Figure 7-17 shows two flow rates of a single heat, the apparent gas flow rate, which is measured during the plant trial, and the gas flow rate predicted from the PLS model. The data shows that the PLS model can be used to estimate the amount of stirring with some error. The flow rates are scaled and normalized using standard deviation.

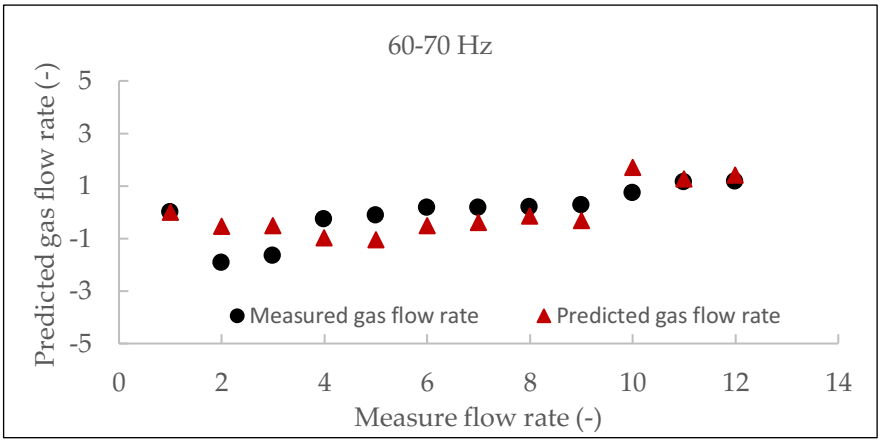

Figure 7-17 Prediction of plant gas flow rate using PLS model developed from cold model data

The water model study found that the structure and degree of linear correlation were affected by the variation in the thickness of top layer/oil. When the top layer is varied, the structure as well as the strength of linear relationship decreases. In a similar manner, plant trials showed that the structure is high when heats with constant slag weight are combined and analysed. Industrial data that has variable slag weight were less structured. The linear relationship is stronger for cold model data than in the plant data of a single heat. The vibration data that comes from various heats show no linear relationships with stirring power and gas flow rate. This relationship could be improved by carrying out separate and sufficient plant measurements for each parameter and analyzing the combined data by both linear and nonlinear data analysis techniques.

7.9 Conclusions and Recommendations

Plant scale studies showed that vibration data at low gas bubbling rates are highly structured when investigated using linear principal component analysis. The three signals were able to be linearly compressed into a single latent variable. This latent variable preserves above 80% of the variation in the stirring process. The frequency ranges where maximum information lies are in the range of 60 to 70, 70 to 80, 80 to 90, and 90 to 100 Hz. These frequency ranges were consistent in the plant and in the water model studies.

The data within the informative frequencies were analysed by partial least squares to assess the linear relationship between the latent variables and process parameters such as apparent gas flow rate. The cold model data gave a strong linear correlation whereas the investigated plant data showed poor linear relationship for most of the cases. Plant data was taken from each heat and analysed independently to show a comparable degree of linear relationship as the cold model data for the frequency range of 60 to 70 Hz. The vibration signals in the x, y and z direction contributed comparable information which indicates the importance of three-dimensional vibration in stirring process control.

In the plant data, those heats that had similar slag weight gave high values of first principal components, which signifies that the slag weight may affect the underlying structure. However, these should be verified by accommodating additional industrial data. Vibration data taken with different plug lives also showed a further decrease in vibration magnitude when plugs are used for a long time indicating major liquid metal build-up allowing less gas flow rate.

The size of the plant data taken in this study is very small compared to the number of parameters varying during ladle operation. Current results should be verified by incorporating additional industrial data to see the effect of different parameters separately. Typical noise sources such as crane movement and other nearby operations should also be identified and measured separately to easily filter them and reduce their effect on the correlation and structure of the data.

In summary, these findings show that the stirring process may be monitored by combining the three axes vibration signals if the right frequency ranges are chosen carefully and the relationship is further studied using adequate plant trials and proper noise filtering techniques.

8 Bubbling Sound Signal Analysis

8.1 Introduction

Stirring using bottom gas injection is the common mechanism used to achieve uniform temperature and homogeneous composition in steel melts in ladle metallurgy. When injected, inert gas naturally rises through the molten metal or slag forming bubbles. The formation and disintegration of bubbles generate sound. Researchers found that the sound pulse is created when two bubbles, primary and secondary, are coalesced.[25, 26, 124, 129, 269] Bubble coalescence is the merging of two small bubbles to form a relatively large bubble. During the coalescence period, the sound pressure tends to increase [25, 26, 124]. The emission of sound can also be due to bubbles' harmonic oscillation.[270] When a liquid entrains gas bubbles, the volume pulsation of the bubble imparts high sound pressure in the medium. The volume pulsation is explained by the bubble wall oscillation that decays with time due to damping characteristics.[123] The importance of acoustic signal in steelmaking has been described by Zhang et al. [271]

There is no study in the open literature that explains the behavior of sound pressure when molten steel is stirred at low flow rates, varying molten metal depth, and varying slag thickness. Hence, the objective of this study was to measure the sound pressure created during bath stirring in the laboratory scale cold model. The present work investigated the effect of bottom layer depth, top layer thickness and volumetric flow rate on the magnitude and frequency of the sound pressure. This may benefit ladle operators in estimating the exact amount of molten metal and slag depth in the ladle. This information is also important in evaluating the stirring status.

8.2 Experiment Setup

A cold model apparatus made of Perspex shown in Figure 8-1 was used to undertake sound pressure measurements. This cold model simulates a 200-tonne capacity industrial ladle by fulfilling geometric and dynamic similarity criteria proposed by Krishnapisharody and Irons.[36] This ladle is scaled down by 1/10 i.e. every geometric dimension and process parameters on the cold model were computed based on this scaling factor. The diameter and height of the cold model vessel are 0.42 m and 0.5 m respectively. The volumetric flow similarity is based on plume Froude number similarity and is given in Equation 4-10 [35]

A centrally located 0.003 m diameter nozzle was assembled at the bottom for compressed air injection. Water and oil (ϱ= 850 kg/m^3) are used to simulate molten steel and slag respectively. The selection of water was due to its kinematic similarity with molten steel at working temperature, its easy availability and being widely used in cold model steelmaking studies.[35, 154] However, the physical and dynamic property of slag is highly variable and it is difficult to mimic it with a single material. Although oil is not an ideal choice to simulate slag, due to its immiscibility with water and availability, it has been successfully used in steelmaking cold model investigations in the plant.[7, 8, 14-16, 18, 37, 73, 76-80, 97, 214, 215]

An integrated circuit piezoelectric (ICP) array microphone was used to sense the sound pressure. This microphone is of the condenser type and is "Free-Field" i.e. it is direction sensitive. The microphone was located centrally above the apparatus and pointed directly to the bath. A low impedance cable where the signal can be transported over long distances with a negligible signal loss was utilized to connect the microphone to a data logger. The data logger was NI 9234, which is a 4-channel C Series dynamic signal acquisition module from National Instruments. It digitized the sound pressure signals at a maximum rate of 51.2 kHz. The amount of pressurized air was controlled by a standard acrylic rotameter (±3 % full-scale errors). The air pressure was made to be at a fixed value by a pressure regulator to prevent any fluctuations. Figure 8-1 shows the scheme of the experimental setup.

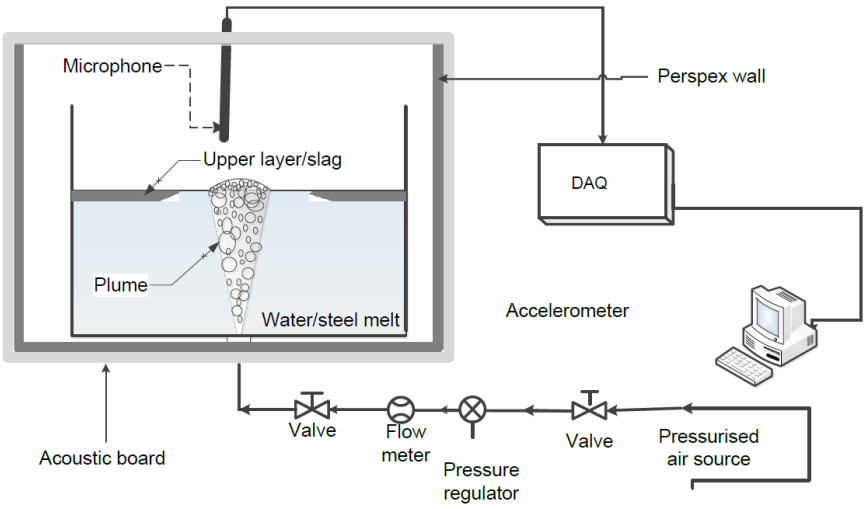

Figure 8-1 Experimental setup for acoustic measurement

National Instrument SignalExpresss 2013 software was used to acquire, generate and save signals. The analysis of the collected data was performed in Matlab2013a.

8.3 Experimental Conditions

Applying geometric and dynamic similarity criteria, the parameters' values in the lab-scale were determined. Equation 4-10 which is based on plume Froude number similarity ($(Fr_p)_m = (Fr_p)_f$) was applied to determine the volumetric flow rates for cold model study. Flow rates taken for this study were determined using Equation 4-10 ($Q_m = \lambda^{2.5} Q_f$) in order to be within the range of flow rates applied in ladle metallurgy.

Table 8-1 Experimental conditions for sound pressure experiment

Layers	Water Level (m)	Oil Depth (m)	Air Flow Rate (m^3/s)
single	0.1	0.00	1 to $4x10^{-5}$
single	0.15	0.00	1 to $4x10^{-5}$
single	0.15	0.00	1 to $4x10^{-5}$
single	0.2	0.00	1 to $4x10^{-5}$
single	0.25	0.00	1 to $4x10^{-5}$
single	0.25	0.00	0.83 to $10.33x10^{-5}$
double	0.1	0.005 to 0.02	1 to $4x10^{-5}$
double	0.15	0.005 to 0.02	1 to $4x10^{-5}$
double	0.25	0.005 to 0.02	1 to $4x10^{-5}$
double	0.25	0.02	0.83 to $10.33x10^{-5}$

In the previous experimental study of ladle vibration[154], the experimental conditions considered were four bottom layer heights, four top layer heights and low volumetric air flow rate ranging from 0.83 to 4.17 x 10^{-5} m^3/s. To be able to draw general conclusions in this study, similar experimental conditions were taken in the sound pressure measurement. The sound pressure data was gathered when the bath was stirred by pressurized air in the presence and absence of the top layer. The single layer experiment was carried out on four different water depths. During the double layer experiment, the top layer was varied from 0.005 to 0.02 m. For each bath level, the volumetric airflow rate was varied from 1 $x10^{-5}$ to $4x10^{-5}$ m^3/s at 0.33 x 10^{-5} m^3/s interval. Table 8.1 shows the flow rate intervals, water levels and oil depths considered in this experiment. Single layer refers to only water being used and double refers to the presence of a layer of oil on

the top of the water. All flow rate ranges considered in this study are within the operational range of flow rates in ladle metallurgy.[38, 105, 262].

8.4 Analysis Procedure

The analysis process began by evaluating the level of background noise, which came from various sources. All necessary steps were taken to ensure that the noise does not interfere with the main signal. The next step was to determine the sampling frequency and the sampling time. The sound pressure data obtained at various experimental conditions were analysed in the time and frequency domains. The time domain investigates the magnitude of the sound signal in relation to flow rate and bath height. The FFT of the data was analysed to uncover certain properties of the sound pressure by taking specific frequency ranges at a time. Detail descriptions of the FFT are found in the literature.[141, 145, 228, 230]

8.5 Signal Analysis

8.5.1 External Noise

In order to check whether the background noise is a significant part of the main signal, external sources of sound were measured in the absence of air bubbling at various times to detect spurious signals. This was initially performed without an acoustic insulator on the apparatus as shown in Figure 8-2a.

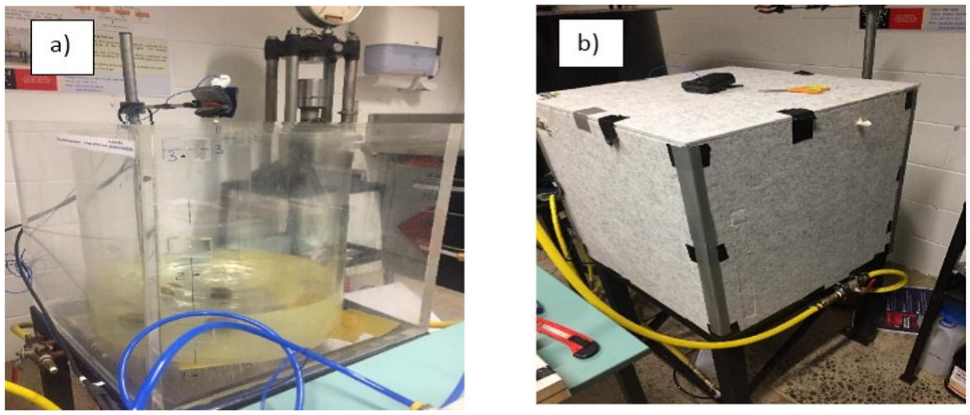

Figure 8-2 Cold model apparatus a) without insulation b) with insulation

Figure 8-3 shows the temporal variation of sound pressure of air conditioning equipment (external source) and water bubbling due to gas stirring at 16.67x10-6 m^3/s and 33.33x10-6 m^3/s

respectively. Figure 8-3 shows that the magnitude of the external noise is comparable to the main signal.

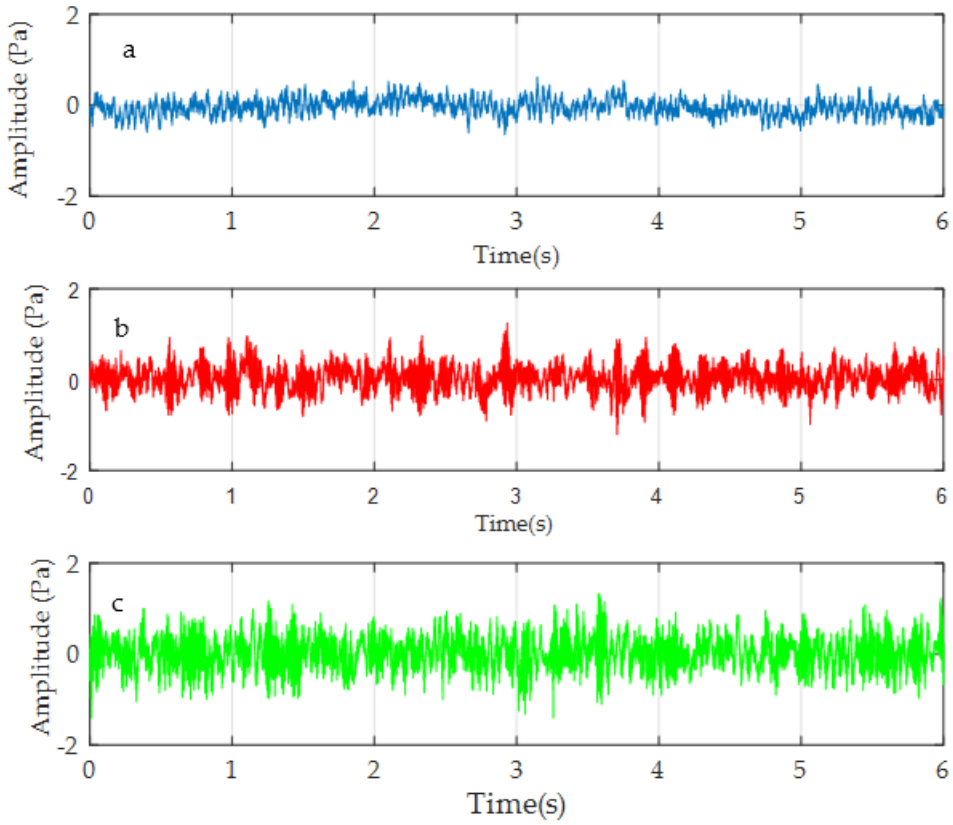

Figure 8-3 Sound pressure at 0.25 m water level a) background noise b) noise + main signal at 16.67x10-6 m^3/s c) noise + main signal at 33.33x10-6 m^3/s

To minimize the effect of background noise and increase the strength of the main signal, the apparatus was covered with a 0.009 m thick acoustic pin board, which is a sound dampening material made of woven polyester (see Figure 8-2b). This material has the ability to absorb and attenuate sound energy coming from external sources.[272]As shown in Figure 8-4a the magnitude and intensity of the external noise was reduced. This improved the signal to noise ratio (SNR) from almost 1 to 4.4.

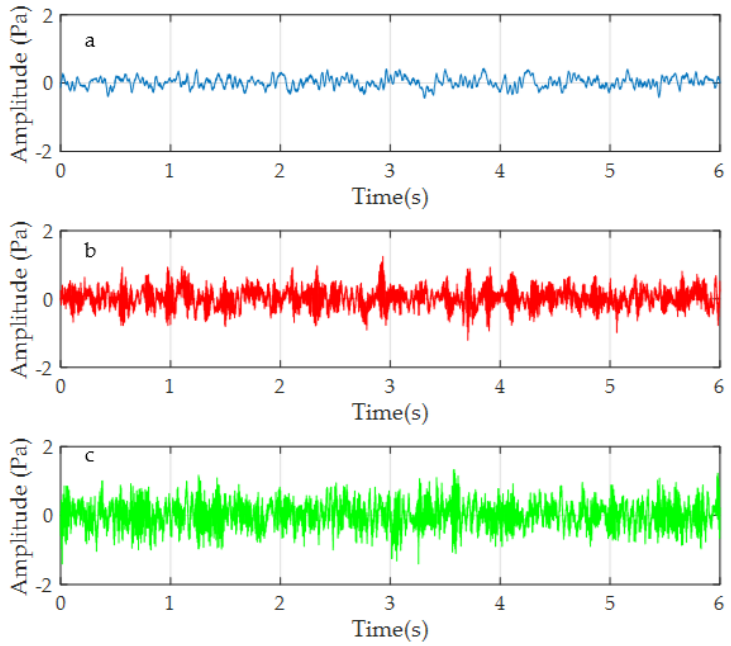

Figure 8-4 Comparison of noise signal with main signal containing noise a) no stirring (external noise) and with insulation b) flow rates of 16.67x10-6 m³/s and c) flow rates of 33.33x10-6 m³/s)

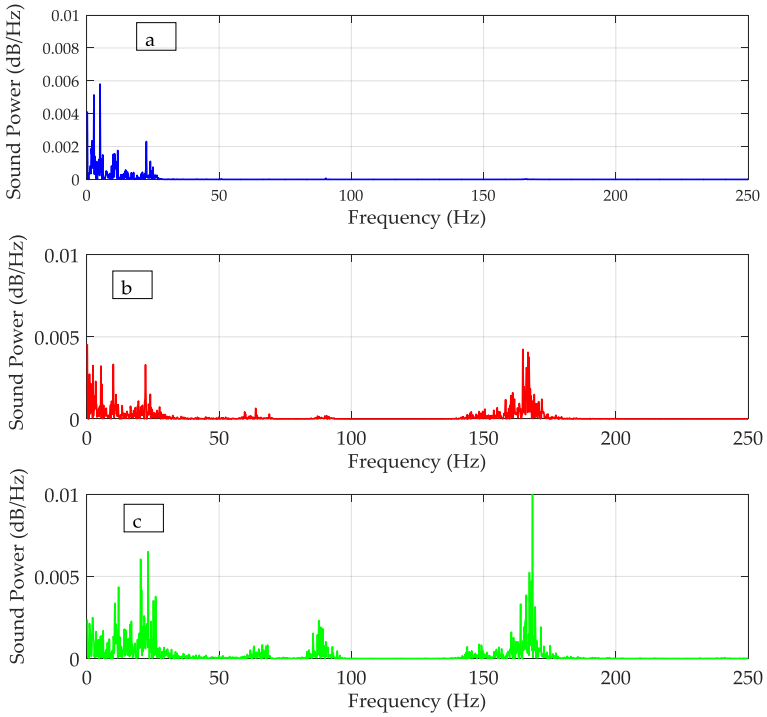

Figure 8-5 Sound pressure level (dB) for a) no stirring (external noise) b) flow rates of 16.67x10-6 m³/s and c) flow rates of 33.33x10-6 m³/s)

In addition, the ambient/external noise alone and the main signals containing the external noise was analysed in the frequency domain using power spectral density (PSD). The concept of PSD

is described briefly in Chapter 4. The analysis was aimed at identifying the frequency range where the power of the signal is concentrated. Figure 8-5 shows the sound pressure level of external noise and the main signal containing external noise. It can be concluded that the power of the external noise signal is concentrated at low frequencies i.e. between 0 and 50 Hz. Consequently, to increase the strength of the signal, the signal in this frequency range was filtered out during frequency domain analysis.

8.5.2 Sample Time Determination

The recording length for this data acquisition was determined by observing the spectral wave pattern at different sampling times. First, the signal was recorded for 60 seconds. This sample time is subdivided into different recording lengths (30, 10, 6 and 5 seconds). The frequency domain of each recording length is given in Figures 8-6 to 8-9. The spectral patterns of 30, 10, and 6 are very similar within the divisions while for the 5 sec sample time, the dividends start to show a difference. This was also reported in previous vibration signal analysis.[18, 154] Hence, it was determined that using a sampling time of 6 seconds would have little impact on the overall signal and could, therefore, be used as a data acquisition time.

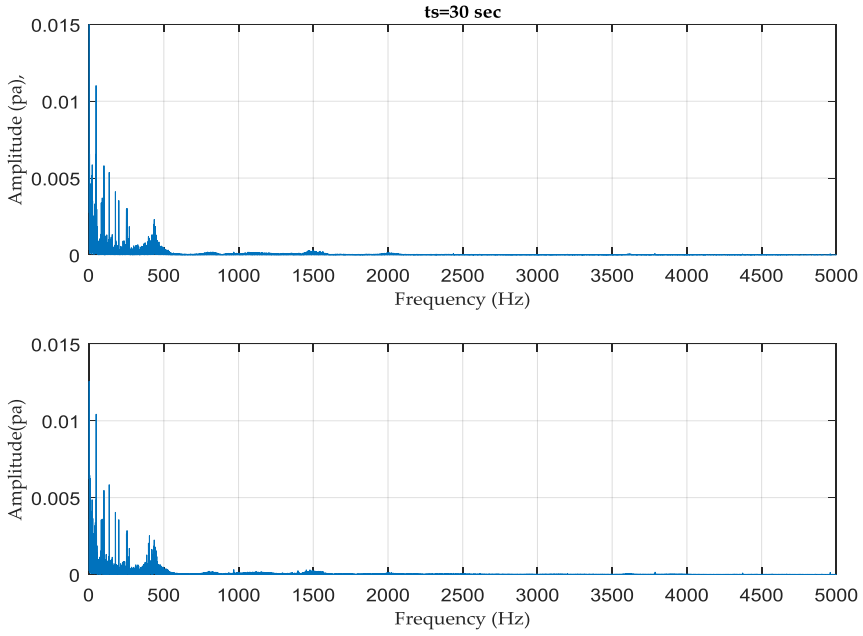

Figure 8-6 Spectral patterns of sound pressure at sample time of 30 seconds

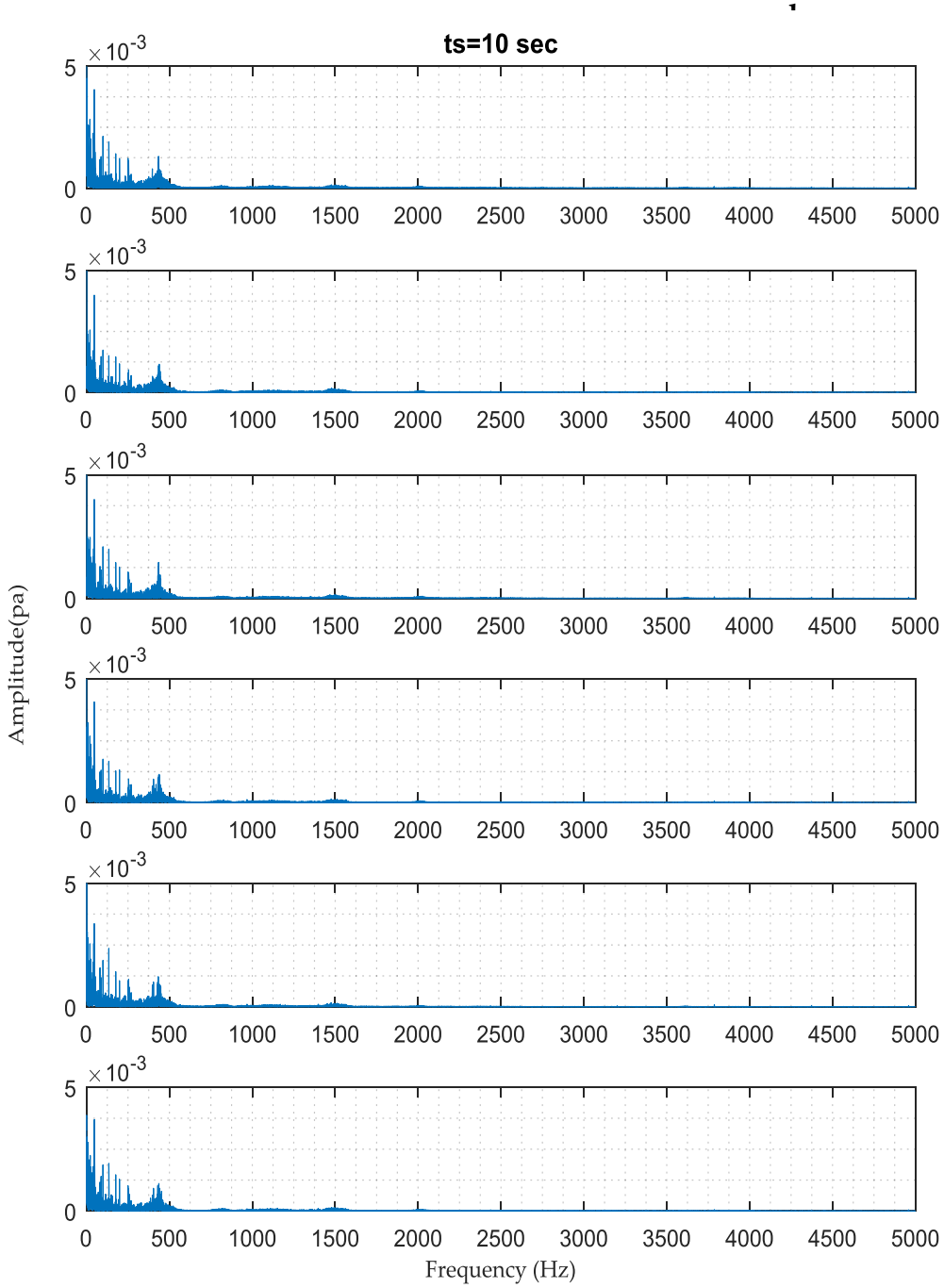

Figure 8-7 Spectral patterns of sound pressure at sample time of 10 seconds

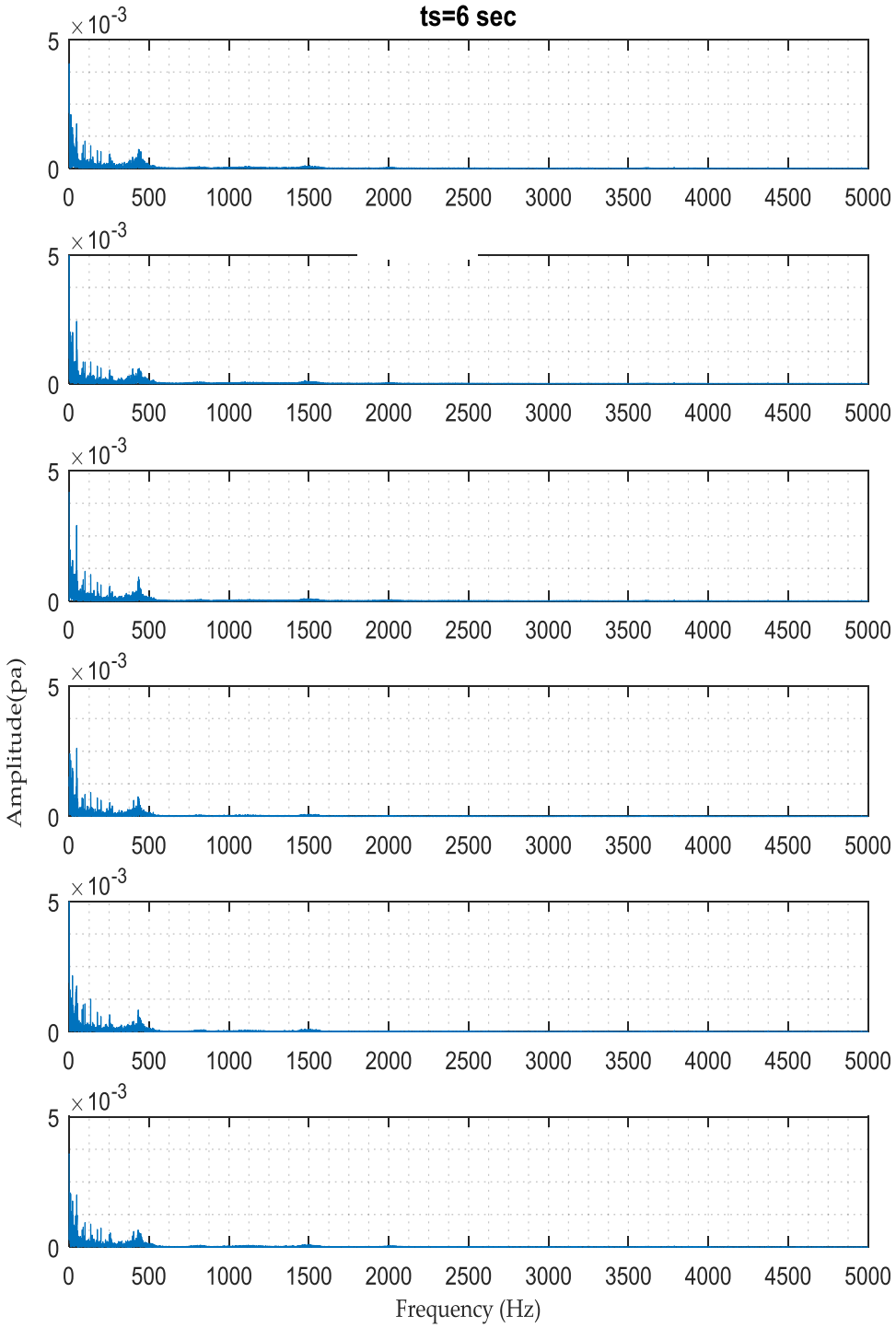

Figure 8-8 Spectral patterns of sound pressure at sample time of 6 seconds

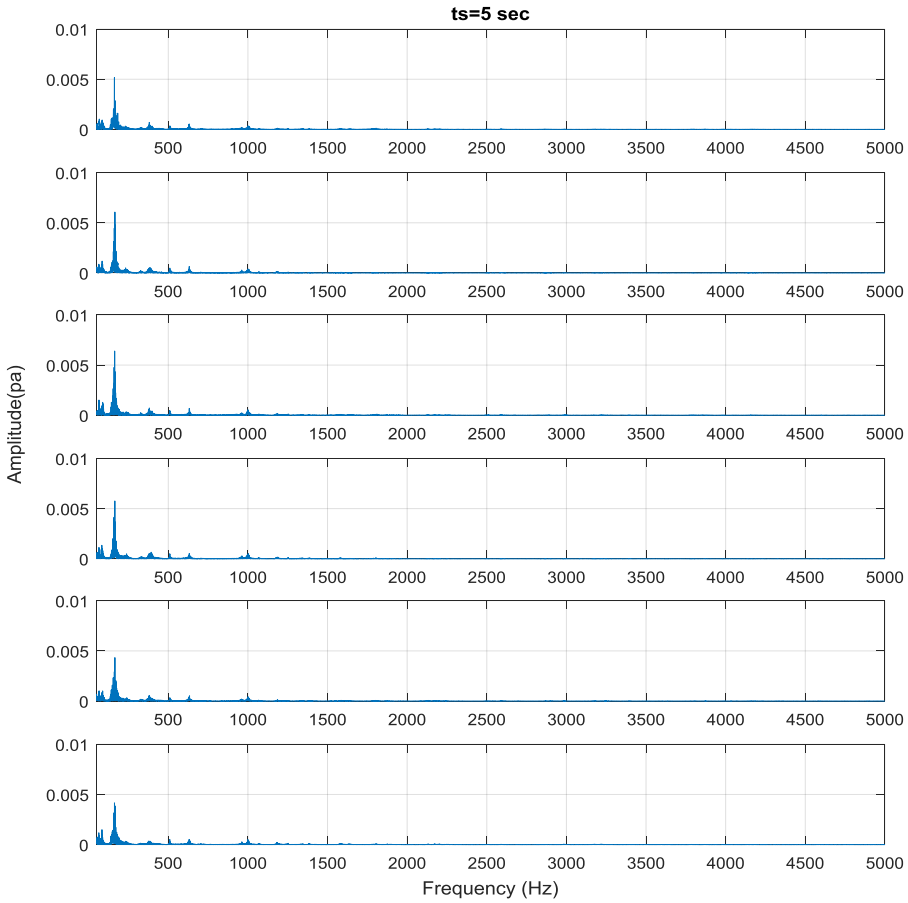

Figure 8-9 Spectral patterns of sound pressure at sample time of 5 seconds

8.6 Result and Discussion

8.6.1 Bubbling Sound in the Single Layer

8.6.1.1 Low Flow Rate Bubbling

Data collected at four different water levels and low volumetric flow rates of 10^{-5} to $40x10^{-6}$ m^3/s, without the upper layer, was analysed in the time and frequency domains. Time domain analysis of data shows that the average amplitude of sound pressure increases with flow rate when keeping the bath level constant. This profile is shown in Figure 8-10. However, this amplitude does not show any trend when the flow rate was fixed and bath height was varied. Figure 8-10 and Figure 8-11 shows this result. The temporal patterns in Figure 8-11 show no clear distinction among the four levels by keeping the flow rate constant.

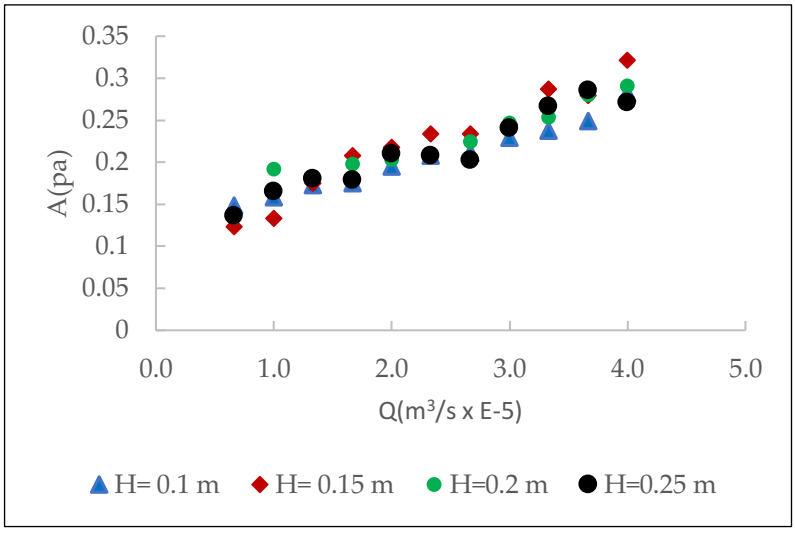

Figure 8-10 Relationship between average sound pressure and flow rate

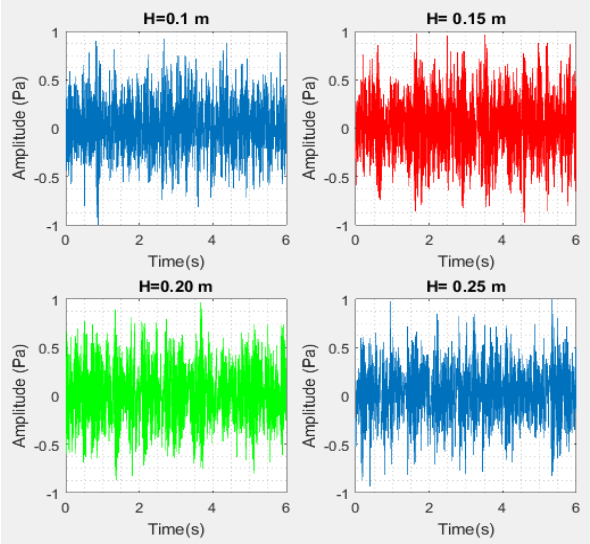

Figure 8-11 Sound waves for a fixed flow rate of 1.67×10^{-6} m^3/s and variable bath level

As the time domain analysis could not unveil any difference in sound pressure created at different water levels when keeping the air flow rate constant, the data were analysed in the frequency domain using the Fast Fourier Transform. In the frequency spectrum, the highest magnitude peak, f_1, and second highest magnitude peak, f_2, frequencies were investigated in each experimental condition as shown in Figure 8-9. Table 8-2 displays these peaks with respect to their air flow rate and water heights in the apparatus.

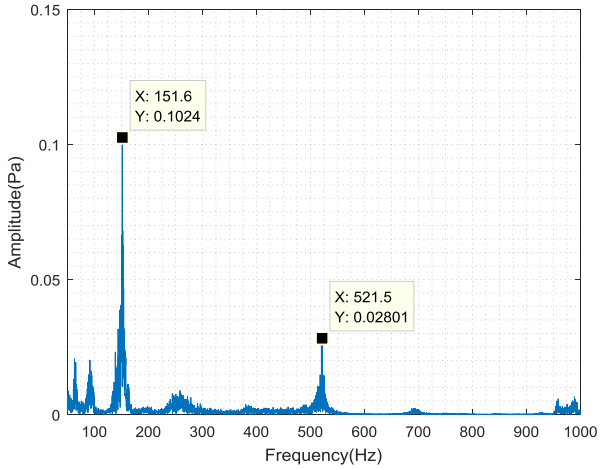

Figure 8-12 Peak frequencies at 0.15 m water level and 10^{-5} m^3/s volumetric air flow rate

The data in Table 8-2 displays the maximum peak frequencies under various experimental parameters. It has been found that the global peak frequencies exhibit negligible variation with flow rate. However, as the level increases, the peak frequency shows a persistent increment of approximately 8 Hz for a 0.050 m bath level rise from 0.10 to 0.25 m. Figure 8-13 shows how the peak frequency changes as a function of water depth and volumetric flow rate.

Table 8-2 First and second peak frequencies for four water levels and varying flow rates

	H=0.1 m									
Q (m3/s)x10^{-6}	**10**	**13.33**	**16.67**	**20**	**23.33**	**26.67**	**30**	**33.33**	**36.67**	**40**
***f1*(Hz)**	145	142.4	144.4	143.7	144.5	143	142	143.6	142	142.5
***f2*(Hz)**	473.4	473.5	473.2	472.4	472	472.9	471	142	144.7	472
	H=0.15 m									
***f1*(Hz)**	150.9	152.5	150.4	152.6	151.1	152	152	151.8	152	152.6
***f2*(Hz)**	521.2	520.3	521.1	65.8	69	65	68.8	521	66.9	66
	H=0.2 m									
***f1*(Hz)**	159.5	160.2	158.7	159.5	159.5	159	158.9	159.9	159.6	157.8
***f2*(Hz)**	68.7	61.7	62.1	65.7	67	91.8	95.5	92.87	94.1	93.2
	H=0.25 m									
***f1*(Hz)**	165.6	167.3	166.9	169.2	168.8	168.6	168	167.3	168.2	166.5
***f2*(Hz)**	60.25	64.6	62.7	65.92	89.6	66.6	90.1	61.6	66.8	67.19

Further analysis in the frequency domain was performed by analyzing the power spectral density (PSD). This was aimed at identifying frequency ranges where the energy content of the signal varies with the rise or fall of the bath level for the single layer study. When the signal amplitude or power of the signal is observed in the whole frequency range by computing the power spectral

density (PSD) of the sound pressure (shown in Figure 8-14) no difference could be visualized. Close examination of the PSD curve at various smaller frequency ranges reveals that the magnitude of the sound power either increases or decreases with the bath level depending on which frequency range is taken. For most of the flow rates considered, the sound power increases with bath level in the frequency range of 125 to 130 Hz as it can be observed in Figure 8-15.

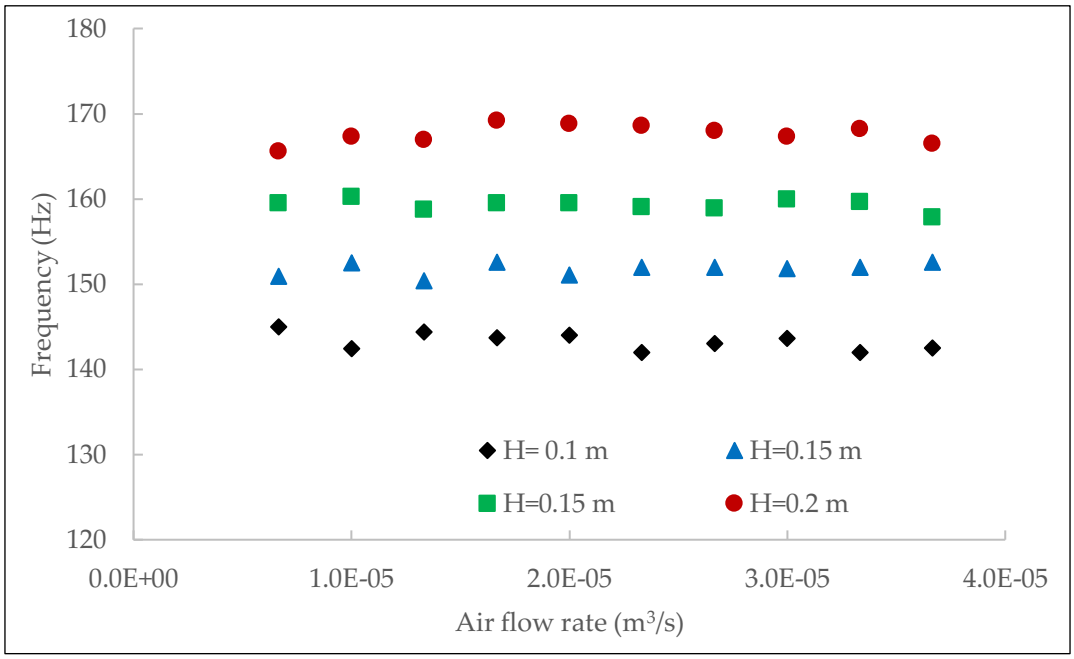

Figure 8-13 Global peak frequency at different flow rate and bath heights

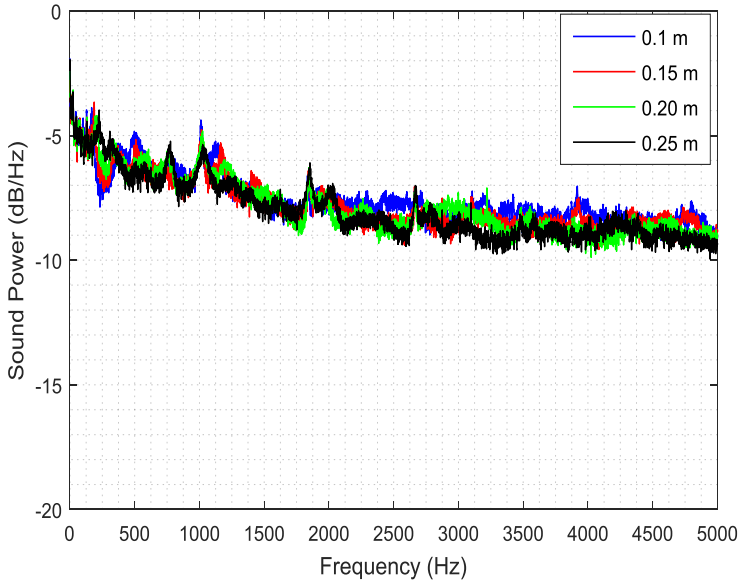

Figure 8-14 PSD of sound pressure at 10^{-5} m^3/s flow rate and the various heights

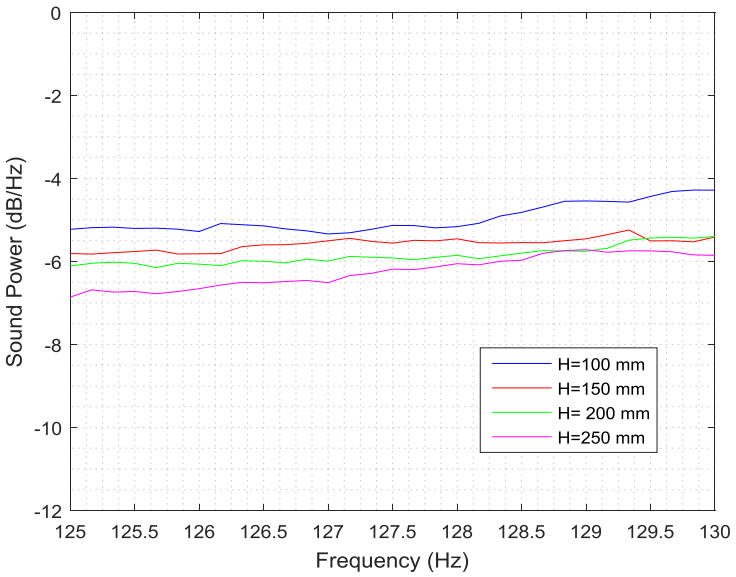

Figure 8-15 Sound power at 33.3x10^{-6} m^3/s and 125 to 130 Hz

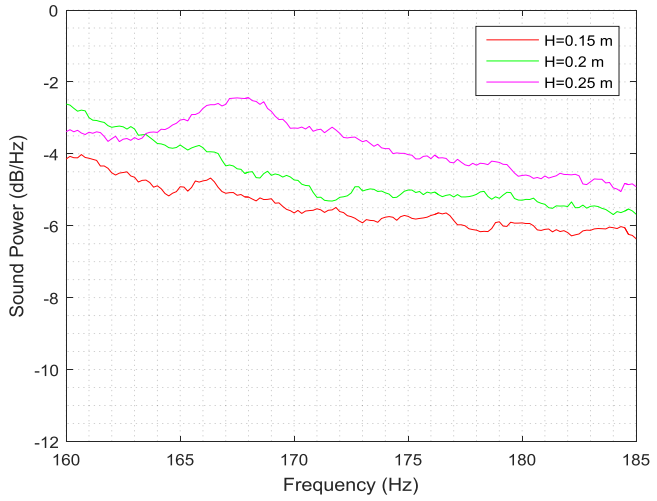

Figure 8-16 Sound pressure at 33.3x10^{-6} m^3/s and 160 to 185 Hz frequency range

There are other frequency ranges, which show a trend, but for three bath heights only: 150, 200 and 300 mm. Figure 8-16 shows that the sound power decreases with increasing water depth in the frequency range of 160 to 185 Hz. In comparison, the sound power increases with increasing water depth in the frequency range of 685 to 700 Hz for the three water depths taken in this study. This is presented in Figure 8-17.

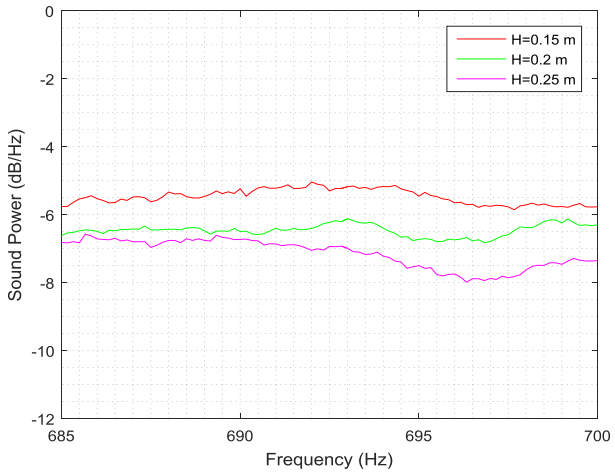

Figure 8-17 Sound pressure at 33.3x10^{-6} m^3/s and 160 to 185 Hz frequency range

8.6.1.2 High Flow Rates

In ladle metallurgy, stirring occurs at different flow rates to satisfy various objectives. In the previous section, the study of ladle stirring at low flow rates has been investigated by analyzing the sound signal measured from the cold model.

To observe how the bubbling sound pressure behaves at a relatively high flow rate, measurements were taken from the same cold model for the flow rate of 41.7x10^{-6} to 10.83 x10^{-6} m^3/s and two bath levels of 0.15 and 0.25 m.

Table 8-3 First and second peak frequencies at different flow rate and water height

	H=0.15 m , h=0 (without the upper layer)								
Q (3x10^{-6} m^3/s)	**41.67**	**50**	**58.33**	**66.67**	**75**	**83.33**	**91.67**	**100**	**108.33**
f1(Hz)	151	152	151	152	151	152	153	154	152
f2(Hz)	66	522	522	522	523	521	522	521	522
	H= 0.25 m								
f1(Hz)	167	168	167	168	167	165	166	168	168
f2(Hz)	89	66	89	86	89	88	86	86	89

Analyses in the time domain show that the sound wave magnitude increases with flow rate but the relationship with bath level is not linear. Figure 8-18 shows the relationship between the average sound pressure and the volumetric flow rates. Peak frequency analysis as shown in

Figure 8-19 shows that the highest peak occurs at a higher frequency for the 0.25 m bath level than the 0.15 m bath level whereas the second peak occurs at higher frequency in the 0.15 m than the 0.25 m. This is shown in Figure 8-19 and Table 8-3. However, the frequency at which both peaks occur remains more or less constant with flow rate. Figures 8-20 and 8-21 show the relationships between peak frequency and volumetric airflow rate and bath level for a single layer and higher flow rates. It suggests that the peak frequencies remain almost constant as flow rate changes. The peak frequencies only shifts when the bath level changes.

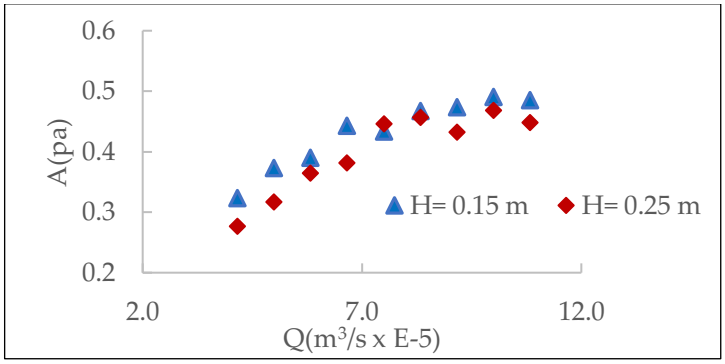

Figure 8-18 Relationship between air flow rate and average sound pressure

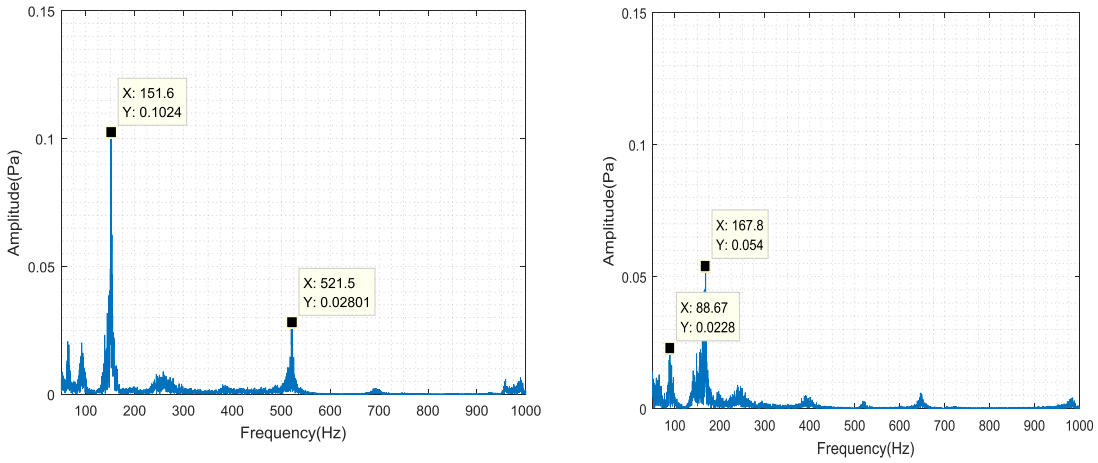

(a) (b)

Figure 8-19 Peak frequencies at 10.83 x10^{-6} m3/s a) 0.15 m and b) 0.25 m bath level

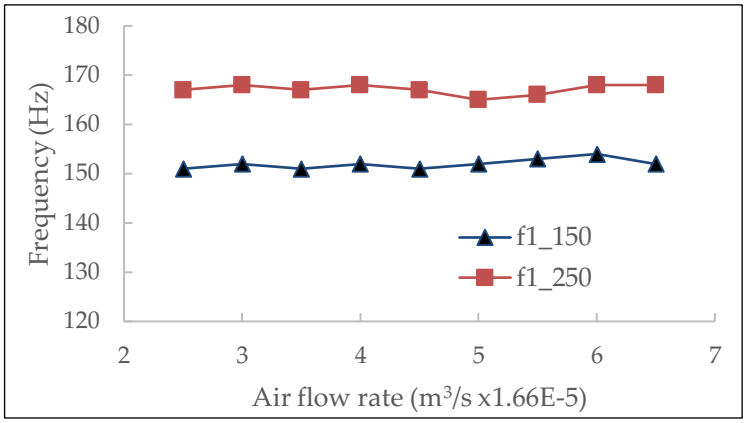

Figure 8-20 First peak frequency at different flow rate and bath heights

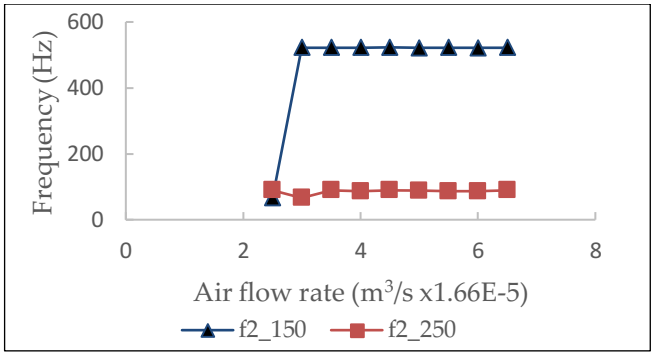

Figure 8-21 Second peak frequency at different flow rate and bath heights

8.6.2 Bubbling Sound in Double Layer

In ladles, the upper surface of the melt is usually covered by a slag of a certain thickness. This forms an upper layer and can affect the quality of the steel in different ways. In this study, this slag layer was replicated with oil. The water level was fixed and the oil depth was varied between 0.005 and 0.02 m at intervals of 0.005 m. The study analysed the variation of sound pressure with flow rate, and upper layer/oil depth. The bottom layer depths taken in this study are 0.10, 0.15 and 0.25 m.

8.6.2.1 H=0.25 m

The sound signal from the double layer stirring was collected at a fixed water level and varying top/oil depth. This data was analysed in the time and frequency domains. The analysis result shows that the average sound pressure linearly increases with flow rate as shown in Figure 8-22 for the four oil depths.

However, the data shows that the average amplitude calculated over the whole time span rarely changes with oil depth in the volumetric airflow rate of the range of 6.67x10-6 to 40 x10-6 m3/s. To examine the effect of varying the upper layer while keeping the airflow constant, the data were analysed in the frequency domain. Figure 8-23 and Table 8-4 show the values of peak frequency and their respective amplitude for each flow rate and oil depth. Computing the peak frequencies for each flow rate and oil depth shows that the global peak frequencies remain at a nearly constant value as both the injected volumetric airflow rate and upper layer thickness increases. This reveals that the global peak frequency is a function of the bottom layer thickness

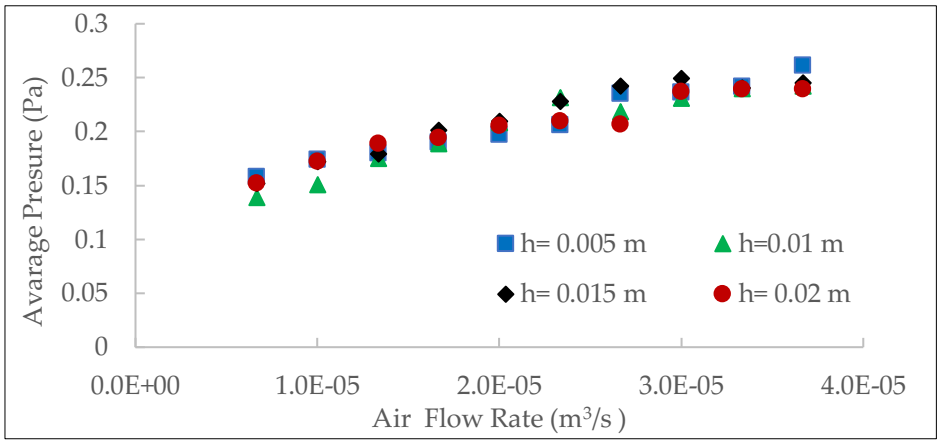

Figure 8-22 Relationship between sound pressure and flow rate

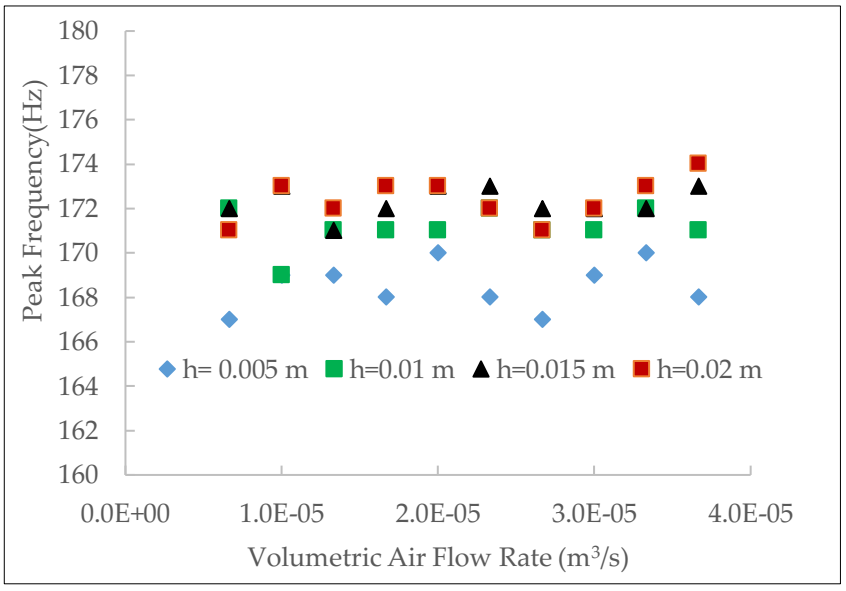

Figure 8-23 Peak frequencies as a function of flow rate.

Table 8-4 First and second peak frequencies and their respective sound pressure amplitude value

	H=0.250 m, h=0.005 m (with upper layer)									
Q (m3/s)x10^{-6}	**10**	**13.33**	**16.67**	**20**	**23.33**	**26.67**	**30**	**33.33**	**36.67**	**40**
f1(Hz)	167	169	169	168	170	168	167	169	170	168
A1(Pa)	0.025	0.029	0.033	0.023	0.036	0.028	0.045	0.034	0.031	0.038
f2(Hz)	658	60	88	86	85	85	86	87	84	85
A2(Pa)	0.004	0.006	0.009	0.011	0.009	0.012	0.013	0.013	0.013	0.014
	H=0.25 m, h=0.01 mm									
f1(Hz)	172	169	171	171	171	172	171	171	172	171
A1(Pa)	0.018	0.020	0.026	0.035	0.046	0.048	0.030	0.029	0.041	0.033
f2(Hz)	662	58	59	61	62	63	61	62	84	87
A2(Pa)	0.004	0.003	0.007	0.008	0.014	0.015	0.016	0.019	0.019	0.020
	H=0.25 m, h=0.15 m									
f1(Hz)	172	173	171	172	173	173	172	172	172	173
A1(Pa)	0.022	0.028	0.028	0.030	0.040	0.041	0.050	0.049	0.032	0.026
f2(Hz)	62	63	62	62	62	61	62	60	60	89
A2(Pa)	0.048	0.006	0.007	0.008	0.016	0.016	0.018	0.017	0.02	0.017
	H=0.25 m, h= 0.20 m									
f1(Hz)	171	173	172	173	173	172	171	172	173	174
A1(Pa)	0.023	0.028	0.028	0.029	0.030	0.029	0.030	0.028	0.034	0.034
f2(Hz)	763	764	765	63	88	87	91	89	64	87
A2(Pa)	0.004	0.005	0.005	0.005	0.007	0.009	0.011	0.013	0.010	0.012

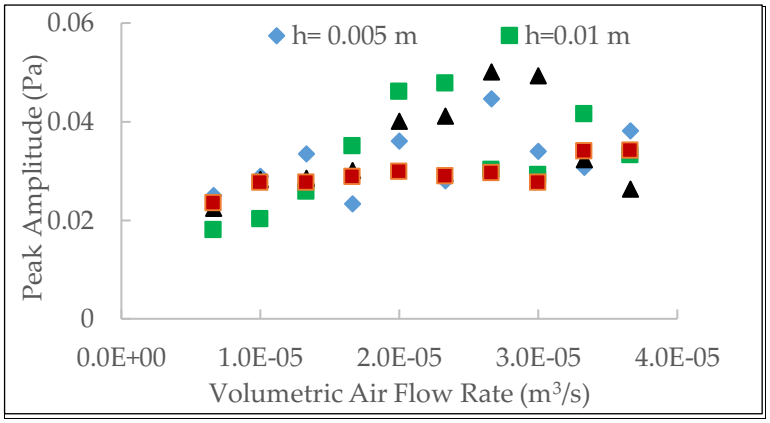

Figure 8-24 Relationship between amplitude at peak frequencies and flow rate at four oil depths.

To assess how the amplitude of the sound pressure at peak frequencies varies with experimental conditions, the amplitude at peak frequencies was plotted against the volumetric airflow rate as

shown in Figure 8-24. This figure suggests that no clear correlation has been found to detect the effect of the upper layer on the amplitude at peak frequency. In a similar manner, the spectral variation of the sound pressure level was also examined to reveal any relationship that can tell the influence of increasing or decreasing oil/slag depth.

Figure 8-25 shows the power (dB) of the sound wave in the frequency spectrum at a volumetric flow rate of 36.67×10^{-6} m^3/s at a fixed water level of 0.25 m and four oil depths. Taking the whole frequency range, the power of the signal shows no clear difference between different depths of the upper layer. Considering the sound power in a narrow frequency range, it is found that the sound power (dB) varies in magnitude as the depth of the oil increases. Figure 8-26 shows the sound power (dB) in the frequency range of 760 to 775 Hz where the sound pressure level decreases with oil depth for the volumetric air flow rate of 36.67×10^{-6} m^3/s. The arrows in Figure 8-26 indicate the range where this tendency is observed for the four top layer thicknesses simultaneously. To check if this result repeats for the other volumetric airflow rates, the average sound power (dB) within the frequency range of 760 to 775 Hz was calculated for each upper layer thickness and plotted against the flow rate. Figure 8-27 shows that the average sound power exhibits negligible variation with volumetric airflow rate but increases with oil depth.

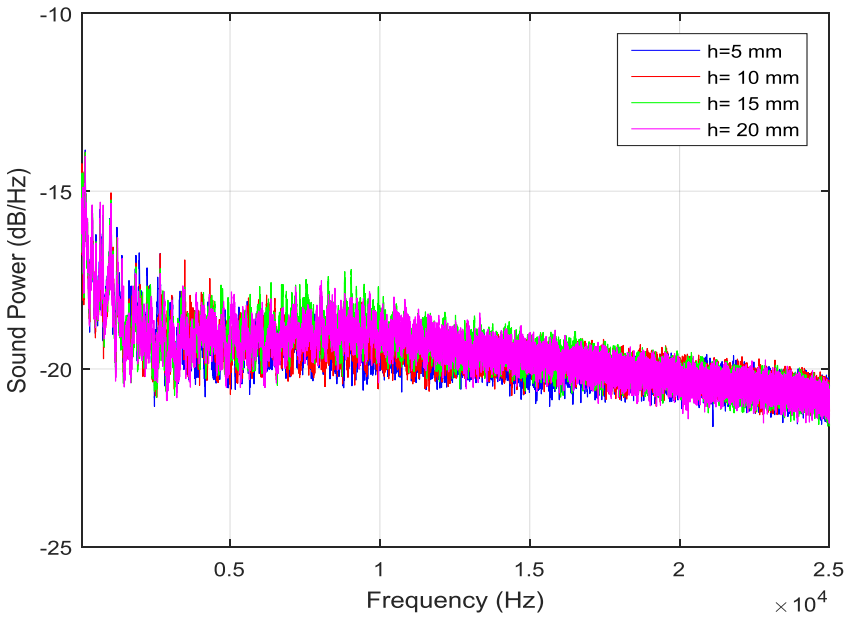

Figure 8-25 Sound pressure level at 36.67×10^{-6} m^3/s, 0.250 m thick lower layer and varying upper layer

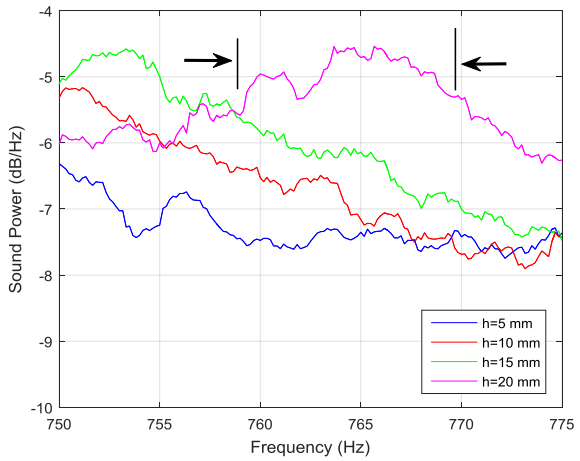

Figure 8-26 Sound pressure level for the flow rate of 36.67x10^{-6} m3/s and H=0.25 m

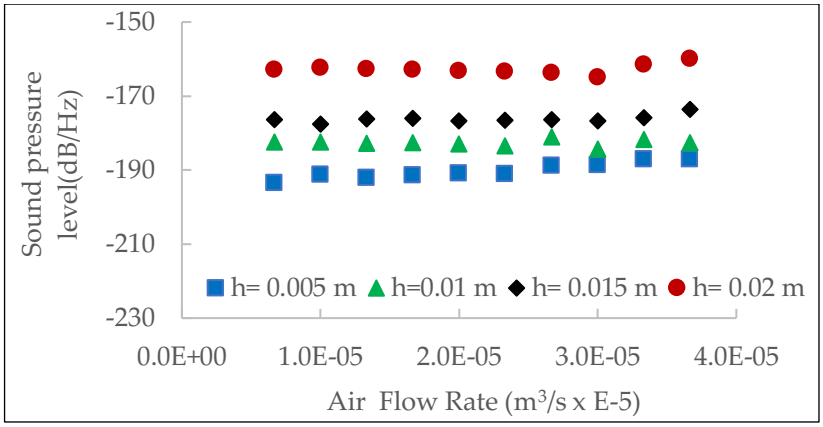

Figure 8-27 Variation of average sound pressure level with the depth of the upper layer in between 760 and 775 Hz

Table 8-5 Peak frequency values within the frequency range of 700 to 800 Hz

	H=0.25 m, h= 0.5 m (with upper layer)									
Q (m3/s)x10^{-6}	**10**	**13.33**	**16.67**	**20**	**23.33**	**26.67**	**30**	**33.33**	**36.67**	**40**
f1(Hz)	736	737	737	739	738	738	738	738	740	739
	H=0.250 m, h= 0.10 m									
f1(Hz)	747	747	748	745	746	746	767	747	747	749
	H= 0.25 m, h= 0.15 m									
f1(Hz)	753	752	754	755	753	754	755	752	752	755
	H= 0.25 m, h= 0.20 m									
f1(Hz)	765	767	765	765	765	765	766	765	764	766

Further analysis around this frequency range, i.e. 700 to 800 Hz, also revealed that the local peak frequency in this frequency range increases with an increase of oil depth. Table 8-5 contains the

values of the peak frequencies at each airflow rate and bath level while Figure 8-28 shows the trend of peak frequency with flow rate and oil depth.

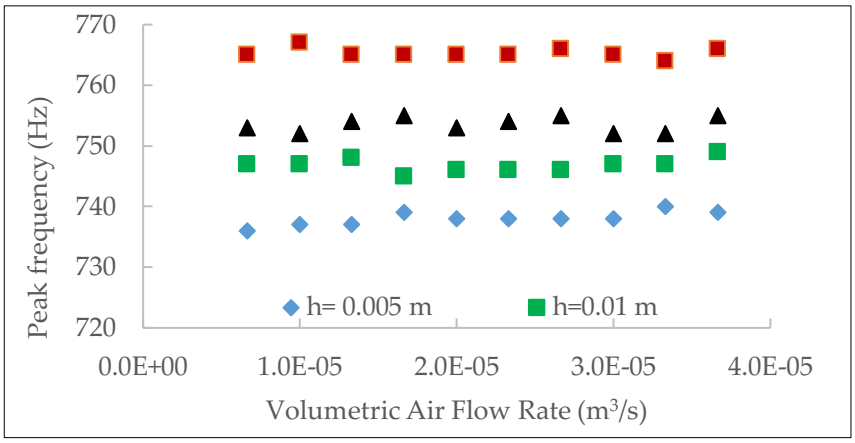

Figure 8-28 Peak frequency values at different upper layer depths

Figure 8-29 presents the frequency-amplitude plot for single and double layer air stirring. From this plot, it is clear that no peak is observed between 700 and 800 Hz in the single layer. The new peak appears during double layer bubbling. The spectral analysis shows that the peaks are generated during the double layer bubbling.

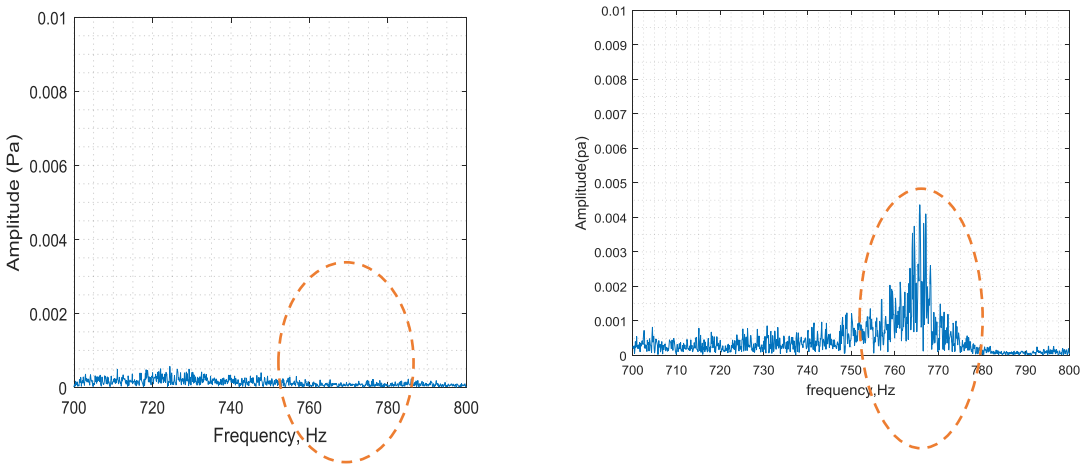

Figure 8-29 Spectral patterns of sound pressure in the range of 700 to 800 Hz a) single layer: H= 0.250 m, Q= 40x10^{-6} m^3/s b) double layer: H=0.25 m, h= 0.20 m and Q= 40x10^{-6} m^3/s

8.6.2.2 H=0.10 m

To determine if these peak frequencies persist when different water levels and same upper layer depths are used, a 0.01 m water level and an oil depth that varies from 0.005 to 0.020 m, was

stirred by identical volumetric airflow rate. The result shows that the peak frequencies exist in a different frequency range i.e. 800 to 900 Hz and 1300 to 1350 Hz. These peak frequencies do not exist in the single layer of identical bath depths and airflow rates. They only appear when the bath contains an upper layer/oil. Figure 8-31 shows the new frequency at 890 Hz.

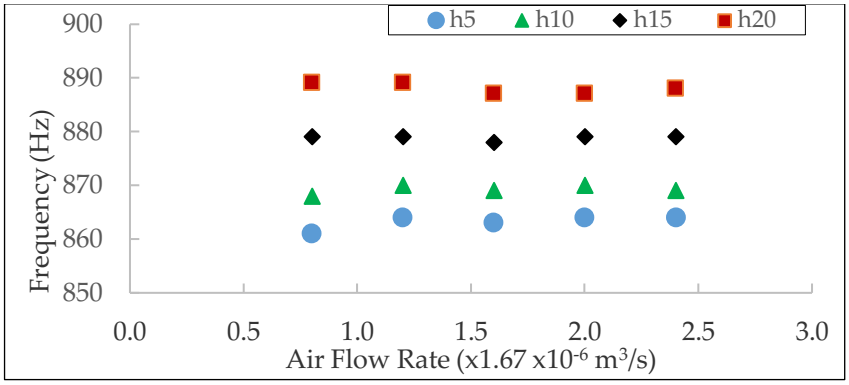

Figure 8-30 Peak frequencies when H= 0.10 and h=0.005 to 0.020 m.

The values of peak frequencies when the flow rate and oil depth are varied is shown in Figure 8-30. Other frequency ranges that show similar results were also found. As observed in Figures 8-32 and 8-33, within the frequency range of 1700 to 1715 Hz the sound power and the average sound power for each flow rate decreases as oil depth increases.

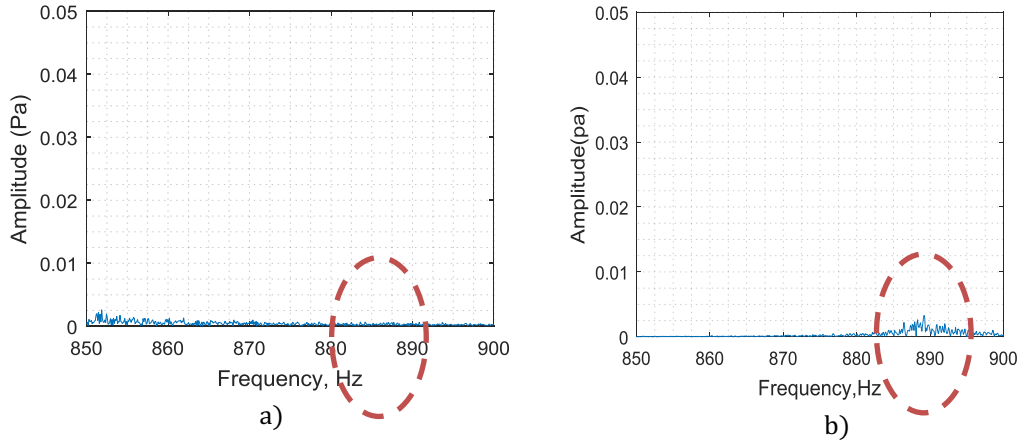

Figure 8-31 Peak frequencies at 66.67 m³/s a) single layer: H= 0.10 m and b) double layer, H=0.10 and 0.020 m thick oil

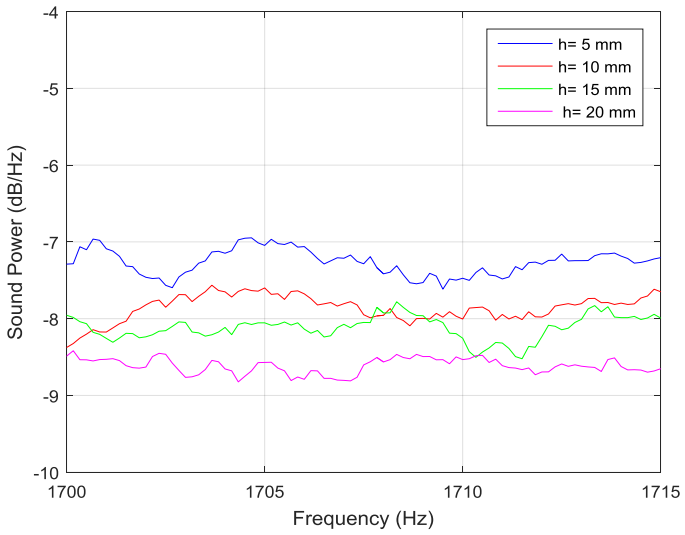

Figure 8-32 Sound pressure level at 36.67x10^{-6} m^3/s and water level of 0.25 m with oil as an upper layer

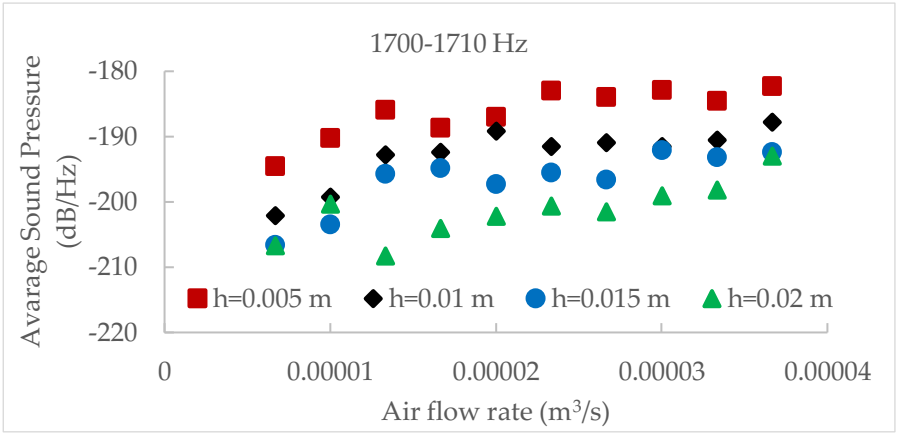

Figure 8-33 Variation of sound pressure level with the depth of the upper layer in between 1700 and 1710 Hz

8.6.2.3 H= 0.15 m

The effect of the upper layer was studied by varying height of the bottom layer. These findings show that the peak frequencies increase with top layer thickness in a specific frequency range. Figure 8-34 shows two frequency ranges that exhibit this result. These are 1400 to 1450 Hz and 500 to 550 Hz. This strengthens the analysis result made on a 0.25 m bottom layer depth.

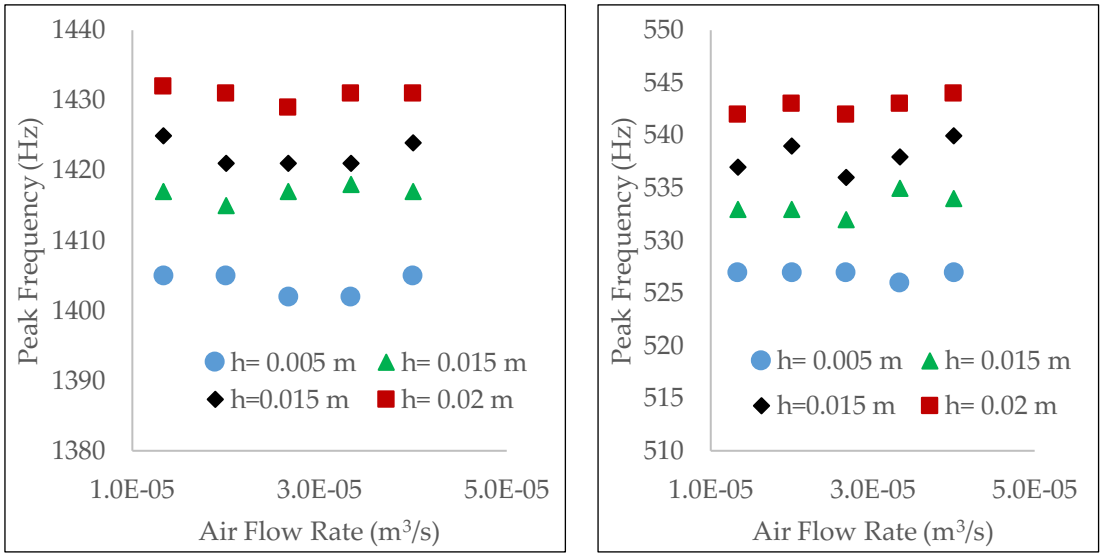

Figure 8-34 Peak frequency variation in the double layer for water level of 0.15 m and oil depth that varies from 0.005 to 0.020 m

The bubble breakup and coalescence are some mechanisms of sound generation. In ladles, some studies show that the bubble coalescence rate is function of gas volume fraction, α, and energy dissipates per unit mass of liquid, ε.[273] In addition, the bubble break up frequency is also function rate of energy dissipation, ε, to the liquid.[274] The gas volume fraction is function of the distance from bottom of the ladle, z whereas the rate of energy dissipation is dependent on mass of the liquid. Hence, the change in peak frequencies when bath height varies may be related to the change in bubble breakup and coalescence frequencies. The reason why the peak frequencies remain constant with volumetric gas flow rate remains unclear.

8.7 Conclusions

The sound pressure measured from a bottom stirred laboratory-scale cold model was studied by varying the volumetric airflow rate, lower and upper layer depths. The data was analysed in the time and frequency domains. The time domain analysis clearly reveals an increase of sound pressure magnitude as the flow rate increases both for the single and double layer models. The effect of the water level height and the oil depths were not clear from the time domain analysis. The frequency domain analysis was able to uncover the effect of the bath level change. For the single layer, the increase in bath level resulted in an increase in peak frequency and, in the frequency range of 125 to 130 Hz, a decrease in sound power (dB). In the double layer study where the lower layer was fixed at 250 mm and the upper layer was varied from 0.005 to 0.020 m,

the frequency analysis uncovers certain results. In the frequency range of 700 to 800 Hz, the local peak frequency has shown a linear increase with an increase of the oil depth. In addition, the average sound power increases in the frequency range of 760 to 775 Hz and decreases in the frequency range 1700 to 1710 Hz with oil depth. For the double layer investigation, other water levels were also considered. The result was similar except that the frequency ranges where these peaks show an increase was different. On the other hand, the peak frequencies rarely change with volumetric airflow rate for both the single and double layer stirring.

To sum up, the relationships found between sound amplitude and flow rate, peak frequency and top layer/slag height, peak frequency, and bottom layer/liquid metal are vital to control ladle stirring and steelmaking in general. More comprehensive investigations need to be carried out in the plant to verify these findings, apply or extend their applications in other steelmaking operations.

9 Discussion

The steel melt poured into continuous casting operations should have a minimal temperature and chemical gradients as well as tight control of its impurities and inclusions to improve the quality of the final steel product. This is in part achieved by stirring molten steel by a pressurized gas, usually argon, in ladles. Low gas flow rates are intended to rinse the steel and attain thermal and/or chemical homogenization while intense stirring is often practiced to facilitate slag-metal reactions.[38, 103, 275] Hence, monitoring the status of the stirring is vital in attaining the desired homogeneity, purity and cleanness, as well as ensuring optimization of gas/argon consumption.

The current monitoring system is largely dependent on experienced operators which use feedback signals from the gas line back pressure, indicated flow rates, surface turbulence, and the size of the slag opening on the top surface.[18, 189] Variable back pressure and gas leaks in the argon supply system, variable back pressure because of variable plug conditions and resistance to flow are some of the difficulties facing ladle operators in accurately evaluating stirring status in ladles.[7, 103] It is obvious that the most reliable measurement of stirring is to make direct quantification of temperature and composition of the liquid metal over time. However, this is difficult because of the plant operating conditions and may not satisfy the criterion of real-time control. This is because it takes a significant length of time to measure the chemistry of the melt. Therefore, an indirect measurement of effect stirring needs to be established to address this problem.[18] The signals such as bubbling sound and ladle vibration due to gas stirring have been used to quantify the level of agitation.[8, 10, 12, 13, 15, 16, 154, 155] This online monitoring system is most beneficial when the operator cannot see the slag surface in a ladle and for weak purging conditions.[8]

Mucciardi[19] used an accelerometer to measure ladle vibration due to stirring to correlate the mixing power and vibration signal. The study reported that an accelerometer is a suitable transducer for monitoring the interaction between liquids and gases when direct contact with the liquid phase is not possible.

The work of Minion et al. [10] focused in developing vibration signal based monitoring technique for ladle stirring. Kemeny and his co-researchers developed commercial sensors based on ladle vibration to predict the degree of stirring.[12, 189] Others like Burty et al.[13, 15, 16],Yuri et al.[8] and Kostetskii et al.[14] have measured vibration, sound and/or ladle eye size on industrial and laboratory scales to characterize the stirring process. Xu et al.[7] used a different approach by combining the vibration, bubbling sound and ladle eye size to find the latent variable to predict the stirring power. Relationships developed between one-dimensional vibration and flow rate and Froude number by some researchers were not working for double layer water model data. This suggests that a detailed study is required for metal bubbling that consists significant amount of slag. Detecting the stirring status at low flow rates as well as the effect of vibration sensor location is also not fully understood. In addition, the effect of the top and bottom layers on the bubbling sound was not given much attention. Hence, this study focused on studying low flow rate stirring process using vibration and sound signals to automate the stirring process online. This research had several key objectives described in Chapter 3.

The first key objective was to select an optimum vibration-sensor location. Industrial working conditions are harsh. The high-temperature surfaces, in particular, may affect the performance of the contact sensor. In some studies, the contactless laser vibrometer has been taken as a solution to cope with hot surfaces of the ladle.[15, 16] However, Laser Doppler Vibrometer (LDV) has limitations related to directional uncertainty, stand-off distance, poor signal to noise ratio for low diffusive surfaces, generation of image interference with rough surfaces and vulnerability to harsh industrial working conditions.[276, 277] An accelerometer was therefore chosen to measure vibration. The optimum location of the accelerometer was selected to undertake successful measurements.

The factors that were considered in the selection criteria were; the amount information obtained, accessibility for installation and safety issues. The study of the sensor location was carried out at a laboratory scale using physical cold models. Six locations were studied. Three were on the external wall of the cold model apparatus whereas the other three are on the ladle/vessel support, the external wall of a tank of a vacuum degasser and on the exterior wall of the vessel/ladle. In each location, the accelerometer was mounted on a flat smooth surface using a stud to have the test surface and the accelerometer well fused together due to the clamping force. This ensures

exact replication of motion of both bodies at all frequencies i.e. critical dynamic information can be obtained during vibration data acquisition.

The study found that that the average vibration amplitudes are not similar in magnitude when identical axes are compared. To examine the amount of information available in each vibration dataset captured from each position, principal component analysis was applied. This revealed that the structure of the data is similar in the six locations. The sum of the first two latent variables can pick almost all of the information regarding the stirring process variation. However, the informative frequency ranges may shift their position with sensor location. The sensor can be mounted on wall, support or tank because all positions provide the equivalent magnitude of information. This implies that the amount of information of the stirring process of the cold model does not depend on the sensor locations considered in this study. This result is useful in the industrial applications in many ways. It simplifies the difficulty of locating the sensor caused by temperature, accessibility and safety issues. Hence, the outcome of this research shows the use of contact sensor/ accelerometer is not limited by a blistering heat of a ladle surface since the sensor can be mounted on a less hot surface of a part that is well assembled to the ladle system.

Once the sensor optimum location was determined ladle vibration data was collected over a wide range of experimental conditions in the cold model study. Two physical cold models that replicate ladles of different capacity were used to investigate bottom gas stirring at different flow rate ranges. One model is made of plastic material, which is 1/10 of a 200-tonne ladle, and the other is made of stainless steel and is 1/10 of a 160-tonne ladle. In both cases, geometric and mechanical similarities are respected. The plastic cold model did not consider the wall material and vessel shape. This material property and geometric shape may influence the vibration signal. Hence, a second physical cold model was designed that has similar wall material and geometric shape with the industrial ladle to improve the accuracy of the vibration signal. The cold model was built from steel material to have comparable vibration dampening characteristics with the actual industrial ladle. The steel walled cold model study was part of an industrial project undertake in collaboration with Tata Steel. A plant trial was carried out to compare the results of the corresponding steel-walled cold model.

In the cold model studies. Equation 4-10 ($Q_m = \lambda^{2.5} Q_f$) which is based on plume Froude number similarity criterion ($(Fr_p)_m = (Fr_p)_f$) was applied to determine the volumetric flow rates. This helped the flow rates to be within the range of flow rates applied in ladle metallurgy.

For the plastic-walled water model, the study was carried out at three flow rate intervals. The corresponding flow intervals in industrial scale are 0.53 to 2.63x10^{-3} m^3/s, 2.63 to 13.02x10^{-3} m^3/s, and 13.02 to 34.23x10^{-3} m^3/s based on Froude number similarities. The top and bottom layers were also varying in each flow interval. The sensor was mounted on the external wall of the rig.

The main analysis methods used in this study were linear PCA and PLS. The choice of PLS was due to its ability to handle extraneous, collinear and missing data. Another essential characteristic of PLS is its accuracy improves with more observations. The selection PCA based on its reliability and ability to detect the structure in a large dataset. Both PLS and PCA are simple and convenient for online monitoring. These techniques also have good success stories in industrial multivariate monitoring.[28, 30, 31, 166, 172, 256]

The study showed that the triaxial vibration data from each interval has maximum underlying structure. The first latent variable, which is a combination of the three axes vibration signals, can efficiently predict both the amount of stirring energy and bath recirculation speed adequately for vibration data without the top layer. This indicates that ladles that operate with little or no slag, the vibration latent variables from principal component analysis can accurately and efficiently predict the stirring intensity. In most cases, tapping of steel into a ladle leads to the uncontrolled amount of slag carry over. The carryover slag may affect the level of melt recirculation and degree of turbulence in the liquid bath.[222] This means the dynamics of the ladle wall is also affected by the slag presence. Hence, a layer of oil was added at the top and varied throughout the experiment. The correlation between PCA latent variable and stirring indicators is not linear for this data. To find the linear relationship between the stirring process parameters and the corresponding induced vibration, partial least squares (PLS) was applied to the input parameters (flow rate and bath height) and vibration (response) matrices simultaneously. As a result, the linear combinations of the responses that explain maximum variation in the input parameters have a good linear relationship with stirring indicators. The relationship is stronger at fixed bottom and top layers. This robust linear relationship is exhibited in specific frequency ranges and the frequency ranges vary with sensor location and flow rate range.

A similar study carried out on a steel-walled water model, which is 1/10 of a 160-tonne ladle, showed that vibration data has underlying structure and the majority of this structure can be explained by the first latent variable. The common variation between vibration and process parameters were discovered in certain frequency ranges by applying PLS. To verify the results of the water model investigations, plant trials were performed on a 160-tonne vacuum degasser ladle. Six heat with different working conditions were considered in this plant trial. The study was carried out individually and in combination.

Similar to cold model data, PCA showed that the vibration data of each heat and the combined are highly structured. The first two principal components can pick most of the stirring process variation. The frequency ranges that pick this structure are 60 to 70, 70 to 80, 80 to 90 and 90 to 100 Hz. These frequency ranges were also observed in the water model studies. In the combined plant data, when slag weight shows little or no variation, the underlying data structure tends to be stronger. This was also the case in the cold model investigation where the variation of the top layer reduces the strength of the linear relationship.

The data within the informative frequency ranges was further investigated by PLS to develop a model that predicts the stirring status. The prediction is good when considering only one heat in the frequency range of 60 to 70 Hz. On the other hand, when data from all heats are combined and analysed by PLS, the prediction was not possible i.e. the correlation between the latent variable of the process parameters and vibration is not linear. There are several possible explanations, which need to be addressed to identify which factor affects the relationship. Firstly, the underlying relationship could be nonlinear. Secondly, the data comes from heats that have different process parameter values such as plug position, plug number, steel weight, slag weight, plug life, slag line life, and barrel life. In addition, some heats were carried out with new porous plugs and others with old plugs that served from two to four heats. The location of these plugs was also different in the six heats. Some heats had sidewall plugs whereas others were stirred by a sidewall and a central plug. Studies reported that flow patterns are strongly dependent on the number and positions of the porous plugs.[278] In Chapter 7, the effect of plug life on vibration magnitude was studied using four-plug lives. The vibration slightly decays with plug life. This may be a sign of plug blockage by metal build-up allowing less gas flow rates. In a similar manner, the current study found that the variability in slag depth affects the structure of the vibration data. From Newton's Laws, the mass of the molten metal also affects the acceleration.[279]

Hence, the variability of these parameters, steel weight, plug life, position and number, and slag weight, may have partly played a role in this relationship. The influence of barrel life and slag line life on bubble flow and then vibration is not available in the open literature. This suggests that comprehensive plant trials are necessary to establish an accurate stirring prediction model for plant data.

Water model studies and plant trials show that the overall stirring process variation can be explained by the comparable variations of the oscillation along the x, y and z axes. This supports the notion that three-dimensional vibration signals are equally important in monitoring the stirring process online.

In order to use the PLS regression model, knowledge of the liquid metal and slag weight is required. The peak frequencies of the sound signal can provide information on the thickness of the slag/top layer and depth of liquid metal. This helps in predicting the stirring power and amount of metal circulation using the developed models. Thus, the stirring process can be monitored by combining the three axes vibration with the sound signals if the right frequency ranges are chosen carefully, and the relationship for plant data is further studied with adequate plant trials and proper noise filtering techniques.

In general, the key findings of this study can be summarized as follows:

- The accelerometer can be mounted on the ladle wall, the ladle support or the external wall of the tank (in the case of vacuum degasser). The location of the sensor does not affect the quality and amount of information found in the vibration signal.
- There is a strong underlying structure in the laboratory as well as plant vibration data.
- There is a strong linear relationship between first latent variable, which is a linear combination of the three axes vibration signal, and stirring indicators such as stirring power, molten metal recirculation speed, and gas flow rate.
- There are specific informative frequency ranges where the high data structure and strong relationships exist.
- The depth of the bottom layer/molten metal and thickness of the top layer/slag can predict from peak frequencies of the sound pressure signal.

- There is a strong linear relationship between average sound pressure generated during stirring and air/gas flow rate.

Though this study contributed significant outcomes, it had also some weaknesses attributed to different scenarios. PLS and PCA have a weakness in that they do not detect any nonlinear relationships. Other techniques such as artificial neural networks may be applied in the future to discover any nonlinear correlations. During physical modeling, not all operating conditions and geometric configurations were replicated. For example, the physical and dynamic property of slag is highly variable and was difficult to mimic with a single material. The study used oil merely based on its immiscibility with and being lighter than water. Hence, the dynamic behavior of oil and slag may not be equivalent. The vibroacoustic method for ladle stirring monitoring appeared to be sensitive to the surface tension of the liquid.[8] In addition, a change of metal chemistry such as sulfur content may influence the size of the bubbles[280] which in turn can affect the bubble dynamics . The bubble dynamics has direct relationships with the sound and vibration signal. During the water model study, the issue of surface tension and chemistry variation were not considered which might alter the result somehow. Plant vibration study as well has not included the effect of variation in chemical composition during stirring on vibration signal. In the plant, a general relationship could not be established due to variability in plant operations and inadequate data. This means the separate measurement of all operating parameters may be required before the vibration signal can be used as a reliable measurement of stirring. The results obtained in this study apply only to stationary ladle. For ladle in ladle cars, the movement can create gravity modes that can give false vibration.

However, beside these problems , the results from the cold model studies and plant trials show that ladle gas stirring can be automated using triaxial vibration and sound signals to meet high steel quality demands.

10 Conclusions and Recommendations

10.1 Conclusions

In the present work, vibration and sound signals were used to investigate ladle gas stirring. In the laboratory, two physical cold models of different capacity and design were used. A plastic-walled and steel-walled cold models simulated 1/10 of 200 and 160-tonne ladles respectively. Geometric and Froude number similarity criteria were applied to replicate the geometry and the flow in these gas stirred ladles. Water and oil were used to simulate the molten metal and the top-layer slag respectively. Air at high pressure was injected through nozzles, located at the bottom of the laboratory apparatus, to stir the water-oil bath. Vibration and sound signals were acquired during stirring by a tri-axial accelerometer and a microphone respectively at different volumetric airflow rates, water levels, and oil thicknesses. Vibration measurements were also carried out on an industrial scale. The vibration data was mainly analysed by PCA and PLS in the frequency domain whereas the sound signals were investigated using the FFT and the power spectral density.

One aim of this study was to assess if the location of the accelerometer affects the amount of information about the stirring. In each cold model, three candidate locations were investigated. In the plastic-walled model, the locations were on the external wall of the apparatus whereas in the steel walled model the accelerometer was mounted on the ladle wall, the ladle support and the tank external wall. PCA was applied to compare and contrast the information in the data measured from the considered locations. Data were collected from the selected locations on each laboratory scale and full scales to carry out the study on ladle stirring. This study discovered important findings that can help in improving the online stirring process control.

The study of optimum sensor location showed that the amount of information about stirring obtained from vibration data measured from the candidate location (the ladle external wall, the ladle supports, or the tank external wall) is very similar. The frequency range where this information is situated may slightly vary with accelerometer location with no significant differences in the size of the information. Hence, the quality of the vibration signal captured during melt stirring is not affected by the accelerometer location. This is an important finding for industrial applications as the accelerometer can be mounted on relatively cooler surfaces/parts

such as the ladle support or tank external wall to get similar information regarding the stirring process.

The laboratory study as well as plant scale investigation found that the vibration data associated with stirring is highly structured. The x , y and z accelerations are equally important in obtaining highly structured data. Specific frequency ranges that retain this structure are found in the cold model and plant trials. The frequency ranges tend to shift when different air/gas volumetric flowrate ranges were used to agitate the bath. This is a vital finding in addressing the low flow rate stirring detection problem in industrial ladles. Vibration latent variables (combination of x , y and z accelerations) computed in these frequency ranges have strong linear relationships with stirring indicators: the stirring power and bath recirculation speed models developed in water models by other researchers. These correlations are strong when known fixed water/liquid metal depth and oil/slag thickness are considered. The information about the metal and slag depths can be found from the sound signal analysis.

The investigation of sound pressure generated from water model bubbling found that the peak frequencies increase when the depth of the bottom layer/water was increased. An increase in volumetric flow rate does not result in shifting the peak frequency when maintaining the bath level is constant. In addition, at a fixed bottom layer depth and variable top layer/oil thickness varies, new local frequencies emerge. The location of the local peak frequency that appears when a top layer is present in the bath is different for different water/molten metal depths. Moreover, the average sound pressure was found to increase linearly with an increase of volumetric airflow rate but no clear relationship is observed with bath height. Hence, the change in flow rate is related to the magnitude of sound pressure whereas peak frequencies are useful to detect the bottom and top layer depths.

In summary, the accelerometer location does not affect the information content of the signal. Vibration data collected from two water models and the plant has maximum structure. The relationship between this structured data and stirring power is strong in specific frequency ranges for each volumetric gas flow rate range. The sound pressure signal is able to predict the water depth and oil thickness. PCA was used to find the structure of the dataset whereas PLS was an important tool to discover the linear relationship between input and output variables. The sound signal can provide information on the amount of metal and slag, which are vital inputs

to the PLS model. Hence, combining the results of vibration and bubbling sound study, the online monitoring of ladle stirring can be effective.

To sum up, the accelerometer location does not affect the information content of the signal. Vibration data collected from two water models and the plant has maximum structure. The relationship between this structured data and stirring power is maximum at specific frequency ranges for each volumetric gas flow rate range. The sound pressure is able to predict the water depth and oil thickness. Hence, combining the results of vibration and bubbling sound study, the online monitoring of ladle stirring can be effective.

10.2 Limitations, Recommendations, and Future Directions

The results of the study are important in developing an effective online control system for ladle stirring process. However, the current study has some limitations that need to be addressed in future research.

- The physical cold models may not be ideal replications of the industrial ladles. Water and oil are approximate substitutions of molten metal and slag and the complex structure of the ladle and its accessories are difficult to model in the laboratory. This means a perfect flow that mimics the flows in gas stirred ladles may not be achieved in the laboratory. In addition, fluid properties such as damping and surface tension, chemistry change and gas properties at operating condition may not be appropriately replicated. This may affect the strength and quality of the vibration and sound signal. Hence, laboratory as well as plant scale studies should consider these factors.
- The current vibration measurement was undertaken only on two ladle capacities. This study can be repeated for other ladle capacities to verify the result and check its reproducibility for the studied experimental conditions. In addition, apparent gas flow rates were used to build relationships, which may generate some errors due to gas leakage.
- Considering the variability of the stirring process parameters in ladle operations, the plant trials need to be carried out in a comprehensive manner to draw important conclusions and verify water model results

- The sound pressure was measured from a cold model only. Industrial trials should be performed and analysed using efficient noise filtering techniques.
- It is also important to apply a different analysis technique if the current results are consistent. Artificial neural network and fuzzy logic and nonlinear forms of PCA can be applied to the vibration data to detect any nonlinear relationship that exists in the stirring process.
- Noise filtering is a big issue in vibration and sound signal measurement in an industry where various sources of noise can distract the main signal. Hence, this needs to be addressed by considering a wide range sources of noise to develop to filter out irrelevant signals.
- Future research should focus on measuring vibration and sound stirring process parameters such as slag, plug life, position and number variability to measure vibration and sound to control the stirring process online. Relationships between chemical/ thermal homogeneity and vibration/acoustic signals can be studied for a more direct stirring control.

To conclude, the current study has achieved encouraging results and if the above issues are resolved, online stirring process control in ladles can be undertaken efficiently and accurately.

References

1. Fruehan, R.J., *The making, shaping, and treating of steel*. 1999: AISE Steel Foundation.

2. Fruehan, R., *Overview of steelmaking processes and their development.* The Making, Shaping and Treating of Steel: Steelmaking and Refining volume, 1998: p. 2-3.

3. Fruehan, R.J. and Wakelin, D.H., *The Making, shaping, and treating of steel*. 11th ed.. ed, ed. Foundation, A.S. 1998, Pittsburgh, Pau.: Pittsburgh, Pau. : AISE Steel Foundation.

4. Ghosh, A., *Secondary Steelmaking Principles and Applications*. 2000, Hoboken : Taylor and Francis: Hoboken. p. 14-20.

5. Ghosh, A., *Secondary Steelmaking : Principles and Applications*. 2000, CRC Press: Baton Rouge. p. 248-250.

6. Millman, M.S., *Secondary steelmaking developments in British Steel.* Ironmak. Steelmak., 1999. 26(3): p. 169-175.

7. Xu, X., Brooks, G.A., and Yang, W., *Online analysis of stirring processes in ladle metallurgy.* Metallurgical and Materials Transactions B, 2010. 41(5): p. 1025-1032.

8. Yuriy, K., David, K., Iluya, K., Vadim, K., Ilya, D., and Andrey, O. *Application Of Vibroacoustic Monitoring Technique on A Ladle Furnace Unit During Steel Treatment*. in *METAL 2007: 16 th International Metallurgical and Materials Conference*. 2007.

9. Subagyo and Brooks, G., *Online Monitoring of Dynamic Slag Behavior in Ladle Metallurgy.* ISIJ International, 2003. 43(8): p. 1286-1288.

10. Minion, R., Leckie, C., Legeard, K., and Richardson, B., *Improved ladle stirring using vibration technology at Stelco Hilton Works.* Iron & steelmaker, 1998. 25(7): p. 25-31.

11. Tan, D., Ji, S., Li, P., and Pan, X., *Development of vibration style ladle slag detection methods and the key technologies.* Science China Technological Sciences, 2010. 53(9): p. 2378-2387.

12. Kemeny, F.L., Walker, D.I., and Jones, J.A., *Process for controlling the stirring energy delivered by a gas flowing through a liquid*. 2001, Google Patents. p. 1-11.

13. Burty, M., Pusse, C., Wetta, P., Sulin, F., Bertoletti, C., Borneque, Y., Pernet, D., and Carioli, E., *Method for controlling a molten metal bath bubbling in a metallurgical vessel and a device for carrying out said method*. 2011, Google Patents. p. 1-8.

14. Kostetskii, Y., Kvasov, I., Degtyarenko, I., and Kukui, D., *Control and management of the out-of-furnace treatment of metal using ladle vibrations.* Russian Metallurgy (Metally), 2009. 2009(7): p. 595-597.

15. Burty, M., Pussé, C., Sheng, D., DANNERT, C., KOCHNER, H., SANCHO, L., DIAZ, J., VALENTIN, P., BRUCH, C., and ARTEAGA, A., *Development of advanced methods for the control of ladle stirring process.* EUR, 2007(22988): p. 1-139.

16. Burty, M., Pussé, C., Bertoletti, C., Wetta, P., and Cariola, E., *Kettlor: efficient stirring in ladle metallurgy.* Revue de Métallurgie, 2006. 103(11): p. 493-499.

17. McLean, A., *The science and technology of steelmaking—Measurements, models, and manufacturing.* Metallurgical and Materials Transactions B, 2006. 37(3): p. 319-332.

18. Xu, B.X., *Analysis of Bubble Flow in Metallurgical operations Using Multivariate Statistical Technique*, in *Mathematics*. 2010, Swinburne University of Technology: Melbourne, Australia. p. 247.

19. Mucciardi, F., *Monitoring Liquid-Gas Interactions with an Accelerometer.* Canadian Metallurgical Quarterly, 1987. 26(4): p. 351-357.

20. Singiresu, S.R., in *Mechanical Vibrations*. 2004, Prentice Hall: USA. p. 1-31.

21. Inman, D.J., *Engineering Vibration*. 3rd ed. 2008, New Jersey, USA: Pearson, Prentice Hall. 669.

22. Thomson, W.T., Dahleh, M. D., *Theory of Vibration with Application*. 5th ed. 1998, New Jersey,USA: Prentice Hall. 524.

23. Norton, M.P., *Fundamentals of Noise and Vibration Analysis for Engineers*, Karczub, D.G., Editor. 2003, Cambridge : Cambridge University Press: Cambridge. p. 2-127.

24. E., M., *Detail Practice-Acoustics and Sound Insulation*. 2009, Architetur-Dockumentaio GmbH: Munich. p. 110-115.

25. Manasseh, R., Riboux, G., Bui, A., and Risso, F., *Sound emission on bubble coalescence: imaging, acoustic and numerical experim*, in *16th Australasian Fluid Mechanics Conference (AFMC)*. 2007, School of Engineering, The University of Queensland. p. 167-173.

26. Pistorius, P.C., *Chapter 2.3 - Bubbles in Process Metallurgy A2 - Seetharaman, Seshadri*, in *Treatise on Process Metallurgy*. 2014, Elsevier: Boston. p. 179-196.

27. Rencher, A.C., *Methods of Multivariate Analysis*, Christensen, W.F., Editor. 2012, Hoboken : Wiley: Hoboken. p. 390-408.

28. Shlens, J., *A tutorial on principal component analysis.* arXiv preprint arXiv:1404.1100, 2014.

29. Smith, L.I., *A tutorial on principal components analysis.* Cornell University, USA, 2002. 51: p. 52.

30. de Jong, S., *SIMPLS: An alternative approach to partial least squares regression.* Chemometrics and Intelligent Laboratory Systems, 1993. 18(3): p. 251-263.

31. Kourti, T., *Application of latent variable methods to process control and multivariate statistical process control in industry.* International Journal of Adaptive Control and Signal Processing, 2005. 19(4): p. 213-246.

32. Barker, K., Paules, J., Rymarchyk Jr, N., and Jancosko, R., *Oxygen steelmaking furnace mechanical description and maintenance considerations.* The Making, Shaping and Treating of Steel, Steelmaking and Refining Volume, Pittsburgh, PA: AISE Steel Foundation, 1998: p. 431-474.

33. Mincu, V. and Ittu, S., *Gas Removal and Increase of Purity by Conventional Methods of Steel Ladle Refining In Secondary Treatment.* Metalurgia, 2012. 64(5): p. 41-46.

34. Ghosh, A., *Secondary Steel Making Principles and Application*. 2001, CRC Press LLC: USA. p. 4.

35. Mazumdar, D., *Modeling of Steelmaking Processes*. 2009, CRC Press. p. 7-15.

36. Krishnapisharody, K. and Irons, G.A., *A Critical Review of the Modified Froude Number in Ladle Metallurgy.* Metallurgical and Materials Transactions B, 2013. 44(6): p. 1486-1498.

37. Mazumdar, D., Kim, H., and Guthrie, R., *Modelling criteria for flow simulation in gas stirred ladles: experimental study.* Ironmaking & steelmaking, 2000. 27(4): p. 302-309.

38. Mazumdar, D. and Guthrie, R.I., *The physical and mathematical modelling of gas stirred ladle systems.* ISIJ international, 1995. 35: p. 1-1.

39. Brooks, G. *Advances in ladle metallurgy control*. in *Ladle and Tundish Metallurgy: as held at the 41 st Annual Conference of Metallurgists of CIM(COM 2002)*. 2002.

40. Guthrie, R., *Process metallurgy for ladle-tundish-mould operations*, in *Ladle and Tundish Metallurgy:*. 2002, MET Soc: Ontario. p. 3-26.

41. Pretorius, E., *Fundamentals of EAF and Ladle Slags and Ladle Refining Principles.*

42. Horii, K., Tsutsumi, N., Kitano, Y., and Kato, T., *Processing and reusing technologies for steelmaking slag.* Nippon Steel Technical Report, 2013. 104: p. 123-129.

43. Yildirim, I.Z. and Prezzi, M., *Chemical, Mineralogical, and Morphological Properties of Steel Slag.* Advances in Civil Engineering, 2011. 2011: p. 13.

44. Erven, K.A., Matlock, D.K., and Krauss, G., *Effect of sulfur on bending fatigue of carburized steel.* Journal of Heat Treating, 1991. 9(1): p. 27-35.

45. Holappa, L., *Ladle injection metallurgy.* Int. Met. Rev., 1981. 27(2): p. 53-76.

46. Väinölä, R.V., Holappa, L.E.K., and Karvonen, P.H.J., *Modern steelmaking technology for special steels.* Journal of Materials Processing Technology, 1995. 53(1): p. 453-465.

47. Okumura, K., Ban, M., Hirasawa, M., Sano, M., and Mori, K., *Rate of SiO₂ Inclusion Removal from Molten Cu to Slag under Gas Injecion Stirring Condition.* ISIJ International, 1995. 35(7): p. 832-837.

48. Mapelli, C., Nicodemi, W., Vedani, M., and Zoppi, A., *Control of inclusions in a resulphurised steel.* Steel Research, 2000. 71(5): p. 161-168.

49. Becker, J.-U. and Oeters, F., *Model experiments of mixing in steel ladles with continuous addition of the substance to be mixed.* Steel Research, 1998. 69(1): p. 8-16.

50. Jauhiainen, A., Jonsson, L., and Sheng, D.-Y., *Modelling of alloy mixing into steel.* Scandinavian Journal of Metallurgy, 2001. 30(4): p. 242-253.

51. Scott, F.W., *Effect of Nitrogen on Steel.* Industrial & Engineering Chemistry, 1931. 23(9): p. 1036-1051.

52. Llewellyn, D., *Nitrogen in steels.* Ironmaking & steelmaking, 1993. 20(1): p. 35-41.

53. Kleimt, B., Köhle, S., Johann, K., Jungreithmeier, A., and Molinero, J., *Dynamic process model for denitrogenation and dehydrogenation by vacuum degassing.* Scandinavian journal of metallurgy, 2000. 29(5): p. 194-205.

54. Kor, G. and Glaws, P., *Ladle refining and vacuum degassing.* The Making, Shaping and Treating of Steel, 1998: p. 661-713.

55. Albert, L., *Method and apparatus for continuously degassing molten metals, particularly steel, by evacuation*. 1959, Google Patents. p. 1-6.

56. Dittrich, R., Tembergen, D., and Teworte, R., *Method of degassing molten steel*. 2003, Google Patents.

57. Yano, M., Kitamura, S.-y., Harashima, K., Inomoto, T., Azuma, K., and Nagahama, H., *Recent advances in ultralow-carbon steel refining technology by vacuum degassing processes.* Nippon Steel Technical Report, 1994: p. 15.

58. Mondal, M.K., Maruoka, N., Kitamura, S., Gupta, G.S., Nogami, H., and Shibata, H., *Study of Fluid Flow and Mixing Behaviour of a Vacuum Degasser.* Transactions of the Indian Institute of Metals, 2012. 65(3): p. 321-331.

59. Ishimura, K., Saito, F., Yoshikawa, M., Okada, M., and Nakajima, S., *Vacuum degassing method and its apparatus*. 1994, Google Patents. p. 1-16.

60. Kuwabara, T., Umezawa, K., Mori, K., and Watanabe, H., *Investigation of Decarburization Behavior in RH-reactor and Its Operation Improvement.* Transactions of the Iron and Steel Institute of Japan, 1988. 28(4): p. 305-314.

61. Zulhan, Z. and Schrade, C., *Vacuum Treatment of Molten Steel: RH (Rurhstahl Heraeus) versus VTD (Vacuum Tank Degasser)*, in *SEAISI*. 2014: Kuala Lumpur. p. 1-10.

62. Satyendra. *Vacuum degassing processes for liquid steel*. ISPA7 guru 2016 May 16 2017]; Available from: http://ispatguru.com/vacuum-degassing-processes-for-liquid-steel/.

63. Themelis, N. and Goyal, P., *Gas Injection in Steelmaking: Mechanism and Effects.* Canadian Metallurgical Quarterly, 1983. 22(3): p. 313-320.

64. Pan, S.M., Chiang, J.D., and Hwang, W.S., *Effects of gas injection condition on mixing efficiency in the ladle refining process.* Journal of Materials Engineering and Performance, 1997. 6(1): p. 113-117.

65. Szekely, J., Carlsson, G., and Helle, L., *The Fundamental Aspects of Injection Methalurgy*, in *Ladle metallurgy*. 1989, Springer-Verlag, : New York, New York , USA. p. 27-71.

66. Khajavi, L.T. and Barati, M., *Cold Model Study of Emulsification Behavior in Bottom Blown Metallurgical Baths Covered with Thick Slag.* ISIJ International, 2010. 50(5): p. 654-662.

67. Tafaghodi Khajavi, L. and Barati, M., *Liquid Mixing in Thick-Slag-Covered Metallurgical Baths—Blending of Bath.* Metallurgical and Materials Transactions B, 2010. 41(1): p. 86-93.

68. Sahai, Y. and Guthrie, R.I.L., *Hydrodynamics of gas stirred melts: Part I. Gas/liquid coupling.* Metallurgical Transactions B, 1982. 13(2): p. 193-202.

69. Hwang , H., A. Pratt, M., and Bury, K., *Optimal Mixing Condition for Top Stir Gas Injection at ArcelorMittal Burns Harbor*, in *AISTech 2015*, AIST, Editor. 2015, AIST: U.S.A. p. 296.

70. Chhabra, R.P., *Bubbles, Drops, and Particles in Non-Newtonian Fluids, Second Edition*, in *Bubbles, Drops, and Particles in Non-Newtonian Fluids, Second Edition*. 2012, Hoboken : Taylor and Francis: Hoboken.

71. KUO, T.-Y.K.a.J.-C., *Determination of Mixing Time in a Ladle-Refining Process Using Optical Image Processing*. Vol. 51. 2011, Tokyo, JAPON: Iron and Steel Institute of Japan.

72. Peranandhanthan, M. and Mazumdar, D., *Modeling of slag eye area in argon stirred ladles.* ISIJ international, 2010. 50(11): p. 1622-1631.

73. Krishnapisharody, K. and Irons, G., *Modeling of slag eye formation over a metal bath due to gas bubbling.* Metallurgical and Materials Transactions B, 2006. 37(5): p. 763-772.

74. Yonezawa, K. and Schwerdtfeger, K., *Correlation for area of spout eyes in ladle metallurgy.(Comments on spout eye area correlation in ladle metallurgy by Subagyo, brooks and irons).* ISIJ international, 2004. 44(1): p. 217-219.

75. Yonezawa, K. and Schwerdtfeger, K., *Dynamics of the spout of gas plumes discharging from a melt: Experimental investigation with a large-scale water model.* Metallurgical and Materials Transactions B, 2000. 31(3): p. 461-468.

76. Yonezawa, K. and Schwerdtfeger, K., *Height of the spout of a gas plume discharging from a metal melt.* Metallurgical and Materials Transactions B, 1999. 30(4): p. 655-660.

77. Yonezawa, K. and Schwerdtfeger, K., *Spout eyes formed by an emerging gas plume at the surface of a slag-covered metal melt.* Metallurgical and Materials Transactions B, 1999. 30(3): p. 411-418.

78. Krishnapisharody, K. and Irons, G., *A study of spouts on bath surfaces from gas bubbling: Part I. Experimental investigation.* Metallurgical and Materials Transactions B, 2007. 38(3): p. 367-375.

79. Guo, D. and Irons, G., *A water model and numerical study of the spout height in a gas-stirred vessel.* Metallurgical and Materials Transactions B, 2002. 33(3): p. 377-384.

80. Xu, X., Brooks, G., and Yang, W., *Modelling of Ladle Eye Phenomena.* Chemeca 2008: Towards a Sustainable Australasia, 2008: p. 796.

81. Mazumdar, D. and Evans, J., *A model for estimating exposed plume eye area in steel refining ladles covered with thin slag.* Metallurgical and Materials Transactions B, 2004. 35(2): p. 400-404.

82. Krishnapisharody, K. and Irons, G.A., *An extended model for slag eye size in ladle metallurgy.* ISIJ international, 2008. 48(12): p. 1807-1809.

83. Graham, K., Krishnapisharody, K., Irons, G., and MacGregor, J., *Ladle eye area measurement using multivariate image analysis.* Canadian Metallurgical Quarterly, 2007. 46(4): p. 397-405.

84. *Slag atlas*, Verein Deutscher, E., Editor. 1995, Düsseldorf : Verlag Stahleisen: Düsseldorf. p. 328-429.

85. Xu, X., Brooks, G., Yang, W., and Curic, S., *Rapid image analysis of ladle eye area using threshold technique.* Ironmaking & Steelmaking, 2010. 37(8): p. 620-623.

86. Graham, K.J., *Integrated Ladle Metallurgy Control*. 2008, McMaster University: Canada. p. 418.

87. *Ladle furnace on-line reckoner for prediction and control of steel temperature and composition.* Ironmaking & Steelmaking, 2006. 33(2): p. 140-150.

88. Zhang, L., Thomas, B.G., Wang, X., and Cai, K. *Evaluation and control of steel cleanliness-review*. in *Steelmaking Conference Proceedings*. 2002.

89. Carlsson, G., Lehner, T., Brunner, M., and Thoren, T., *Instrumentation for Ladle Metallurgical Control--Review.* Scaninject IV, 1986: p. 1986.

90. Nirschel, W., Stone, R., and Carr, C., *Overview of steelmaking process control sensors for the BOF, ladle and continuous casting tundish.* Iron & steelmaker, 2001. 28(3): p. 61-65.

91. Chiba, K., Ono, A., Saeki, M., Yamauchi, M., Kanamoto, M., and Ohno, T., *Development of direct analysis method for molten iron in converter: hotspot radiation spectrometry.* Ironmaking & steelmaking, 1993. 20(3): p. 215-220.

92. He, F., Xu, A., Wang, H., He, D., and Tian, N., *End temperature prediction of molten steel in LF based on CBR.* steel research international, 2012. 83(11): p. 1079-1086.

93. Dogan, N., Monaghan, B.J., Longbottom, R.J., Reid, M.H., and Tsekouras, X.C., *Why do we need new inclusion experimental techniques?* 2012.

94. Zhang, L. and Thomas, B.G., *State of the Art in Evaluation and Control of Steel Cleanliness.* ISIJ International, 2003. 43(3): p. 271-291.

95. Hagglund, H., *Device for determining the level of melt in a ladle or the like*. 1982, Google Patents.

96. Meszaros, G., ESTOCIN, T., Marquart, R., KEMENY, E., and Walker, D., *Optimal ladle slag conditioning using US Steel's DepthWave noncontact slag measurement system.* Iron & steelmaker, 2000. 27(6): p. 31-34.

97. Estocin, J.G., Kemeny, F.L., Marquart, R., Meszaros, G.A., and Walker, D.J., *Measuring the thickness of hot slag in steelmaking*. 2000, Google Patents.

98. Meszaros, G.A., Marquart, R., Walker, D.J., Estocin, J.G., and Kemeny, F.L., *Measuring the thickness of hot slag in steelmaking*. 2000, Google Patents.

99. Meszaros, G.A., Marquardt, R., Walker, D.I., Estocin, J.G., and Kemeny, F.L., *Measuring the thickness of materials*. 2000, Google Patents.

100. Lee, G. and Bertermann, K., *Implementation of a slag thickness measurement tool*, in *Seventy Ninth Conference of the Steelmaking Division of the Iron and Steel Society*. 1996. p. 61-65.

101. Kracich, R. and Goodson, K., *Ladle slag depth measurement.* Iron & steelmaker, 1996. 23(7): p. 41-46.

102. Kennedy, T.R., *Molten metal stirring apparatus*. 1967, Google Patents.

103. Satyendra. *Argon Rinsing of Steels*. 2014 [cited 2015; Available from: http://ispatguru.com/argon-rinsing-of-steels/.

104. Hammerer, W., Raidl, G., and Barthel, H., *Gas Purging Plugs for Steel Ladles*, in *Steelmaking Conference Proceedings.* 1992. p. 291-298.

105. Patil, S.P., Satish, D., Peranandhanathan, M., and Mazumdar, D., *Mixing Models for Slag Covered, Argon Stirred Ladles.* ISIJ International, 2010. 50(8): p. 1117-1124.

106. Grüner, H., Wiemer, H., Bardenheuer, F., and Fix, W., *Metallurgische Massnahmen und Bedingungen zur Stahlentschwefelung über das Schlackenreaktionsverfahren.* Stahl und Eisen, 1979. 99(14): p. 725-737.

107. MA, D.H. and FIM, M., *Ladles and Ladle Control Systems-5.* Steel Times, 1976. 204(6): p. 479.

108. Meyer, H., Walter, M., Baum, R., and Zorcher, H., *Vacuum Refining of High-Chromium Melts.* Stahl und Eisen, 1979. 99(23): p. 1315-1318.

109. Burgmann, W., Holtermann, H., EIIebrecht, C., and Wahlster, M., *Vacuum Process Engineering and Ladle Metallurgy in the Production of Steel.* Steel Times International, 1980. 208(6): p. 11.

110. Mobley, R.K. and Mobley, R.K., *Vibration Fundamentals*. 1999, Burlington : Elsevier Science: Boston, Burlington. p. 1-60.

111. Wikepedia. *Vibration*. 2014 [cited 2017 30/05/17]; Available from: https://en.wikipedia.org/wiki/Vibration.

112. Mangiarotty, R., *Acoustic radiation damping of vibrating structures.* The Journal of the Acoustical Society of America, 1963. 35(3): p. 369-377.

113. J.M., C., *HandBook of Acoustics*. 1998, A Wiley-Interscience Publication: New York, USA. p. 675-688.

114. Larsson, H.G., Ostlund, A., and Westman, E., *Ladle or tundish*. 1986, Google Patents.

115. Br, auml, mming, M., Millman, S., Overbosch, A., Kapilashrami, A., Malmberg, D., Bj, ouml, and rkman, B., *BOS Vessel Vibration Measurement for Foam Level Detection.* ISIJ International, 2011. 51(1): p. 71-79.

116. O'Leary, K.E., *The accelerometer as an end-point control sensor for the basic oxygen steelmaking process.* 1992.

117. Randall, R.B., *vibration Signature Analysis-Techniques and instrumentations.* 1974: p. 15.

118. Licht, M.S.a.T.R., *Piezoelectric Accelerometers and Vibration Preamplifiers-Theory and Application Handbook*. 1987, K.larsen & sonA/s: Denmark.

119. McConnell, K.G., *Vibration testing : theory and practice*, Varoto, P.S., Editor. 1995, Hoboken, N.J. : John Wiley & Sons: Hoboken, N.J. p. 212-221.

120. Fahy, F., *Foundation of Engineering Acoustics.* 2007, Elsevier Acadamic press: London, UK. p. 1-136.

121. Rossing T.D. , M.F.R.a.W.P.A., *The Sceince of Sound*. 3rd ed. 2002, SanFrancisco: Addison Wesley. 783.

122. Wolfe, J. *Music Acoustics*. What is acoustic impedance and why is it important? [cited 2014 April 2014]; Available from: http://newt.phys.unsw.edu.au/jw/z.html.

123. Strasberg, M., *Gas Bubbles as Sources of Sound in Liquids.* Journal of the Acoustical Society of America, 1956. 28(1): p. 20-26.

124. Manasseh, R., Riboux, G., and Risso, F., *Sound generation on bubble coalescence following detachment.* International Journal of Multiphase Flow, 2008. 34(10): p. 938-949.

125. Xia, J.L., Ahokainen, T., and Holappa, L., *Analysis of flows in a ladle with gas-stirred melt.* Scandinavian Journal of Metallurgy, 2001. 30(2): p. 69-76.

126. Xiaopeng, Q. and Huihe, Q., *Bubble dynamics under a horizontal micro heater array.* Journal of Micromechanics and Microengineering, 2009. 19(9): p. 095008.

127. Lin, T.J., Tsuchiya, K., and Fan, L.S., *Bubble flow characteristics in bubble columns at elevated pressure and temperature.* AIChE Journal, 1998. 44(3): p. 545-560.

128. Johansen, S.T. and Boysan, F., *Fluid dynamics in bubble stirred ladles: Part II. Mathematical modeling.* Metallurgical Transactions B, 1988. 19(5): p. 755-764.

129. Kulkarni, A.A. and Joshi, J.B., *Bubble Formation and Bubble Rise Velocity in Gas–Liquid Systems: A Review.* Industrial & Engineering Chemistry Research, 2005. 44(16): p. 5873-5931.

130. Davidson, J.F. and Schüler, B.O.G., *Bubble formation at an orifice in a viscous liquid.* Chemical Engineering Research and Design, 1997. 75: p. S105-S115.

131. Lubetkin, S., *Bubble nucleation and growth*. 1994, Butterworth-Heinemann Ltd, Oxford. p. 159-186.

132. Hoefele, E.O. and Brimacombe, J.K., *Flow regimes in submerged gas injection.* Metallurgical Transactions B, 1979. 10(4): p. 631-648.

133. Gerlach, D., Biswas, G., Durst, F., and Kolobaric, V., *Quasi-static bubble formation on submerged orifices.* International Journal of Heat and Mass Transfer, 2005. 48(2): p. 425-438.

134. Stewart, C.W., *Bubble interaction in low-viscosity liquids.* International Journal of Multiphase Flow, 1995. 21(6): p. 1037-1046.

135. Kitscha, J. and Kocamustafaogullari, G., *Breakup criteria for fluid particles.* International Journal of Multiphase Flow, 1989. 15(4): p. 573-588.

136. Štrubelj, L. and Tiselj, I., *Numerical simulations of basic interfacial instabilities with incompressible two-fluid model.* Nuclear Engineering and Design, 2011. 241(4): p. 1018-1023.

137. Anagbo, P. and Brimacombe, J., *Plume characteristics and liquid circulation in gas injection through a porous plug.* Metallurgical and Materials Transactions B, 1990. 21(4): p. 637-648.

138. Lerch, R., *Sensors for Measuring Sound*, in *Sensors*. 2008, Wiley-VCH Verlag GmbH. p. 577-644.

139. Bendat, J.S., *Engineering Applications of Correlation and Spectral Analysis*, Piersol, A.G., Editor. 1980, New York : Wiley: New York. p. 300-472.

140. Cohen, L., *Time-frequency analysis*. 1995, Englewood Cliffs, N.J. : Prentice Hall PTR: Englewood Cliffs, N.J. p. 2-25.

141. Brigham, E.O., *The fast Fourier transform and its applications*, Brigham, E.O., Editor. 1988, Englewood Cliffs, N.J. : Prentice Hall: Englewood Cliffs, N.J. p. 3-8.

142. Julius S.B, J.G.A., *Random Data: Analysisi and Measurement Procedures*. 4th ed. ed. 2011: Wiley, Hoboken

143. Kido, K.i., *Discrete Fourier Transform*, in *Digital Fourier Analysis: Fundamentals*. 2015, Springer. p. 77-105.

144. Itiki, C., *Discrete Fourier Transform.* Wiley Encyclopedia of Biomedical Engineering, 2006: p. 1-17.

145. Girgis, A.A. and Ham, F.M., *A quantitative study of pitfalls in the FFT.* Aerospace and Electronic Systems, IEEE Transactions on, 1980(4): p. 434-439.

146. Shreve, D.H., *Signal processing for effective vibration analysis.* IRD Mechanalysis, Inc. Columbus, Ohio, 1995: p. 1-11.

147. Abed, S.T., Dallalbashi, Z.E., and Taha, F.A., *Studying The Effect of Window type On Power Spectrum Based On MATLAB.* Tikrit Journal of Engineering Science (TJES), 2012. 19(2).

148. Zjajo, A. and de Gyvez, J.P., *Analog to Digital Conversion*, in *Low-Power High-Resolution Analog to Digital Converters*. 2011, Springer. p. 11-40.

149. D.H, S., *Signal Processing for Effective vibration Analysis*. 1995, IRD Mechanalysis, Inc: Columbus, Ohio. p. 11.

150. Taylor, J., *The Vibration Analysis Handbook*. p. 1-34.

151. Piersol, A.G., Paez, T.L., and Harris, C.M., in *Harris' shock and vibration handbook*. 2010, New York McGraw-Hill: New York. p. 463-525.

152. Lebold, M., McClintic, K., Campbell, R., Byington, C., and Maynard, K., *Review of vibration analysis methods for gearbox diagnostics and prognostics*, in *Proceedings of the 54th meeting of the society for machinery failure prevention technology*. 2000. p. 16.

153. Xu, X.B., *Analysis of bubble flow in metallurgical operations using multivariate statistical techniques*, Swinburne University of Technology. Faculty of, E. and Industrial, S., Editors. 2010. p. 247.

154. Yenus, J., Brooks, G., and Dunn, M., *Multivariate Analysis of Ladle Vibration.* Metallurgical and Materials Transactions B, 2016. 47(4): p. 2681-2689.

155. Yenus, J., Brooks, G., and Dunn, M., *Vibration analysis in ladle metallurgy*, in *Asia Pacific Confederation of Chemical Engineering Congress 2015: APCChE 2015, CHEMECA 2015*. 2015, Engineers Australia. p. 2665-2676.

156. Tumer, I.Y. and Huff, E.M., *Principal components analysis of triaxial vibration data from helicopter transmissions.* 2001: p. 1-11.

157. Liu, X., Chen, X., Wu, W., and Zhang, Y., *Process control based on principal component analysis for maize drying.* Food control, 2006. 17(11): p. 894-899.

158. Brito Palma, L., Vieira Coito, F., Sousa Gil, P., and Neves-Silva, R., *Process control based on PCA models*, in *Emerging Technologies and Factory Automation (ETFA), 2010 IEEE Conference on*. 2010, IEEE. p. 1-4.

159. Suhr, D.D., *Principal component analysis vs. exploratory factor analysis.* SUGI 30 Proceedings, 2005: p. 203-230.

160. Child, D., *The essentials of factor analysis, 2nd ed*. 1990, New York, NY, US: Cassell Educational. viii, 120.

161. Romesburg, C., *Cluster analysis for researchers*. 2004: Lulu. com.

162. Torgerson, W.S., *Multidimensional scaling: I. Theory and method.* Psychometrika, 1952. 17(4): p. 401-419.

163. Scholz, M., Kaplan, F., Guy, C.L., Kopka, J., and Selbig, J., *Non-linear PCA: a missing data approach.* Bioinformatics, 2005. 21(20): p. 3887-3895.

164. Scholz, M. and Vigário, R. *Nonlinear PCA: a new hierarchical approach*. in *ESANN*. 2002.

165. Kruger, U. and Xie, L., *Principal Component Analysis*. 2012, Chichester, UK: Chichester, UK: John Wiley & Sons, Ltd. 355-374.

166. MacGregor, J.F. and Kourti, T., *Statistical process control of multivariate processes.* Control Engineering Practice, 1995. 3(3): p. 403-414.

167. van der Linde, A., *Variational Bayesian functional PCA.* Computational Statistics & Data Analysis, 2008. 53(2): p. 517-533.

168. Raghunathan, T.E., Lepkowski, J.M., Van Hoewyk, J., and Solenberger, P., *A multivariate technique for multiply imputing missing values using a sequence of regression models.* Survey methodology, 2001. 27(1): p. 85-96.

169. Abdi, H., *Partial least square regression (PLS regression).* Encyclopedia for research methods for the social sciences, 2003: p. 792-795.

170. de Jong, S. and Phatak, A., *Partial least squares regression.* Recent advances in total least squares techniques and errors-in-variables modeling, 1997: p. 311-338.

171. Geladi, P. and Kowalski, B.R., *Partial least-squares regression: a tutorial.* Analytica Chimica Acta, 1986. 185: p. 1-17.

172. Wold, S., Sjöström, M., and Eriksson, L., *PLS-regression: a basic tool of chemometrics.* Chemometrics and Intelligent Laboratory Systems, 2001. 58(2): p. 109-130.

173. Hsu, K.l., Gupta, H.V., and Sorooshian, S., *Artificial Neural Network Modeling of the Rainfall-Runoff Process.* Water resources research, 1995. 31(10): p. 2517-2530.

174. Tu, J.V., *Advantages and disadvantages of using artificial neural networks versus logistic regression for predicting medical outcomes.* Journal of Clinical Epidemiology, 1996. 49(11): p. 1225-1231.

175. Jager, M. and Hamprecht, F.A., *Principal Component Imagery for the Quality Monitoring of Dynamic Laser Welding Processes.* IEEE Transactions on Industrial Electronics, 2009. 56(4): p. 1307-1313.

176. Tumer, I.Y. and Huff, E.M., *Analysis of triaxial vibration data for health monitoring of helicopter gearboxes.* Journal of vibration and acoustics, 2003. 125(1): p. 120-128.

177. Raykov, T., *An Introduction to Applied Multivariate Analysis*. 2008, Hoboken : Taylor & Francis: Hoboken. p. 211-241.

178. Abdi, H. and Williams, L.J., *Principal component analysis.* Wiley Interdisciplinary Reviews: Computational Statistics, 2010. 2(4): p. 433-459.

179. Yeung, K.Y. and Ruzzo, W.L., *Principal component analysis for clustering gene expression data.* Bioinformatics, 2001. 17(9): p. 763-774.

180. Seggiani, M. and Pannocchia, G., *Prediction of Coal Ash Thermal Properties Using Partial Least-Squares Regression.* Industrial & Engineering Chemistry Research, 2003. 42(20): p. 4919-4926.

181. Bhattacharya, T., *Prediction of Silicon Content in Blast Furnace Hot Metal Using Partial Least Squares (PLS).* ISIJ International, 2005. 45(12): p. 1943-1945.

182. Wold, S., Ruhe, A., Wold, H., and W. J. Dunn, I., *The Collinearity Problem in Linear Regression. The Partial Least Squares (PLS) Approach to Generalized Inverses.* SIAM Journal on Scientific and Statistical Computing, 1984. 5(3): p. 735-743.

183. Lindgren, F., Geladi, P., and Wold, S., *The kernel algorithm for PLS.* Journal of Chemometrics, 1993. 7(1): p. 45-59.

184. Rannar, S., Geladi, P., Lindgren, F., and Wold, S., *The kernel algorithm for PLS II, Few observations and many variables.* J Chemom, 1994. 8: p. 111-125.

185. Wold, S., Albano, C., Dunn, W., Esbensen, K., Hellberg, S., Johansson, E., and Sjöström, M., *Pattern recognition: finding and using regularities in multivariate data.* Food research and data analysis, 1983. 3: p. 183-185.

186. Naes, T., Irgens, C., and Martens, H., *Comparison of Linear Statistical Methods for Calibration of NIR Instruments.* Journal of the Royal Statistical Society. Series C (Applied Statistics), 1986. 35(2): p. 195-206.

187. Halland, D. and Thomas, E., *Partial least-squares methods for spectral analysis.* Anal. Chem, 1988. 60: p. 1193.

188. Wise, B.M., *Properties of Partial Least Squares (PLS) Regression, and Differences between Algorithms*. p. 1-51.

189. Kemeny, F.L., Walker, D., and Jones, J. *Accurate argon stirring in the ladle by vibration measurement*. in *58 th Electric Furnace Conference and 17 th Process Technology Conference*. 2000.

190. Behera , N., Wohaishi, A., Subramanian, R., Tewari, N., and Bommaraju, R. *Optimization of Argon Stirring at Hadeed Ladle Furnace by Application of Trustir*

Technology. in *AISTech Conference 2014*. 2014. USA: AIST.

191. Min, D.R., Jung, C.H., Kim, K.Y., and Kemeny, F.L., *Secondary refining optimization by applying Ar-gas bottom bubbling auto-control system*. Vol. 2. 2013. 2075-2081.

192. Pylvänäinen, M., Visuri, V.-V., Liedes, T., Laurila, J., Karioja, K., Pikkupeura, S., Ollila, S., Fabritius, T., and Oy, S.E., *VIBRATION-BASED ASSESSMENT OF GAS STIRRING INTENSITY IN LADLE TREATMENTS.*

193. Fabritius, T., Kurkinen, P., Mure, P., and Härkki, J., *Vibration of argon–oxygen decarburisation vessel during gas injection.* Ironmaking & steelmaking, 2005. 32(2): p. 113-119.

194. McLeod, S. *Experimental Methods*. SimplyPschology 2012 [cited 2017 31/01/17]; SimplyPschology].

195. Verhelst, D., *Physical modelling of gas stirred metallurgical reactors containing two liquids.* 1991.

196. Mazumdar, N., Mahadevan, A., Madan, M., and Mazumdar, D., *Impact of ladle design on bath mixing*. ISIJ international, 2005. 45(12): p. 1940-1942.

197. Mazumdar, D., Internal Report No. MME-20040129, 2005.

198. SINGH, R.K., *in (Partiaf Tufi 'z 'llment qf tlie Requirements for tlie® egree qf.* 2007.

199. Engineer, I.a.S., *Riveted, Welded or Furnace, Blast Hearth, Open Cars, Ladle Transfer Bails, Ladle Hooks*, in *Ladle*. 1952. p. 2-16.

200. Austin, P., He, Q., Rex, A., and O'Rourke, S. *Thermal modelling of steel ladles*. in *Steelmaking Conference Proceedings.* 1992.

201. Kathait, D.S., *Ladle Furnace Refractory Lining: A review.*

202. Trummer, B., Fellner, W., Viertauer, A., Kneis, L., and Hackl, G., *A Water Modelling Comparison of Hybrid Plug, Slot Plug and Porous Plug Designs.* RHI worldwide: p. 35.

203. Mazumdar, D. and Evans, J.W., *Macroscopic Models for Gas Stirred Ladles.* ISIJ International, 2004. 44(3): p. 447-461.

204. Guthrie, R.I.L., *Dimesional Analysis and Reactor Design*, in *Engineering in process metallurgy*. 1992, Oxford : Clarendon Press ; New York : Oxford University Press, 1992.; Oxford : Clarendon Press ; New York : Oxford University Press, 1992. p. 151-211.

205. Hughes, S.A., *Physical models and laboratory techniques in coastal engineering*. 1993, World Scientific. p. 81-164.

206. Yalin, M., *Fundamentals of hydraulic physical modelling*, in *Recent Advances in Hydraulic Physical Modelling*. 1989, Springer. p. 1-37.

207. Svendsen, I., *Physical modelling of water waves.* Physical Modelling in Coastal Engineering. AA Balkema, Rotterdam, 1985: p. 13-48.

208. Price, A. and Fattah, A., *Hydrodynamic characteristics of a plate heat exchanger channel.* Trans. Inst. of Chem. Eng, 1978. 56: p. 217-228.

209. Mazumdar, D., *Dynamic similarity considerations in gas-stirred ladle systems.* Metallurgical Transactions B, 1990. 21(5): p. 925-928.

210. Michalek, K., Gryc, K., and Morávka, J., *Physical modelling of bath homogenisation in argon stirred ladle.* Metalurgija-Zagreb, 2009. 48(4): p. 215.

211. Saternus, M., Pieprzyca, J., and Merder, T., *Physical Modelling of Metallurgical Processes*, in *Materials Science Forum*. 2017, Trans Tech Publ. p. 1685-1690.

212. Shi, C., *Steel slag—its production, processing, characteristics, and cementitious properties.* Journal of Materials in Civil Engineering, 2004. 16(3): p. 230-236.

213. Seok, S.-H., Jung, S.-M., Lee, Y.-S., and Min, D.-J., *Viscosity of Highly Basic Slags.* ISIJ International, 2007. 47(8): p. 1090-1096.

214. Wu, L., Valentin, P., and Sichen, D., *Study of open eye formation in an argon stirred ladle.* steel research international, 2010. 81(7): p. 508-515.

215. Krishnapisharody, K. and Irons, G.A., *A Unified Approach to the Fluid Dynamics of Gas-Liquid Plumes in Ladle Metallurgy.* ISIJ international, 2010. 50(10): p. 1413-1421.

216. Singh, L., Khan, R., and Aggarwal, M., *Influence of residual stress on fatigue design of AISI 304 stainless steel.* The Journal of Engineering Research, 2011. 8(1): p. 44-52.

217. Colakoglu, M., *Damping behaviour of cyclically deformed 304 stainless steel.* Indian journal of engineering & materials sciences, 2003. 10: p. 480-485.

218. Kling, C., *Damping Effects on a Down Scale*, in *Investigations into damping in building acoustics by use of downscaled models*. 2008, Logos. p. 89-108.

219. Buehrle, R., Gibbs, G., Klos, J., and Mazur, M., *Modeling and validation of damped plexiglas windows for noise control.* NASA Technical Report, 2003: p. 1870-2003.

220. Zhang, J., Perez, R., and Lavernia, E., *Documentation of damping capacity of metallic, ceramic and metal-matrix composite materials.* Journal of materials science, 1993. 28(9): p. 2395-2404.

221. Lai, K.Y.M., Salcudean, M., Tanaka, S., and Guthrie, R.I.L., *Mathematical modeling of flows in large tundish systems in steelmaking.* Metallurgical Transactions B, 1986. 17(3): p. 449-459.

222. Mazumdar, D., Nakajima, H., and Guthrie, R.I.L., *Possible roles of upper slag phases on the fluid dynamics of gas stirred ladles.* Metallurgical Transactions B, 1988. 19(3): p. 507-511.

223. Klingholz, F., *The measurement of the signal-to-noise ratio (SNR) in continuous speech.* Speech Communication, 1987. 6(1): p. 15-26.

224. Cimbala, J.M., *How to Analyze the Frequency Content of a Signal*. 2013, Penn State University: USA. p. 1-5.

225. Alan, V.O., Ronald, W.S., and John, R., *Discrete-time signal processing*, in *New Jersey, Printice Hall Inc*. 1989. p. 648-709.

226. Duhamel, P. and Vetterli, M., *Fast fourier transforms: A tutorial review and a state of the art.* Signal Processing, 1990. 19(4): p. 259-299.

227. Brigham, E.O. and Morrow, R.E., *The fast Fourier transform.* IEEE Spectrum, 1967. 4(12): p. 63-70.

228. Donnelly, D. and Rust, B., *The Fast Fourier Transform for Experimentalists, Part I: Concepts.* Computing in Science & Engineering, 2005. 7(2): p. 80-88.

229. Shutin, D., Witrisal, K., Rank, E., Képesi, M., and Meissner, P., *Discrete Fourier Transform.* TU Graz, SPSC Laboratory Handout, 2009. 6.

230. Cochran, W.T., Cooley, J.W., Favin, D.L., Helms, H.D., Kaenel, R.A., Lang, W.W., Maling, G.C., Jr., Nelson, D.E., Rader, C.M., and Welch, P.D., *What is the fast Fourier transform?* Proceedings of the IEEE, 1967. 55(10): p. 1664-1674.

231. Selesnick, I., *Short time fourier transform.* 2005: p. 1-13.

232. Owens, F.J. and Murphy, M.S., *A short-time Fourier transform.* Signal Processing, 1988. 14(1): p. 3-10.

233. He, Q., Wang, J., Hu, F., and Kong, F., *Wayside acoustic diagnosis of defective train bearings based on signal resampling and information enhancement.* Journal of Sound and Vibration, 2013. 332(21): p. 5635-5649.

234. Wang, K., Liu, Z., Liu, G., Yi, L., Yang, K., Peng, S., and Chen, M., *Vibration Sensor Approaches for the Monitoring of Sand Production in Bohai Bay.* Shock and Vibration, 2015. 2015.

235. Bromba, M.U. and Ziegler, H., *Application hints for Savitzky-Golay digital smoothing filters.* Analytical Chemistry, 1981. 53(11): p. 1583-1586.

236. Krishnan, S.R. and Seelamantula, C.S., *On the Selection of Optimum Savitzky-Golay Filters.* IEEE Transactions on Signal Processing, 2013. 61(2): p. 380-391.

237. Press, W.H. and Teukolsky, S.A., *Savitzky-Golay Smoothing Filters.* Computers in Physics, 1990. 4(6): p. 669-672.

238. Schafer, R.W., *What is a Savitzky-Golay filter?[lecture notes].* IEEE Signal Processing Magazine, 2011. 28(4): p. 111-117.

239. Eilers, P.H., *A perfect smoother.* Analytical chemistry, 2003. 75(14): p. 3631-3636.

240. Savitzky, A. and Golay, M.J.E., *Smoothing and Differentiation of Data by Simplified Least Squares Procedures.* Analytical Chemistry, 1964. 36(8): p. 1627-1639.

241. Persson, P.-O. and Strang, G., *Smoothing by Savitzky-Golay and Legendre Filters*, in *Mathematical Systems Theory in Biology, Communications, Computation, and Finance*, Rosenthal, J. and Gilliam, D.S., Editors. 2003, Springer New York: New York, NY. p. 301-315.

242. Quan, Q. and Cai, K.-Y., *Time-domain analysis of the Savitzky–Golay filters.* Digital Signal Processing, 2012. 22(2): p. 238-245.

243. Frost, O., *Power-spectrum estimation*, in *Aspects of Signal Processing*. 1977, Springer. p. 125-162.

244. Tubaro, S., *Some notes on the power spectral density of random processes*. 2011. p. 6-11.

245. Stoica, P. and Moses, R.L., *1 Basic Concepts*, in *Spectral analysis of signals*

2005, Pearson Prentice Hall Upper Saddle River, NJ. p. 1-14.

246. Bello, J.P., Daudet, L., Abdallah, S., Duxbury, C., Davies, M., and Sandler, M.B., *A Tutorial on Onset Detection in Music Signals.* IEEE Transactions on Speech and Audio Processing, 2005. 13(5): p. 1035-1047.

247. Priestley, M.B., *Power spectral analysis of non-stationary random processes.* Journal of Sound and Vibration, 1967. 6(1): p. 86-97.

248. Paschotta, R., *Power Spectral Density*, in *Encyclopedia of Laser Physics and Technology*. October 2008, Wiley-VCH: Germany.

249. Bhadeshia, H.K.D.H., *Neural Networks in Materials Science.* ISIJ International, 1999. 39(10): p. 966-979.

250. Fuji, H., *Automation and mechanization in steelmaking process.* Nippon Steel Technical Report, 1994: p. 77-77.

251. Hair Jr, J.F., Anderson, R.E., Tatham, R.L., and William, C., *Black (1995), Multivariate data analysis with readings*. New Jersy: Prentice Hall. 1995. 10-20.

252. Rencher, A.C., *Methods of Multivariate Analysis*. 2003, Hoboken : Wiley: Hoboken. p. 400-408.

253. Rencher, A.C., *Methods of Multivariate Analysis*. 2002, A JOHN WILEY & SONS, INC. PUBLICATION: USA. p. 380-727.

254. Qu, X., *Multivariate data analysis*. 2007, Taylor & Francis. p. 103-104.

255. Tabachnick, B.G., *Multivariate Statistics: Why?* , in *Using multivariate statistics*, Fidell, L.S., Editor. 2013, Boston : Pearson: Boston. p. 1-16.

256. Kourti, T., Lee, J., and Macgregor, J.F., *Experiences with industrial applications of projection methods for multivariate statistical process control.* Computers & Chemical Engineering, 1996. 20: p. S745-S750.

257. Shlens, J., *A tutorial on principal component analysis (2005)*. 2010, Institute for Nonlinear Science, UCSD: USA. p. 1-13.

258. Mevik, B.-H. and Cederkvist, H.R., *Mean squared error of prediction (MSEP) estimates for principal component regression (PCR) and partial least squares regression (PLSR).* Journal of Chemometrics, 2004. 18(9): p. 422-429.

259. G.A., C., *Experimental Errors and Uncertainty*. 2002. p. 1-6.

260. Coleman, H.W. and Steele, W.G., *Experimentation, Errors, and Uncertainty*, in *Errors and Uncertainities in a Measure Variable*. 2009, John Wiley & Sons, Inc. p. 31-60.

261. Crittenden, J.C., Trussell, R.R., Hand, D.W., Howe, K.J., and Tchobanoglous, G., *Appendix C: Physical Properties of Water*, in *MWH's Water Treatment: Principles and Design, Third Edition*. 2012, John Wiley & Sons, Inc. p. 1861-1862.

262. Anagbo, P.E., Brimacombe, J.K., and Castillejos, A.H., *A Unified Representation of Gas Dispersion in Upwardly Injected Submerged Gas Jets.* Canadian Metallurgical Quarterly, 1989. 28(4): p. 323-330.

263. Capurro, C., Cerrutti, G., and Cicutti, C., *Influence of vacuum degassing on steel cleanliness.* 2015.

264. Chung, D., *Review: Materials for vibration damping.* Journal of Materials Science, 2001. 36(24): p. 5733-5737.

265. Crandall, S.H., *The role of damping in vibration theory.* Journal of Sound and Vibration, 1970. 11(1): p. 3-IN1.

266. Alam, N. and Asnanit, N.T., *Vibration and Damping Analysis of a Multilayered Cylindrical Shell, Part 11: Numerical Results.* AIAA Journal, 1984. 22(7): p. 975-981.

267. Cupiał, P. and Nizioł, J., *Vibration and damping analysis of a three-layered composite plate with a viscoelastic mid-layer.* Journal of Sound and Vibration, 1995. 183(1): p. 99-114.

268. Tassot, P., *Innovative concepts for steel ladle porous plugs.* Millenium Steel, 2006: p. 111-115.

269. Leighton, T., White, P., and Finfer, D. *Bubble acoustics in shallow water: possible applications in Nature*. in *Proc. Int. Conf. on Boundary influences in high frequency, shallow water acoustics*. 2005. N. Pace.

270. Leighton, T.G. and Walton, A.J., *An experimental study of the sound emitted from gas bubbles in a liquid.* European Journal of Physics, 1987. 8(2): p. 98.

271. Zhang, X., McLean, A., and Sommerville, I. *Potential Applications of Acoustic Techniques in Iron and Steelmaking Operations*. in *Steelmaking Conference Proceedings.* 1991.

272. Sanborn, D.M., *Acoustical insulation panel*. 2001, Google Patents.

273. Prince, M.J. and Blanch, H.W., *Bubble coalescence and break-up in air-sparged bubble columns.* AIChE Journal, 1990. 36(10): p. 1485-1499.

274. MartÍNez-BazÁN, C., MontaÑÉS, J.L., and Lasheras, J.C., *On the breakup of an air bubble injected into a fully developed turbulent flow. Part 1. Breakup frequency.* Journal of Fluid Mechanics, 1999. 401: p. 157-182.

275. Ghosh, A., *Secondary steelmaking: principles and applications*. 2000, USA: CRC Press.

276. Castellini, P., Martarelli, M., and Tomasini, E.P., *Laser Doppler Vibrometry: Development of advanced solutions answering to technology's needs.* Mechanical Systems and Signal Processing, 2006. 20(6): p. 1265-1285.

277. Johansmann, M., Siegmund, G., and Pineda, M., *Targeting the limits of laser Doppler vibrometry.* Proc. IDEMA, 2005: p. 1-12.

278. Joo, S. and Guthrie, R.I.L., *Modeling flows and mixing in steelmaking ladles designed for single- and dual-plug bubbling operations.* Metallurgical Transactions B, 1992. 23(6): p. 765-778.

279. Seeger, R.J., *Newton's Second Law.* American Journal of Physics, 1962. 30(12): p. 930-930.

280. Zhang, Y. and Fruehan, R.J., *Effect of the bubble size and chemical reactions on slag foaming.* Metallurgical and Materials Transactions B, 1995. 26(4): p. 803-812.

Appendix A: Relationships Between PC1 and PC2

The following figures show that the first two principal components are uncorrelated with each other, as would be expected in PCA. The data was taken from cold model as well as plant trials for selected frequency ranges. In the cold model, the volumetric air/gas flow rate varied from 8.33×10^{-6} to 41.67×10^{-6} m^3/s where as in the plant from 583.33 to 16650 $\times 10^{-6}$ m^3/s.

Plastic-Walled Cold Model

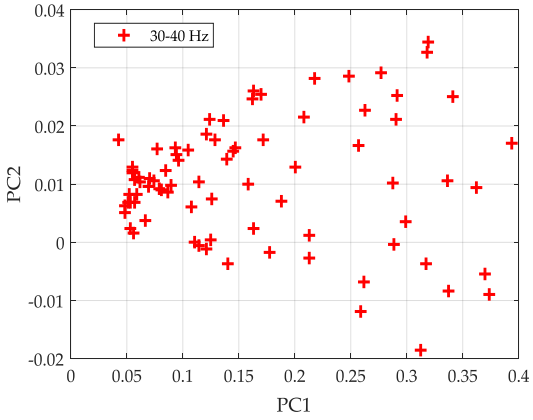

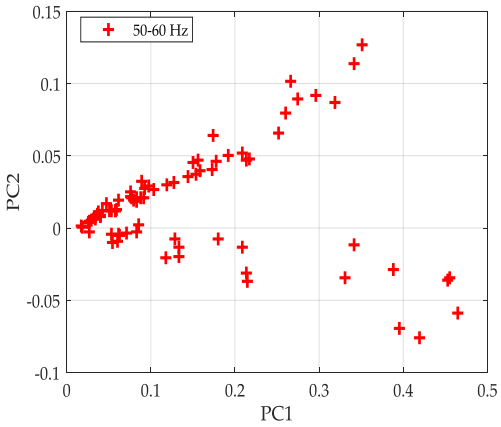

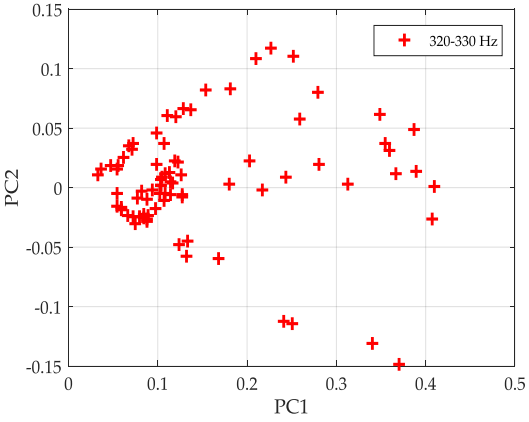

Steel-walled Cold Model

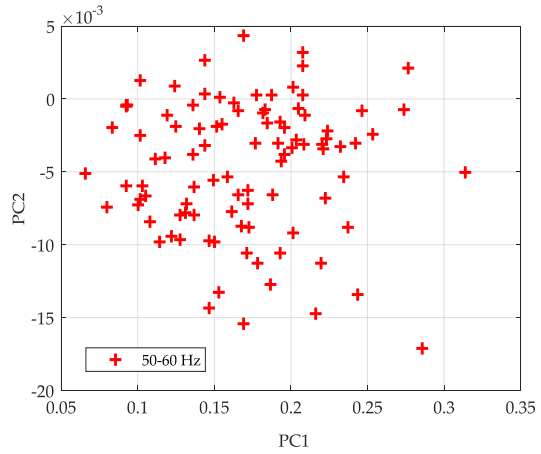

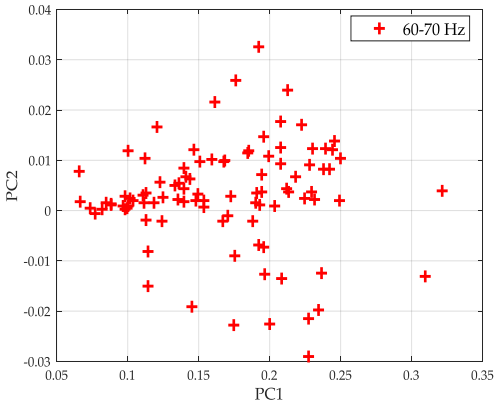

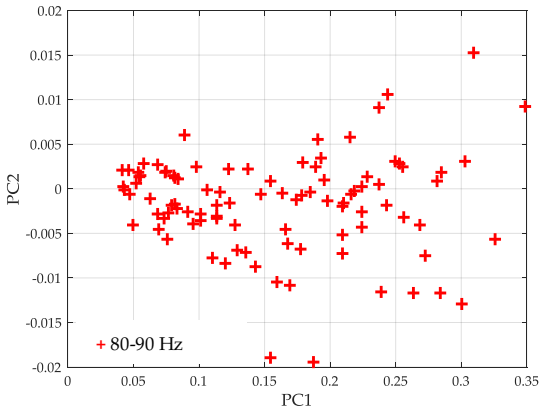

Plant Trails (Combined Heats)

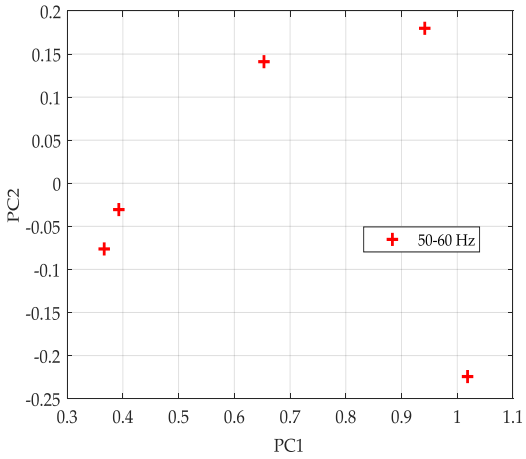

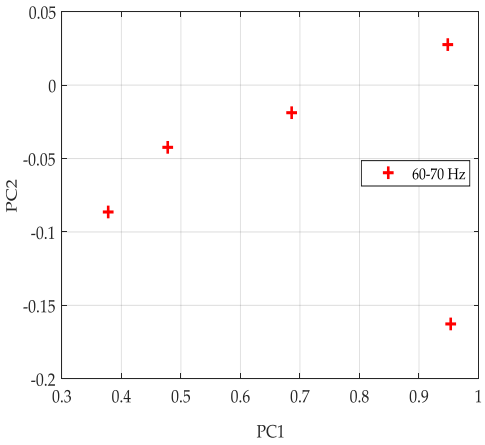

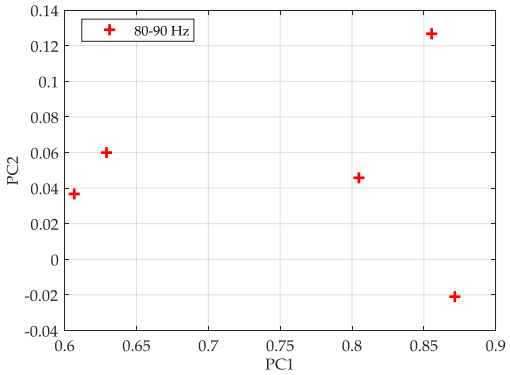

Appendix B Mean Square Error (MSE) of PLS Regressions

The correlation between MSE and number of PLS components for sample frequency ranges is shown below.

Plastic-Walled Cold Model

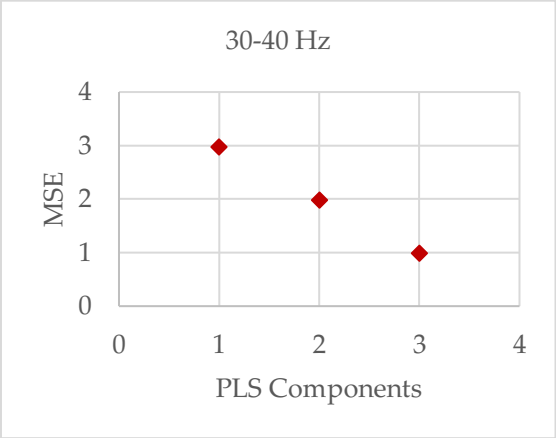

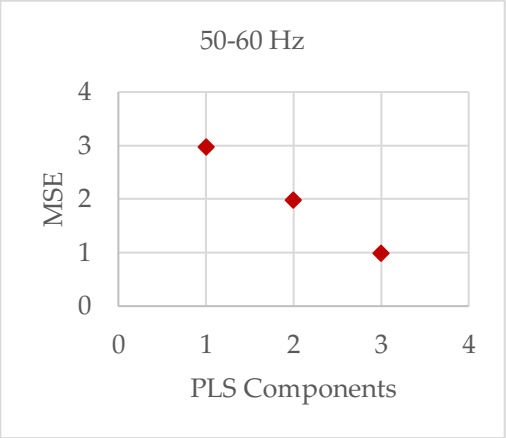

Steel-walled Cold Model

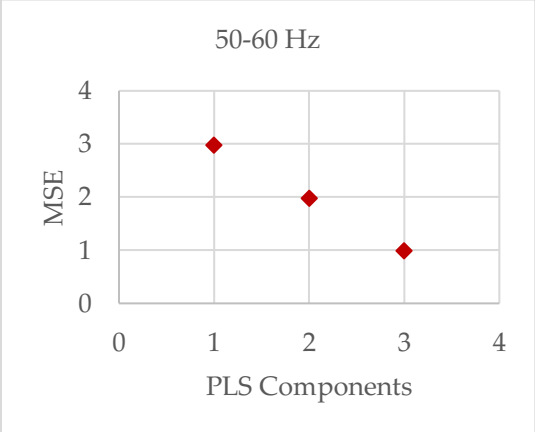

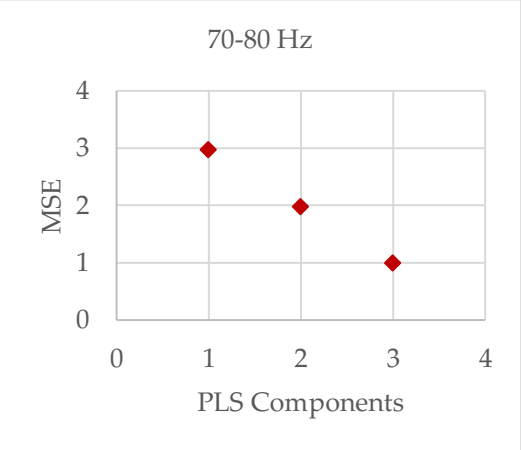

Plant Trails (one Heat)

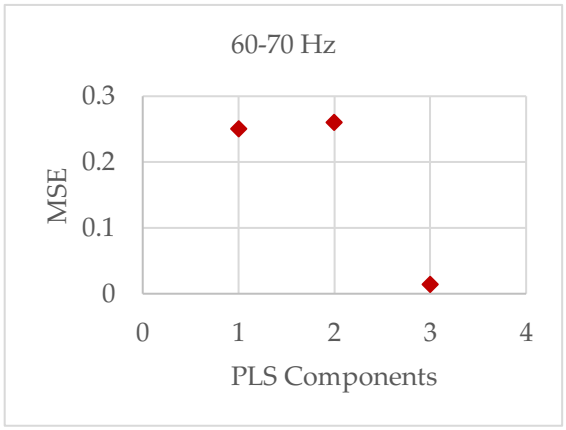

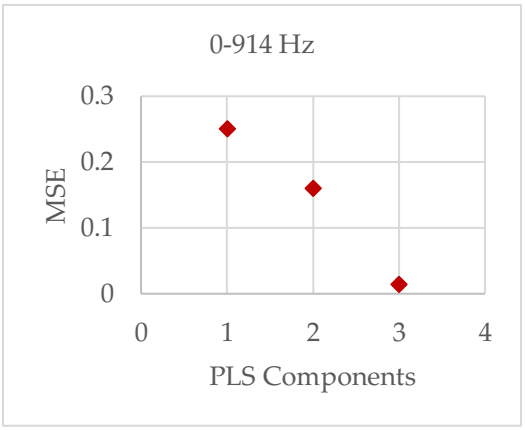

Appendix C: Matlab Based PCA and PLS Programs

This sample program shows how cold model and plant vibration data are analysed. This sample is part of a program used to analyse the steel-walled cold model vibration data. It performs the following tasks:

- Data collection
- Vibration magnitude analysis
- Vibration spectrum analysis
- PCA on vibration signals
- PLS on vibration signals

Program

```
%% **Stee-Walled Cold Model Data **
%% PCA and PLSR Analysis
%Data collected at the following experimtal conditions
%Water height, H= 0.22: 0.02:0.280 m,
%top layer thickness, h=0.005:0.005:0.020 m
% Air flowrate, Q=6.67xE-6:6.67xE-6:40E-6 m^3/s**
%% PCA inputs: Vibration along x-, y and z axes

%% PCA
clc
clear all
p=1;
for i=0.22:0.02:0.280;
   for n=5:5:20;
       for j=0.4:0.2:1.4 %:0.1:0.5;
          for k=1:1;



file=['PT1H',num2str(i),'h',int2str(n),'Q',num2str(j),'LPM_',int2str(k
),'.xlsx'];
        [type,sheets] = xlsfinfo(file);

        sheetx=char(sheets(1,3));
        sheety=char(sheets(1,2));
        sheetz=char(sheets(1,1));
        x=xlsread(file, sheetx,'B11:B11010');
        y=xlsread(file, sheety,'B12:B11011');
        z=xlsread(file, sheetz,'B12:B11011');
        allData(:,p:p+2)=[x y z];
        p=p+3;
          end
      end
```

```
  end
end
xdata=allData(:,1:3:end);
x1data=xdata;
X1=abs(fft(x1data));

ydata=allData(:,2:3:end);
y1data=ydata;
Y1=abs(fft(y1data));

zdata=allData(:,3:3:end);
z1data=zdata;
Z1=abs(fft(z1data));

%% FFT Analysis

Fs=1828;                            % sampling frequency
T=1/Fs;                             %  sample time
L=length(X1) ;      % length of the signal
t=(0:L-1)*T ;                       %  Time vector
NFFT=2^nextpow2(L);
f=Fs/2*linspace(0,1,NFFT/2);        %  vibration frequencies
length(f);

for v=1:96;
  Xfft_X1=abs(fft(x1data,NFFT)/L);
  Xfft_X1_v=Xfft_X1(:,v);
 figure(v)
 plot(f,Xfft_X1_v(1:NFFT/2)),xlabel('Frequency,
Hz'),ylabel('Amplitude, g'), grid minor;
axis([0 914 0 0.6e-3])
end

% y-axis
for v2=1:96;
Yfft_Y1=abs(fft(y1data,NFFT)/L);
Yfft_Y1_v2=Yfft_Y1(:,v2);
 figure(v2)
 plot(f,Yfft_Y1_v2(1:NFFT/2)),xlabel('frequency,
HZ'),ylabel('Amplitude, g'),title('Frequency vs Amplitude(X3)'), grid
minor
end

%z-axis
for v3=1:96;
Zfft_Z1=abs(fft(z1data,NFFT)/L);
Yfft_Z1_v3=Zfft_Z1(:,v3);
figure(v3)
plot(f,Yfft_Z1_v3(1:NFFT/2)),xlabel('frequency,
HZ'),ylabel('Amplitude, g'),title('Frequency vs Amplitude(X3)'), grid
minor
end

%% PCA for 1-914 based sum of values
% frrequency
```

```
fx=sum(1:8192)*ones(44,1);
fy=sum(1:8192)*ones(44,1);
fz=sum(1:8192)*ones(44,1);

%amplitude
X=sum(Xfft_X1(1:8192,:));
Y=sum(Yfft_Y1(1:8192,:));
Z=sum(Zfft_Z1(1:8192,:));

M=[ X'  Y'  Z'];
M=normc(M);
% pca for 1-914 Hz
coefff=pca(M);
[coeff,score,latent] = pca(M);

% principal componenets
PC1=(latent(1)/sum(latent))*100;
PC2=(latent(2)/sum(latent))*100;
PC=[PC1;PC2];

%% PCA for 1-914 based sum of values
% sum of amplitude in the freq. band of 0-300 ,301-600 and 601-914 Hz
X1_1=sum(Xfft_X1(1:2689,:));   % 0-300 Hz
X1_2=sum(Xfft_X1(2690:5378,:));
X1_3=sum(Xfft_X1(5379:8192,:));

Y1_1=sum(Yfft_Y1(1:2689,:));
Y1_2=sum(Yfft_Y1(2690:5378,:));
Y1_3=sum(Yfft_Y1(5379:8192,:));

Z1_1=sum(Zfft_Z1(1:2689,:));
Z1_2=sum(Zfft_Z1(2690:5378,:));
Z1_3=sum(Zfft_Z1(5379:8192,:));

%forming main matrix and applying pca 1-300 Hz
M_1=[X1_1' Y1_1' Z1_1'];
M_1=normc(M_1);
coeff1=pca(M_1);
[coeff,score,latent1] = pca(M_1);

% Percent of variation explained by first and second latent variable
PC11=(latent1(1)/sum(latent1))*100;
PC21=(latent1(2)/sum(latent1))*100;

%forming main matrix and applying pca 300-600 Hz
M_2=[X1_2' Y1_2' Z1_2'];
M_2=normc(M_2);
% pca 1-300
coeff2=pca(M_2);
[coeff,score,latent2] = pca(M_2);

% Percent of variation explained by first and second latent variable
PC12=(latent2(1)/sum(latent2))*100;
PC22=(latent2(2)/sum(latent2))*100;
```

```
%forming main matrix and applying pca 600-914 Hz
M_3=[X1_3' Y1_3' Z1_3'];
M_3=normc(M_3);
% pca 1-300
coeff3=pca(M_3);
[coeff,score,latent3] = pca(M_3);

% Percent of variation explained by first and second latent variable
PC13=(latent3(1)/sum(latent3))*100;
PC23=(latent3(2)/sum(latent3))*100;
PC_300=[PC11 PC12 PC13 ]; % 0 to 914 at interval of 300

%% %% PCA for 1-300  based on sum of values
% sum of amplitude in the freq. band of 0-100 , 101-200 and 200-300 Hz
X1_1a=sum(Xfft_X1(1:896,:));
X1_1b=sum(Xfft_X1(897:1793,:));
X1_1c=sum(Xfft_X1(1794:2689,:));

Y1_1a=sum(Yfft_Y1(1:896,:));
Y1_1b=sum(Yfft_Y1(897:1793,:));
Y1_1c=sum(Yfft_Y1(1794:2689,:));

Z1_1a=sum(Zfft_Z1(1:896,:));
Z1_1b=sum(Zfft_Z1(897:1793,:));
Z1_1c=sum(Zfft_Z1(1794:2689,:));

%forming main matrix and applying pca 1-100 Hz
M_1a=[X1_1a' Y1_1a' Z1_1a'];
M_1a=normc(M_1a);
coeff1a=pca(M_1a);
[coeff,score,latent1a] = pca(M_1a);

% Percent of variation explained by first and second latent variable
PC11a=(latent1a(1)/sum(latent1a))*100;
PC21a=(latent1a(2)/sum(latent1a))*100;

%forming main matrix and applying pca 100-200 Hz
M_1b=[X1_1b' Y1_1b' Z1_1b'];
M_1b=normc(M_1b);

coeff1b=pca(M_1b);
[coeff,score,latent1b] = pca(M_1b);

% Percent of variation explained by first and second latent variable
PC11b=(latent1b(1)/sum(latent1b))*100;
PC21b=(latent1b(2)/sum(latent1b))*100;

%forming main matrix and applying pca 200-300 Hz
M_1c=[X1_1c' Y1_1c' Z1_1c'];
M_1c=normc(M_1c);
coeff1c=pca(M_1c);
[coeff,score,latent1c] = pca(M_1c);

% Percent of variation explained by first and second latent variable
```

```
PC11c=(latent1c(1)/sum(latent1c))*100;
PC21c=(latent1c(2)/sum(latent1c))*100;

PC100=[PC11a PC11b PC11c ];   % 0 to 300 at interval of 100

%% PCA for 300-600  based on sum of values
% sum of amplitude in the freq. band of 300-401 , 300-400 and 400-600
Hz
X1_2a=sum(Xfft_X1(2690:3585,:));
X1_2b=sum(Xfft_X1(3586:4481,:));
X1_2c=sum(Xfft_X1(4482:5378,:));

Y1_2a=sum(Yfft_Y1(2690:3585,:));
Y1_2b=sum(Yfft_Y1(3586:4481,:));
Y1_2c=sum(Yfft_Y1(4482:5378,:));

Z1_2a=sum(Zfft_Z1(2690:3585,:));
Z1_2b=sum(Zfft_Z1(3586:4481,:));
Z1_2c=sum(Zfft_Z1(4482:5378,:));

%forming main matrix and applying pca 300-400 Hz
M_2a=[X1_2a' Y1_2a' Z1_2a'];
M_2a=normc(M_2a);
coeff2a=pca(M_2a);
[coeff,score,latent2a] = pca(M_2a);

% Percent of variation explained by first and second latent variable
PC12a=(latent2a(1)/sum(latent2a))*100;
PC22a=(latent2a(2)/sum(latent2a))*100;

%forming main matrix and applying pca 400-600 Hz
M_2b=[X1_2b' Y1_2b' Z1_2b'];
M_2b=normc(M_2b);
coeff2b=pca(M_2b);
[coeff,score,latent2b] = pca(M_2b);
PC12b=(latent2b(1)/sum(latent2b))*100;
PC22b=(latent2b(2)/sum(latent2b))*100;

%forming main matrix and applying pca 500-600 Hz
M_2c=[X1_2c' Y1_2c' Z1_2c'];
M_2c=normc(M_2c);
coeff2c=pca(M_2c);
[coeff,score,latent2c] = pca(M_2c);

% Percent of variation explained by first and second latent variable
PC12c=(latent2c(1)/sum(latent2c))*100;
PC22c=(latent2c(2)/sum(latent2c))*100;

PC300=[PC12a PC12b PC12c ];
%% %% PCA for 1-100
% sum of amplitude in the freq. band of 0-50 , 50-100
X1_1a1=sum(Xfft_X1(1:448,:));
X1_1a2=sum(Xfft_X1(449:896,:));
```

```
Y1_1a1=sum(Yfft_Y1(1:448,:));
Y1_1a2=sum(Yfft_Y1(497:992,:));

Z1_1a1=sum(Zfft_Z1(1:448,:));
Z1_1a2=sum(Zfft_Z1(497:992,:));

%forming main matrix and applying pca 1-50 Hz
M_1a1=[X1_1a1' Y1_1a1' Z1_1a1'];
M_1a1=normc(M_1a1);
coeff1a1=pca(M_1a1);
[coeff,score,latent1a1] = pca(M_1a1);

% Percent of variation explained by first and second latent variable
PC11a1=(latent1a1(1)/sum(latent1a1))*100;
PC21a1=(latent1a1(2)/sum(latent1a1))*100;

%forming main matrix and applying pca 50-100 Hz
M_1a2=[X1_1a2' Y1_1a2' Z1_1a2'];
M_1a2=normc(M_1a2);
coeff1a2=pca(M_1a2);
[coeff,score,latent1a2] = pca(M_1a2);

% Percent of variation explained by first and second latent variable
PC11a2=(latent1a2(1)/sum(latent1a2))*100;
PC21a2=(latent1a2(2)/sum(latent1a2))*100;

PC50=[ PC11a1 PC11a2 ];

%% %% PCA for 1-100 ()  based on sum of values
% sum of amplitude in the freq. band of 0-25, 25-50, 50-75, 50-100 Hz
X1_1a11=sum(Xfft_X1(1:224,:));
X1_1a12=sum(Xfft_X1(225:448,:));
X1_1a21=sum(Xfft_X1(449:672,:));
X1_1a22=sum(Xfft_X1(673:896,:));

Y1_1a11=sum(Yfft_Y1(1:224,:));
Y1_1a12=sum(Yfft_Y1(225:448,:));
Y1_1a21=sum(Yfft_Y1(449:672,:));
Y1_1a22=sum(Yfft_Y1(673:896,:));

Z1_1a11=sum(Zfft_Z1(1:224,:));
Z1_1a12=sum(Zfft_Z1(225:448,:));
Z1_1a21=sum(Zfft_Z1(449:672,:));
Z1_1a22=sum(Zfft_Z1(673:896,:));

%forming main matrix and applying pca 1-25 Hz
M_1a11=[X1_1a11' Y1_1a11' Z1_1a11'];
M_1a11=normc(M_1a11);
coeff1a11=pca(M_1a11);
[coeff,score,latent1a11] = pca(M_1a11);

% Percent of variation explained by first and second latent variable
PC11a11=(latent1a11(1)/sum(latent1a11))*100;
PC21a11=(latent1a11(2)/sum(latent1a11))*100;
```

```
%forming main matrix and applying pca 25-50 Hz
M_1a12=[X1_1a12' Y1_1a12' Z1_1a12'];
M_1a12=normc(M_1a12);
coeff1a12=pca(M_1a12);
[coeff,score,latent1a12] = pca(M_1a12);

% Percent of variation explained by first and second latent variable
PC11a12=(latent1a12(1)/sum(latent1a12))*100;
PC21a12=(latent1a12(2)/sum(latent1a12))*100;

%forming main matrix and applying pca 50-75 Hz
M_1a21=[X1_1a21' Y1_1a21' Z1_1a21'];
M_1a21=normc(M_1a21);
coeff1a21=pca(M_1a21);
[coeff,score,latent1a21] = pca(M_1a21);

% Percent of variation explained by first and second latent variable
PC11a21=(latent1a21(1)/sum(latent1a21))*100;
PC21a21=(latent1a21(2)/sum(latent1a21))*100;

%forming main matrix and applying pca 75-100 Hz
M_1a22=[X1_1a22' Y1_1a22' Z1_1a12'];
M_1a22=normc(M_1a22);
coeff1a22=pca(M_1a22);
[coeff,score,latent1a22] = pca(M_1a22);

% Percent of variation explained by first and second latent variable
PC11a22=(latent1a22(1)/sum(latent1a22))*100;
PC21a22=(latent1a22(2)/sum(latent1a22))*100;

PC25=[ PC11a11 PC11a12 PC11a21 PC11a22]; %
%% %% PCA for 1-50
% sum of amplitude in the freq. band of 0-10, 10-20, 20-30, 30-40, 40-
50 Hz
X1_1a111=sum(Xfft_X1(1:90,:));
X1_1a112=sum(Xfft_X1(91:179,:));
X1_1a113=sum(Xfft_X1(180:269,:));
X1_1a114=sum(Xfft_X1(270:359,:));
X1_1a115=sum(Xfft_X1(360:448,:));

Y1_1a111=sum(Yfft_Y1(1:90,:));
Y1_1a112=sum(Yfft_Y1(91:179,:));
Y1_1a113=sum(Yfft_Y1(180:269,:));
Y1_1a114=sum(Yfft_Y1(270:359,:));
Y1_1a115=sum(Yfft_Y1(360:448,:));

Z1_1a111=sum(Zfft_Z1(1:90,:));
Z1_1a112=sum(Zfft_Z1(91:179,:));
Z1_1a113=sum(Zfft_Z1(180:269,:));
Z1_1a114=sum(Zfft_Z1(270:359,:));
Z1_1a115=sum(Zfft_Z1(360:448,:));

%forming main matrix and applying pca 1-10 Hz
```

```
M_1a111=[X1_1a111' Y1_1a111' Z1_1a111'];
M_1a111=normc(M_1a111);
coeff1a111=pca(M_1a111);
[coeff,score,latent1a111] = pca(M_1a111);

% Percent of variation explained by first and second latent variable
PC11a111=(latent1a111(1)/sum(latent1a111))*100;
PC21a111=(latent1a111(2)/sum(latent1a111))*100;

%forming main matrix and applying pca 10-20 Hz
M_1a112=[X1_1a112' Y1_1a112' Z1_1a112'];
M_1a112=normc(M_1a112);
coeff1a112=pca(M_1a112);
[coeff,score,latent1a112] = pca(M_1a112);

% Percent of variation explained by first and second latent variable
PC11a112=(latent1a112(1)/sum(latent1a112))*100;
PC21a112=(latent1a112(2)/sum(latent1a112))*100;
%forming main matrix and applying pca 20-30 Hz
M_1a113=[X1_1a113' Y1_1a113' Z1_1a113'];
M_1a113=normc(M_1a113);
coeff1a113=pca(M_1a113);
[coeff,score,latent1a113] = pca(M_1a113);

% Percent of variation explained by first and second latent variable
PC11a113=(latent1a113(1)/sum(latent1a113))*100;
PC21a113=(latent1a113(2)/sum(latent1a113))*100;

%forming main matrix and applying pca 30-40 Hz
M_1a114=[X1_1a114' Y1_1a114' Z1_1a114'];
M_1a114=normc(M_1a114);
coeff1a114=pca(M_1a114);
[coeff,score,latent1a114] = pca(M_1a114);

% Percent of variation explained by first and second latent variable
PC11a114=(latent1a114(1)/sum(latent1a114))*100;
PC21a114=(latent1a114(2)/sum(latent1a114))*100;

%forming main matrix and applying pca 40-50 Hz
M_1a115=[X1_1a115' Y1_1a115' Z1_1a115'];
M_1a115=normc(M_1a115);
coeff1a115=pca(M_1a115);
[coeff,score,latent1a115] = pca(M_1a115);

% Percent of variation explained by first and second latent variable
PC11a115=(latent1a115(1)/sum(latent1a115))*100;
PC21a115=(latent1a115(2)/sum(latent1a115))*100;

PC10_0t50=[PC11a111 PC11a112 PC11a113 PC11a114 PC11a115];
%% %% PCA for 50-100 Hz
% sum of amplitude in the freq. band of 50-60, 60-70, 70-80, 80-90,
90-100 Hz
X1_1a121=sum(Xfft_X1(448:538,:));
X1_1a122=sum(Xfft_X1(539:627,:));
X1_1a123=sum(Xfft_X1(628:717,:));
```

```
X1_1a124=sum(Xfft_X1(718:807,:));
X1_1a125=sum(Xfft_X1(808:896,:));

Y1_1a121=sum(Yfft_Y1(448:538,:));
Y1_1a122=sum(Yfft_Y1(539:627,:));
Y1_1a123=sum(Yfft_Y1(628:717,:));
Y1_1a124=sum(Yfft_Y1(718:807,:));
Y1_1a125=sum(Yfft_Y1(808:896,:));

Z1_1a121=sum(Zfft_Z1(448:538,:));
Z1_1a122=sum(Zfft_Z1(539:627,:));
Z1_1a123=sum(Zfft_Z1(628:717,:));
Z1_1a124=sum(Zfft_Z1(718:807,:));
Z1_1a125=sum(Zfft_Z1(808:896,:));
%forming main matrix and applying pca 50-60 Hz
M_1a121=[X1_1a121' Y1_1a121' Z1_1a121'];
M_1a121=normc(M_1a121);
coeff1a121=pca(M_1a121);
[coeff,score,latent1a121] = pca(M_1a121);

%forming main matrix and applying pca 60-70 Hz
M_1a122=[X1_1a122' Y1_1a122' Z1_1a122'];
M_1a122=normc(M_1a122);
coeff1a122=pca(M_1a122);
[coeff,score,latent1a122] = pca(M_1a122);

%forming main matrix and applying pca 70-80 Hz
M_1a123=[X1_1a123' Y1_1a123' Z1_1a123'];
M_1a123=normc(M_1a123);
coeff1a123=pca(M_1a123);
[coeff,score,latent1a123] = pca(M_1a123);

%forming main matrix and applying pca 80-90Hz
M_1a124=[X1_1a124' Y1_1a124' Z1_1a124'];
M_1a124=normc(M_1a124);
coeff1a124=pca(M_1a124);
[coeff,score,latent1a124] = pca(M_1a124);

%forming main matrix and applying pca 90-100 Hz
M_1a125=[X1_1a125' Y1_1a125' Z1_1a125'];
M_1a125=normc(M_1a125);
coeff1a125=pca(M_1a125);
[coeff,score,latent1a125] = pca(M_1a125);

% Percent of variation explained by first and second latent variable
PC11a121=(latent1a121(1)/sum(latent1a121))*100;
PC21a121=(latent1a121(2)/sum(latent1a121))*100;

PC11a122=(latent1a122(1)/sum(latent1a122))*100;
PC21a122=(latent1a122(2)/sum(latent1a122))*100;

PC11a123=(latent1a123(1)/sum(latent1a123))*100;
PC21a123=(latent1a123(2)/sum(latent1a123))*100;
```

```
PC11a124=(latent1a124(1)/sum(latent1a124))*100;
PC21a124=(latent1a124(2)/sum(latent1a124))*100;

PC11a125=(latent1a125(1)/sum(latent1a125))*100;
PC21a125=(latent1a125(2)/sum(latent1a125))*100;

PC10_50t100=[PC11a121 PC11a122 PC11a123 PC11a124 PC11a125];
%% %% PCA for 100-200 Hz
% sum of amplitude in the freq. band of 100-150 ,150-200 Hz

X3_1b1=sum(Xfft_X1(896:1344,:));
X3_1b2=sum(Xfft_X1(1345:1793,:));

Y3_1b1=sum(Yfft_Y1(896:1344,:));
Y3_1b2=sum(Yfft_Y1(1345:1793,:));

Z3_1b1=sum(Zfft_Z1(896:1344,:));
Z3_1b2=sum(Zfft_Z1(1345:1793,:));

%forming main matrix and applying pca 100-150 Hz
M_1b1=[X3_1b1' Y3_1b1' Z3_1b1'];
M_1b1=normc(M_1b1);
coeff1b1=pca(M_1b1);
[coeff,score,latent1b1] = pca(M_1b1);

%forming main matrix and applying pca 150-200Hz
M_1b2=[X3_1b2' Y3_1b2' Z3_1b2'];
M_1b2=normc(M_1b2);
coeff1b2=pca(M_1b2);
[coeff,score,latent1b2] = pca(M_1b2);

% Percent of variation explained by first and second latent variable
PC11b1=(latent1b1(1)/sum(latent1b1))*100;
PC21b1=(latent1b1(2)/sum(latent1b1))*100;

PC11b2=(latent1b2(1)/sum(latent1b2))*100;
PC21b2=(latent1b2(2)/sum(latent1b2))*100;



PC50_100to200=[ PC11b1 PC11b2 ];
%% %% PCA for 100-150 Hz
% sum of amplitude in the freq. band of 100-110,110-120, 120-130, 130-
140, 140-150 Hz
X1_1b111=sum(Xfft_X1(896:986,:));
X1_1b112=sum(Xfft_X1(987:1076,:));
X1_1b113=sum(Xfft_X1(1077:1165,:));
X1_1b114=sum(Xfft_X1(1166:1255,:));
X1_1b115=sum(Xfft_X1(1256:1344,:));

Y1_1b111=sum(Yfft_Y1(896:986,:));
Y1_1b112=sum(Yfft_Y1(987:1076,:));
Y1_1b113=sum(Yfft_Y1(1077:1165,:));
Y1_1b114=sum(Yfft_Y1(1166:1255,:));
Y1_1b115=sum(Yfft_Y1(1256:1344,:));
```

```
Z1_1b111=sum(Zfft_Z1(896:986,:));
Z1_1b112=sum(Zfft_Z1(987:1076,:));
Z1_1b113=sum(Zfft_Z1(1077:1165,:));
Z1_1b114=sum(Zfft_Z1(1166:1255,:));
Z1_1b115=sum(Zfft_Z1(1256:1344,:));
%forming main matrix and applying pca 100-110 Hz
M_1b111=[X1_1b111' Y1_1b111' Z1_1b111'];
M_1b111=normc(M_1b111);
coeff1b111=pca(M_1b111);
[coeff,score,latent1b111] = pca(M_1b111);

%forming main matrix and applying pca 110-120 Hz
M_1b112=[X1_1b112' Y1_1b112' Z1_1b112'];
M_1b112=normc(M_1b112);
coeff1b112=pca(M_1b112);
[coeff,score,latent1b112] = pca(M_1b112);

%forming main matrix and applying pca 120-130 Hz
M_1b113=[X1_1b113' Y1_1b113' Z1_1b113'];
M_1b113=normc(M_1b113);
coeff1b113=pca(M_1b113);
[coeff,score,latent1b113] = pca(M_1b113);

%forming main matrix and applying pca 130-140Hz
M_1b114=[X1_1b114' Y1_1b114' Z1_1b114'];
M_1b114=normc(M_1b114);
coeff1b114=pca(M_1b114);
[coeff,score,latent1b114] = pca(M_1b114);

%forming main matrix and applying pca 140-150 Hz
M_1b115=[X1_1b115' Y1_1b115' Z1_1b115'];
M_1b115=normc(M_1b115);
coeff1b115=pca(M_1b115);
[coeff,score,latent1b115] = pca(M_1b115);

% Percent of variations explained by first and second latent variable
PC11b111=(latent1b111(1)/sum(latent1b111))*100;
PC21b111=(latent1b111(2)/sum(latent1a121))*100;

PC11b112=(latent1b112(1)/sum(latent1b112))*100;
PC21b112=(latent1b112(2)/sum(latent1b112))*100;

PC11b113=(latent1b113(1)/sum(latent1b113))*100;
PC21b113=(latent1b113(2)/sum(latent1b113))*100;

PC11b114=(latent1b114(1)/sum(latent1b114))*100;
PC21b114=(latent1b114(2)/sum(latent1b114))*100;

PC11b115=(latent1b115(1)/sum(latent1b115))*100;
PC21b115=(latent1b115(2)/sum(latent1b115))*100;

PC10_100t150=[PC11b111 PC11b112 PC11b113 PC11b114 PC11b115]; % 100 to
150 Hz at interval of 10
```

```
%% %% PCA for 150-200 Hz
% sum of amplitude in the freq. band of 150-160,160-170, 170-180,180-
190, 190-200 Hz
X1_1b121=sum(Xfft_X1(1344:1434,:));
X1_1b122=sum(Xfft_X1(1435:1524,:));
X1_1b123=sum(Xfft_X1(1525:1613,:));
X1_1b124=sum(Xfft_X1(1614:1703,:));
X1_1b125=sum(Xfft_X1(1704:1793,:));

Y1_1b121=sum(Yfft_Y1(1344:1434,:));
Y1_1b122=sum(Yfft_Y1(1435:1524,:));
Y1_1b123=sum(Yfft_Y1(1525:1613,:));
Y1_1b124=sum(Yfft_Y1(1614:1703,:));
Y1_1b125=sum(Yfft_Y1(1704:1793,:));

Z1_1b121=sum(Zfft_Z1(1344:1434,:));
Z1_1b122=sum(Zfft_Z1(1435:1524,:));
Z1_1b123=sum(Zfft_Z1(1525:1613,:));
Z1_1b124=sum(Zfft_Z1(1614:1703,:));
Z1_1b125=sum(Zfft_Z1(1704:1793,:));
%forming main matrix and applying pca 150-160 Hz
M_1b121=[X1_1b121' Y1_1b121' Z1_1b121'];
M_1b121=normc(M_1b121);
coeff1b121=pca(M_1b121);
[coeff,score,latent1b121] = pca(M_1b121);

%forming main matrix and applying pca 160-170 Hz
M_1b122=[X1_1b122' Y1_1b122' Z1_1b122'];
M_1b122=normc(M_1b122);
coeff1b122=pca(M_1b122);
[coeff,score,latent1b122] = pca(M_1b122);

%forming main matrix and applying pca 170-180 Hz
M_1b123=[X1_1b123' Y1_1b123' Z1_1b123'];
M_1b123=normc(M_1b123);
coeff1b123=pca(M_1b123);
[coeff,score,latent1b123] = pca(M_1b123);

%forming main matrix and applying pca 180-190Hz
M_1b124=[X1_1b124' Y1_1b124' Z1_1b124'];
M_1b124=normc(M_1b124);
coeff1b124=pca(M_1b124);
[coeff,score,latent1b124] = pca(M_1b124);

%forming main matrix and applying pca 190-200 Hz
M_1b125=[X1_1b125' Y1_1b125' Z1_1b125'];
M_1b125=normc(M_1b125);
coeff1b125=pca(M_1b125);
[coeff,score,latent1b125] = pca(M_1b125);

% Percent of variation explained by first and second latent variable
PC11b121=(latent1b121(1)/sum(latent1b121))*100;
PC21b121=(latent1b121(2)/sum(latent1b121))*100;
```

```
PC11b122=(latent1b122(1)/sum(latent1b122))*100;
PC21b122=(latent1b122(2)/sum(latent1b122))*100;

PC11b123=(latent1b123(1)/sum(latent1b123))*100;
PC21b123=(latent1b123(2)/sum(latent1b123))*100;

PC11b124=(latent1b124(1)/sum(latent1b124))*100;
PC21b124=(latent1b124(2)/sum(latent1b124))*100;

PC11b125=(latent1b125(1)/sum(latent1b125))*100;
PC21b125=(latent1b125(2)/sum(latent1b125))*100;

PC10_150t200=[PC11b121 PC11b122 PC11b123 PC11b124 PC11b125]; % 150 to
200 Hz at interval of 10
%% %% PCA for 200-300 Hz
% sum of amplitude in the freq. band of 0-50 , 50-100 Hz
X1_1c1=sum(Xfft_X1(1793:2241,:));
X1_1c2=sum(Xfft_X1(2242:2689,:));

Y1_1c1=sum(Yfft_Y1(1793:2241,:));
Y1_1c2=sum(Yfft_Y1(2242:2689,:));

Z1_1c1=sum(Zfft_Z1(1793:2241,:));
Z1_1c2=sum(Zfft_Z1(2242:2689,:));

%forming main matrix and applying pca 200-250 Hz
M_1c1=[X1_1c1' Y1_1c1' Z1_1c1'];
M_1c1=normc(M_1c1);
coeff1c1=pca(M_1a1);
[coeff,score,latent1c1] = pca(M_1c1);

%forming main matrix and applying pca 250-300 Hz
M_1c2=[X1_1c2' Y1_1c2' Z1_1c2'];
M_1c2=normc(M_1c2);
coeff1c2=pca(M_1c2);
[coeff,score,latent1c2] = pca(M_1c2);

% Percent of variation explained by first and second latent variable
PC11c1=(latent1c1(1)/sum(latent1c1))*100;
PC21c1=(latent1c1(2)/sum(latent1c1))*100;

PC11c2=(latent1c2(1)/sum(latent1c2))*100;
PC21c2=(latent1c2(2)/sum(latent1c2))*100;

PC50_200to300=[ PC11c1 PC11c2 ];
%% PCA for 200-250 Hz
% sum of amplitude in the freq. band of 200-210, 210-220,220-230, 230-
240, 240-250 Hz
X1_1c121=sum(Xfft_X1(1793:1882,:));   % 200-210 Hz
X1_1c122=sum(Xfft_X1(1883:1972,:));
X1_1c123=sum(Xfft_X1(1973:2061,:));
X1_1c124=sum(Xfft_X1(2062:2151,:));
X1_1c125=sum(Xfft_X1(2152:2241,:));
```

```
Y1_1c121=sum(Yfft_Y1(1793:1882,:));
Y1_1c122=sum(Yfft_Y1(1883:1972,:));
Y1_1c123=sum(Yfft_Y1(1973:2061,:));
Y1_1c124=sum(Yfft_Y1(2062:2151,:));
Y1_1c125=sum(Yfft_Y1(2152:2241,:));

Z1_1c121=sum(Zfft_Z1(1793:1882,:));
Z1_1c122=sum(Zfft_Z1(1883:1972,:));
Z1_1c123=sum(Zfft_Z1(1973:2061,:));
Z1_1c124=sum(Zfft_Z1(2062:2151,:));
Z1_1c125=sum(Zfft_Z1(2152:2241,:));

%forming main matrix and applying pca 200-210 Hz
M_1c121=[X1_1c121' Y1_1c121' Z1_1c121'];
M_1c121=normc(M_1c121);
coeff1c121=pca(M_1c121);
[coeff,score,latent1c121] = pca(M_1c121);

%forming main matrix and applying pca 210-220  Hz
M_1c122=[X1_1c122' Y1_1c122' Z1_1c122'];
M_1c122=normc(M_1c122);
coeff1c122=pca(M_1c122);
[coeff,score,latent1c122] = pca(M_1c122);

%forming main matrix and applying pca 220-230 Hz
M_1c123=[X1_1c123' Y1_1c123' Z1_1c123'];
M_1c123=normc(M_1c123);
% pca for 1-100 Hz
coeff1c123=pca(M_1c123);
[coeff,score,latent1c123] = pca(M_1c123);

%forming main matrix and applying pca 230-240 Hz
M_1c124=[X1_1c124' Y1_1c124' Z1_1c124'];
M_1c124=normc(M_1c124);
coeff1c124=pca(M_1c124);
[coeff,score,latent1c124] = pca(M_1c124);

%forming main matrix and applying pca 240-250 Hz
M_1c125=[X1_1c125' Y1_1c125' Z1_1c125'];
M_1c125=normc(M_1c125);
coeff1c125=pca(M_1c125);
[coeff,score,latent1c125] = pca(M_1c125);

% Percent of variation explained by first and second latent variable
PC11c121=(latent1c121(1)/sum(latent1c121))*100;
PC21c121=(latent1c121(2)/sum(latent1c121))*100;

PC11c122=(latent1c122(1)/sum(latent1c122))*100;
PC21c122=(latent1c122(2)/sum(latent1c122))*100;

PC11c123=(latent1c123(1)/sum(latent1c123))*100;
PC21c123=(latent1c123(2)/sum(latent1c123))*100;
```

```
PC11c124=(latent1c124(1)/sum(latent1c124))*100;
PC21c124=(latent1c124(2)/sum(latent1c124))*100;

PC11c125=(latent1c125(1)/sum(latent1c125))*100;
PC21c125=(latent1c125(2)/sum(latent1c125))*100;

PC10_200t250=[PC11c121 PC11c122 PC11c123 PC11c124 PC11c125];
%% %% PCA for 250-300 Hz
% sum of amplitude in the freq. band of 250-260, 250-260, 260-270,270-
280, 280-290, 290-300 Hz
X1_1c221=sum(Xfft_X1(2240:2330,:));
X1_1c222=sum(Xfft_X1(2330:2419,:));
X1_1c223=sum(Xfft_X1(2419:2509,:));
X1_1c224=sum(Xfft_X1(2509:2599,:));
X1_1c225=sum(Xfft_X1(2599:2688,:));

Y1_1c221=sum(Yfft_Y1(2240:2330,:));
Y1_1c222=sum(Yfft_Y1(2330:2419,:));
Y1_1c223=sum(Yfft_Y1(2419:2509,:));
Y1_1c224=sum(Yfft_Y1(2509:2599,:));
Y1_1c225=sum(Yfft_Y1(2599:2688,:));

Z1_1c221=sum(Zfft_Z1(2240:2330,:));
Z1_1c222=sum(Zfft_Z1(2330:2419,:));
Z1_1c223=sum(Zfft_Z1(2419:2509,:));
Z1_1c224=sum(Zfft_Z1(2509:2599,:));
Z1_1c225=sum(Zfft_Z1(2599:2688,:));

%forming main matrix and applying pca 200-210 Hz
M_1c221=[X1_1c221' Y1_1c221' Z1_1c221'];
M_1c221=normc(M_1c221);
coeff1c221=pca(M_1c221);
[coeff,score,latent1c221] = pca(M_1c221);

%forming main matrix and applying pca 2210-220  Hz
M_1c222=[X1_1c222' Y1_1c222' Z1_1c222'];
M_1c222=normc(M_1c222);
coeff1c222=pca(M_1c222);
[coeff,score,latent1c222] = pca(M_1c222);

%forming main matrix and applying pca 220-230 Hz
M_1c223=[X1_1c223' Y1_1c223' Z1_1c223'];
M_1c223=normc(M_1c223);
coeff1c223=pca(M_1c223);
[coeff,score,latent1c223] = pca(M_1c223);

%forming main matrix and applying pca 230-240 Hz
M_1c224=[X1_1c224' Y1_1c224' Z1_1c224'];
M_1c224=normc(M_1c224);
coeff1c224=pca(M_1c224);
[coeff,score,latent1c224] = pca(M_1c224);

%forming main matrix and applying pca 240-250 Hz
M_1c225=[X1_1c225' Y1_1c225' Z1_1c225'];
M_1c225=normc(M_1c225);
```

```
coeff1c225=pca(M_1c225);
[coeff,score,latent1c225] = pca(M_1c225);

% Percent of variation explained by first and second latent variable
PC11c221=(latent1c221(1)/sum(latent1c221))*100;
PC21c221=(latent1c221(2)/sum(latent1c221))*100;

PC11c222=(latent1c222(1)/sum(latent1c222))*100;
PC21c222=(latent1c222(2)/sum(latent1c222))*100;

PC11c223=(latent1c223(1)/sum(latent1c223))*100;
PC21c123=(latent1c223(2)/sum(latent1c223))*100;

PC11c224=(latent1c224(1)/sum(latent1c224))*100;
PC21c224=(latent1c224(2)/sum(latent1c224))*100;

PC11c225=(latent1c225(1)/sum(latent1c225))*100;
PC21c225=(latent1c225(2)/sum(latent1c225))*100;

PC10_250t300=[PC11c221 PC11c222 PC11c223 PC11c224 PC11c225];


%% PC1 vs stirring Energy relationship
clear CSM11
h2=10e-
3*[225*ones(6,1);230*ones(6,1);235*ones(6,1);240*ones(6,1);245*ones(6,
1);250*ones(6,1);255*ones(6,1);260*ones(6,1);265*ones(6,1);270*ones(6,
1);275*ones(6,1);280*ones(6,1);285*ones(6,1);290*ones(6,1);295*ones(6,
1);300*ones(6,1)];

q2=10e-
3*[(0.4:0.2:1.4)';(0.4:0.2:1.4)';(0.4:0.2:1.4)';(0.4:0.2:1.4)';(0.4:0.
2:1.4)';(0.4:0.2:1.4)';(0.4:0.2:1.4)';(0.4:0.2:1.4)';(0.4:0.2:1.4)';(0
.4:0.2:1.4)';(0.4:0.2:1.4)';(0.4:0.2:1.4)';(0.4:0.2:1.4)';(0.4:0.2:1.4
)';(0.4:0.2:1.4)';(0.4:0.2:1.4)'];
Q=1.67e-5*(0.4:0.2:2.4)';
CSM=M_1a124*coeff1a124; % components of state matrix
CSM1=CSM(:,1)';
CSM11=CSM1';

CSM2=CSM(:,2)';
CSM22=CSM2';
% Relationship between PC1 and PC2
 plot (CSM11,CSM22, 'r+'), xlabel('PC1'),ylabel('PC2'),legend ('50-60
Hz'), grid on

Rhowater=1000 ;                     % water density in kg/m3
Rhosteel=7500;                      % steel density in kg/m3
r=210e-3;                           % rig radius in m
h2=0.001*h2;                        % bath height in m
q2=(0.001)*q2;                      % flow rate in m3/min

Mbw1=((pi*r.^2.*h2)*Rhowater/1000);       % bath weight in tonn
```

```
P0=1;                                          % atmospheric pressure in
atm
T=293;                          % temperature in kelvin
%% stirring power based on szekley model

e1=14.23*(q2*T./Mbw1).*log(1+ (h2/1.46)*P0); % stirring power in w/t
e1=normc(e1);

%Relationship between PC1 and  stirring power

figure(1)
plot(CSM1',e1,'r.'), xlabel('PC1'),ylabel('Normalized stirring energy
(w/t)'), title('180-190 Hz'), grid on
mdl1 = fitlm(CSM1,e1);
R1 = corrcoef(CSM1,e1);      % corrcoeff between PC1 and striing power
Rsq1=mdl1.Rsquared.Adjusted;  % corrcoeff between PC1 and striing
power

% Relatinship between flow rate and vibration amplitude
figure(2)
plot(q2,Y','r.') ,xlabel('Q(l/min)'),ylabel('Normalized stirring
energy(w/t)'), title('180-190 Hz'), grid on
R2 = corrcoef(q2,Y1_1b124');   % corrcoeff between Q-flow rate and
vibration magnitude
mdl2 = fitlm(q2,Y1_1b124');
Rsq2=mdl2.Rsquared.Adjusted;  % corrcoeff between PC1 and striing
power

% Relatinship between PC1 and air flowrate
figure(3)
plot(CSM1(12:22),Q,'r.') , xlabel('PC1'),ylabel('Q(l/min)'),
title('180-190 Hz'), grid on
mdl3 = fitlm(CSM1(12:22),Q);
Rsq3=mdl3.Rsquared.Adjusted;  % corrcoeff between PC1 and striing
power
R3 = corrcoef(CSM1(12:22),Q);        % corrcoeff between PC1 and Q-
flow rate

%Relatinship between avarage speed of bath recirculation and PC1
figure (4)
U=0.86*q2.^0.33.*h2.^0.25*r^(-0.58);
U=normc(U);
plot(CSM1, U, 'r.'), xlabel('PC1'),ylabel('Normalized Steel
Recirculation Speed (w/t)'), title(' 180-190 Hz'), grid on

R4 = corrcoef(CSM1,U);
mdl4 = fitlm(CSM1,U); % linear model
Rsq4=mdl4.Rsquared.Adjusted;  % coefficient of determination between
PC1 and striing power
% disp ( 'pce qvi pcq pcu')
Rsq = [ Rsq1 Rsq2 Rsq3 Rsq4 ];

%%  ++++++++++++++++++++++++++++++++++++++++++++Partial least squares
++++++++++++++++++++++++++++++++++++++++++++++++++++++++++++++++++++
```

```
 % the PLS analysis takes the the flow rate, water depth and oil
thickness
 % as input/predictor matrix and the vibration as output/response
matrix
 % two types
%% Input/predictor variables
H=[0.22*ones(24,1);0.24*ones(24,1);0.26*ones(24,1);0.28*ones(24,1)];
Q=1.67E-
05*[(0.4:0.2:1.4)';(0.4:0.2:1.4)';(0.4:0.2:1.4)';(0.4:0.2:1.4)';(0.4:0
.2:1.4)';(0.4:0.2:1.4)';(0.4:0.2:1.4)';(0.4:0.2:1.4)';(0.4:0.2:1.4)';(
0.4:0.2:1.4)';(0.4:0.2:1.4)';(0.4:0.2:1.4)';(0.4:0.2:1.4)';(0.4:0.2:1.
4)';(0.4:0.2:1.4)';(0.4:0.2:1.4)'];
ho1=1e-
3*[5*ones(6,1);10*ones(6,1);15*ones(6,1);20*ones(6,1);5*ones(6,1);10*o
nes(6,1);15*ones(6,1);20*ones(6,1);5*ones(6,1);10*ones(6,1);15*ones(6,
1);20*ones(6,1);5*ones(6,1);10*ones(6,1);15*ones(6,1);20*ones(6,1)];

ho=ho1;
Xin=[ H ho Q ]; % Input Matrix

Xin=zscore(Xin) % Normalizing the input matrix
                                                                    %%
full frequency range
%% Pls for 1-914 Hz
M=zscore(M_1c334);
[XLz,YLz,XSz,YSz,BETAz,PCTVARz,MSEz] = plsregress(Xin,M,3);
figure(3)
plot (XSz(:,1),YSz(:,1), '+')
% plot(1:3,cumsum(100*PCTVAR(2,:)),'-bo');
xlabel('Xscore');
ylabel('Yscore');
% prediction
A=M;
Y0=A-repmat(mean(A),size(A,1),1);

Yresidualsfz=Y0-XSz*YLz';
n=size(Xin,1);
Yfz = [ones(n,1),Xin]*BETA ; %+Yresiduals;

figure (31)
plot(e1(1:5),Yfz(1:5), '+') , xlabel('stirring energy'),
ylabel('response in vibration'), grid on
figure (32)
plot(U(1:5),Yfz(1:5), '+') , xlabel('Recirculation Speed (m/s)'),
ylabel('response in vibration'), grid on
%% 180-190 Hz (manually chnnge the frequency range to perform the
PLSR)
M_1a122=zscore(M_1a122);
[XL4z,YL4z,XSb4z,YSb4z,BETA4z,PCTVAR4z,MSE4z] = plsregress(M_1a122,
Xin,3);

figure (4)
plot (XSb4z (:,1) ,YSb4z (:,1), '+')
xlabel('Xscore');
ylabel('Yscore');
```

```
% prediction
A=M_1b124;
Y0=A-repmat(mean(A),size(A,1),1);

Yresidualsz=Y0-XSb4z*YL4z';
n=size(Xin,1);
Yz = [ones(n,1),Xin]*BETA4z; % + Yresiduals;
figure (41)
plot(e1(1:5),Yz(1:5), '+') , xlabel('stirring energy'),
ylabel('response in vibration'), grid on
figure (42)
plot(U(1:5),Yz(1:5), '+') , xlabel('Recirculation Speed (m/s)'),
ylabel('response in vibration'), grid on
```

Appendix D: Summary of Publications and Presentations

- List of Publications:

1. **Yenus, Jaefer**; Brooks, Geoffrey; Dunn, Michelle; 2015. Vibration analysis in ladle metallurgy. APCChE 2015 Congress incorporating Chemeca 2015, Melbourne, Australia, 27 September - 1 October 2015. Paper no. 3126426.
2. **Yenus, Jaefer**, Brooks, Geoffrey, and Dunn, Michelle. 2016. Stirring Process Control in Ladle Metallurgy, 8th High-Temperature Processing Symposium 2016, Melbourne, Australia, 1-2 February 2016.
3. **Yenus, Jaefer**; Brooks, Geoffrey; Dunn, Michelle; 2016. Multivariate analysis of ladle vibration. Metallurgical and Materials Transactions B: Process Metallurgy and Materials Processing Science. Vol. 47, no. 4 (Aug 2016), pp. 2681–2689.
4. **Yenus, Jaefer.** Brooks, G.; Dunn, M.; 2016. Principal component analysis of vibration signal in ladle metallurgy. Proceedings AISTech 2016, Pittsburgh, Pennsylvania, 16-19 May 2016. Vol. 2, pp. 1245-1253.

- Paper under review:

  Yenus, J., Brooks G., and Dunn M., Goodwin T., Adderley M., and Li Z. "Study of Low Flow Rate Ladle Bottom Gas Stirring Using Triaxis Vibration Signals". Paper submitted to Metallurgical and Materials Transaction B, May 2017.

- List of Presentations:

1. "*Vibration Analysis of Ladle Gas Stirring Using a Physical Cold Model*" at MPDE biweekly seminar, Swinburne University of Technology, Melbourne, Australia, May 23, 2017.
2. "*Vibration Analysis of Ladle Gas Stirring Using Cold Model and Plant Data*" at AISTech 2017 conference, Nashville, Tenn., USA , 9 May 2017.
3. "*Principal component analysis of vibration signal in ladle metallurgy*" at AISTech 2016 conference in Pittsburgh, Pennsylvania, USA, 18 May 2016.
4. "*Stirring Process Control in Ladle Metallurgy*" at 8th High-Temperature Processing Symposium 2016, Melbourne, Australia, 2 February 2016.
5. "*Vibration analysis in ladle metallurgy*" at APCChE 2015 Congress incorporating Chemeca 2015 conference in Melbourne, Australia, 28 September 2015.
6. "*Vibration and Sound Signal Analysis in Ladle Metallurgy*" at BlueScope Steel in Wollongong, Australia, 20 August 2014.

7. "*Ladle Wall Vibration Measurement in Ladle Metallurgy*" Poster presentation at The 6th Australia-China-Japan Joint Symposium on Iron and Steelmaking, Melbourne, Australia, 24 November 2016.